Science and Technology of Nuclear Installations

Selected Papers from TopSafe 2008: Safety at Nuclear Installations

Guest Editors: Michel Giot, Nikola Čavlina, Dubravko Pevec, and Alessandro Petruzzi

Selected Papers from TopSafe 2008: Safety at Nuclear Installations

Selected Papers from TopSafe 2008: Safety at Nuclear Installations

Guest Editors: Michel Giot, Nikola Čavlina, Dubravko Pevec, and Alessandro Petruzzi

Contents

Hindawi Publishing Corporation
Science and Technology of Nuclear Installations
Volume 2010, Article ID 168298, 2 pages
doi:10.1155/2010/168298

Editorial
Selected Papers from TopSafe 2008: Safety at Nuclear Installations

Michel Giot,[1] Nikola Čavlina,[2] Dubravko Pevec,[2] and Alessandro Petruzzi[3]

[1] *Louvain School of Engineering, Université Catholique de Louvain, 1348 Louvain-la-Neuve, Belgium*
[2] *Faculty of Electrical Engineering and Computing, University of Zagreb, 1000 Zagreb, Croatia*
[3] *Department of Mechanical, Nuclear and Production Engineering, University of Pisa, 56126 Pisa, Italy*

Correspondence should be addressed to Michel Giot, michel.giot@uclouvain.be

Received 12 April 2010; Accepted 12 April 2010

At the end of 2008, a conference on the safety of nuclear installations was successfully organized in Dubrovnik by the European Nuclear Society (ENS). A selection of the papers of this TOPSAFE Conference is proposed in this special issue after the usual long review process. We thank the authors who submitted a revised version of their paper and the distinguished scientists who accepted to review them carefully.

The selected papers of the TOPSAFE Conference presented here are grouped around six themes, all very relevant to safety. A first series of three papers deals with the role of *nuclear safety codes in general*. Presenting several examples of applications, the paper by Thomas Höhne et al. of the Research Centre of Dresden-Rossendorf emphasizes the role of CFD as a tool in the detailed analysis of safety issues of Pressurized Water Reactors, like coolant mixing and stratification, debris transport phenomena, and subcooled boiling in a fuel rod bundle. The quality requirements of the models contained in the CFD codes are outlined. Among the system codes, the advanced capabilities of RELAP/SCDAPSIM are presented in the paper by Chris Allison and Judith K. Hohorst of Innovative Systems Software, LLC. Besides improvements of the models included in the code, improvements in coding and numerics enable the code to be run on complex multidimensional problems faster than real time on inexpensive personal computers and to be used to support training activities. Finally, the paper by Eugenijus Uškpuras of the Lithuanian Energy Institute illustrates the impact of a set of deterministic and probabilistic studies on the decisions regarding the Ignalina NPP safety improvement program.

Containment integrity in a severe accident is the subject of the next two papers proposed by IRSN (Institut de Radioprotection et Sûreté Nucléaire). Ahmed Bentaib et al. present a methodology and its application to Level 2 Probabilistic Safety Assessment to evaluate the impact of the passive autocatalytic recombiners on the hydrogen risk. A set of 35 scenarios have been examined and, subject to further experimental verification, it is concluded that the use of recombiners significantly reduces but does not totally eliminate the risk of flame acceleration and transition to detonation. The other paper on containment integrity, by Renaud Meignen and Tanguy Janin, deals with direct containment heating that could occur after the eventual failure of the reactor vessel. This process is related to dynamical, thermal, and chemical phenomena associated with the possible fine fragmentation and dispersal of the corium melt out of the vessel pit. It may threaten the integrity of the containment by pressurization of its atmosphere. Here the MC3D code has been used. Further developments will require a model for the combustion of hydrogen.

Other aspects of *severe accidents* are studied in the next series of three papers. A comparison between two codes, RELAP5/SCDAPSIM and MAAP4, has been performed by Siniša Šadek et al. in the framework of cooperation between the University of Zagreb, ENCONET Company and NPP Krško. The case study postulates a blackout of the NPP with on-site unavailable supply and with a leakage from reactor coolant pump seals, leading to core degradation. It is shown that both phenomenological and mechanistic models in severe accident codes (MAAP4 and RELAP5/SCDAPSIM) have their own benefits and drawbacks. Their usage can pose

challenges to the user, in first case due to need for model parameters selection and in second case due to more detailed input preparation.

A step for the uncertainty analysis of large-break LOCAs is presented in the paper of Francesc Reventos et al. showing the results of the BEMUSE (Best Estimate Methods plus Uncertainty and Sensitivity Evaluation) programme. This programme involves 13 participants using different codes or different versions of codes.

Nowadays the increased industrial competition and constraints result in more aggressive conditions for the fuel (higher burnup, higher power, load follow, ...) and create incentive conditions for the development of advanced fuel designs with improved performance (new fuel types with additives, cladding material with better resistance to corrosion, ...). These developments involve the need for new investigations of irradiated fuel behavior under reference accidents in order to check the adequacy of the current criteria, evaluate the safety margins, provide new technical bases for modelling, and allow an evolution of these criteria. The paper by François Barré et al. discusses this issue and presents the IRSN strategy.

The next three papers deal with the *safety of VVERs*. The paper by Ivan Spasov et al. (INRNE-Sofia and IRSN) presents validation results for multichannel vessel thermal-hydraulic models in CATHARE used in coupled 3D neutronic/thermal hydraulic calculations. The test cases are from the OECD VVER-1000, coolant transient benchmark (V1000CT) and include asymmetric vessel flow transients and main steam line break (MSLB) transients. Another paper dealing with the qualification of coupled codes for reactor safety evaluations is proposed by Victor Sánchez et al. (FZK). In the frame of the VVER-1000, coolant transient benchmark RELAP5/PARCS has been extensively assessed and multidimensional thermal hydraulic phenomena as well as core physics were examined. Plant data were used to qualify the 3D models of TRACE and RELAP5/CFX, which were coupled for this purpose.

Finally, based on cooperation between IRSN and the University of Lappeenranta, the paper by Luben Sobitonov et al. summarizes the analysis results of three PACTEL experiments, carried out with the thermal-hydraulic system computer CATHARE 2 code. The three LOCA experiments, conducted on the Finnish test facility PACTEL (VVER-440 model), represent 7.4% cold leg breaks with combination of secondary bleed and primary bleed and feed and different actuation modes of the passive safety injection.

Two papers are devoted to the *simulation of passive emergency heat removal systems*. The paper by Lorenzo Santini et al. describes a new experimental facility built and operated at SIET laboratory. in Piacenza, while Davide Papini and Antonio Cammi report on their modeling of heat transfer phenomena for vertical or horizontal configurations of in-pool condensers. A set of correlations are compared with data obtained with the PERSEO facility at SIET laboratory.

The last paper deals with RELAP5/MOD3.3 best estimate for *human reliability*. Proposed by Andrej Prošek and Borut Mavko of the Jožef Stefan Institute, this paper estimates the time windows for successful operator action in scenarios where the human actions are supplement to safety system actuations. The times needed for performing operator actions were determined based on simulator experience.

The editors are convinced that the broad spectrum of safety aspects dealt with in this special issue will be of interest to many readers of the journal.

Michel Giot
Nikola Čavlina
Dubravko Pevec
Alessandro Petruzzi

Hindawi Publishing Corporation
Science and Technology of Nuclear Installations
Volume 2010, Article ID 198758, 8 pages
doi:10.1155/2010/198758

Research Article

Application of CFD Codes in Nuclear Reactor Safety Analysis

T. Höhne, E. Krepper, and U. Rohde

Forschungszentrum Dresden-Rossendorf (FZD), Institute of Safety Research, P.O. Box 51 01 19, D-01314 Dresden, Germany

Correspondence should be addressed to T. Höhne, t.hoehne@fzd.de

Received 16 January 2009; Accepted 29 June 2009

Academic Editor: Michel Giot

Computational Fluid Dynamics (CFD) is increasingly being used in nuclear reactor safety (NRS) analyses as a tool that enables safety relevant phenomena occurring in the reactor coolant system to be described in more detail. Numerical investigations on single phase coolant mixing in Pressurised Water Reactors (PWR) have been performed at the FZD for almost a decade. The work is aimed at describing the mixing phenomena relevant for both safety analysis, particularly in steam line break and boron dilution scenarios, and mixing phenomena of interest for economical operation and the structural integrity. For the experimental investigation of horizontal two phase flows, different non pressurized channels and the TOPFLOW Hot Leg model in a pressure chamber was build and simulated with ANSYS CFX. In a common project between the University of Applied Sciences Zittau/Görlitz and FZD the behaviour of insulation material released by a LOCA released into the containment and might compromise the long term emergency cooling systems is investigated. Moreover, the actual capability of CFD is shown to contribute to fuel rod bundle design with a good CHF performance.

1. Introduction

The last decade has seen an increasing use of three-dimensional CFD codes to predict steady state and transient flows in nuclear reactors because a number of important phenomena such as pressurized thermal shocks, coolant mixing, and thermal striping cannot be predicted by traditional one-dimensional system codes with the required accuracy and spatial resolution. CFD codes contain models for simulating turbulence, heat transfer, multiphase flows, and chemical reactions. Such models must be validated before they can be used with sufficient confidence in NRS applications. The necessary validation is performed by comparing model results against measured data. However, in order to obtain a reliable model assessment, CFD simulations for validation purposes must satisfy strict quality criteria given in the Best Practice Guidelines (BPGs).

Our partner for CFD code qualification is ANSYS CFX [1], which is one of the leading CFD codes worldwide. Based on this partnership the models developed are implemented into the code and thus contribute to the code qualification. In principle the presented simulation could be performed by any other actual CFD-code. The following topical issues, where CFD calculations have been performed, will be briefly discussed in the paper:

(1) coolant mixing,

(2) corizontal stratified flow phenomena in the Hot Leg of PWR,

(3) Debris transport phenomena in multidimensional water flow,

(4) sub-cooled boiling Application to fuel rod bundle safety assessment.

The material presented has been prepared by FZD partly under the sponsorship by the European Commission and the German Government (BMWi).

2. Coolant Mixing

Numerical investigations on coolant mixing in Pressurized Water Reactors (PWRs) have been performed by other institutes and at the FZD for more than a decade [2–9]. The work was aimed at describing the mixing phenomena relevant for both safety analysis, particularly in steam line

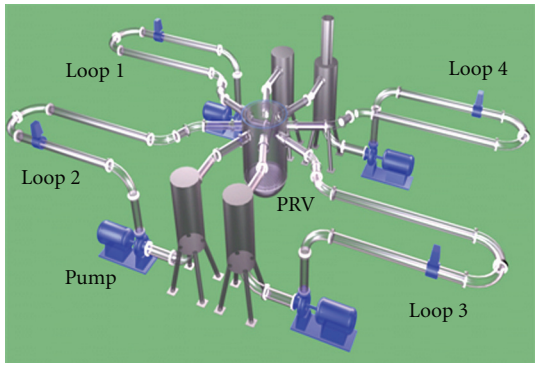

Figure 1: Scheme of ROCOM.

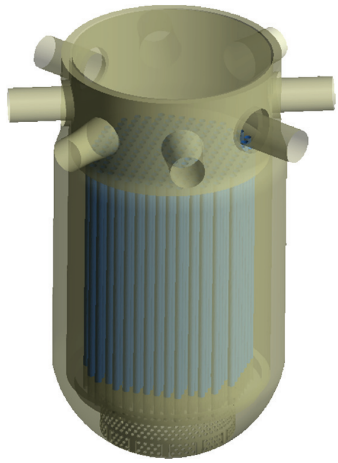

Figure 2: Grid model of ROCOM.

break and boron dilution scenarios, and mixing phenomena of interest for economical operation and the structural integrity.

With the setup of the ROCOM [8, 9] test facility (Figure 1), a unique database has been created to be used for the validation of Computational Fluid Dynamics (CFD) codes for the application to turbulent mixing in nuclear reactors. Benchmark problems based on selected experiments were used to study the effect of different turbulent mixing models under various flow conditions, to investigate the influence of the geometry, the boundary conditions, the grid, and the time step in the CFD analyses. In doing the calculations the Best Practice Guidelines for nuclear reactor safety calculations have been followed [5].

A selection of the performed work is described in [5]:

(i) stationary and transient flow and mixing studies of the coolant in the PWR Konvoi and the ROCOM test facility with CFX-4 and ANSYS CFX-5-11 during boron dilution transients (start-up of the first coolant pump), Figure 3,

(ii) main steam line break scenarios, Figure 4,

(iii) density driven flows after an inherent dilution with ECC injection (generic experiments at the ROCOM test facility) [7].

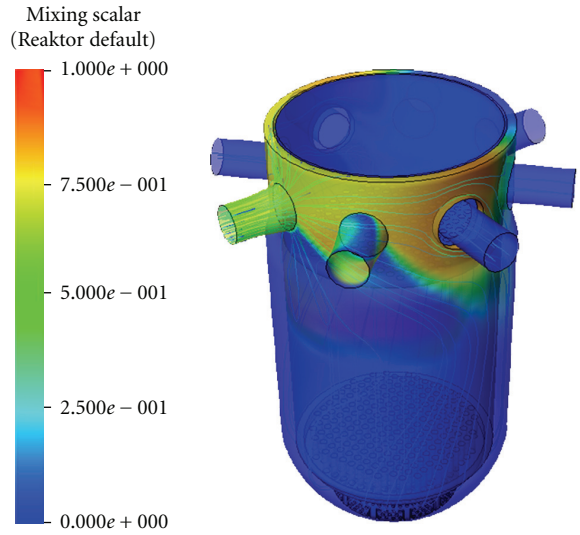

Figure 3: Pump Start-up.

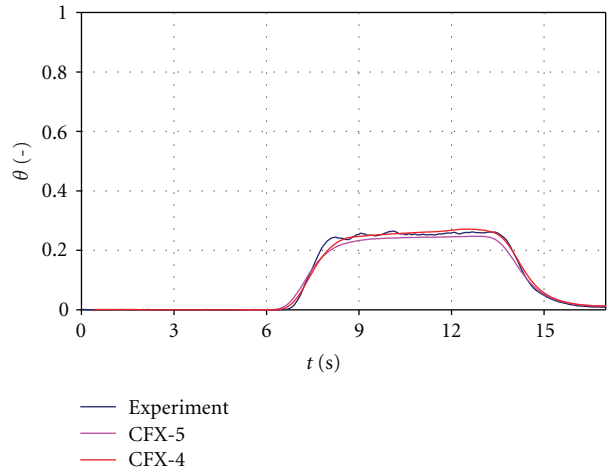

(a) Time dependent global averaged mixing scalar at the core inlet.

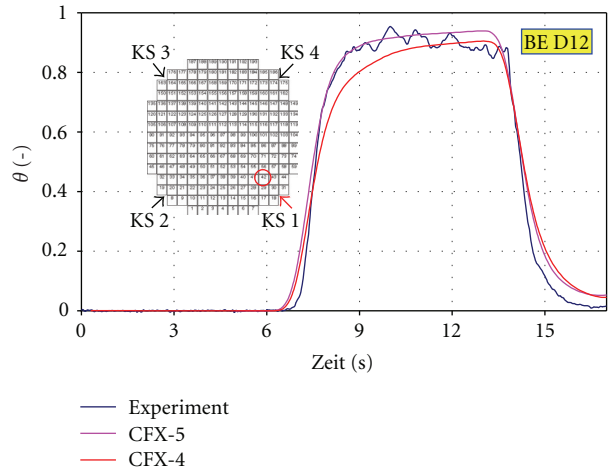

(b) Time dependent local mixing scalar at the core inlet, position near the wall.

Figure 4: Comparison of the measured and calculated mixing scalar (steady state flow field, 185 m^3/h).

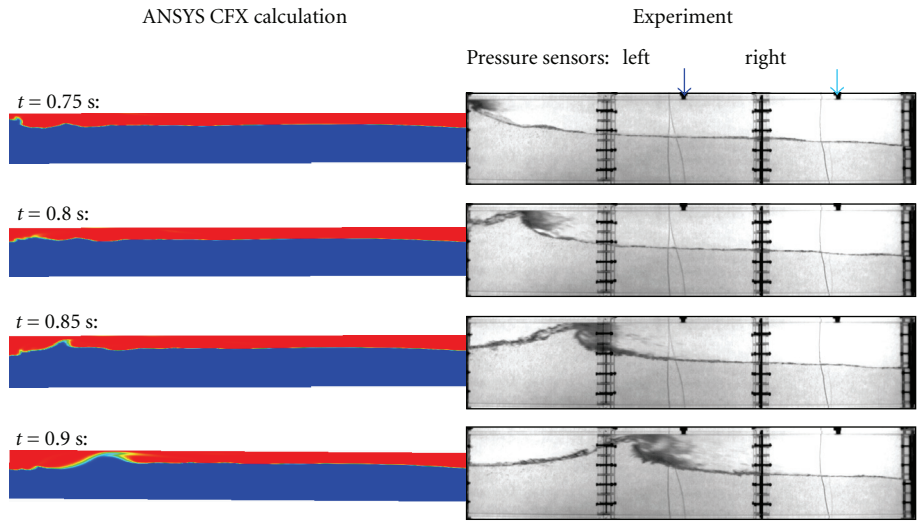

Figure 5: Comparative picture sequence of the recalculated slug.

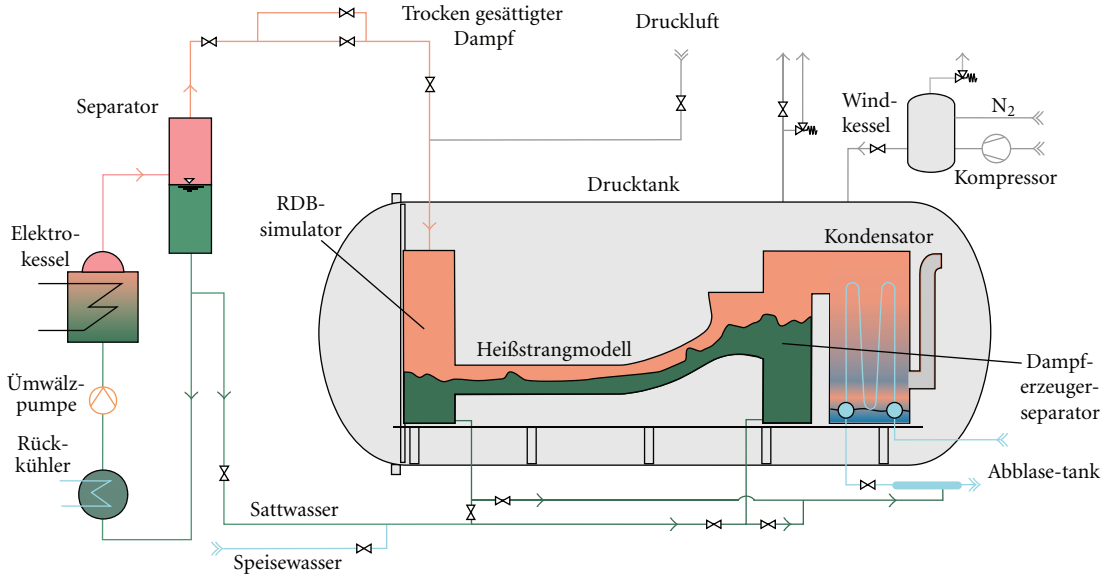

Figure 6: Scheme of the Hot Leg Model in the pressure chamber.

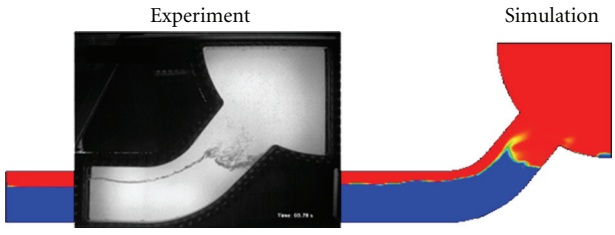

Figure 7: Snapshot of the results of the calculations.

The CFD calculations were carried out with the CFD-codes CFX-4 and CFX-5. Calculations were performed on the FZD LINUX cluster (operating system: Linux Scientific 64 bit, 32 AMD Opteron Computer Nodes, node configuration: 2 × AMD Opteron 285 (2.6 GHz, dual-core), 16 GB Memory). Using the block-structured code CFX-4 internals were modeled using the porous media approach and additional body forces. Sensitivity studies showed that the k-ε turbulence model together with the second-order discretization scheme gives the best results. Within ANSYS CFX-5-11 it was possible to model all internals of the RPV of ROCOM in detail. A production mesh with 7 Million elements was generated (Figure 2). Detailed and extensive grid studies were made. It was shown that a detailed model of the perforated drum in CFX-5 gives the best agreement with the experiments. Sensitivity studies showed that the shear

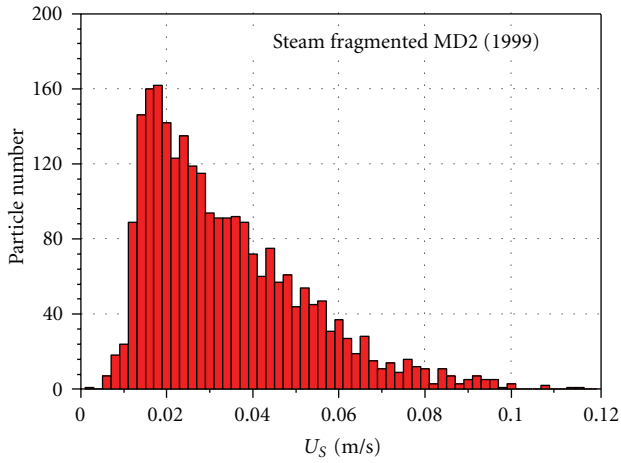

Figure 8: Distributions of the sinking velocities.

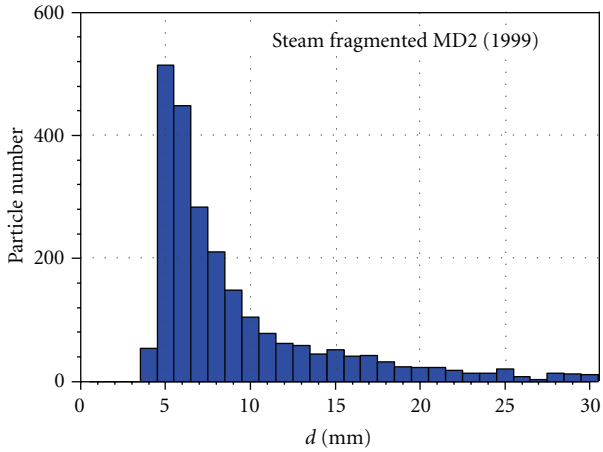

Figure 9: Distributions of the particle size.

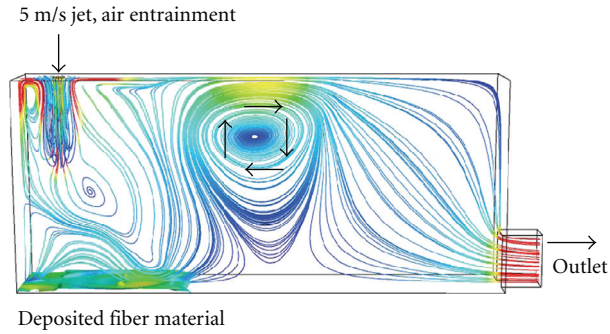

Figure 10: Water flow field induced by the entrained air.

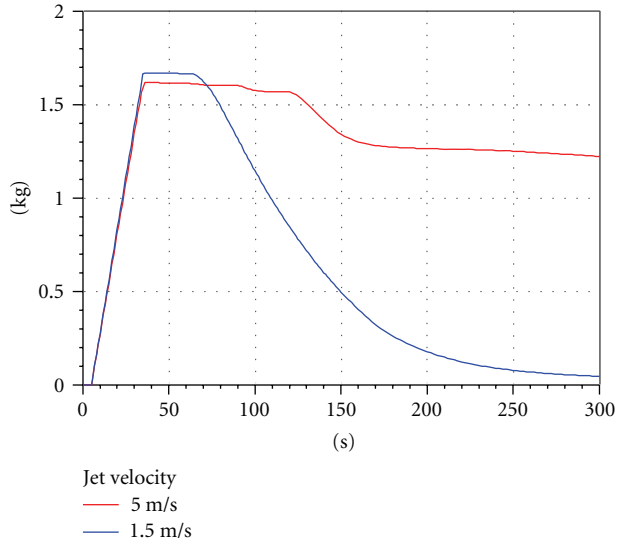

Figure 11: Accumulated fibre mass dependent on the inlet velocity.

stress transport (SST) turbulence model and the automatic wall functions together with higher-order discretization schemes should be used if possible (further details see [5]).

In the case of stationary mixing, the maximum value of the averaged mixing scalar at the core inlet was found in the sector below the inlet nozzle, where the tracer was injected (Figure 4). The mixing scalar is a dimensionless representation of the tracer concentration in the experiment or boron concentration/fluid temperature in reality. There is a good agreement between the measurement and the CFD calculations, especially in the averaged global mixing scalar at the core inlet. At the local position of the maximum mixing scalar the time course of the measurement and the calculations is also in good agreement (see Figure 4).

At the start-up case of one pump due to a strong impulse driven flow at the inlet nozzle the horizontal part of the flow dominates in the downcomer (Figure 3). The injection is distributed into two main jets; the maximum of the tracer concentration at the core inlet appears at the opposite part of the loop where the tracer was injected [6].

3. CFD-Simulations for Stratified Flows

Slug flow as a multiphase flow regime can occur in the cold legs of pressurized water reactors, for instance, after a small break Loss of Coolant Accident (SB-LOCA). Slug flow is potentially hazardous to the structure of the system due to the strong oscillating pressure levels formed behind the liquid slugs. It is usually characterized by an acceleration of the gaseous phase and by the transition of fast liquid slugs, which carry out a significant amount of liquid with high kinetic energy. For the experimental investigation of air/water flows, a horizontal channel with rectangular cross-section was build at Forschungszentrum Dresden-Rossendorf (FZD) [10, 11]. Experimental data were used to check the feasibility to predict the slugging phenomenon with the existing multiphase flow models build in ANSYS CFX. Further it is of interest to prove the understanding of the general fluid dynamic mechanism leading to slug flow and to identify the critical parameters affecting the main slug flow parameters (like e.g., slug length, frequency and propagation velocity, pressure drop). For free surface simulations, the inhomogeneous multiphase model was used, where the gaseous and liquid phases can be partially

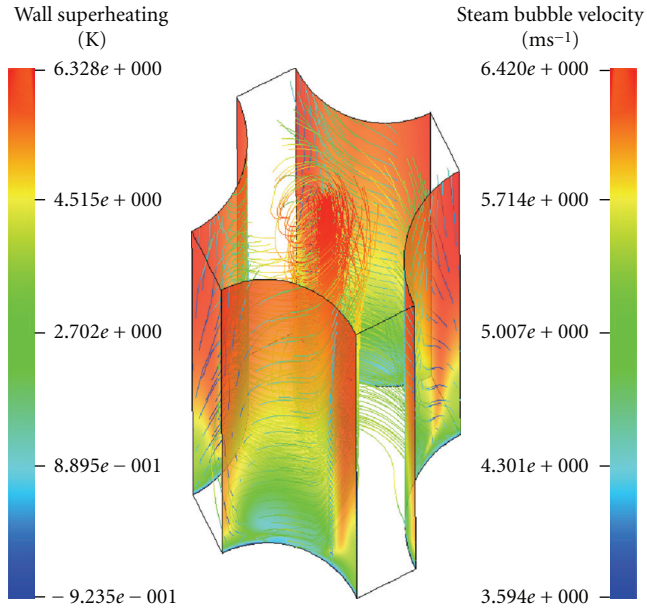

Figure 12: Hot channel vapour flow streamlines and rod surface temperatures.

mixed in certain areas of the flow domain. In this case the local phase demixing after a gas entrainment is controlled by buoyancy and interphase drag and is not hindered by the phase interface separating the two fluids. The fluid-dependent shear stress transport (SST) turbulence models were selected for each phase. Damping of turbulent diffusion at the interface has been considered.

The picture sequence (see Figure 5) shows comparatively the channel flow in the experiment and in the corresponding CFD calculation. In both cases, a slug is developing. The tail of the calculated slug and the flow behind it is in good agreement with the experiment. The entrainment of small bubbles in front of the slug could is not be observed in the calculation. However, the front wave rolls over and breaks. This characteristic of the slug front is clearly to be seen in Figure 5. It is created due to the high air velocity.

Furthermore, pretest calculations CFD were carried out to simulate a slug current in a real geometry and under parameters relevant for the reactor safety. These calculations were performed for a flat model of the hot leg which represents the geometry of a 1 : 3 scaled Konvoi reactor (Figure 6). Steam and water were taken as a model fluid with a pressure of 50 bar and the accompanying saturation temperature of 264°C. To be able to perform the experiments at high pressure, the whole hot leg model is put into a pressure chamber.

The pretest calculations began with a partial water-full channel and quiescent gas phase. At the beginning of the steam supply the surface of the still standing water phase rises in the direction of the steam generator simulator. This effect is caused by the momentum exchange between flowing out steam and quiescent water. The calculation shows spontaneous waves which grow in the elbow to slugs originate in the horizontal part of the hot leg model. Figure 7 shows this state as a snapshot of the results of the calculations.

4. Investigations of Insulation Fiber Transport Phenomena in Water Flow

The investigation of insulation debris generation, transport, and sedimentation becomes more important with regard to reactor safety research for PWR and BWR, when considering the long-term behaviour of emergency core coolant systems during all types of loss of coolant accidents (LOCAs). The insulation debris released near the break during a LOCA incident consists of a mixture of disparate particle population that varies with size, shape, consistency, and other properties. Some fractions of the released insulation debris can be transported into the reactor sump, where it may perturb/impinge on the emergency core cooling systems [12–15].

Open questions of generic interest are the fibre transport in an aqueous flow, the sedimentation of the insulation debris in a water pool, its possible resuspension and transport in the sump water flow, and the fibre load on strainers and the corresponding pressure drop.

A joint research project on such questions is being performed in cooperation of the University of Applied Sciences in Zittau/Görlitz and the Forschungszentrum Dresden-Rossendorf. The project deals with the experimental investigation and the development of CFD models for the description of particle transport phenomena in coolant flow. While the experiments are performed at the University Zittau/Görlitz, the theoretical work is concentrated at Forschungszentrum Dresden-Rossendorf. Details were published by Krepper et al. in 2008 [16].

The main topics of the project are the following

(i) *Primary particle constitution*. Experiments are performed to blast blocks of insulation material by steam under the thermal hydraulic conditions to be expected during a LOCA incident (i.e., at pressures up to 11 MPa). The material obtained by this method is then used as raw material for further experiments.

(ii) *Sedimentation of the fibres*. The transport behaviour of the steam-blasted material is investigated in a water column by optical high-speed video techniques. The sinking velocities of the fibres are then used to derive the drag coefficients and other physical properties of the modelled fibre phase, which is necessary for the implementation of an adequate CFD simulation. Figures 7 and 8 show the measured distribution of sinking velocities and particle size for the insulation material MD2.

(iii) *Transport of fibres in a turbulent water flow*. For these investigations, a narrow channel with a racetrack type configuration was used with defined boundary conditions. Laser PIV measurements and high-speed video were used for the investigation of the water flow-field and the fibre concentration. Besides the drag acting on the particles, the turbulent dispersion force plays an important role in determining the momentum exchanged between the water and the fibrous phase.

(iv) *Deposition and resuspension of fibres*. The deposition and resuspension behaviour at low velocities was investigated by the same techniques and the narrow racetrack channel. Except that, in this case obstacles were inserted into the channel to change locally the flow regime. The experiments are designed to work with laser PIV measurement and high-speed video to investigate the fibre agglomeration in the obstacle region. CFD approaches consider the influence of the fibre material on the mixture viscosity and the dispersion coefficient on the transport of the solids.

(v) *Effect of strainers*. A test rig was used to study the influence of the insulation material loading on the pressure difference observed in the region of the strainers. A CFD model was developed that uses the approach of a porous body. The calculated differential pressure considers compactness of the porous fibre layer. Correlations from the filter theory known in chemical engineering are adapted to the certain fibre material properties by experiments. This concept enables the simulation of a partially blocked strainer and its influence on the flow field.

(vi) *Behaviour of a plunging jet in a large pool and impact on fibre transport*. By using high-speed video and laser (LDA and PIV) measurements, the progression of the momentum by the jet in the pool is investigated. Of special importance is the role that entrained gaseous bubbles play on disturbing the fluid and potentially influencing the fibre sedimentation and re-suspension. Figure 10 shows that under certain flow conditions the entrained air causes a swirl, which transports the injected fibres below the jet. In Figure 11 the fibre mass accumulated in the tank dependent on the inlet jet velocity is shown. In the case of only 1.5 m/s a left turning swirl was found, and the fibre material was transported directly through the tank. For the other case of 5 m/s jet velocity a right turning swirl occurred (see Figure 10), which deposited the fibres below the jet and accumulates fibres for longer time in the tank (see Figure 11).

5. CFD-Calculation of a Hot Channel of a Fuel Rod Bundle

Boiling is a very effective heat transfer mechanism. Liquid cooling including phase transfer very large heat fluxes can be established. Exceeding the critical heat flux, however, the heat transfer coefficient suddenly decreases, and the temperature increases leading to possible damaging of construction material. The critical heat flux depends not only on fluid properties but also on flow conditions and on geometric circumstances [17].

For the case of a fuel rod, the permissible heat flux can be influenced by the geometrical design. Especially the spacer grids equipped with mixing vanes play an important role to increase the permissible heat flux. The verification of design improvements and their influence on the critical heat flux require very expensive experiments. Therefore, the supplementation or even the replacements of expensive experiments by numerical analyses are of relevant interest in fuel assembly design.

Although the CFD modelling of critical heat flux is not yet able to accurately predict CHF, the simulations shall demonstrate the capability of CFD supporting the fuel assembly design. In the calculations only subcooled boiling is simulated, which is here considered as a preliminary phenomenon towards departure of nucleate boiling (DNB). DNB might occur at the thermal hydraulic conditions of a PWR. A situation was investigated, when at full power and full pressure the inlet temperature rise caused undesired boiling in the channel.

A section of coolant channel between two spacer grids having a length of $z = 0.5\,\text{m}$ was simulated. The grid represents a subchannel between 4 rods having a diameter of 9 mm and a rod distance of 12.6 mm. The thermal hydraulic and transport water properties were set for a pressure of 15.7 MPa, typical for PWR conditions. The heat flux at the rod surface was assumed to be $1.0 \cdot 10^6\,\text{W/m}^2$, and the subcooling at the inlet was set to 12 K expecting the generation of vapour in the simulated section. The axial water velocity was set to $V_Z = 5\,\text{m/s}$. The faces at the low and high x respective at low and high y were simulated as periodic boundary conditions, assuming that the channel is infinitely extended in these four directions.

The figure shows the flow condition in the considered channel section (axially shortened presentation). The mixing vanes generate a strong swirl in the actual calculation given

as inlet condition. They are not modelled in this calculation, but a swirl was introduced into the flow as boundary condition at the inlet of the channel section. The overall vapour generation can be decreased by the swirl effect. Due to the centrifugal force, the heavier fluid component—the water—is pushed outwards, whereas a large amount of the lighter component—the vapour—is accumulated in the centre of the channel. The streamlines show vapour bubbles moving in the centre of the channel caused by the centrifugal forces. The colours represent the temperatures of the metal surface. Their distribution can be used as qualitative criterion of the effect of a mixing vane. Further details were published by Krepper et al. (2007), [18].

6. Capability of Actual CFD Codes

The competiveness of CFD is continuously growing due the rapid developments in computer technology. However, computer capacity is still, and will be for a foreseeable future, a limiting factor for the capacity for CFD calculations to produce completely accurate results. Simplified models for describing turbulence therefore have to be used, and the computer capacity put restrictions on the resolution in space and time that one can use in a CFD calculation. This leads to modelling errors and numerical errors that give more or less inaccurate results. Validation of the quality and trust of different approaches in CFD calculations are therefore needed. So-called Best Practice Guidelines (BPGs) have to be used for quality assurance of the validation calculations (see Mahaffy et al., 2007 [19]). The BPGs are built on the concept of an error hierarchy. The different types of errors in CFD simulations are divided into the two main categories:

(i) numerical errors, caused by the discretisation of the flow geometry and the model equations, and by their numerical solution,

(ii) model errors, which arise from the approximation of physical processes by empirical mathematical models

This concept implies that numerical errors are quantified and reduced to an acceptable level, before comparison with experimental data is made. That means that the CFD solution has to be shown to be grid-independent, that is, results that do not change when the grid is refined further. A grid-independent solution can be defined as a solution that has a solution error that is within a range that can be accepted by the end-user, in view of the purpose of the calculations.

7. Conclusion

Computational Fluid Dynamics (CFD) is increasingly being used in nuclear community to model safety relevant phenomena occurring in the reactor coolant system. For this reason the long-term objective of the activities of the FZD R&D program lies in the development of theoretical models for basic phenomena of transient, three-dimensional single and multiphase systems. Local geometry independent models for mass, momentum, heat transfer, and scalar transport are developed and validated. Such models are an essential precondition for the application of complex fluid dynamic codes to the modelling of flow related phenomena in nuclear facilities.

Acknowledgments

The work reported about in this paper was supported by the EU within the FLOMIX Project and the German Federal Ministry of Economics and Labour, Project no 150 1265, 1501270, and 150 1307.

References

[1] ANSYS CFX User Manual, ANSYS-CFX, 2008.

[2] D. Alvarez, et al., "Three dimensional calculations and experimental investigations of the primary coolant flow in a 900 MW PWR vessel," in *Proceedings of the 5th International Topical Meeting on Nuclear Reactor Thermal Hydraulics (NURETH '92)*, vol. 2, pp. 586–592, 1992.

[3] F. Alavyoon, B. Hemström, N. G. Andersson, and R. Karlsson, "Experimental and computational approach to investigating rapid boron dilution transients in PWRs," in *Proceedings of the CSNI Specialist Meeting on Boron Dilution Reactivity Transients*, State College, Pa, USA, October 1995.

[4] B. Woods, *UM 2×4 loop experimental findings on the effect of inertial and buoyancy forces on annular flow mixing for rapid boron dilution transients*, Ph.D. thesis, University of Maryland, Baltimore, Md, USA, 2001.

[5] U. Rohde, T. Höhne, S. Kliem, et al., "Fluid mixing and flow distribution ín a primary circuit of a nuclear pressurized water reactor—validation of CFD codes," *Nuclear Engineering and Design*, vol. 237, no. 15–17, pp. 1639–1655, 2007.

[6] G. M. Cartland Glover, T. Höhne, S. Kliem, U. Rohde, F.-P. Weiss, and H.-M. Prasser, "Hydrodynamic phenomena in the downcomer during flow rate transients in the primary circuit of a PWR," *Nuclear Engineering and Design*, vol. 237, no. 7, pp. 732–748, 2007.

[7] T. Höhne, S. Kliem, and U. Bieder, "Modeling of a buoyancy-driven flow experiment at the ROCOM test facility using the CFD-codes CFX-5 and TRIO_U," *Nuclear Engineering and Design*, vol. 236, no. 12, pp. 1309–1325, 2006.

[8] U. Rohde, S. Kliem, T. Höhne, et al., "Fluid mixing and flow distribution in the reactor circuit—part 1: measurement data base," *Nuclear Engineering and Design*, vol. 235, pp. 421–443, 2005.

[9] H.-M. Prasser, G. Grunwald, T. Höhne, S. Kliem, U. Rohde, and F.-P. Weiss, "Coolant mixing in a PWR—deboration transients, steam line breaks and emergency core cooling injection —experiments and analyses," *Nuclear Technology*, vol. 143, pp. 37–56, 2003.

[10] C. Vallee, T. Höhne, H.-M. Prasser, and T. Sühnel, "Experimental investigation and CFD simulation of horizontal air/water slug flow," *Kerntechnik*, vol. 71, no. 3, pp. 95–103, 2006.

[11] T. Höhne, C. Vallee, and H.-M. Prasser, "Experimental and numerical prediction of horizontal stratified flows," in *Proceedings of the International Conference on Multiphase Flow (ICMF '07)*, Leipzig, Germany, July 2007, paper no. S5_Tue_C_23.

[12] "Knowledge base for emergency core cooling system recirculation reliability," NEA/CSNI/R(95)11.

[13] "Knowledge Base for the Effect of Debris on Pressurized Water Reactor Emergency Core Cooling Sump Performance," NUREG/CR-6808; LA-UR-03-0880.

[14] "Knowledge Base for Strainer Clogging—Modifications Performed in Different Countries Since 1992," NEA/CSNI/R(2002)6.

[15] "Debris impact on Emergency coolant recirculation," in *Proceedings of the OECD Workshop*, Albuquerque, NM, USA, February 2004, NEA no. 5468.

[16] E. Krepper, G. Cartland-Glover, A. Grahn, et al., "Numerical and experimental investigations for insulation particle transport phenomena in water flow," *Annals of Nuclear Energy*, vol. 35, pp. 1564–1579, 2008.

[17] H. Anglart, O. Nylund, N. Kurul, and M. Z. Podowski, "CFD prediction of flow and phase distribution in fuel assemblies with spacers," *Nuclear Engineering and Design*, vol. 177, no. 1–3, pp. 215–228, 1997.

[18] E. Krepper, B. Koncar, and Y. Egorov, "Modelling of subcooled boiling—concept, validation and application to fuel assembly design," *Nuclear Engineering and Design*, vol. 237, pp. 716–731, 2007.

[19] J. Mahaffy, et al., "Best practice guidelines for the use of CFD in nuclear reactor safety applications," NEA/CSNI/R(2007)5, May 2007.

Hindawi Publishing Corporation
Science and Technology of Nuclear Installations
Volume 2010, Article ID 425658, 17 pages
doi:10.1155/2010/425658

Project Report

Role of RELAP/SCDAPSIM in Nuclear Safety

C. M. Allison and J. K. Hohorst

Innovative Systems Software, LLC, 1284 South Woodruff Avenue, Idaho Falls, ID 83404, USA

Correspondence should be addressed to C. M. Allison, iss@srv.net

Received 17 August 2009; Accepted 10 January 2010

Academic Editor: Michel Giot

The RELAP/SCDAPSIM code, designed to predict the behaviour of reactor systems during normal and accident conditions, is being developed as part of the international SCDAP Development and Training Program (SDTP). SDTP consists of nearly 60 organizations in 28 countries supporting the development of technology, software, and training materials for the nuclear industry. The program members and licensed software users include universities, research organizations, regulatory organizations, vendors, and utilities located in Europe, Asia, Latin America, and the United States. Innovative Systems Software (ISS) is the administrator for the program. RELAP/SCDAPSIM is used by program members and licensed users to support a variety of activities. The paper provides a brief review of some of the more important activities including the analysis of research reactors and Nuclear Power Plants, design and analysis of experiments, and training.

1. Introduction

The RELAP/SCDAPSIM code, designed to predict the behaviour of reactor systems during normal and accident conditions, is being developed as part of the international SCDAP Development and Training Program (SDTP) [1, 2]. Three main versions of RELAP/SCDAPSIM, as described in Section 2, are currently used by program members and licensed users to support a variety of activities. RELAP/SCDAPSIM/MOD3.2, and MOD3.4 are production versions of the code and are used by licensed users and program members for critical applications such as research reactor and nuclear power plant applications. The most advanced production version, MOD3.4, is also used for general user training and for the design and analysis of severe accident related experiments such as those performed in the Phebus and Quench facilities. In turn, these experiments are used to improve the detailed fuel behaviour and other severe accident-related models in MOD3.4 and MOD4.0. MOD4.0 is currently available only to program members and is used primarily to develop advanced modelling options and to support graduate research programs and training.

2. RELAP/SCDAPSIM

RELAP/SCDAPSIM uses the publicly available RELAP/MOD3.3 [3] and SCDAP/RELAP5/MOD3.2 [4] models developed by the US Nuclear Regulatory Commission in combination with proprietary (a) advanced programming and numerical methods, (b) user options, and (c) models developed by ISS and other members of the SDTP. These enhancements allow the code to run faster and more reliably than the original US NRC codes. RELAP/SCDAPSIM/MOD3.2 was the first production version released under SDTP sponsorship. It was designed to duplicate the modeling options available from the original US NRC versions of RELAP/MOD3.3 and SCDAP/RELAP5/MOD3.2 but run faster and more reliably. This version used standard RELAP5 and SCDAP/RELAP5 input but included enhanced output options such as integrated 3D and time history plotting options. This version also included a number of coding and numerical improvements to improve the performance of the code. RELAP/SCDAPSIM/MOD3.4 is the current production version and is designed specifically for "faster-than-real-time" simulations on typical Windows or LINUX PCs.

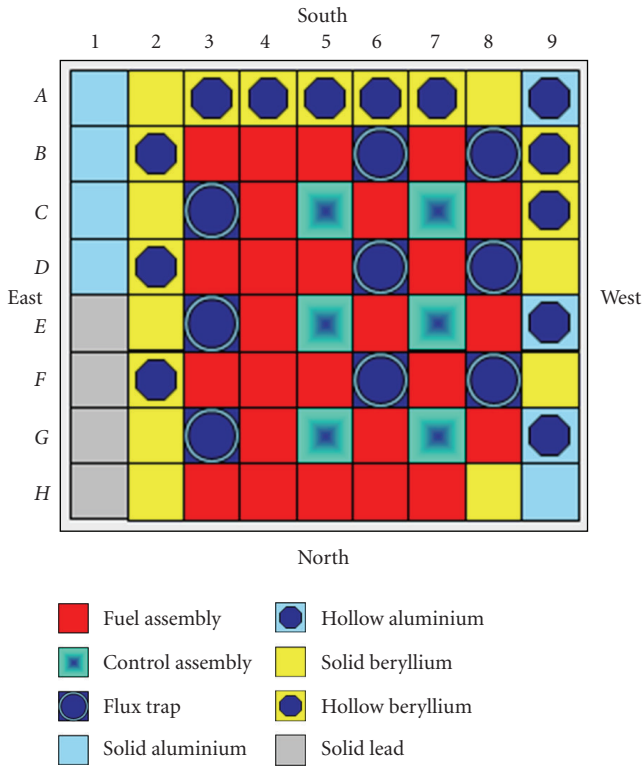

Figure 1: SAFARI reactor core configuration.

The designation MOD3.4 is used to indicate that additional modeling options have been included relative to the original US NRC codes. These modeling options include improved models for a detailed fuel rod, an electrically heated fuel rod simulator, and other SCDAP core components. Other modeling improvements include new models and correlations for air ingression transients and alternative fluids and cladding materials. Continued improvements in the coding and numerics also allow both MOD3.4 and MOD4.0 to run a wider variety of transients including low-pressure transients with the presence of noncondensable gases such as those occurring during mid-loop operations in LWRs, in pool type reactors, or in spent fuel storage facilities.

The most advanced version of the code, RELAP/SCDAPSIM/MOD4.0 [5], is the first version of RELAP or SCDAP/RELAP5 completely rewritten to FORTRAN 90/95/2000 standards. This is a significant benefit for the program members that are using the code for the development of advanced models and user options such as the coupling of the code to other analysis packages. Coupled 3D reactor kinetics and coupled RELAP/SCDAPSIM-SAMPSON [6] calculations are examples where MOD4.0 is used because of a significant reduction in the code development effort and expense to link the packages. MOD4.0 also includes advanced numerical options such as improved time advancement algorithms, improved water property tables, and improved model coding. As a result the code can reliably run complex multidimensional problems faster than real time on inexpensive personal computers. Plant simulation and integrated uncertainty analysis are among the most important applications benefiting from the improved speed and reliability of MOD4.0. MOD4.0 includes many enhanced user options to improve the accuracy of the code or to offer new options for the users. For example, the addition of an alternative material property library designed for Zr-Nb cladding materials is important for VVER and CANDU reactor designs, particularly for severe accident-related transients. The addition of an advanced water property formulation is important for many transients, in particular those involving super critical water applications.

3. Review of Representative Applications

RELAP/SCDAPSIM is being used for a variety of applications. As described in Section 3.1, the code is used for the analysis of research reactors and nuclear power plants. The research reactors analysed by the code include TRIGAs, MTR-plate designs, and other unique designs well as. Nuclear plants analysed include Western designed PWRs and BWRs, Russian designed VVERs and RMBKs, Canadian and Indian designed CANDUs and HWRs, and Chinese designed PWRs. The analysis of experiments, as discussed in Section 3.2, is also an important application of the code, including the design of the experiments, the assessment and development of modelling improvements, and finally for advanced user training. The application of the code to support the development of improved models and analytic capabilities is discussed in Section 3.3. Section 3.4 presents an overview of the application of the code for training.

3.1. Research Reactor and NPP Applications. A combination of RELAP/SCDAPSIM/MOD3.2 and MOD3.4 is being used to analyze research reactors. A brief summary of the early work by several countries was given in [6]. The research reactors noted in this paper include (a) the LVR-15 reactor located at the Nuclear Research Institute in Rez, Czech Republic, (b) the CARR reactor being built in Beijing, China by the China Institute of Atomic Energy, and (c) TRIGA reactors located at the Atomic Energy Research Establishment in Dhaka, Bangladesh, and National Nuclear Energy Agency in Bandung Indonesia. LVR-15 is a light-water moderated and cooled pool type reactor with a nominal thermal power of 15 MW. The pool operates at atmospheric pressure with an average coolant temperature in the core of 320 K. The reactor also has closed high-pressure/temperature loops suitable for testing of materials under PWR and BWR conditions. The reactor core is composed of several fuel assemblies of Al-U alloy arranged in square concentric tubes. CARR is a tank-in-pool design, cooled and moderated by light water and reflected by heavy water. The rated power is 60 MW. The core consists of plate-type fuel assemblies of Al-U alloy. The Indonesian and Bangladesh TRIGA reactors are pool type reactors with 2 MW and 3 MW thermal power, respectively. The reactor cores are composed of solid U-ZrH fuel rods arranged in a hexagonal array and are cooled by water in

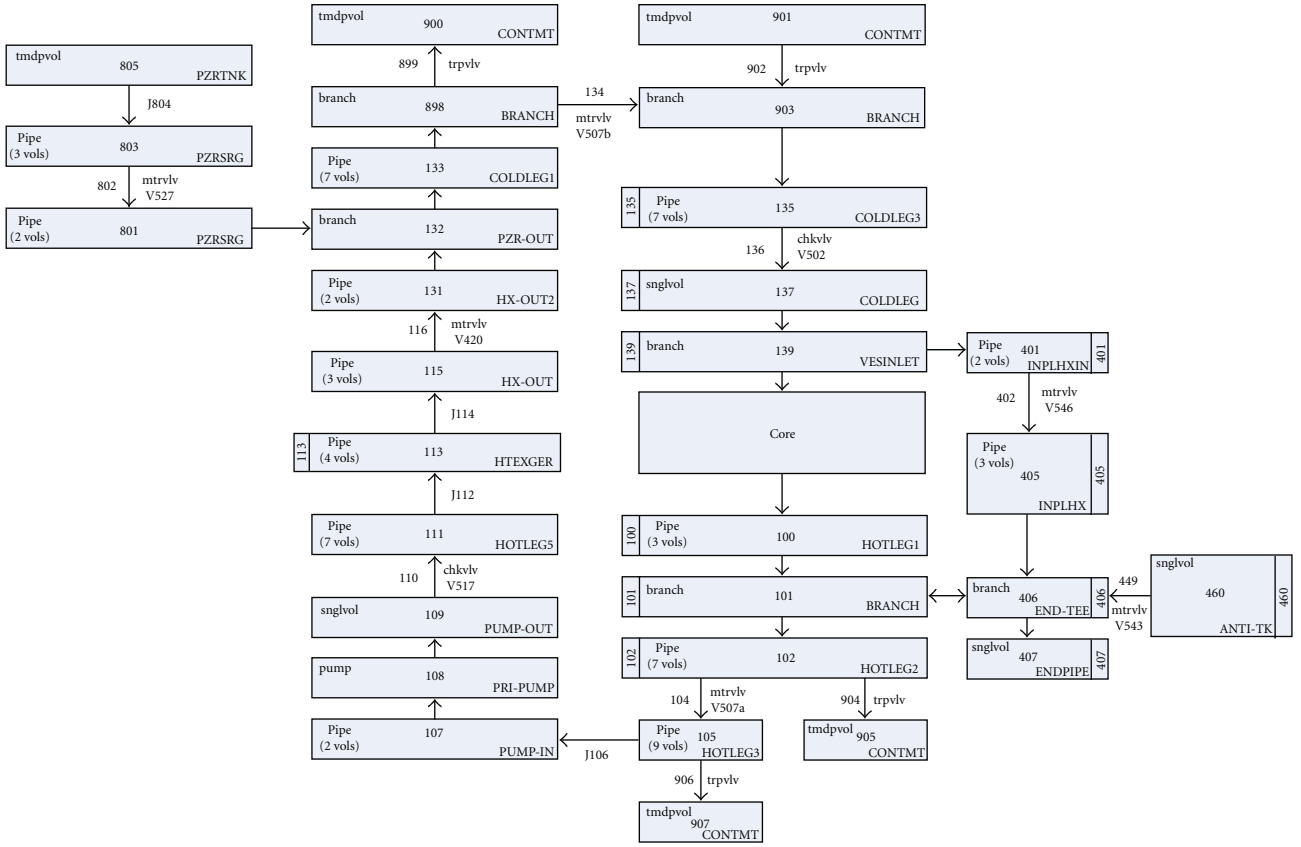

Figure 2: MURR RELAP/SCDAPSIM nodalization of the MURR pressurized primary cooling system.

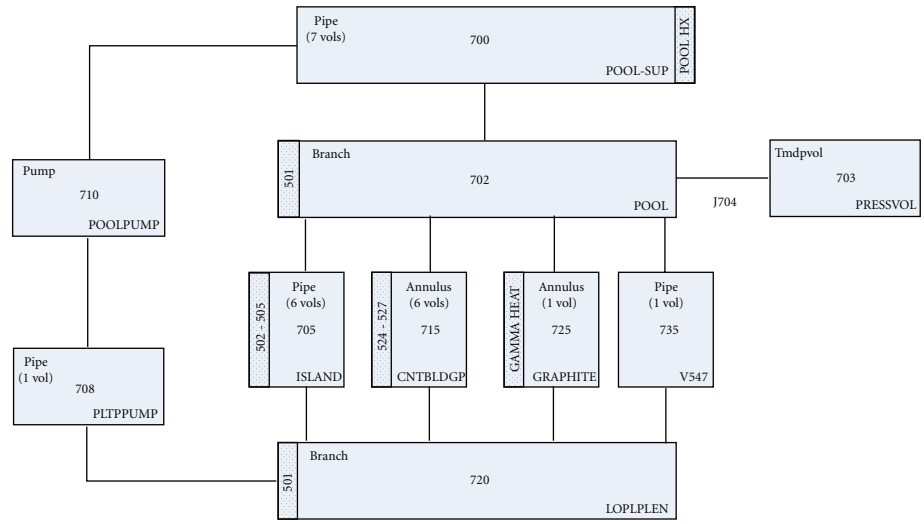

Figure 3: RELAP/SCDAPSIM nodalization of the MURR bulk reactor pool and pool coolant loop.

either forced or natural circulation, depending upon the conditions.

More recently, the analysis of two additional reactor types have been reported in [7–9]. The first is for the SAFARI-1 research reactor located in South Africa [7, 8]. The second is the University of Missouri Research Reactor located in the United States [9]. The SAFARI-1 research reactor is a tank-in-pool type reactor operated at a nominal core power of 20MW. The core is cooled and moderated by forced circulation of light water. The reactor core can be operated in a variety of configurations from 24 to 32 fuel assemblies. Figure 1 shows an example of one such configuration. The fuel is U-Si-Al plate-type fuel elements. MURR is a 10 MW pool type reactor design with a pressurized primary coolant

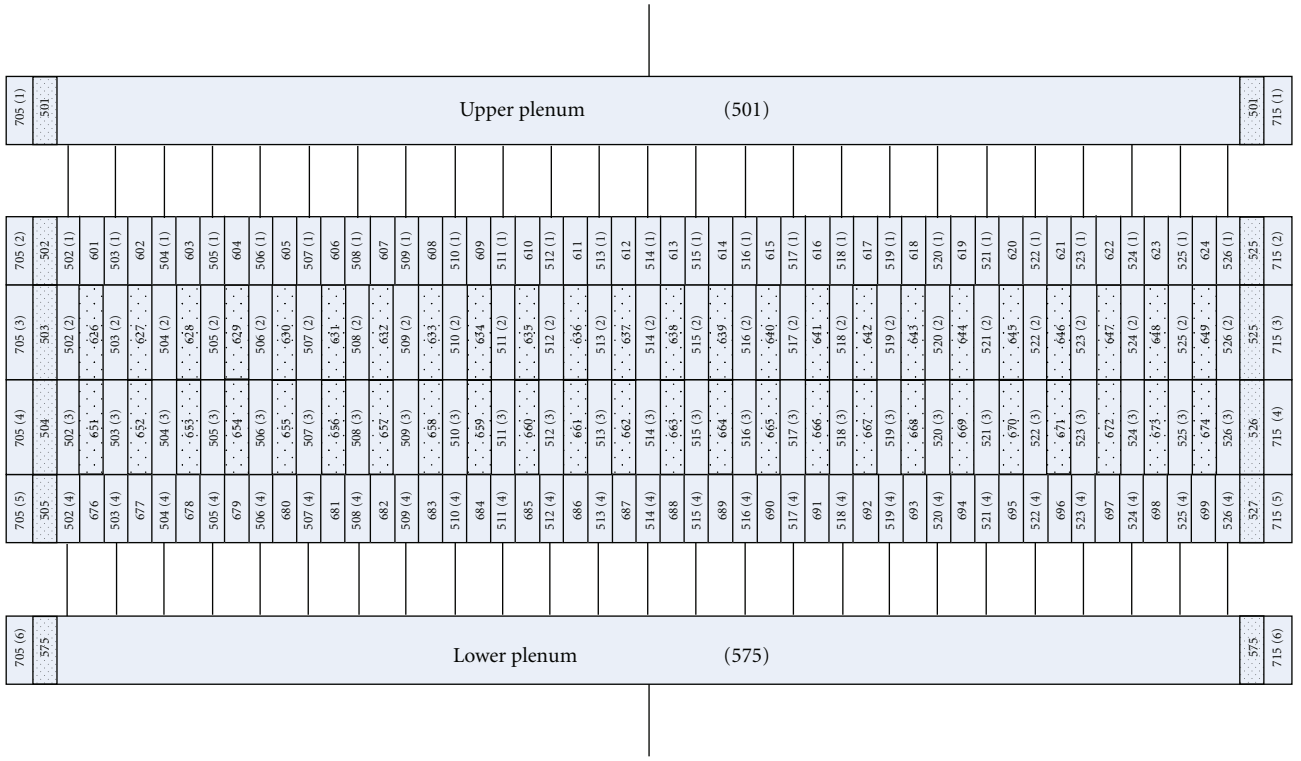

Figure 4: RELAP/SCDAPSIM nodalization of the MURR 24 fuel plate core.

loop to cool the fuel region. The pressurized primary system is located in a pool allowing direct heat transfer during normal operation and transition to natural convection under accident conditions. The reflector region, control blade region, and center test hole are cooled by pool water (natural convection).

Because of the unique reactor designs, the RELAP/SCDAPSIM input models were developed separately by each organization and include a range of different nodalizations as presented in the reference papers. However in general terms, the RELAP/SCDAPSIM input models include all of the major components of each reactor system including the reactor tank, the reactor core and associated structures, and the reactor cooling system including pumps, valves, and heat exchangers. The secondary sides of the heat exchanger(s) are also modelled where appropriate. These input models were qualified through comparison with reactor steady state data, with original vendor safety analysis calculations where available, and with experiments in a limited number of cases. Figures 2 through 4 give examples of the nodalization used for MURR. Figures 2 and 3 show the detailed hydrodynamic nodalization for the pressurized primary cooling system and the bulk pool and pool cooling system, respectively. Figure 4 shows the nodalization of the fuel plates. This input model is also somewhat unique in that all 24 fuel plates were modeled using RELAP5 heat structures.

Figure 5 shows the nodalization used for the SAFARI research reactor. Figure 5 shows the overall system hydrodynamic nodalization with the upper right corner of the figure showing the core nodalization. Note from the insert of the core nodalization diagram that the bypass or unheated channels were modelled separately from the heated fuel assembly channels. The core nodalization also included two separate hot plate channels located on each side of the hottest plate.

A wide variety of transients have been analyzed using the code. Examples are included in the references and include reactivity initiated power excursions and loss of flow or coolant transients. Figure 6 shows one such example for MURR. The figure shows the centerline temperatures for the 24 fuel plates during a cold leg LOCA, indicating that the fuel transients remained well below the assumed fuel damage limits of 900°F.

All three versions of RELAP/SCDAPSIM have been used to analyze a variety of nuclear power plant designs. The applications have included RELAP5-only input models for normal operating or transient conditions where core damage is not expected as well as combined RELAP-SCDAP input models that included the possibility of transients with the loss of core geometry. A few representation examples are discussed in more detail in the remainder of this subsection.

Analysts at the Paul Scherrer Institut (PSI) in Switzerland have applied the code to the TMI-2 accident [10], an analysis of a LOCA during cooldown in the Beznau Westinghouse type 2-Loop PWR [11], and an analysis of a station blackout transient in the Gösgen KWU three-loop 1020 MW PWR [12]. The TMI-2 calculations included comparisons with the limited data available from the accident as well as comparisons with the MELCOR [13] and SCDAP/RELAP5 [14] codes. The Beznau analysis paper summarized the

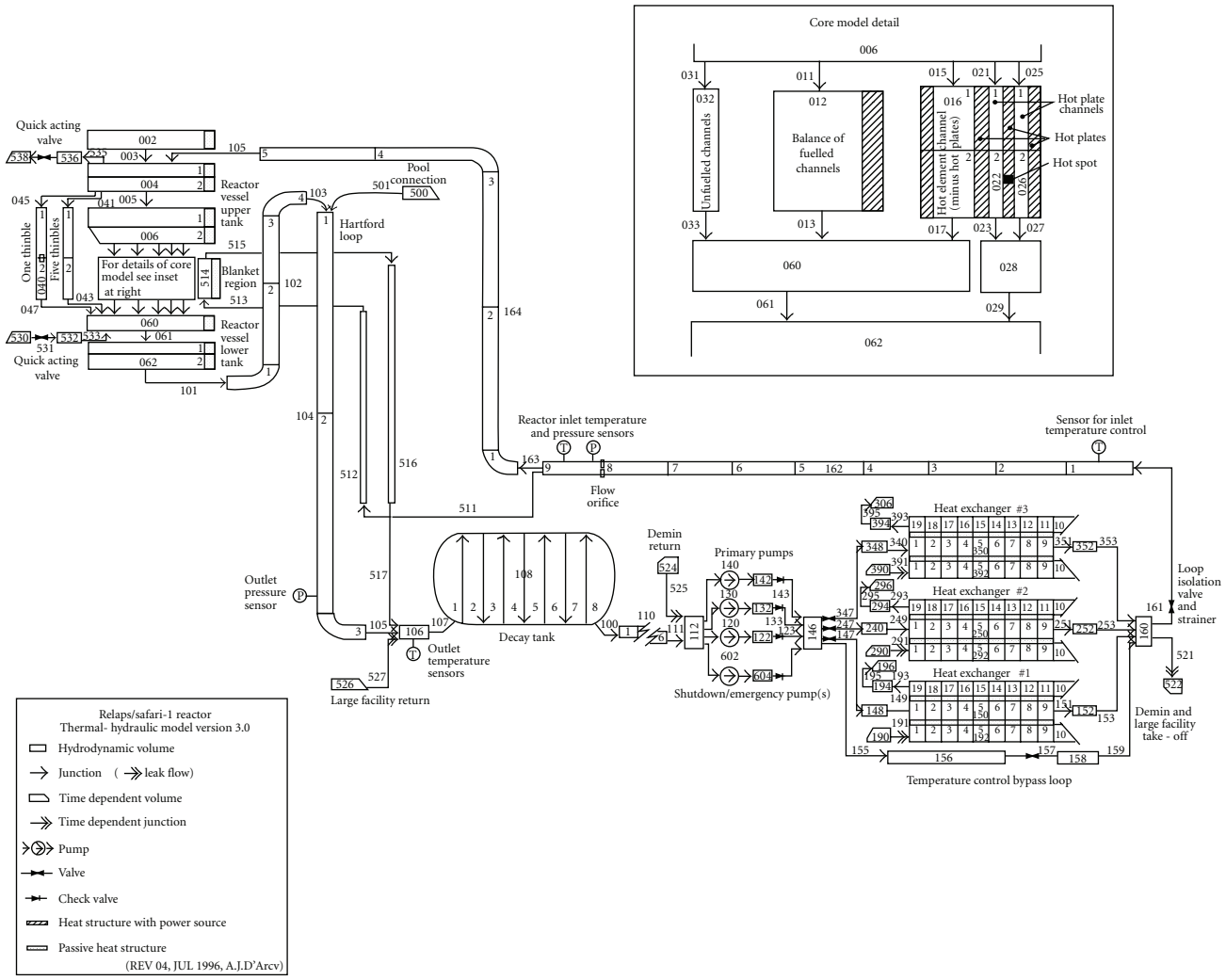

Figure 5: RELAP/SCDAPSIM nodalization of the SAFARI cooling system.

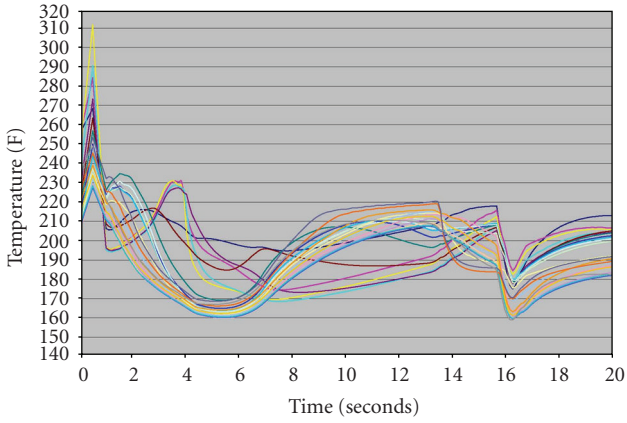

Figure 6: Example of RELAP/SCDAPSIM-calculated fuel plate centerline temperatures for the 24 fuel plates in MURR for a cold leg large break transient.

results of the analyses of postulated LOCAs in the Beznau (KKB) PWR, occurring during hot (HS) and intermediate (IS) shutdown with emphasis on large break LOCAs during hot shutdown. The large break LOCA during HS posed the greatest challenge to the plant safety systems. The analysis of the station blackout transient in the Gösgen Nuclear Plant focused on the impact of a potential failure of the depressurization system. In particular, the analysis focused on the timing of the heatup and failure of the RCS piping relative to the relocation of melt into the lower plenum and failure of the lower head. MELCOR, RELAP/SCDAPSIM, and SCDAP/RELAP5 were also used in both Beznau and Gösgen analyses.

The TMI-2 RELAP/SCDAPSIM and SCDAP/RELAP5 nodalization, as shown in Figure 7, used a 2-dimensional representation of the core region with a detailed SCDAP components being used to describe the behavior of the fuel rods and other core structures within each of the five representative flow channels in the core. The transition from the initial intact core geometry to a damaged state is automatically handled by the SCDAP models including the initial failure of the control rods, liquefaction and relocation of the metallic U-O-Zr fuel rod material, formation and

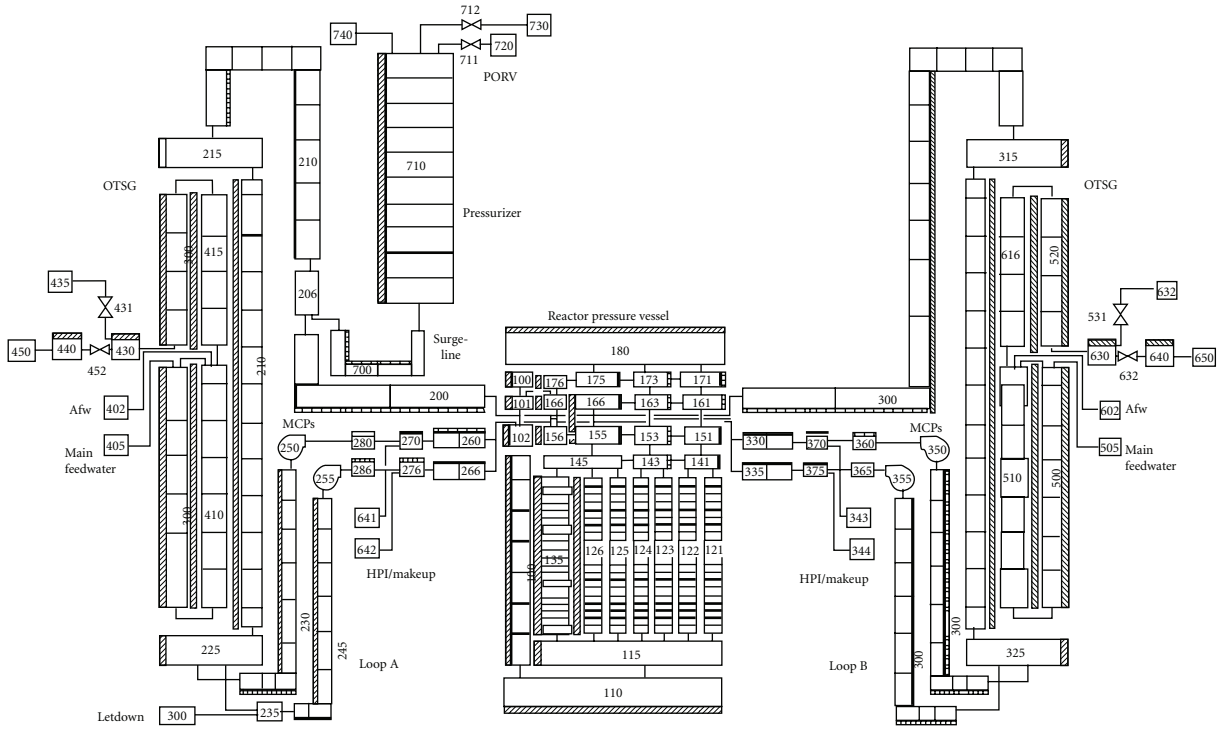

Figure 7: TMI-2 nodalization used for RELAP/SDAPSIM and SCDAP/RELAP5.

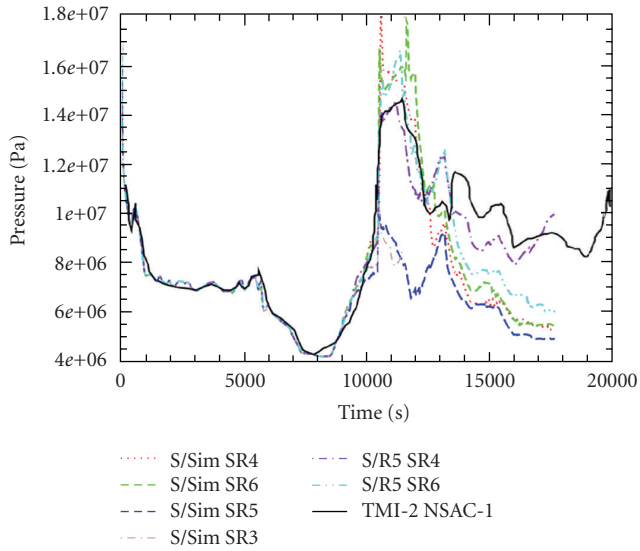

Figure 8: Example of RELAP/SDAPSIM and SCDAP/RELAP5 TMI-2-calculated results for system pressure for a range of metallic fuel rod material relocation modeling parameters.

growth of a ceramic [U-Zr]-O_2 molten pool, and relocation of the molten ceramic into the lower plenum. Figure 8 shows one of the set of representative calculations presented in the paper. The figure shows the variation in predicted system pressure for a range of modeling parameters for the relocation of the metallic U-O-Zr fuel rod material for both RELAP-based codes. It was noted in the paper that both RELAP-based codes correctly calculated an in-core molten pool, of which two RELAP/SCDAPSIM cases predicted relocation to the lower head (via the bypass, as observed), while only one MELCOR case did so. It was further noted that the RELAP-based codes correctly calculated that lower head failure did not occur.

The Beznau RELAP/SCDAPSIM and SCDAP/RELAP5 nodalization, as shown in Figure 9, also used a 2-dimensional representation of the core region with detailed SCDAP components used to describe the behavior of the fuel rods and other core structures within each of the five representative flow channels in the core. Figure 10 shows one of the set of representative calculations presented in the paper. The figure shows the peak cladding temperatures calculated by RELAP/SCDAPSIM and SCDAP/RELAP5 for different assumptions regarding the activation of the Safety Injection pumps including the number of pumps and delays in the actuation of the pumps. The paper concludes that all three codes predict that in the limiting large break case the core is readily quenched without damage, by the nominal operation of the system injection system. However, it was noted that the more mechanistic RELAP-based calculations demonstrated that a larger margin existed (relative to that predicted by MELCOR) with recovery being possible even if only one pump operates after some delay.

The RELAP/SCDAPSIM and SCDAP/RELAP5 nodalization used for the Gösgen analysis also included a detailed core nodalization as described previously. However, the calculations also looked at the effect of hot leg nature circulation using a split hot leg model as shown in Figure 11. The split channel model allows the hotter vapor to move

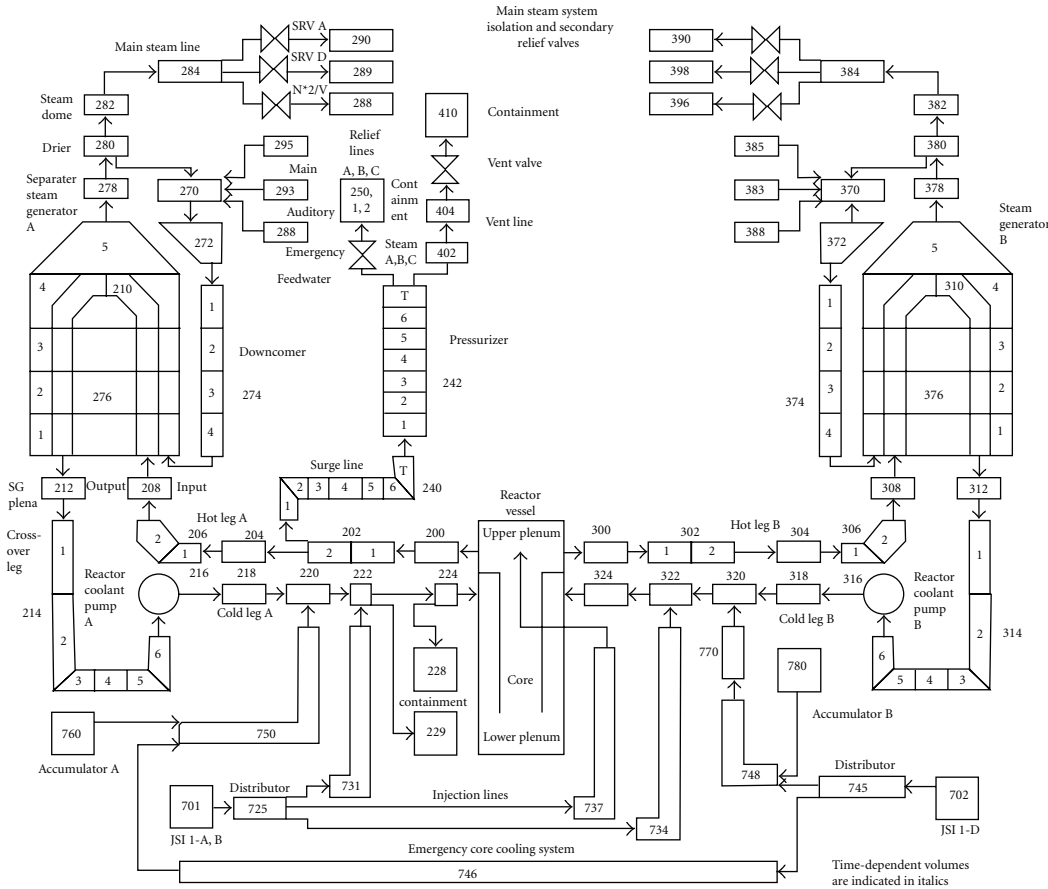

Figure 9: Beznau nodalization used for RELAP/SDAPSIM and SCDAP/RELAP5.

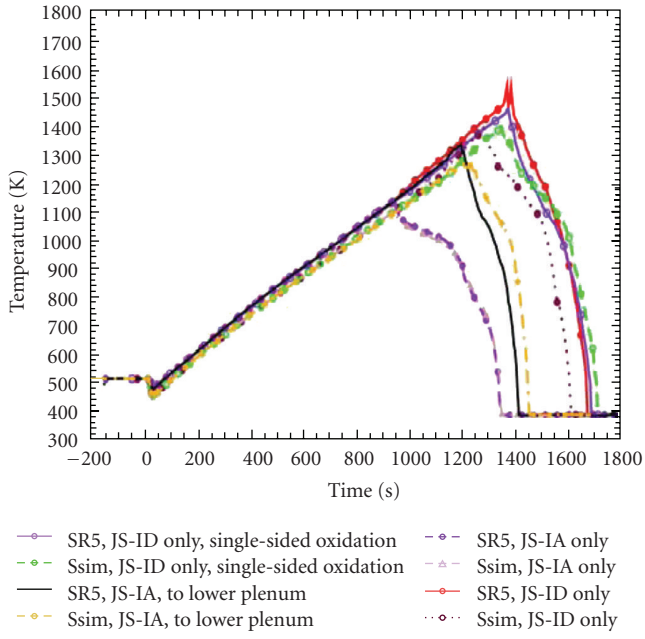

Figure 10: Example of RELAP/SCDAPSIM and SCDAP/RELAP5 Beznau-calculated results for peak cladding temperature for a range of safety injection assumptions.

from the vessel to the steam generators along the top of the hot leg and cooler vapor to return along the bottom of the hot leg. The influence of the split hot leg input model relative to a single channel hot leg (which does not allow countercurrent flow of the vapor within the hot leg) is shown in Figure 12. As shown in the figure the split hot leg model predicted a more gradual heatup of the core but both single channel and split channel models still predict rupture of the surge line or hot leg piping before any molten core material relocates into the lower head.

The Politehnica University, Institute for Nuclear Research, and National Commission for Nuclear Activities Control in Romania have used RELAP/SCDAPSIM/MOD3.4 for a variety of analyses of CANDU reactor designs. The work in [13] presents the analysis of a reactor inlet header break, looking at (a) the size of the break, (b) the choked flow model employed, (c) the emergency core cooling (ECC) performance, and (d) the core nodalization. The results were compared with the original safety analysis results. The work in [14] presents the analysis of the influence of the header manifold modeling for an inlet header break in a CANDU 6. The paper looked at a 35% inlet header break which was expected to produce the highest peak fuel cladding temperatures among all postulated break sizes. The work in [15] presents the analysis of a reactor outlet

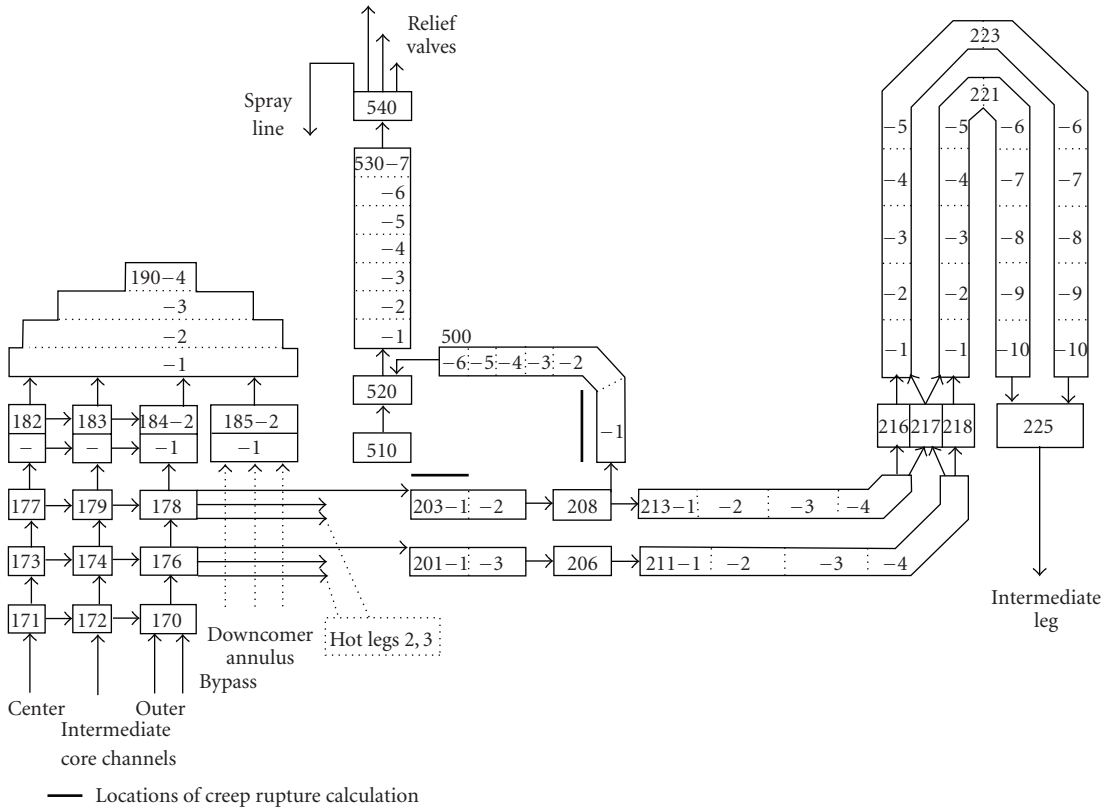

Figure 11: Gösgen split hot leg nodalization used for RELAP/SDAPSIM and SCDAP/RELAP5.

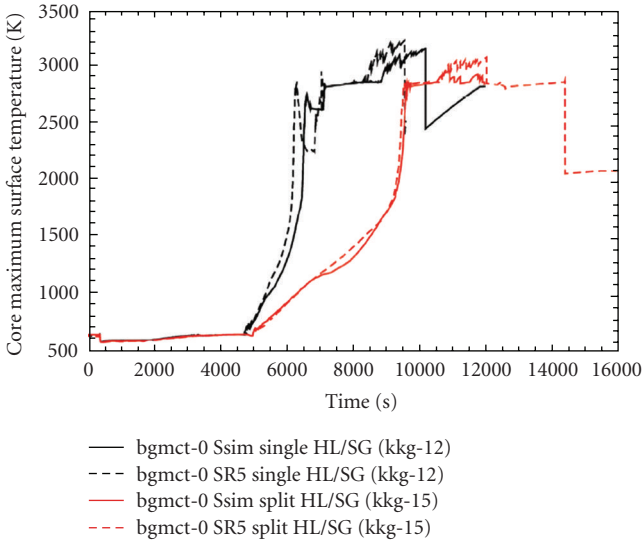

Figure 12:Example of RELAP/SCDAPSIM and RELAP/SCDAPSIM-calculated results for peak core temperature for single and split hot leg model.

header break in a CANDU-6. The paper focused on a 100% reactor outlet header break which had the highest potential for fuel failure and release of radioactivity. The paper also compared the results to earlier calculations performed using the CATHENA code [16]. The work in [17] presents an analysis of the late phase of a severe accident in CANDU 6 where bed of dry solid debris or a molten pool of core material had already formed at the bottom of the calandria vessel and was externally cooled by shield-tank water. The study used the SCDAP COUPLE module and included comparisons with earlier results performed using the ISAAC [18] and MAAP4-CANDU [19] codes.

The general system thermal hydraulic nodalization for the CANDU system thermal hydraulic analysis analyses [13–15] is shown in Figure 13. Portions of this nodalization were varied somewhat depending on the analyses being performed. Figure 14 shows an example of the portion of the nodalization that was used in [14] for the study of the influence of the inlet header model. Figure 15 shows an example of some of the results from the inlet header break model study. In the figure, the reference curve is the results from a single average channel circuit model using a single manifold volume and Cases 1, 2, and 3 represent the break location in the multiple inlet manifold volumes in combination with multiple core channels. The curves shown in the figures are the maximum cladding temperatures in fuel bundles contained within the multiple flow channels.

Figure 16 shows the basic problem analyzed for the late phase of a severe accident in a CANDU-6 where a debris bed is present in the bottom of the calandria vessel along with the RELAP5, SCDAP, and COUPLE nodalization used in the analysis. The RELAP5 thermal hydraulic volumes on

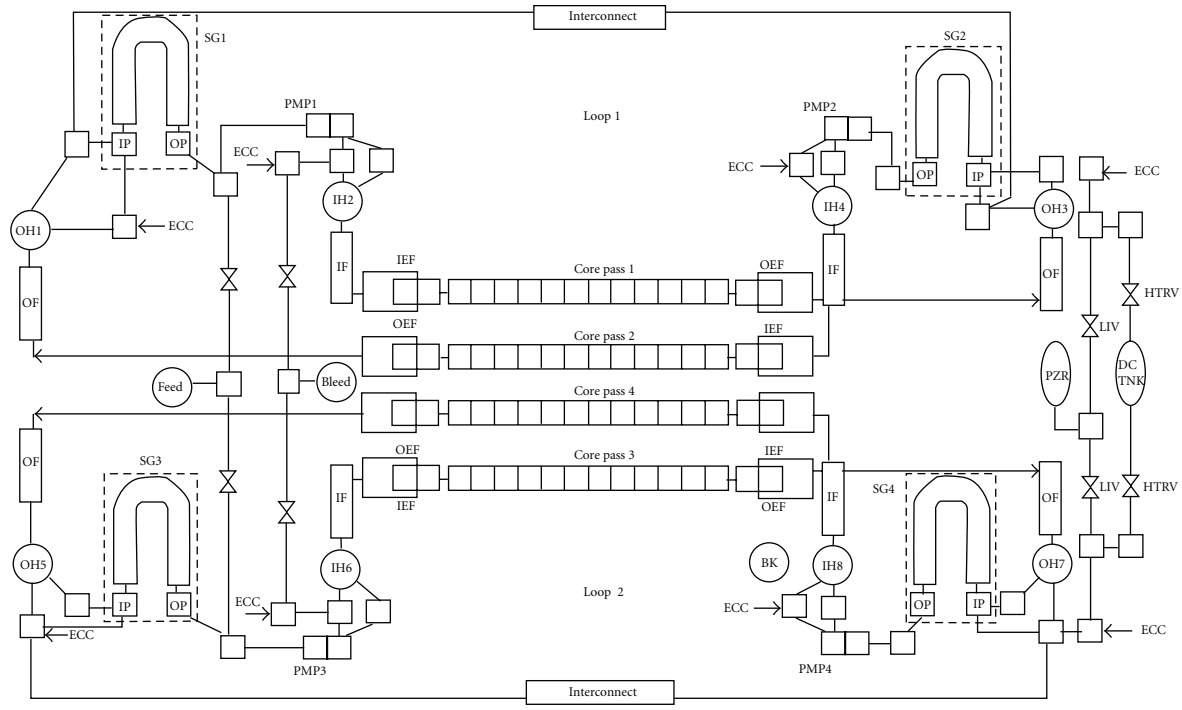

SG	Steam generator	PMP	Pump	ECC	Emergency core cooling injection point
IF	Inlet feeder	IEF	Inlet end fitting	PZR	Pressurizer
OF	Outlet feeder	OEF	Outlet end fitting	DC	Degaser - condenser
IP	SG inlet plenum	IH	Inlet header	LIV	Loop isolation valve
OP	SG outlet plenum	OH	Outlet header	HTRV	Heat transport relief valve

Figure 13: RELAP5 thermal hydraulic nodalization for CANDU-6.

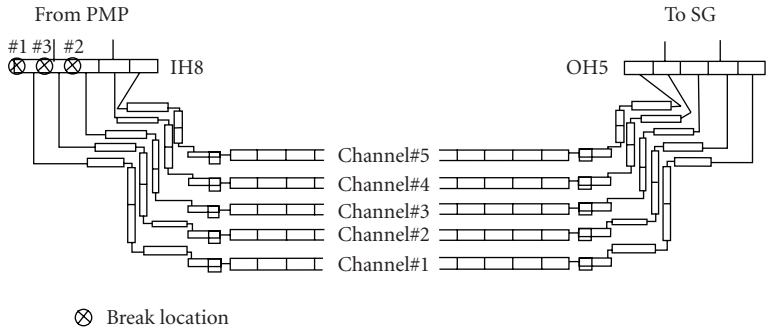

Figure 14: RELAP5 thermal hydraulic nodalization of manifold headers for CANDU-6 Inlet manifold break analysis.

the right of the figure represent the pool on the outside of the calandria vessel. The RELAP5 and SCDAP volumes above and within the COUPLE mesh provide initial and boundary conditions for the debris bed and calandria vessel wall. (The paper also included a more detailed RELAP5 nodalization of the outer pool at the elevations associated with the debris bed. The more detailed nodalization resulted in significantly lower pool containment pressures upon vessel failure due to the more accurate representation of the external cooling of the calandria vessel.)

The papers indicated that RELAP/SCDAPSIM calculations gave comparable results to the CANDU-specific codes, CATHENA for system thermal hydraulics, and ISAAC and MAAP-CANDU for severe accidents. For system thermal hydraulic analysis, RELAP/SCDAPSIM, when using similar input models, provided similar trends as compared to the original safety analysis reports or comparable CATHENA calculations. However, the results were sensitive to the level of detail used in the nodalization; specifically the more detailed nodalization possible using RELAP/SCDAPSIM had

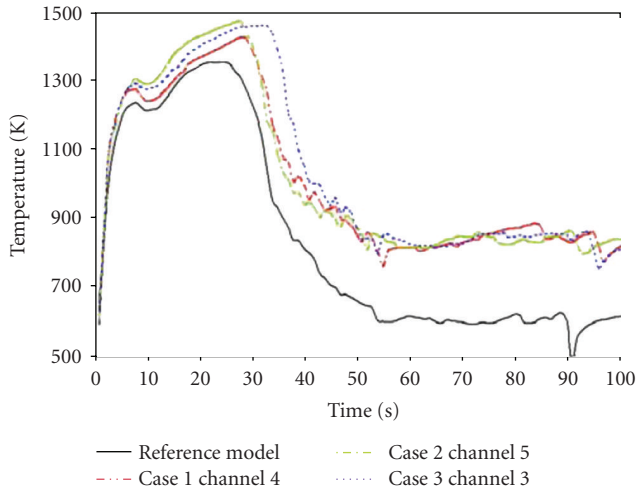

Figure 15: Maximum fuel bundle cladding temperatures for a CANDU-6 Inlet manifold break analysis for different break locations.

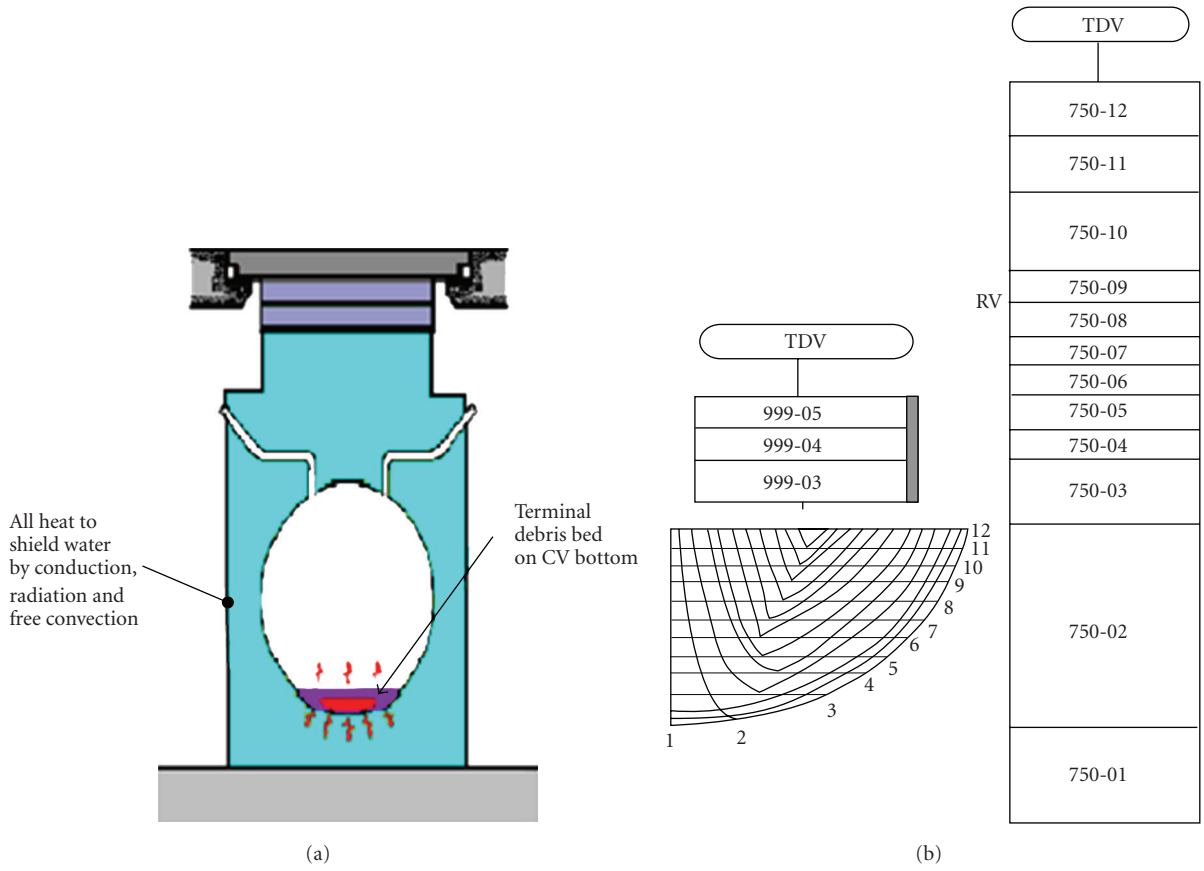

Figure 16: RELAP, SCDAP, and COUPLE module nodalization and conceptual sketch for CANDU-6 calandria vessel analysis.

a noticeable impact on the results for the inlet header manifold [14], the fuel channels (simulating the effects of horizontally stratified flow in the channels) [13], and the outer pool (exterior to the vessel calandria) [17].

RELAP/SCDAPSIM has also been used to analyze VVER reactor designs although the calculations to date have been proprietary and have not been published in the open literature. Figures 17 and 18 show a nonproprietary, but representative, input model for a VVER-1000. This representative VVER-1000 input model and associated detailed input model engineering handbook was provided by Risk Engineering in Bulgaria [20] as an in-kind contribution for use in SDTP-sponsored VVER training activities. The nodalization of the basic components of the reactor (vessel

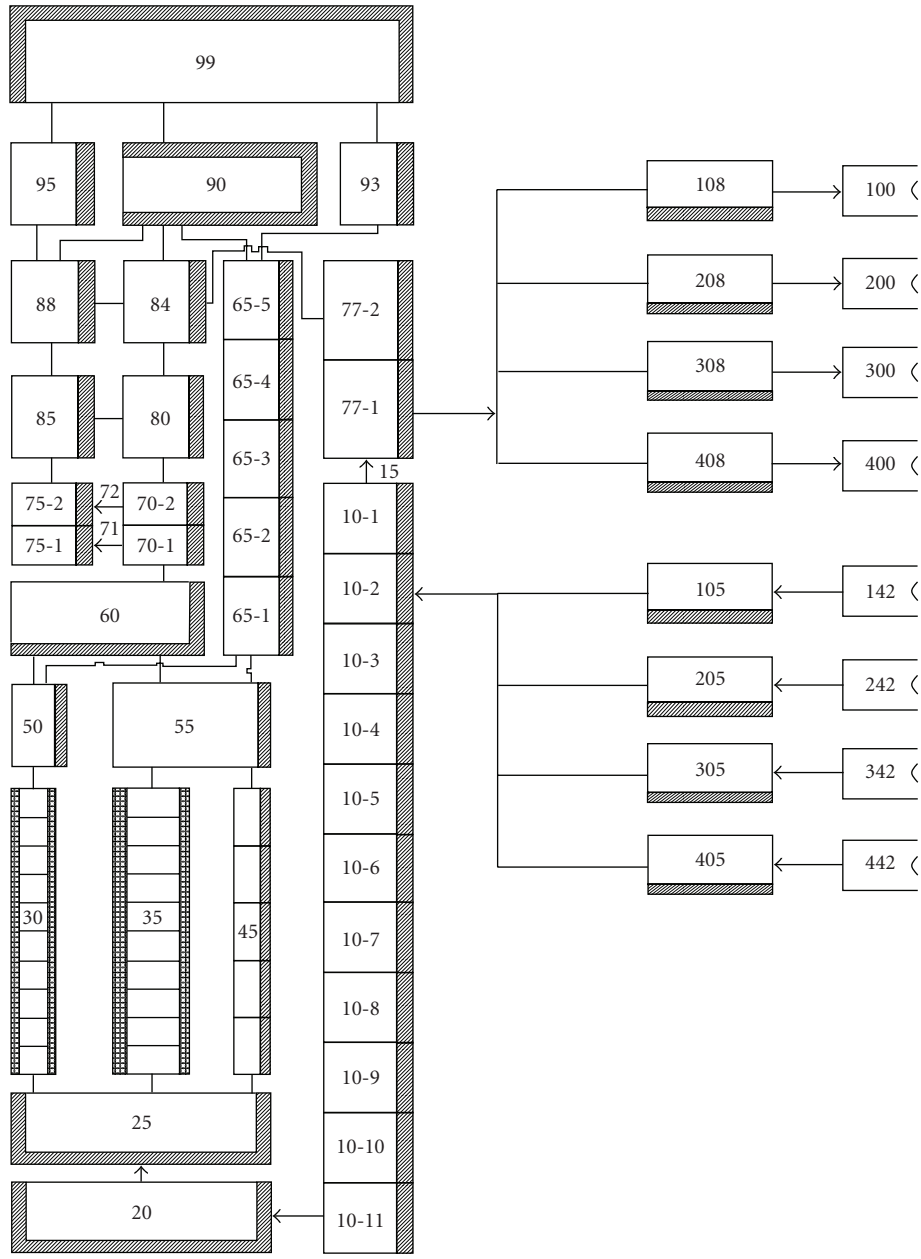

Figure 17: Representative vessel input nodalization for VVER-1000 for transients not including the possibility of loss of core geometry.

and internals) is presented in Figure 17 and includes two channels in the core, the hot and peripheral channels. This basic vessel nodalization would be replaced by a more detailed multidimensional model comparable to that used for the PWR calculations described previously for general applications where core damage transients might be considered. Four separate main circulation loops with their corresponding main coolant pumps and cold and hot circulation pipelines are also included in the representative input model as shown in Figure 17.

Analysts at the Lithuanian Energy Institute (LEI) have published a number of papers describing their use of RELAP/SCDAPSIM/MOD3.2 for the analysis of RBMKs. Recent references are cited as [21–23]. LEI also provided nonproprietary, but representative, input models and associated engineering handbooks for use in SDTP-sponsored training activities. Figure 19 shows the nodalization diagram used for the representative RBMK RCS input model.

All three versions of RELAP/SCDAPSIM have been used to analyze BWRs although few results have been published in the open literature. The work in [24] describes some of the activities related to the use of the code for plant simulation and training for the Laguna Verde plants in Mexico. Figure 20 shows a representative input model, developed by the Nacional de Seguridad Nuclear y Salvaguardias (CNSNS), the Mexican regulatory authority, for the analysis

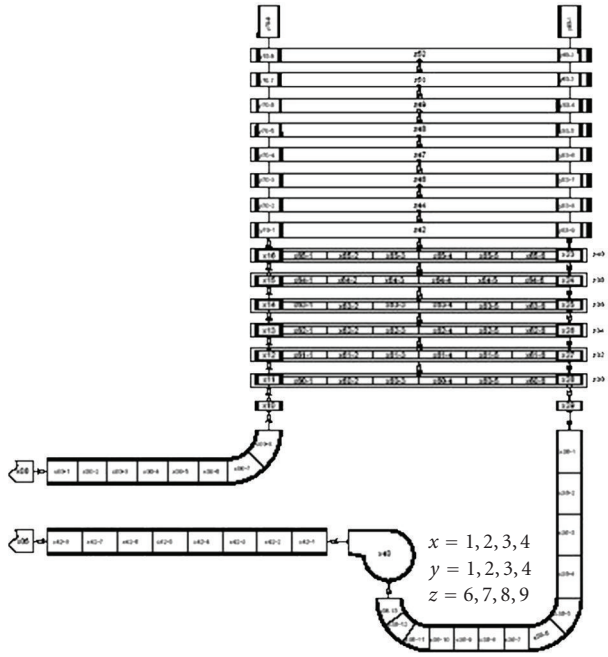

Figure 18: Representative loop input nodalization for VVER-1000.

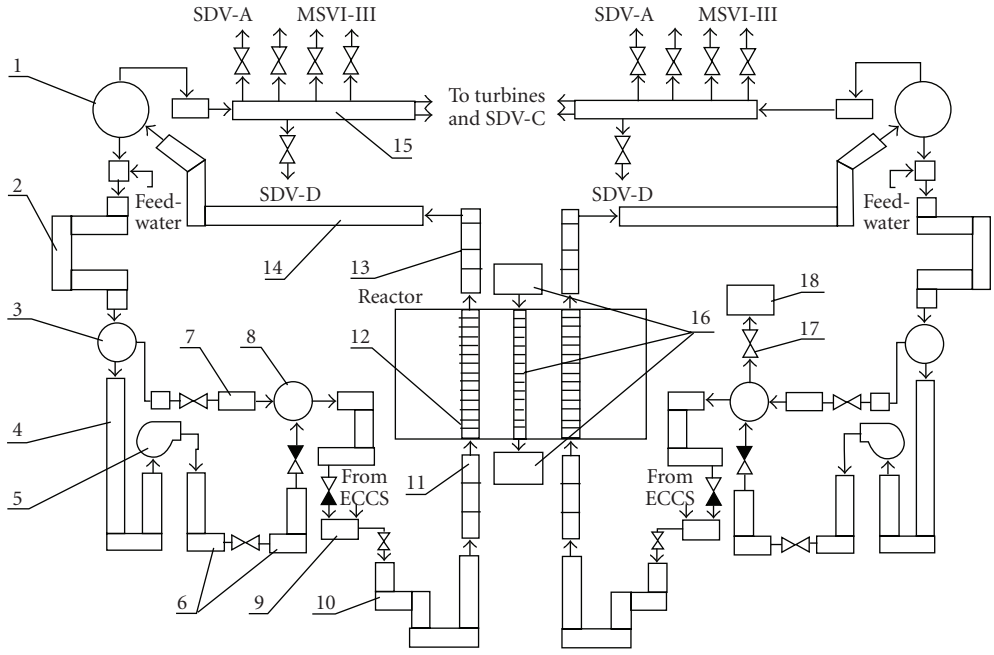

Figure 19: Representative RCS nodalization for RBMK.

of the Laguna Verde plants. This model is also used to support SDTP-sponsored BWR-specific training activities. See Section 3.4 and [24] for more information on these activities in Mexico.

3.2. Experimental Analysis. RELAP/SCDAPSIM/MOD3.4 has been used by a number of organizations to help design experiments, to assess thermal hydraulic and severe accident models, and to support advanced user training. In recent years, the application of the code to experimental analyses have focused on European experimental programs including the German Quench experiments [25–29], French Phebus FPT experiments [30–33], and most recently Russian PARAMETER experiments [34].

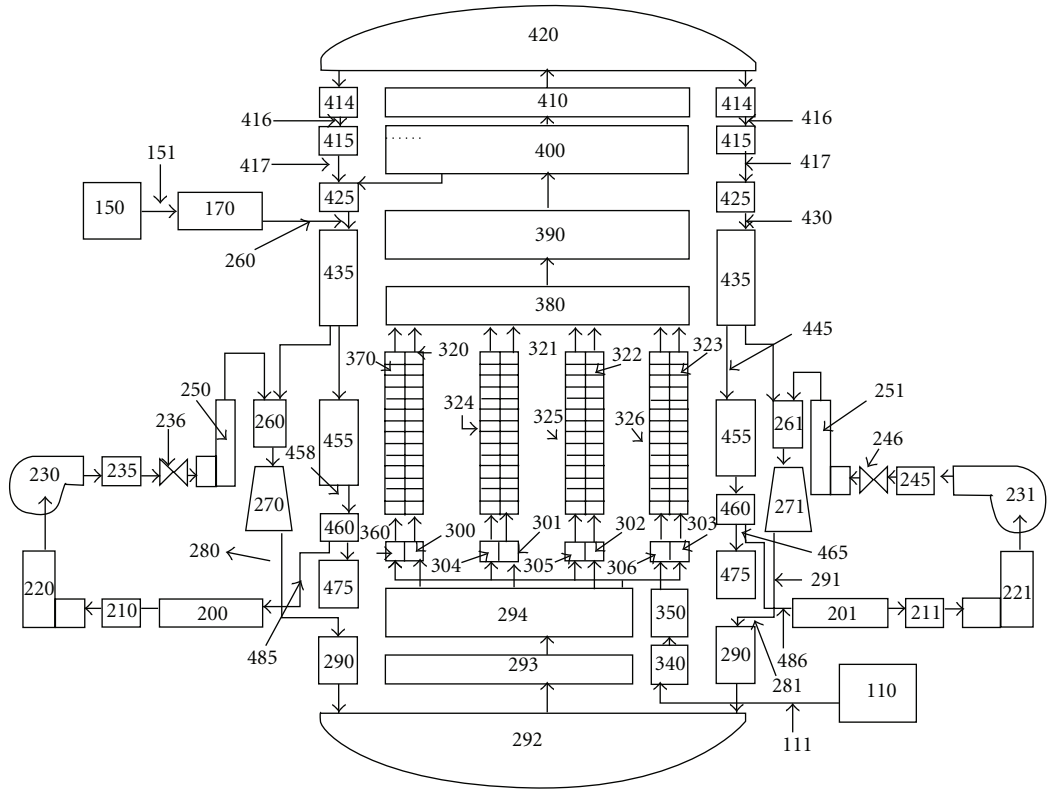

Figure 20: Representative RCS nodalization for BWRs.

The most detailed of the calculations have been involved in the design of new experiments. For example, as described in detail in [26], the design of new experiments requires the development of complex input models to describe the unique features of each experiment and in many cases the development of specialized new models to treat features of the experiments not previously included in the code. In this example, the analysts from PSI and experimentalists from Forschungszentrum Karlsruhe (FzK) describe their use of RELAP/SCDAPSIM/MOD3.4 in conjunction with MELCOR and a special FzK-developed version of SCDAP/RELAP5 [35] to design and analyze three different experiments in the quench facility, Quench-10, Quench 11, and Quench 12. Quench 10 was a unique experiment in that it was the first integral test to look at the influence of air ingression on bundle heating and reflood. The design and analysis of this experiment required PSI to develop and incorporate special SCDAP models to treat the oxidation of Zircaloy in air/steam mixtures. The experimentalist also ran special small separate effects experiments to help develop the correlations that were then used in these new models. Quench 11 was a unique test for the Quench facility in that the test started with the bundle full of water and then the heat up transient was initiated by the boil-down of the water. (Previous Quench experiments used a mixture of steam and argon during the heat up of the bundle prior to reflood.) Although, in this case, it was not necessary to modify any of the RELAP or SCDAP models, the modeling of the auxiliary heaters, added to the lower plenum of the experimental test train to provide realistic boildown rates, proved to difficult because of relatively large heat losses in the lower plenum region. QUENCH-12 was unique in that it was designed to determine the influence of a VVER bundle configuration and cladding on heat-up, oxidation, and quench response. Previous Quench experiments used PWR or BWR configurations and cladding materials. The Quench 12 bundle was significantly modified with changes to cladding material (Zr/1%Nb instead of Zry-4), electrical heating, and geometry. Oxidation correlations for Zr/1%Nb in steam were introduced into SCDAP to support the design and analysis of this experiment. Figure 21 shows a schematic of the Quench facility along with the RELAP/SCDAPSIM nodalization diagram.

The analyses of the German Quench and French Phebus experiments have also played a pivotal role in the assessment of RELAP5/SCDAPSIM, the development of new improved models as discussed in Section 3.3, and in advanced user training as discussed in Section 3.4. The works in [28, 29, 31–33] are examples of the analysis of these experiments to assess the accuracy of the code and to identify areas where the models could be improved. The works in [36, 37] describe the use of these experiments to support advanced user training.

3.3. Development of Improved Models and Analytic Capabilities. The development of improved models and analytic capabilities is also an important part of the overall SDTP cooperative activities. In addition to the modelling

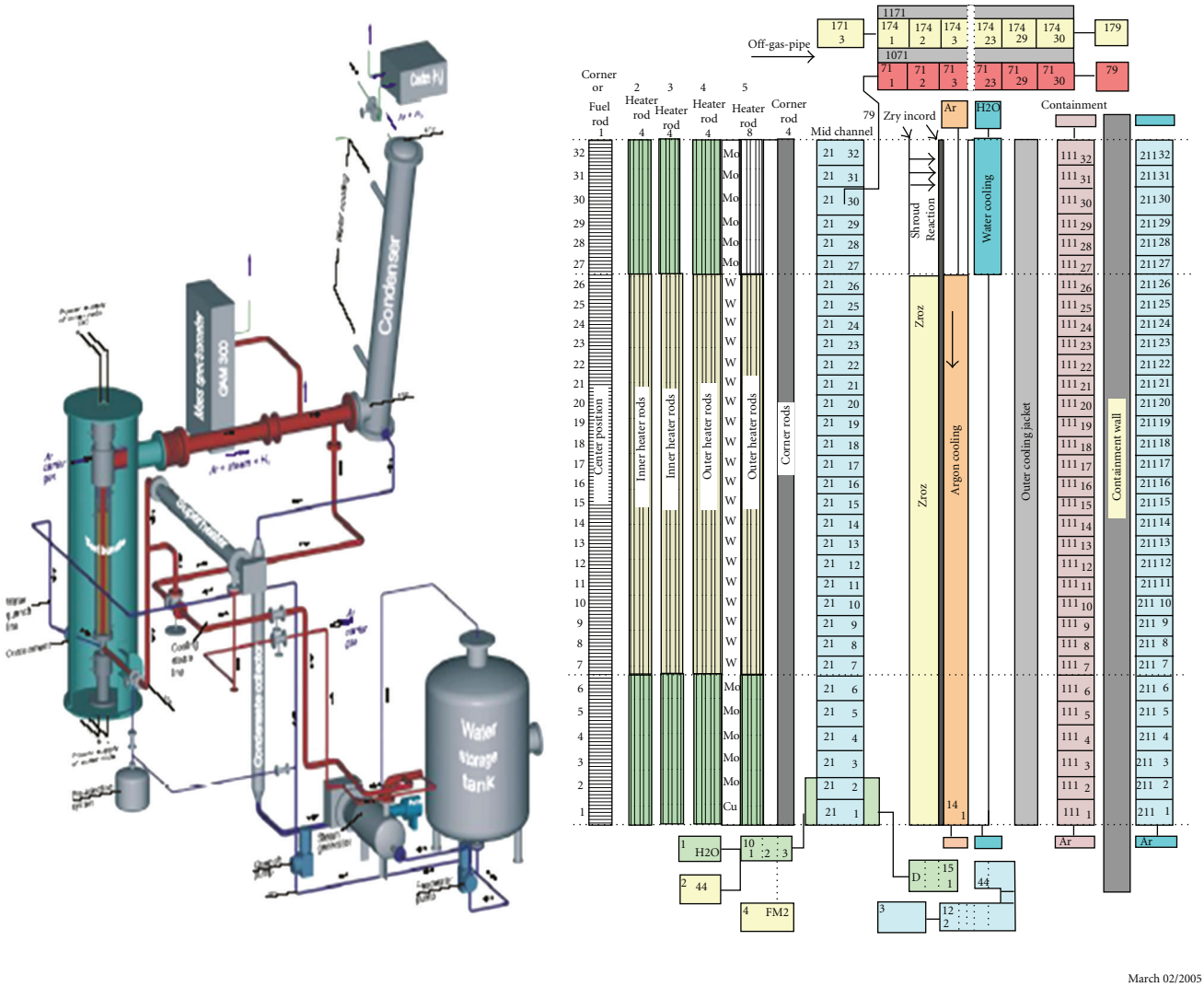

Figure 21: Example of experiment design—quench facility layout and input nodalization.

improvements driven by large-scale experimental programs in the Phebus and Quench facilities as discussed in the previous section, other model and code development activities have been driven by the needs of SDTP members and licensed software users. INSS (Institute of Nuclear Safety System), Japan, one of the original members of SDTP, developed and validated new RELAP/SCDAPSIM models to treat the heat transfer in the gap between a debris bed and the lower plenum wall [38] and improved correlations for condensation in the presence of noncondensable gases [39]. The applications of the improved correlations are described in [40]. IAE/NUPEC (Institute of Applied Energy/Nuclear Power Engineering) Japan, a long-time member of SDTP, has been working with the code to develop improved analytic capabilities to support the Japanese nuclear industry. The merger of RELAP/SCDAPSIM with the IMPACT/SAMPSON package [41] is one of the most significant projects. However, IAE/NUPEC has also been using the code for a variety of other tasks including the development of enhanced analytical capabilities to analyse corrosive conditions in nuclear power plants using coupled system thermal hydraulics and CFD techniques along with corrosion modelling [42]. CNSNS and ININ (Instituto Nacional de Investigaciones Nucleares) in Mexico have added integrated BWR containment models to RELAP/SCDAPSIM/MOD4.0 and are now working on the possible integration of detailed integrated subchannel and containment modules developed by IAE/NUPEC [43]. Nuclear plant analyser graphic packages including VISA [44], developed by KAERI (Korean Atomic Energy Research Institute), and RELSIM, developed by RMA (Risk Management Associates) have been linked to RELAP/SCDAPSIM/MOD3.4 and MOD4.0. Other activities by members and licensed users include the coupling of the code with 3D reactor kinetics packages.

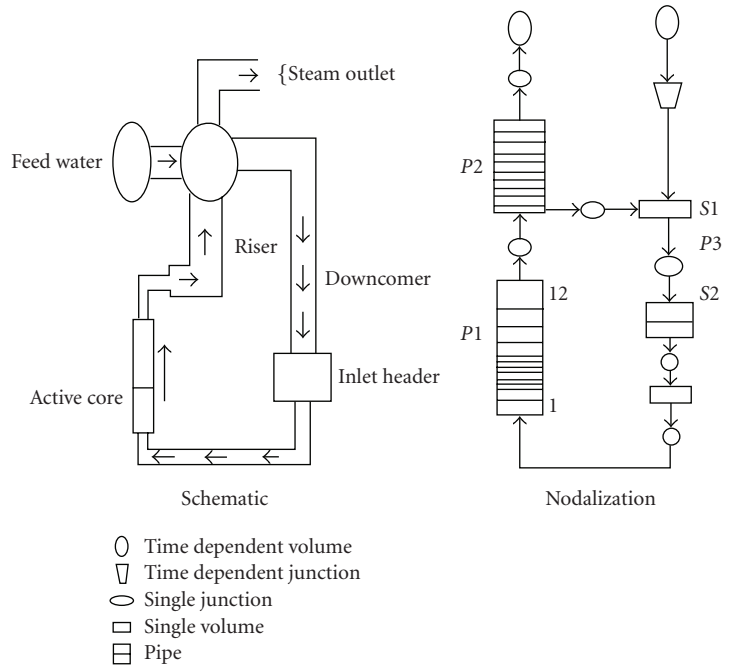

Figure 22: Example of university applications—natural circulation boiling water reactor applications by IIT-Guwahti.

The development of improved models and code capabilities for RELAP/SCDAPSIM/MOD4.0 by university members of SDTP has also been an important factor in the improvement of RELAP/SCDAPSIM/MOD4.0 [5]. The rewriting of the code to Fortran 90/95/2000 version of the code has made it significantly easier for university faculty and students to work with. MOD4.0 also provides a well-characterized framework for university researchers and students to explore new modelling approaches since the tedious programming details associated with use of complex fluid/material properties libraries, reactor component models such as pumps and valves, input/output, and data base management for tasks such as dynamic data allocation are provided through a standard compile library maintained by ISS. The incorporation of integrated fission product transport models by Honaiser, University of Florida, USA [29], and ongoing work to add an integrated uncertainty analysis package by Perez, University of Catalunya, Spain [45, 46], and CANDU-specific models for fuel channel failure by Mladin, Polectechnic University, Romania [17], are good examples where university students are key contributors to the development of the code.

3.4. Training of Analysts and Model/Code Developers. RELAP/SCDAPSIM/MOD3.4 and MOD4.0 are also widely used to support SDTP-sponsored training activities. MOD3.4 is used for basic user and applications training. This includes (a) 1- to 2-week novice and advanced RELAP5 and SCDAP user training workshops and seminars, (b) longer term, 1 to 3 month, user and application training under IAEA and SDTP-sponsored training fellowships, and (c) IAEA-sponsored specialized missions on research reactor applications, severe accident management, and others. For example, novice users will use the code to set up basic thermal hydraulic problems such as the flow of water in a pipe or the boildown and quenching of a representative fuel assembly and then move on to the optimisation or expansion of the input model to a representative full research reactor or NPP. More advanced students or participants in longer term training sessions will typically use the code to develop input models for their own facilities or more typically adapt existing input models to run more reliably or run a much wider variety of possible transients. MOD4.0 and to some extent MOD3.4 are also widely used by the SDTP member universities to support their graduate and faculty research programs. Section 3.3 gave some specific examples of university students that started out participating in SDTP-sponsored training activities using MOD3.4 and MOD4.0 and then going on to make significant contributions to improvement of MOD4.0. Another good example of the use of the codes at universities is provided by Professor Manmohan Pandey and others from the Department of Mechanical Engineering of Indian Institute of Technology Guwahati (IIT-Guwahati), India, in a report submitted as an in-kind contribution for their university membership [47].

IIT-Guwahati used RELAP/SCDAPSIM/MOD4.0 and the Nuclear Plant Analyser RELAP/SCDAPSIM-VISA package (ViSA-RS) for numerical simulations of a natural circulation boiling water reactor (NCBWR) and supercritical water cooled reactor (SCWR). Figure 22 shows the example of the NCBWR schematic and nodalization. Their applications included the following areas:

(a) parametric studies of the primary heat transport loop of NCBWR,

(b) stability analysis of NCBWR,

(c) stability analysis of SCWR,

(d) educational use of RELAP5 and VISA-RS.

Acknowledgment

The contributions of the many SDTP members and licensed users are gratefully acknowledged.

References

[1] http://www.relap.com/.

[2] http://www.sdtp.org/.

[3] RELAP5 Code Development Team, "RELAP5/MOD 3.3 Code Manual, Vol 1–8," NUREG/CR-5535/Rev1, 2001.

[4] SCDAP/RELAP5 Development Team, "SCDAP/RELAP5/MOD3.2 Code Manual, Vol. 1–5," NUREG/CR-6150, INEL-96/0422, July 1998.

[5] C. M. Allison, R. J. Wagner, L. J. Siefken, and J. K. Hohorst, "The development of RELAP5/SCDAPSIM/MOD4.0 for reactor system analysis and simulation," in *Proceedings of the 7th International Conference on Nuclear Option in Countries with Small and Medium Electricity Grids*, Dubrovnik, Croatia, May 2008.

[6] A. R. Antariksawan, Md. Q. Huda, T. Liu, J. Zmitkova, C. M. Allison, and J. K. Hohorst, "Validation of RELAP/SCDAPSIM/MOD3.4 for research reactor applications," in *Proceedings of the 13th International Conference on Nuclear Engineering (ICONE '05)*, Beijing, China, May 2005.

[7] A. Sekhri, A. L. Graham, M. Belal, L. E. Moloko, and A. J. D'Arcy, "Thermal hydraulic and safety analyses of a proposed HEU & LEU core for SAFARI-1 research reactor," in *Proceedings of the 12th International Topical Meeting on Research Reactor Fuel Management (RRFM '08)*, Hamburg, Germany, 2008.

[8] A. Sekhri, A. J. D'Arcy, A. L. Graham, and M. Oliver, "Thermal-hydraulic modelling of the SAFARI-1 research reactor using RELAP/SCDAPSIM/MOD3.4," in *Proceedings of the International Conference on the Physics of Reactors*, Interlaken, Switzerland, September, 2008.

[9] R. C. Nelson, J. C. McKibben, K. Kutikkad, and L. P. Foyto, "Thermal-hydraulic transient analysis of the Missouri University Research Reactor (MURR)," in *Proceedings of the Annual Meeting of Test, Research and Training Reactors (TRTR '07)*, September 2007.

[10] T. Haste, J. Birchley, E. Cazzoli, and J. Vitazkova, "Analysis of TMI-2 with MELCOR and SCDAPSIM," in *Proceedings of the International Congress on Advances in Nuclear Power Plants (ICAPP '05)*, vol. 2, pp. 984–993, Seoul, South Korea, May 2005.

[11] T. Haste, J. Birchley, and M. Richner, "MELCOR and SCDAP analyses of loss-of-coolant accidents during cooldown in a Westinghouse 2-loop PWR," in *Proceedings of the International Conference, Nuclear Energy for New Europe*, Portorož, Slovenia, September 2007.

[12] T. Haste, J. Birchley, and J.-U. Klügel, "Analysis of station blackout in the Gösgen nuclear plant," in *Proceedings of the International Conference on Advances in Nuclear Power Plants (ICAPP '08)*, vol. 2, pp. 1086–1094, Anaheim, Calif, USA, June 2008.

[13] I. Prisecaru, D. Dupleac, P. Ghitescu, and L. Biro, "A parametric study of a large break in reactor inlet header of CANDU6 reactors using RELAP5 code," in *Proceedings of the International Congress on Advances in Nuclear Power Plants (ICAPP '06)*, pp. 1116–1125, Reno, Nev, USA, June 2006.

[14] D. Dupleac, I. Prisecaru, M. Mladin, G. Negut, and P. Ghitescu, "Investigation on header manifold model effect at CANDU6 large loss of cooling accident," in *Proceedings of the 16th International Conference on Nuclear Engineering (ICONE '08)*, vol. 4, pp. 673–679, Orlando, Fla, USA, May 2008.

[15] D. Dupleac, I. Prisecaru, P. Ghitescu, and G. Negut, "Thermal-hydraulic analysis of CANDU 6 100% reactor outlet header break using RELAP5 code," in *Proceedings of the International Congress on Advances in Nuclear Power Plants (ICAPP '07)*, vol. 1, pp. 246–255, Nice, France, May 2007.

[16] B. N. Hanna, N. U. Aydemir, D. K. Baxter, et al., "CATHENA Theoretical Manual: MOD-3.5/Rev. 0," AECL RC-982-31, 1994.

[17] D. Dupleac, I. Prisecaru, M. Mladin, and G. Negut, "SCDAP/RELAP5 investigation on coolability of severely degraded CANDU 6 Core—preliminary results," in *Proceedings of the International Conference on Advances in Nuclear Power Plants (ICAPP '08)*, vol. 2, pp. 1095–1101, Anaheim, Calif, USA, June 2008.

[18] S.-Y. Park, Y.-H. Jin, and Y.-M. Song, "An investigation of an in-vessel corium retention strategy for the Wolsong pressurized heavy water reactor plants," *Nuclear Technology*, vol. 158, no. 1, pp. 109–115, 2007.

[19] S. M. Petoukhov, B. Awadh, and P. M. Mathew, "CANDU 6 severe core damage accident consequence analysis for steam generator tube rupture scenario using MAAP4-CANDU V4.0.5A: preliminary results," in *Proceedings of the International Congress on Advances in Nuclear Power Plants (ICAPP '06)*, pp. 1404–1414, Reno, Nev, USA, June 2006.

[20] E. Borisov, *Personal Communication*, Risk Engineering, Ltd, Sofia, Bulgaria, 2008.

[21] E. Uškuras, A. Kaliatka, J. Augutis, S. Rimkevičius, E. Urbonavičius, and V. Kopustinskas, "Safety analysis of beyond design basis accidents in RBMK-1500 reactors," *Annals of Nuclear Energy*, vol. 34, no. 5, pp. 356–373, 2007.

[22] E. Uspuras and A. Kaliatka, "Development of RBMK-1500 model for BDBA analysis using RELAP/SCDAPSIM code," *Journal of Power and Energy*, vol. 2, 2008.

[23] E. Urbonavicius, E. Uspuras, S. Rimkevicius, and A. Kaliatka, "Application of RELAP/SCOAPSIM and COCOSYS codes for severe accident analysis in RBMK-1500 reactor," in *Proceedings of the International Congress on Advances in Nuclear Power Plants (ICAPP '06)*, pp. 1442–1450, Reno, Nev, USA, June 2006.

[24] C. Chavez-Mercado, J. K. Hohorst, and C. M. Allison, "National Autonomous University of Mexico RELAP/SCDAPSIM-based plant simulation and training applications to the Laguna Verde NPP," in *Proceedings of the 6th International Conference on Nuclear Thermal Hydraulics, Operations and Safety (NUTHOS '04)*, Nara, Japan, October 2004.

[25] http://hikwww2.fzk.de/quench.

[26] J. Birchley, T. Haste, W. Hering, and Ch. Homann, "Pre-test analytical support for experiments Quench-10, -11, and -12," in *Proceedings of the International Conference, Nuclear Energy for New Europe*, Portorož, Slovenia, September 2007.

[27] T. Haste, J. Birchley, J.-S. Lamy, et al., "Pre-test calculational support for the QUENCH-13 experiment," in *Proceedings of the International Conference on Advances in Nuclear Power Plants (ICAPP '08)*, vol. 2, pp. 1182–1190, Anaheim, Calif, USA, June 2008.

[28] S. Šadek, N. Debrecin, and S. Špalj, "QUENCH-11 experiment analysis with RELAP5/SCDAPSIM code," in *Proceedings of the 7th International Conference on Nuclear Option in Countries*

with Small and Medium Electricity Grids, Dubrovnik, Croatia, May 2008.

[29] E. Honaiser and S. Anghaie, "Analysis of RELAP/SCDAPSIM/MOD3.2 computer code using QUENCH experiments," in *Proceedings of the International Congress on Advances in Nuclear Power Plants (ICAPP '04)*, pp. 1420–1425, Pittsburgh, Pa, USA, June 2004.

[30] http://phebus.jrc.nl.

[31] J. K. Hohorst and C. M. Allison, "An assessment of RELAP/SCDAPSIM/MOD3.4 using the phebus FPT-2 bundle heating and melting experiment," in *Proceedings of the International Congress on Advances in Nuclear Power Plants (ICAPP '05)*, vol. 6, pp. 3284–3293, Seoul, South Korea, May 2005.

[32] C. M. Allison and J. K. Hohorst, "An assessment of RELAP/SCDAPSIM/MOD3.2 using bundle heating and melting experiments with irradiated fuel," in *Proceedings of the 11th IEEE International Conference on Networks (ICONE '03)*, Tokyo, Japan, April 2003.

[33] E. Honaiser, "Performance of RELAP/SCDAPSIM code on fission products transport prediction," in *Proceedings of the International Congress on Advances in Nuclear Power Plants (ICAPP '06)*, pp. 1451–1458, Reno, Nev, USA, June 2006.

[34] http://www.istc.ru/istc/sc.nsf/html/projects.htm?open&id=3690.

[35] W. Hering and Ch. Homann, "Improvement of the SCDAP/RELAP5 code with respect to FZK experimental facilities," FZKA Report 6566, Forschungszentrum Karlsruhe in der Helmholtz-Gemeinschaft, June 2007.

[36] J. K. Hohorst and C. M. Allison, "Lessons learned from ISP-46 using RELAP/SCDAPSIM," in *Proceedings of the International Congress on Advances in Nuclear Power Plants (ICAPP '03)*, Córdoba, Spain, May 2003.

[37] J. K. Hohorst and C. M. Allison, "Lessons learned from the Quench-11 training exercise," in *Proceedings of the International Congress on Advances in Nuclear Power Plants (ICAPP '07)*, vol. 3, pp. 1505–1515, Nice, France, May 2007.

[38] T. Kohriyama, M. Murase, T. Nagae, Y. Okano, and A. Ezzidi, "Validation of heat transfer models in narrow gap for RELAP/SCDAPSIM/MOD3.2," *Nuclear Technology*, vol. 147, no. 2, pp. 191–201, 2004.

[39] T. Nagae, M. Murase, T. Chikusa, K. Vierow, and T. Wu, "Reflux condensation heat transfer of steam-air mixture under turbulent flow conditions in a vertical tube," *Journal of Nuclear Science and Technology*, vol. 44, no. 2, pp. 171–182, 2007.

[40] T. Nagae, T. Chikusa, M. Murase, and N. Minami, "Analysis of noncondensable gas recirculation flow in steam generator U-tubes during reflux condensation using RELAP5," *Journal of Nuclear Science and Technology*, vol. 44, no. 11, pp. 1395–1406, 2007.

[41] C. M. Allison, J. K. Hohorst, and M. Naitoh, "Developing and validating severe accident management guidelines using SAMPSON-RELAP/SCDAPIM/MOD3.4," in *Proceedings of the 13th International Conference on Nuclear Engineering (ICONE '05)*, Beijing, China, May 2005.

[42] M. Naitoh, "Evaluation of flow accelerated corrosion by coupled analysis of corrosion and flow dynamics," in *Proceedings of the IAEA Topical Meeting on Advanced Safety Assessment Methods for Nuclear Reactors*, Daejeon, South Korea, October 2007.

[43] Personal communication.

[44] K. D. Kim, S. W. Lee, and C. M. Allison, "Development of visual system analyzer based on the best-estimate code RELAP/SCDAPSIM," in *Proceedings of the 13th International Conference on Nuclear Engineering (ICONE '05)*, Beijing, China, May 2005.

[45] M. Perez, F. Reventos, R. Wagner, and C. M. Allison, "Integrated uncertainty analysis using RELAP/SCDAPSIM/MOD4.0," in *Proceedings of the 7th International Topical Meeting on Nuclear Reactor Thermal Hydraulics, Operation and Safety (NUTHOS '08)*, Seoul, South Korea, October 2008.

[46] F. Reventos, M. Perez, L. Batet, and R. Perca, "Simulation of a LB-LOCA in Zion nuclear power plant," BEMUSE Phase IV Draft Report.

[47] M. Pandey, S. P. Lakshmanan, G. V. Durga Prasad, G. Gopa Kishor, and C. Naveen Kumar, "Numerical simulations using RELAP5 with ViSA-RS," SDTP in-Kind Report, Department of Mechanical Engineering, Indian Institute of Technology Guwahati, Guwahati, India, May 2007.

Hindawi Publishing Corporation
Science and Technology of Nuclear Installations
Volume 2010, Article ID 102078, 11 pages
doi:10.1155/2010/102078

Research Article

State of the Art of the Ignalina RBMK-1500 Safety

E. Uškuras

Laboratory of Nuclear Installation Safety, Lithuanian Energy Institute, Breslaujos street 3, LT-44403 Kaunas, Lithuania

Correspondence should be addressed to E. Uškuras, uspuras@mail.lei.lt

Received 29 April 2009; Accepted 26 October 2009

Academic Editor: Alessandro Petruzzi

Ignalina NPP is the only nuclear power plant in Lithuania consisting of two units, commissioned in 1983 and 1987. Unit 1 of Ignalina NPP was shut down for decommissioning at the end of 2004 and Unit 2 is to be operated until the end of 2009. Both units are equipped with channel-type graphite-moderated boiling water reactors RBMK-1500. The paper summarizing the results of deterministic and probabilistic analyses is developed within 1991–2007 by specialists from Lithuanian Energy Institute. The main operational safety aspects, including analyses performed according the Ignalina Safety Improvement Programs, development and installation of the Second Shutdown System and Guidelines on Severe Accidents Management are discussed. Also the phenomena related to the closure of the gap between fuel channel and graphite bricks, multiple fuel channel tube rupture, and containment issues as well as implication of the external events to the Ignalina NPP safety are discussed separately.

1. Introduction: Historical Context

Preparatory works of construction of the Ignalina NPP have been started in 1974, and the first unit of Ignalina NPP was commissioned in December 31, 1983. At the same time the second unit was under construction and construction of the third unit began. The second unit was planned to start to operate in 1986, but because of accident in Chernobyl, works on preparation to operate this unit have been rescheduled. Second unit was commissioned in August 31, 1987. At that time 60% of the third unit have already been constructed, but later construction was suspended and terminated soon. Nowadays because of political reasons, the first unit of Ignalina NPP is shut down; the second unit is planned to shutdown at the end of 2009.

Ignalina NPP with RBMK-1500 reactors belongs to the second generation of RBMK-type reactors (it means that this is most advanced version of RBMK reactor design series in comparison with other RBMK-type nuclear power plants). In comparison with infamous Chernobyl NPP, Ignalina NPP reactors are by a third more powerfully and already from the beginning of operation substantially advanced emergency protection systems (e.g., emergency core cooling and accident localization systems) [1].

After 1990 Lithuania declared its independence; Ignalina NPP with two largest in the world RBMK-1500 reactors came under authority of the Lithuania Republic; however, nobody in the world did not know about the real safety level of these reactors. The first Safety Justification of Ignalina NPP has been prepared by Russian experts of Research and Design Institute for Power Engineering (RDIPE), organization—designer and developer of RBMK reactors, after Chernobyl NPP accident. In this document the analysis of all design basis accidents (except partial breaks of pipes) is presented in sufficient details. The analysis is performed using at that time existing tool—quasistationary derivative approximation method, being based on conservative assumptions and existing experimental data. From the present-day viewpoint such safety justification [2] has lacks.

(i) It was limited only to the systems description and the analysis of design basis accidents.

(ii) Computer codes, developed in Russia, have been used for simulations, but these codes have not been extensively verified and validated.

(iii) The independent expertise of safety analysis has not been performed.

Therefore, at the beginning of the 90s of the last century there were reasonably doubts how such safety justification of Ignalina NPP, presented in the first safety justification, corresponded to the real situation. In 1992 at G7 Munich Summit the decision of closing Soviet-design nuclear power plants, at first of all the nuclear power plants with RBMK and VVER-440/230 reactor types, was accepted. In 1994 Lithuania signed the agreement with the European Bank for Reconstruction and Development (EBRD) Account of Nuclear Safety by which it had undertaken to perform in-depth safety analysis of the Ignalina NPP and not to change fuel channels in the reactor.

Right from the start, when Lithuania assumed control of the Ignalina NPP, the plant, its design, and operational data have been completely open and accessible to Western experts. A large number of international and local studies have been conducted to verify the operational characteristics of the Ignalina NPP and analyze its level of risk. Ignalina NPP is unique nuclear power plant of RBMK type about which information was collected, checked, systematized, and made accessible. Collected and verified database has allowed

(i) to assess present safety level of NPP,

(ii) to compare its level with other RBMK-type NPPs safety level,

(iii) to plan improvements of plant equipment and operating procedures increasing safety of the NPP.

Below, the results of the State of the Art deterministic and probabilistic safety analyses for Ignalina NPP, developed within 1991–2007 by specialists from Lithuanian Energy Institute, are discussed.

2. Deterministic and Probabilistic Ignalina NPP Safety Analyses

In this Section the main Ignalina NPP safety analyses, performed since 1991 till these days, are discussed:

(i) Ignalina NPP Units 1 and 2 safety analysis reports and their review,

(ii) modifications of activation algorithms for reactor shutdown and emergency core cooling systems,

(iii) second diverse reactor shutdown system development, safety justification, and implementation,

(iv) studies of Ignalina NPP 1 and 2 levels of Probabilistic Safety Assessment (PSA),

(v) external events at Ignalina NPP Analysis.

2.1. Deterministic Ignalina NPP Safety Justification. In 1995-1996 was prepared In-depth Ignalina NPP Unit 1 Safety Analysis Report, using USA and Western Europe methodology and computer codes for providing safety analysis [3]. It was comprehensive international study sponsored by EBRD. The purpose of this international study was to provide a comprehensive overview of plant status with special emphasis placed on its safety aspects. Specialists from the Ignalina NPP, Russia (RDIPE), Canada, and Sweden contributed. During implementation of the project, they have been described more than 50 systems of normal operation, safety important systems, and auxiliary systems. Also analysis of these systems has been performed, considering compliance of these systems to the Lithuanian standards and rules as well to practice of safety used in the West. Analyzing systems, the attention has been concentrated on their consistency to criterion of single failure, as well as to auxiliary safety aspects: maintenance, inspections, and impact of external factors (fire, flooding by water). This analysis of systems has defined the main lacks of systems and has developed conditions for elimination of the deficiencies. The performed review on operation and safety has allowed to identify all possible malfunctions, which can potentially cause an emergency situation.

In the safety analysis report of the Ignalina NPP Unit 1, the comprehensive accident analysis and equipment assessment have been provided; discussed questions concerning equipment ageing, investigated topics related to operators action, and power plant control provided conclusions about safety of Ignalina NPP (NPP safety level was assessed realistically); main lacks have been defined and measures for elimination of the deficiencies have been foreseen. It is the first western-type report on safety for nuclear power plants with RBMK reactors.

One of the basic conclusions in this safety analysis report was such that in this case there was no problem, which would demand immediate shutdown of the Ignalina NPP. Detailed accident analysis (accidents because of different pipelines ruptures, reactivity initiating accidents, equipment failures, transients with additional failure of reactor shutdown system, and fuel channel ruptures in the reactor cavity) has shown that accident occurring because of equipment failures does not cause such condition of the plant station which would cause violation of acceptance criteria; safety system ensures a safe condition of the plant even doing the assumption that operator does not take any action for 10 minutes from the beginning of accident to mitigate an emergency situation. Because of reactivity initiating accidents (exactly such type of initiating event became the reason of accident in the Chernobyl NPP), acceptance criteria of power plant also are not violated, even postulating single failures additionally. It has been shown that Ignalina NPP is reliably protected against loss of the coolant accidents if ruptures of pipelines do not cause local stagnation of flow. In case of one steam line rupture, the acceptance criteria will not be exceeded. But there are two steam lines located in the shaft at the Ignalina NPP; thus, rupture of one steam line can cause rupture of other steam lines, and in this case radiological dozes can be exceeded. Being based on these results of accident analysis, the recommendations for modifications of activation algorithms for reactor shutdown and emergency core cooling systems have been prepared.

It is necessary to note that in parallel with the Ignalina NPP Unit 1 safety analysis report in 1995–1997 it was performed independent Review of the Ignalina Nuclear Power Plant Safety Analysis Report [4]. This study was performed by experts from USA, Great Britain, France,

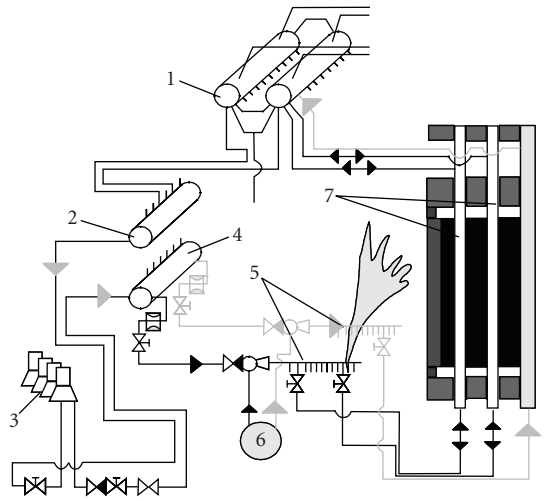

Figure 1: Ignalina NPP reactor cooling circuit (one loop) and coolant flow diagram in case of partial GDH rupture: (1) drum-separators, (2) suction header, (3) main circulation pumps, (4) pressure header, (5) group distribution headers, (6) water supply from emergency core cooling system, and (7) affected fuel channels

Germany, Italy, Russia, and Lithuania. Independent Review has confirmed the main conclusions of safety analysis report.

In recommendations of Ignalina NPP Unit 1 safety analysis report, it has been shown that Ignalina NPP will be reliably protected from any ruptures of pipelines and steam lines after improving of activation algorithms for reactor shutdown and emergency core cooling systems. According to these algorithms the system will automatically activate on coolant flow rate decrease in single Group Distribution Header (GDH) and sharp pressure decrease in drum-separators. These modifications have been implemented in both Ignalina NPP units. Safety justification of these modifications has been performed in Lithuanian Energy Institute (LEI). Further discussed situation, when conditions for local flow stagnation because of GDH rupture in the fuel channels connected to this affected GDH, is developed [5]. The flow stagnation occurs in the case of the certain size break in GDH. Due to discharge of a part of the coolant through this break, the zero gradient of pressure is developed in fuel channels (7—see Figure 1), that is, pressure in a bottom of the channel is close to pressure in drum separators (1). Coolant flow rate stagnation in fuel channels can be destroyed only in case of early activation of Emergency Core Cooling System (ECCS) (see Figure 2(a)). Thus if ECCS would operate according to design algorithm (reactor cooling water started to supply only after approximately 400 seconds from the beginning of accident); acceptance criteria for both fuel rod cladding and fuel channel walls temperatures in high-power channel would be exceeded (see Figure 2(b) and Figure 2(c)). After implementation of ECCS activation algorithms according to coolant flow rate decrease in separate group distribution headers, water from ECCS starts to supply already after 5–10 seconds from the beginning of flow stagnation. Thus stagnation is broken and fuel channels, connected to affected GDH are reliably cooled (see Figure 2). These modifications of activation algorithms for reactor shutdown and emergency core cooling systems are installed in power plant Unit 1 in 1999, and Unit 2 in 2000.

In the Ignalina NPP Unit 1 safety analysis report, they have been investigated not only basic design accidents (discussed above) but also Anticipated Transients Without reactor Shutdown (ATWS). Investigations of such accidents are carried out at the licensing process for USA and Western Europe nuclear power plants; however, for the NPPs with RBMK-type reactors such analysis has been performed for the first time. Consequences of accident for RBMK-1500 reactor during which loss of preferred electrical power supply and failure of automatic reactor shutdown occur [6] are presented in Figure 3. Due to loss of preferred electrical power supply, all pumps are switched (see Figure 3(a)) off; therefore, the coolant circulation through fuel channels is terminated. Because of the lost circulation, fuel channels are not cooled sufficiently; therefore, temperature of the fuel channels walls starts to increase sharply. As it is seen from Figure 3(b), already after 40 seconds from the beginning of the accident, the peak fuel channel wall temperature in the high-power channels reaches acceptance criterion 650°C. It means that because of the further increase of temperature in fuel channels plastic deformations begin—the channels because of influence of internal pressure can be ballooned and ruptured. On the first seconds of accident the main electrical generators and turbines are switched off as well. Steam generated in the core is discharged through the steam discharge valves; however, their capacity is not sufficient. Therefore the pressure in reactor cooling circuit increases and approximately after 80 seconds from the beginning of accident reaches acceptance criterion 10.4 MPa (see Figure 3(c)). The further increase of pressure can lead to rupture of pipelines.

Thus the analysis of anticipated transients without shutdown has shown that in some cases the consequences can be dramatic enough. Therefore the priority recommendation has been formulated: to implement the second, based on other principles of operation, diverse shutdown system. However development, designing, and implementation of such system needed few years (in the Ignalina NPP Unit 2, this system was installed in 2004), so the compensating means, which were used in transition period while second diverse shutdown system was developed, has been implemented. This temporary system was called according Russian abbreviation "DAZ", "Dopolnitelnaja avarijnaja začita"—"Additional emergency protection". This system used the same control rods as well as design reactor shutdown system; however, signals for this system control were generated independently in respect of design reactor shutdown system. In Lithuanian Energy Institute for DAZ system, they have been selected not only set points of activation but also the safety justification was performed. Performed analysis has shown that after implementation of DAZ system the reactor is shut down in time and cooled reliably as well; acceptance criteria are not violated even in case of transients when design reactor shutdown system is not functioning. In Figure 3 is shown the behavior of the main parameters of

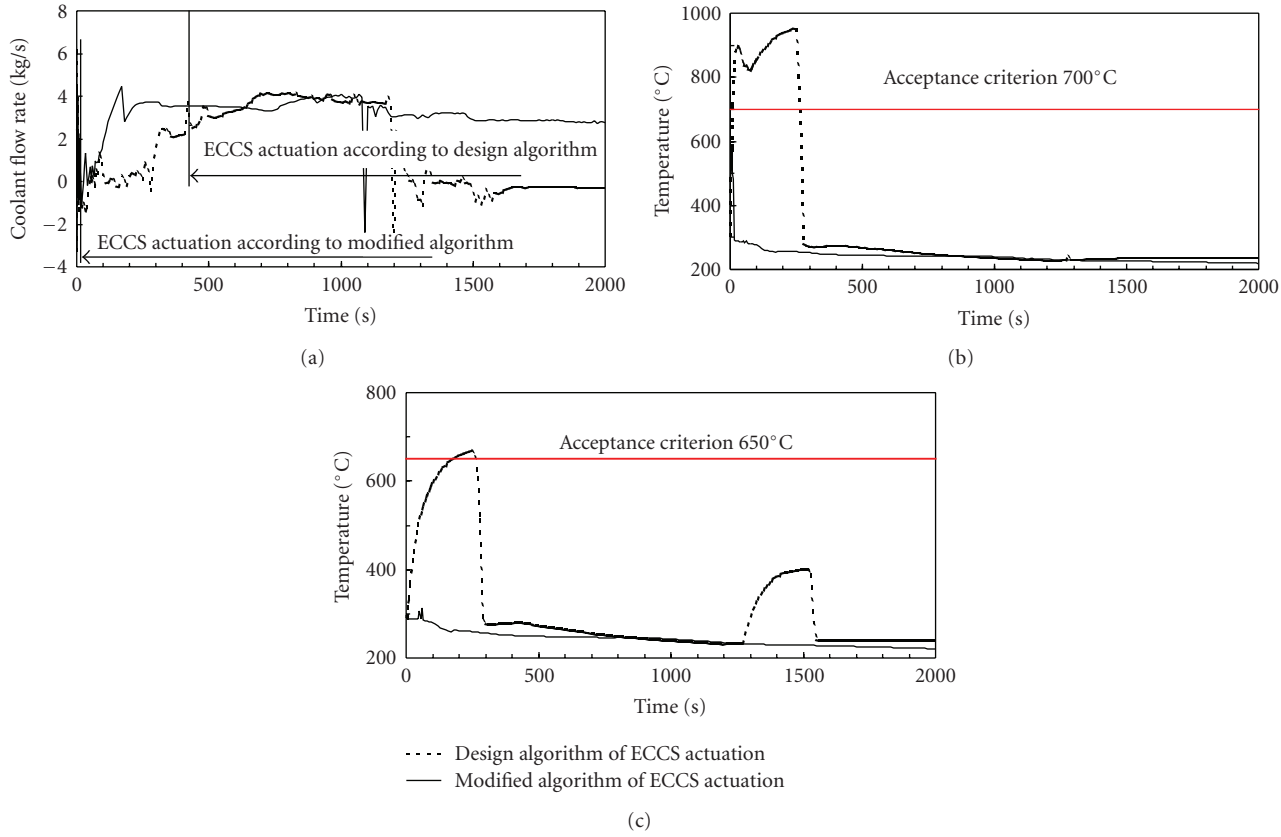

Figure 2: Analysis of partial GDH rupture considering modification of ECCS algorithm: (a) coolant flow rate through fuel channels, (b) fuel rod cladding temperature in high-power channel connected to ruptured GDH, and (c) behavior of fuel channel wall temperature.

reactor cooling circuit in case of loss of preferred electrical power supply and simultaneous failure of design reactor shutdown system. In this case two signals for activation of DAZ system (reactor shutdown) are generated: on increase of pressure in drum separators and on decrease in the coolant flow rate through the main circulation pumps. In Unit 1 DAZ system was installed in 1999 and in Unit 2 in 2000.

The Second Diverse Shutdown System (DSS) has been designed and installed in Ignalina NPP Unit 2 in 2004. In the first unit of Ignalina NPP this system has not been installed because reactor has been shut down in 2004. Therefore, nowadays Ignalina NPP reactor emergency protection (emergency shutdown) system consists of two independent shutdown systems: first, BSM controls manual control rods and shortened absorber rods, which are inserted into the core from bottom. This system performs the normal reactor shutdown function and can maintain a reactor in subcritical state. Second system AZ controls 24 fast acting reactor shutdown rods as well as additionally 49 rods, which belong to both—BSM and AZ systems. AZ system performs emergency protection function. Also the Additional Hold-down System of the reactor is installed. This system allows to prepare and inject water and neutron absorber gadolinium mixture into control rods cooling circuit. Thus, the reactor remains in subcritical state even in the case of failure of BSM system.

DSS justification was one of the main projects increasing a level of NPP safety. Specialists from LEI together with experts from the countries of Western Europe checked and have assessed the design documentation, carrying out independent calculations, thus helping Lithuanian regulatory body (VATESI) to make the appropriate decisions concerning implementation of mentioned system at Ignalina NPP [7]. In conclusions of review it has been shown that implementation of second diverse reactor shutdown system protects a reactor in case of failure of design reactor shutdown system. Implementation of this system has ensured that any initiating event cannot cause accident with damage of the reactor core as well as decreases core damage probability from $4 \cdot 10^{-4}$ up to $5 \cdot 10^{-6}$.

In 2002 the safety analysis report for Ignalina NPP Unit 2 has been developed. This report contains the description of systems, list of postulated accidents, engineering assessment of reactor cooling system, accident analysis, assessment of fuel channels structural integrity, assessment of reactor safety acceptability, and other chapters. The accident analysis in this report was performed using best estimate approach with uncertainty and sensitivity analysis. According to the international practice, the best estimate approach is used mainly for analysis of loss of coolant accidents in reactor cooling system. In Lithuania the best estimate approach was successfully applied not only for loss of coolant accidents

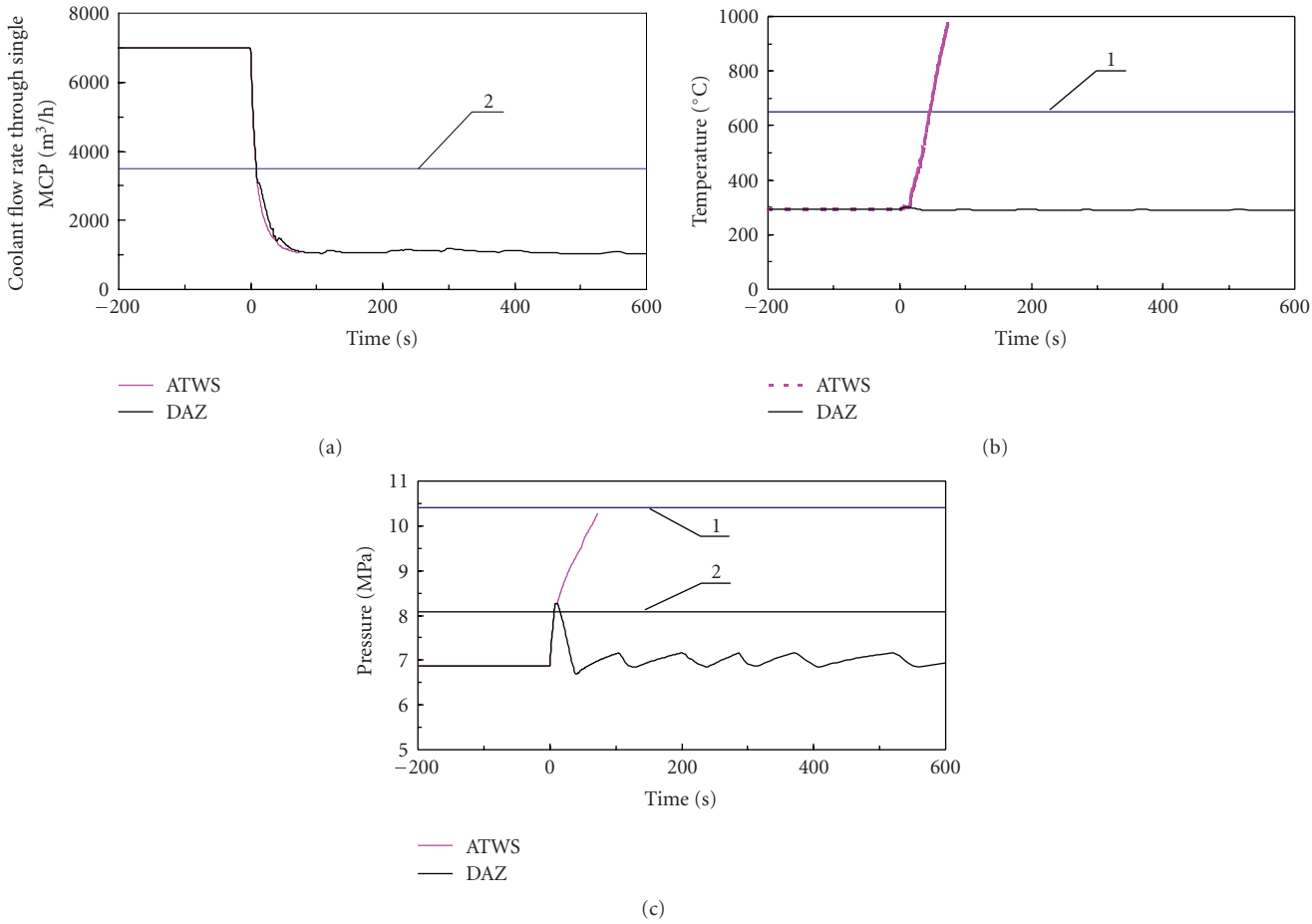

Figure 3: Analysis of loss of preferred electrical power supply and simultaneous failure of design reactor shutdown system, when DAZ system was installed: (a) coolant flow rate through one main circulation pump, (b) the peak fuel channel wall temperature in the high-power channel, (c) pressure behavior in drum separators, (1) acceptance criterion, and (2) set points of DAZ system activation (reactor shutdown).

but also for reactor transients and accident confinement system response analyses. The uncertainty and sensitivity analysis allows to avoid the unnecessary conservatisms as well as to assess and address the existing safety margins. The safety analysis report and its review were the main documents required for license for Ignalina NPP Unit 2. Both documents demonstrated the increased safety level after implementation of above mentioned modifications and satisfaction to requirements of regulating documents.

2.2. Ignalina NPP Probabilistic Safety Assessment. The Ignalina NPP first-level PSA "BARSELINA" project (1991–1996) was initiated in 1991 [8]. It was the first PSA for nuclear power plants with RBMK-type reactors. From the beginning this project was carried out by nuclear energy experts from Lithuanian, Russian, and Swedish institutions, and since 1995 it was carried out by efforts of experts from Lithuania (Ignalina NPP, LEI) and Sweden. Main objective of deterministic analysis was to show that nuclear power plant reliably copes with accidents, and basic purpose of PSA 1 level is to assess probability of reactor core damage to create a basis for severe accident risk assessment and management. Performed Ignalina NPP PSA 1 level study is predicted by assumption that the main radioactive source is reactor core. This PSA is performed for maximum permissible reactor operating power. Only internal initiating events have been analyzed—transients, loss of the coolant accidents, common cause failure, and internal hazards (fire, flooding, and missiles). Results of the analysis have shown that after implementation of recommendations from BARSELINA [8], safety analysis report, and its independent review [3, 4], probability of Ignalina NPP core damage is about $6 \cdot 10^{-6}$. According to the international requirements, this parameter for the operating nuclear power plants should not exceed 10^{-4} per year and for new NPPs, which are in process of construction, -10^{-5}. Therefore Ignalina NPP fulfils this requirement. Analysis has shown that, in Ignalina NPP, risk topography dominates transients, instead of loss of the coolant accidents. The risk of core damage most of all increases transients with loss of long-term core cooling. It is the positive fact meaning that up to consequences of severe accidents there is enough time. Thus operators supervising reactor operation can undertake corrective measures, and it means that Ignalina NPP has great potential opportunities

for implementation of the program on management of severe accidents. It is necessary to note that procedures and means on severe accident management are already implemented at Ignalina NPP Unit 2 [9, 10].

According to the international requirements, probability of the large reactivity release outside nuclear power plant should not exceed 10^{-7} per year for new NPPs, which are in process of construction and for NPPs in operation -10^{-6}. Scenarios and probabilities of the large reactivity release outside nuclear power plant are objects of investigations for PSA level 2. Ignalina NPP PSA level 2 project was performed in 1999–2001 [11] and it was the first project of such type for nuclear power plants with RBMK reactors. This project was carried out by efforts of experts from Lithuania (LEI) and Sweden. Performing PSA level 2 as initial data used results of level 1. According to PSA level 1 investigated accident scenarios consequences and its similarity criteria on radioactive contamination, the conditions of damage of the reactor have been developed and possibilities of accident management were assessed. Results of PSA level 2, it have shown that barrier of the large reactivity release after core damage is 1.5. This barrier is smaller in comparison with modern nuclear power plants having function of containment, which reaches 10 and more. Being based conservative assumptions and estimation of parameters, in PSA level 2 was calculated that general estimation of large discharge frequency is $3.8 \cdot 10^{-6}$ per year. Therefore, Ignalina NPP according to the probability of large reactivity release outside nuclear power plant is not the worst in comparison with the plants of the USA and Western Europe, constructed in the same years.

Carrying out the complex analysis about influence on Ignalina NPP units safety [12] by LEI, the following external events have been investigated:

(i) aircraft crash,

(ii) extreme wind and tornado,

(iii) flooding and extreme showers,

(iv) external fire.

Aircraft or other flying objects crash that caused accidents in Ignalina NPP will have local character because of its big territory. According to the Lithuanian civil aviation data, it has been assumed that average congestion is up to 50000 flights per one year within the 50-kilometer zone around NPP. Three zones have been defined by a radius up to 15, 50, and 85 meters around the reactor in the territory at Ignalina NPP (15—according to reactor dimensions, 85—according to reactor building size). Probability of air crash on a 85-meter zone around the reactor center, assuming that aircraft weight is 5700 kg as well as assuming that half of these flights carry out planes of western manufacturers and other half—Soviet, is $2.06 \cdot 10^{-9}$ 1/year. Even doing more conservative assumptions (heavy planes falling frequency equalized to easy planes falling frequency), probability of air crash on a 85-meter zone around the reactor center will be $1.64 \cdot 10^{-7}$ 1/year. The obtained heavy plane crash probabilities are less than the probabilities obtained in probability analyses for the majority of the West-European and American NPPs.

Tornado may cause huge damage and destruction. From all buildings of nuclear power plant, the tornado is most dangerous for a technical water supply system building, because it is located in the open territory on a coast of lake. Tornado and hurricane winds do not create danger for buildings of reactor and technical systems. Contrariwise probability of tornado and hurricane winds is $5.3 \cdot 10^{-6}$ 1/year. Therefore it is possible to approve that their influence on reactor safety is insignificant.

Rise of a water level in Lake Druksiai represents the greatest danger to pump station on the lake, since the service water system is the nearest NPP construction to the lake. Water level elevation of Lake Druksiai up to a level of 144.1 m is not possible practically; therefore, there is no danger on flooding of pump station. The platform of the other Ignalina NPP construction is located at a level of 148-149 m above the sea level. Rise of a water level in the lake Druksiai up to such mark is impossible and flooding does not represent the direct danger for Ignalina NPP.

Besides lake, another external flooding source is *extreme showers*. In territory of Ignalina NPP there is drainage system and all compartments which are located below a critical mark of a level are connected to this system; therefore, the water leaks in case of internal flooding. Thus, extreme showers do not cause external flooding of the reactor building. For probabilistic external flooding analysis the mathematical model to assess peak water level elevations of the lake Druksiai has been developed. Probabilistic assessment of water level elevation in the lake has been performed. Maximum amount of precipitation (not less than 279.7 mm in 12 hours) probability is $1 \cdot 10^{-6}$ 1/year. Such event will not have influence on reactor safety.

Probabilistic analysis of external fire. Ignalina NPP is situated in the region, where 30% of territory is occupied by forests (40% are grassland and 30% are occupied by lakes and swamps). The edge of the closest forest is less than one kilometre from territory of Ignalina NPP. On the territory of the NPP there are only separate trees and grass. The global fire of a forest with a high wind to the NPP side can cause the smoke cover on the territory of Ignalina NPP. The smoke does not influence work of reactor mechanisms but will complicate work of the personnel. Fire probability of forest, which is in 10-kilometer zone around Ignalina NPP and there are more than 2000 ha woods, is $2.7 \cdot 10^{-3}$ 1/year. It is a high probability, but any fire cannot affect safety of the reactor considerably.

3. Ignalina NPP Safety Assessment in Case of Specific RBMK Problems

Discussing safety of RBMK-type nuclear power plants, three vulnerabilities more often are mentioned generally:

(i) containment issue,

(ii) problem of gas gap closing between fuel channels and graphite blocks,

(iii) problem of multiple fuel channel ruptures.

Below, specificity of RBMK-1500 in respect of these problems is discussed.

3.1. RBMK Reactor Containment Issue. In case of accident in nuclear power plant (rupture of reactor cooling circuit pipelines), the coolant with radioactive materials will spread into reactor and compartment-enclosed reactor cooling circuit. In many (but not in all) reactors of the USA and the Western Europe, function of containment carries out visible from afar, photogenic, semicircle form protection enclosure. Usually nonexistence of containment is treated as deficiency of RBMK reactors. However such containment as for vessel-type reactors is technically impossible to implement for RBMK reactors. In the Ignalina NPP the function of containing accidentally released radioactive material is accomplished by an extensive system of interconnected steel lined, reenforced concrete compartments called the Accident Localization System (ALS). The ALS uses the "pressure suppression" principle employed by G.E. designed boiling-water reactors. The ALS encloses the large Ignalina NPP reactor core, the coolant pumps, and all of the piping providing coolant to the core. It is not necessary to enclose the pipes above the reactor core, which carry the exiting two-phase (steam-water) mixture to the drum separators, because if one of them is breached, coolant flow to the fuel channels (which is provided by pipes entering the core from below) will not be interrupted. Significant amounts of radioactive material can escape only if fuel rods are overheated. Breaches in the exiting pipes will not reduce coolant flow; therefore, the fuel rods will not overheat.

The effectiveness of the ALS has been verified by extensive international analysis and experimental programs. They all show that even if events leading to release of radioactive materials are postulated, these materials will be contained by the ALS; thus, the ALS performs the function of containment [13]. The minimal amounts (due primarily to non-condensable noble gases) which would eventually reach the environment, would not exceed the amounts that would be released by Western built reactors provided with the more familiar, prominently visible "dome containments".

3.2. Problem of Gas Gap Closing between Fuel Channels and Graphite Blocks. The fuel channels of RBMK-type reactor are separated from the graphite bricks by gaps maintained by graphite rings. These rings are arranged next to one another in such a manner that one is in contact with the channel, and the other with the graphite stack block (see Figure 4). As a result of exposure to neutron radiation and temperature, the diameters of graphite columns gaps decrease, and fuel channel tube expands; thus, the gap between them decreases.

The availability of the gap between graphite bricks and fuel channels is the main condition limiting the operation of RBMK-type reactors. These graphite fuel channel tubes gaps allow

(i) unimpeded (axial and radial) thermal expansion and contraction of the fuel channels,

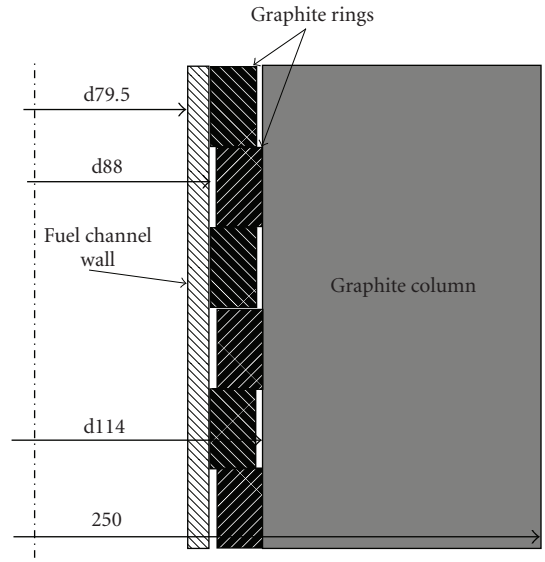

Figure 4: Fuel channel and graphite column interaction. All measurements are in millimeters.

(ii) predictable noncontacting heat transfer from graphite bricks (temperature higher than 500°C) to fuel channels (temperature 300–320°C) across the gaps,

(iii) leakage of helium-nitrogen mixture, which provides heat transfer from graphite to coolant and protects graphite against oxidation. Furthermore helium-nitrogen mixture is part of fuel channel integrity monitoring system.

The control of gap between fuel channels and graphite blocks at Ignalina NPP Unit 1 and 2 is carried out from the beginning of its operation and now the largest database and experience of assessment of gap among all RBMK type reactors is saved. After gap closure some functions of the control not only are lost but also worsen characteristics of the reactor. Increasing probabilities of damage of the channel and deformations of graphite, withdrawing of the channel from a reactor if necessary becomes complicated and the temperature of graphite and the fuel channel changes. In Ignalina NPP Unit 1 reactor the average gap between fuel channels and graphite up to final shutdown of the reactor from an initial level (3–2.7 mm) has decreased three to four times. This decreasing in Unit 2 is insignificant. Estimation of such small gap is very sensitive to errors of measurements, uncertainties of used models, and strategy of selection of fuel channels for measurements.

As it is known, after signing the agreement with the EBRD Account of Nuclear Safety in 1994, Lithuania has undertaken not to change fuel channels and not to operate Ignalina NPP reactor after closing even one gas gap between graphite stack and fuel channels. In Ignalina NPP in-depth safety report [3], which has been prepared by the international experts in 1996, it was predicted that at Ignalina NPP Unit 1 it happens not later than in the beginning of 1999.

In Lithuanian Energy Institute complex investigations on the problem of gap closure between fuel channels and graphite blocks at Ignalina NPP have been carried out. Assessment of the gap between graphite stack and fuel channels has very big importance because results of this problem are very important in making of the decision on duration of Ignalina nuclear power plant operation. At development of a technique on assessment of gap and strategy of measurements, the thermal-hydraulic, structural and probabilistic calculations have been performed. The detailed analysis [14] has shown that in Ignalina NPP In-depth safety analysis report [3] the assessment of the gap between fuel channels and graphite blocks at Ignalina NPP Unit 1 reactor has been performed using simplified deterministic calculations. Therefore obtained results were too pessimistic and conservative, predicting closure of the gap in set of channels in 1998–2000.

The specialists from LEI developed the integrated technique on assessment and control of risk of gas gap reduction. This allowed to develop strategy of measurement of holes diameters in graphite columns and replacement of fuel channels. This strategy has ensured existing of gap in Unit 1 reactor up to its final shutdown and by that has allowed considerably to prolong time of Ignalina NPP Unit 1 operation (until the end of 2004).

Change of a gas gap in the second unit of a reactor very much differs from that of the first unit because in a reactor of Unit 2 they are used zirconium tubes of fuel channels having different hardened surfaces and the rate of their ballooning is two times slower in comparison with tubes in reactor of Unit 1. Tendencies of change of graphite stack diameters in the second Unit are very similar to those of the first unit.

3.3. Problem of Multiple Fuel Channel Ruptures. In case of fuel channel rupture a two-phase flow is discharged to gaps between graphite stack. Part of graphite blocks can be and damaged cracked by coolant jet impingement; graphite columns can be displaced and coolant passes into the reactor cavity. Because graphite stack is hotter than the coolant, the pressure in tight reactor cavity increases. The leak tight Reactor Cavity (RC) performs the function of containment in the region immediately surrounding the nuclear fuel and graphite. The RC is formed by a cylindrical metal structure together with bottom and top metal plates. The reactor cavity confines the steam release in case of rupture of fuel channels. The steam-water-gas mixture from the reactor cavity is directed via Reactor Cavity Venting System (RCVS) pipelines to two steam-distribution devices of the 5th (upper) condensing tray in the Accident Localization System (Figure 5). Two pipelines $d = 400$ mm that come from a branch pipe $d = 600$ mm located above the top plate of RC are interconnected to a pipe $d = 600$ mm which connects to one steam-distribution device [1]. In the same way the other two pipelines $d = 400$ mm from the top plate of RC are connected to the second steam-distribution device. On their way these pipelines have branches, which are interconnected in a leak-tight corridor and end up with three Membrane Safety Devices (MSDs). The blowdown pipes from the bottom of RC pass directly to the leak-tight corridor and also end up with three MSDs.

In the case of multiple fuel channel tube ruptures, if the RCVS does not assure relief of steam-water-gas mixture from RC, the pressure increase in the RC will lift top plate of the RC. Those structural integrity of the RC and the rest fuel channels would be lost as well. Such event would cause very severe consequences similar to Chernobyl accident. Therefore it is important to maintain RC integrity, which is assured if pressure in the RC is below permissible pressure (314 kPa, abs), that is, the pressure of upper plate of biological reactor shielding weight [15].

Rupture of one fuel channel is design basis accidents for RBMK-1500 reactors. Probability of such rupture is -10^{-2} 1/year. According to design, the reactor cavity venting system assured the integrity of RC in the case of up to 3 fuel channels ruptures. This system has been modernized in 1996 as shown in Figure 5.

Moscow Research and Design Institute for Power Engineering (RDIPE), designer and developer of RBMK reactors, specialists in 1996 have analyzed pressure behavior in the Reactor Cavity in case of multiple fuel channel rupture [15]. Results of these calculations have shown that acceptance criterion maximum permissible load (310 kPa) to upper reactor cavity plate will be exceeded in case of 9 fuel channels rupture (according to RDIPE calculations). In RDIPE calculations the coolant discharge through the rupture conservatively was assumed equal to 32 kg/s through one fuel channel. This flow rate has been selected as constant versus time. Because of such conservative assumptions, amount of discharged coolant into reactor cavity is largest and number of channels, when permissible pressure in reactor cavity is not exceeded, will be minimal.

Such analysis is conservative with impact of uncertainties. The best estimate analysis of Ignalina NPP response to multiple fuel channels tubes rupture was performed at the Lithuanian Energy Institute. Sensitivity and uncertainty analysis was performed as well [16]. At performance of the analysis it has been considered that results of calculations can be influenced by uncertainties such as the plant initial conditions, assumed at the modeling, as well as assumptions and correlations of CONTAIN code. Summarizing the results of the uncertainty and sensitivity analysis, it was concluded that the capacity of RCVS comprises from 11 up to 19 ruptured fuel channels, that is, 15 ± 4 channels (Figure 6).

It is necessary to note that the analysis was performed for the case with reactor cooling system filled by coolant (the water levels in drum separators are nominal). Thus, after the fuel channels rupture, the steam-water mixture is discharged into the gaps of graphite stack. If the "dropout" model is used in CONTAIN 1.1 code, it is assumed that all the water released from the ruptured fuel channels in liquid fraction leaves from RC to the water drain. If the "dropout" model is not used in CONTAIN 1.1 code, it is assumed that not all evaporated water remains in a dispersed condition, and it may be transferred into RC and through the pipelines into ALS. The last assumption leads to higher calculated pressure in the RC (see Figure 6).

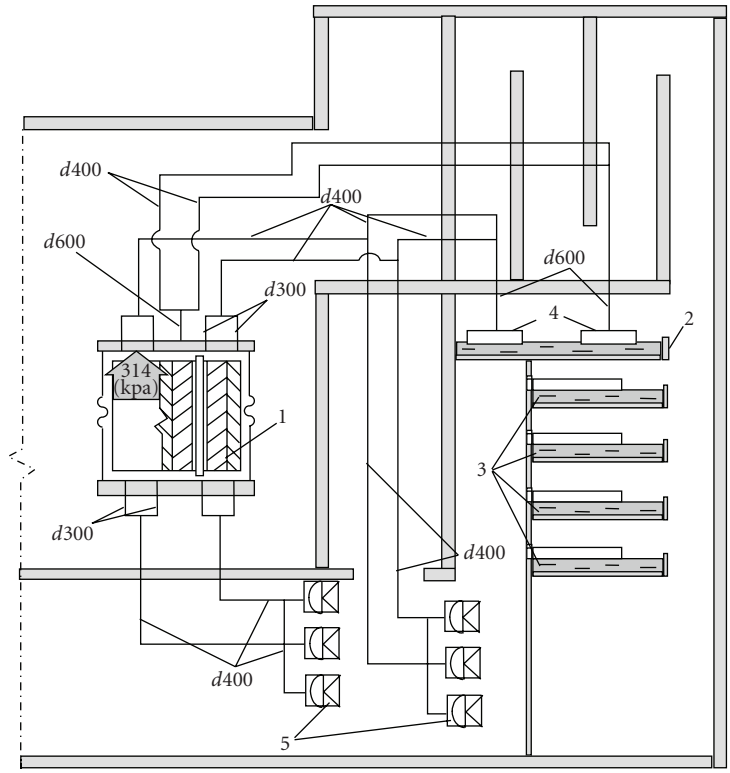

Figure 5: Simplified schematic of the reactor cavity venting system: (1) reactor, (2) the fifth ALS suppression pool, (3) suppression pools 1–4, (4) steam distribution devices, and (5) membrane safety devices (350 mm diameter)

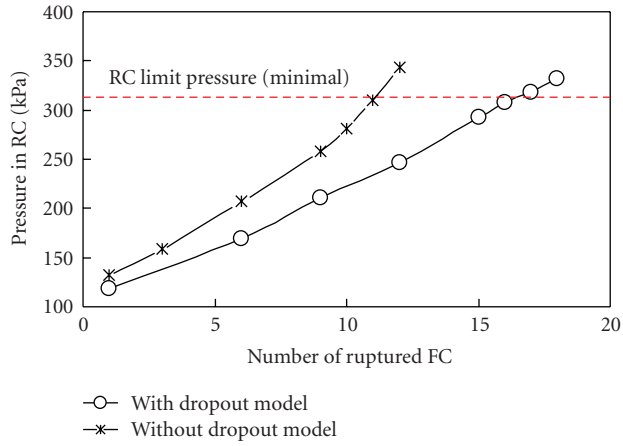

Figure 6: Pressure in the reactor cavity as a function of a number of ruptured fuel channels.

It is necessary to note that during operation of RBMK reactors there were only three cases of ruptures of separate fuel channels:

(i) at Leningrad NPP Unit 1 in 1975,

(ii) at Chernobyl NPP Unit 1 in 1982,

(iii) at Leningrad NPP Unit 3 in 1992.

In any of these cases adjacent channels have not been damaged. Thus, in reality there was no so-called "cascade rupture of fuel channels" when rupture of one channel causes ruptures of other channels. Experiments made on the large-scale TKR-Test facility at Electrogorsk Research and Engineering center for NPP safety [17] have shown also that cascade rupture of fuel channels is impossible.

4. Conclusions

Requirements of nuclear power plants safety depend on the accumulated experience, a level of a technical society evolution, which always raises, and from position of the state. About safety level of Ignalina NPP it was worried after Chernobyl accident in 1986. The first modernizations of reactors have been implemented at that time. RDIPE, designer and developer of RBMK reactors, experts have prepared the first safety justification for operating power plant in 1989. When Lithuania assumed control of the Ignalina NPP in 1991, a large number of studies on safety level have been conducted. It is necessary to note Safety Analysis Reports for Ignalina NPP Units 1 and 2, Safety Justifications of Reactor Cooling System, and Accident Localization System. The Ignalina nuclear power plant is distinguished from all RBMK-type reactors for the matter is that many international studies to investigate design parameters as well as level of their risk have been performed. Ignalina NPP, its design, and operational data have been

completely open and accessible to Western experts. At first the effective initial help in questions of nuclear safety has been provided by Sweden and after by other countries (Germany, United Kingdom, USA, etc.), capable to perform expertises of the safety analysis. A public list of EC Phare projects, supporting the modernization of Ignalina NPP, is available under http://ie.jrc.ec.europa.eu/dissem/.

The detailed analysis of accidents has shown that design basis accidents do not cause such condition of the plant, which postulates violation of acceptance. As well safety systems of the plant ensure a safe condition of the plant even doing the assumption that operator does not take any action for 30 minutes from the beginning of accident to mitigate an emergency situation.

The performed Probabilistic Safety Analysis of levels 1 and 2 has allowed to compare safety level of Ignalina NPP with the reached level on other nuclear power plants and to plan how to improve NPP safety systems and operational procedures. Investigations have shown that Ignalina NPP according to the probability of large radioactivity release outside nuclear power plant is not the worst in comparison with the plants of the USA and the Western Europe, constructed in the same years.

On the basis of the performed investigations the recommendations on safety improvement were developed by efforts of local and foreign experts. These recommendations were brought into Ignalina NPP Safety Improvement Programs (SIP-1, SIP-2, or SIP-3) which implementation strictly was checked by Lithuanian regulatory body VATESI. These means have allowed to improve safety level of the Ignalina NPP constantly. These works do not stop even on forthcoming final shutdown of the plant. In outcome of last significant project the Severe Accident Management Guide is developed. Now this guide is under implementation at Ignalina NPP. Severe Accident Management Guide will supplement Symptom-Oriented Emergency Operating Procedures and will provide safe elimination of accident consequences in all range of accidents.

Nomenclature

ALS: Accident localization system
ATWS: Anticipated transients without reactor shutdown
AZ: Russian acronym for "emergency protection system"
BSM: Russian acronym for "normal reactor shutdown system"
DAZ: Russian acronym for "additional emergency protection"
DSS: Diverse shutdown system
EBRD: European Bank for Reconstruction and Development
EC: European Community
ECCS: Emergency core cooling system
GDH: Group distribution header
LEI: Lithuanian Energy Institute
MSD: Membrane safety device
NPP: Nuclear Power Plant
PSA: Probabilistic Safety Assessment
RC: Reactor Cavity
RCVS: Reactor Cavity Venting System
RBMK: Russian Acronym for "Water-Graphite Boiling Reactor"
RDIPE: Research and design institute for power engineering
VATESI: Lithuanian acronym for "lithuanian state nuclear power safety inspectorate".

References

[1] K. Almenas, A. Kaliatka, and E. Uškuras, *Ignalina RBMK-1500. A Source Book. Extended and Updated Version*, Lithuanian Energy Institute, Kaunas, Lithuania, 1998.

[2] RDIPE, "Technical safety justification of Ignalina NPP with RBMK-1500 reactors," Tech. Rep. D040-1110, RDIPE, Moscow, Russia, 1989.

[3] Ignalina NPP, "In-depth safety assessment of Ignalina Nuclear Power Plant," Tech. Rep., Ignalina NPP, Visaginas, Lithuania, 1996.

[4] RISKAUDIT, "Review of the Ignalina Nuclear Power Plant safety analysis report, summary," Tech. Rep. 55, RISKAUDIT, Paris, France, 1997.

[5] A. Kaliatka and E. Uškuras, "Thermal-hydraulic analysis of accidents leading to local coolant flow decrease in the main circulation circuit of RBMK-1500," *Nuclear Engineering and Design*, vol. 217, no. 1-2, pp. 91–101, 2002.

[6] A. Kaliatka and E. Uškuras, "Development and evaluation of additional shutdown system at the Ignalina NPP by employing RELAP5 code," *Nuclear Engineering and Design*, vol. 217, no. 1-2, pp. 129–139, 2002.

[7] Independent review calculations of the accidents for Ignalina NPP Unit 2 DSS safety substantiation, LEI report according to project, "TSO support to VATESI during review and licensing of the diverse shutdown system at Ignalina NPP Unit 2," LEI, Kaunas, 2004.

[8] The BARSELINA Project Phase 4 Summary Report, "Ignalina unit 2 probabilistic safety analysis," *Ignalina NPP report*, Visaginas, Lithuania, 1996.

[9] E. Uškuras, A. Kaliatka, and V. Vileiniškis, "Development of accident management measures for RBMK-1500 in the case of loss of long-term core cooling," *Nuclear Engineering and Design*, vol. 236, no. 1, pp. 47–56, 2006.

[10] V. Vlaskin, G. Kryvošein, B. Dizik, V. Stebenev, A. Kaliatka, and E. Urbanavičius, "Development of beyond-design-basis accident management guidelines for RBMK-1500 reactors of the INPP," *Energetika*, vol. 4, no. 2, pp. 19–25, 2007 (Russian).

[11] E. Uškuras, A. Kaliatka, J. Augutis, S. Rimkevičius, E. Urbonavičius, and V. Kopustinskas, "Probabilistic and deterministic analysis of BDBA in RBMK-1500," *Energetika*, vol. 3, no. 3, pp. 8–23, 2006.

[12] J. Augutis and E. Uškuras, "Safety of Ignalina nuclear power plant in relation to external events," in *Proceedings of the 5th International Conference on Reliability, Maintainability and Safety (ICRMS '01)*, vol. 2, pp. 884–891, Dalian, China, August 2001.

[13] O. Novoselsky, A. Moskalev, V. Radkevitch, et al., "Software development for accident analysis of VVER and RBMK reactors in Russia. Part B (RBMK)," Final Technical Report DIMNP NT 580 (05), TACIS Project: R2.03/97, University of Pisa, Pisa, Italy, 2005.

[14] J. Augutis, E. Uškuras, and M. Liaukonis, "Ignalina NPP RBMK-1500 gas gap evaluation," *Nuclear Engineering and Design*, vol. 203, no. 2-3, pp. 195–207, 2001.

[15] Ignalina NPP Safety Analysis Report. Volume 3 Task Group 5, "Assessment of reactor cavity integrity," Ignalina NPP Report, VATTENFALL, Visaginas, Lithuania, 1996.

[16] B. Česna, S. Rimkevičius, E. Urbonavičius, and E. Babilas, "Reactor cavity and ALS thermal-hydraulic evaluation in the case of fuel channels ruptures at Ignalina NPP," *Nuclear Engineering and Design*, vol. 232, no. 1, pp. 57–73, 2004.

[17] N. Medvedeva, S. Timkin, A. Andrejev, et al., "Analysis of piping behavior in the graphite stack of RBMK-1000 in case of single technological channel rupture," Annual Report, Elektrogorsk Research Centre on Safety of Nuclear Power Plants, Elektrogorsk, Russia, 2004.

Hindawi Publishing Corporation
Science and Technology of Nuclear Installations
Volume 2010, Article ID 320396, 7 pages
doi:10.1155/2010/320396

Research Article

Evaluation of the Impact That PARs Have on the Hydrogen Risk in the Reactor Containment: Methodology and Application to PSA Level 2

Ahmed Bentaib, Cataldo Caroli, Bernard Chaumont, and Karine Chevalier-Jabet

Service d'évaluation des Accidents Graves et des rejets Radioactifs, Institut de Radioprotection et de Sûreté Nucléaire, Direction de la Sûreté des Réacteurs, BP 17, 92262 Fontenay aux Roses, France

Correspondence should be addressed to Ahmed Bentaib, ahmed.bentaib@irsn.fr

Received 16 April 2009; Revised 8 February 2010; Accepted 11 May 2010

Academic Editor: Michel Giot

This paper presents a methodology and its application to a Level 2 Probabilistic Safety Assessment (PSA-2), to evaluate the impact of the Passive Autocatalytic Recombiners (PARs) on the hydrogen risk in the reactor containment in case of a severe accident. Among the whole set of accidental scenarios calculated in the framework of the PSA-2, nine have been selected as representative in terms of the in-vessel hydrogen production rate and in-vessel total produced hydrogen mass. Five complementary scenarios have been added as representative of the core reflooding situations. For this set of selected scenarios the evolution of the conditions in the containment (i.e., pressure, temperature, and composition) during the in-vessel phase of the accident has been evaluated by means of a lumped parameter approach. The use of spray systems in the containment has also been considered as well as the presence of recombiners. Moreover, the ignition by recombiners of the flammable atmosphere has been considered.

1. Introduction

In the theoretical case of a severe accident in a nuclear reactor with core meltdown, the interaction of the hot core with the cooling water can generate large amounts of hydrogen. Hydrogen may be produced by oxidation of metals present in the corium pool or in the base mat during the molten corium-concrete interaction phase. This hydrogen is transferred into the containment (and transported therein) by convection loops arising mainly from condensation of steam released via the RCS break or during corium-concrete interaction. Depending on mixing in the containment atmosphere, the distribution of hydrogen is more or less homogeneous. If considerable hydrogen stratification exists, local concentrations of hydrogen may become substantial, exceeding the lower flammability limit for the gas mixture. The distribution and concentration of hydrogen in the containment building may also be modified by its spray systems. Spraying does homogenize the distribution of hydrogen in the containment and lead to "deinertization" of the mixture through the condensation of steam on water droplets.

To limit the hydrogen concentration in the containment, several methods can be proposed [1]:

(i) the deliberate ignition of the mixture as soon as the flammability limit is reached,

(ii) the consumption of hydrogen,

(iii) the removal of oxygen,

(iv) the dilution of the atmosphere to prevent the formation of flammable mixtures either by the increase in the volume of the containment or by the injection of an inert gas.

Hydrogen risk management can be implemented by one or a combination of the previous methods. The choice of a mitigation strategy depends primarily on the design of the containment. For PWRs with large dry containment, the strategy usually consists in combining large free volume to allow dilution, a high value of the design pressure, and the

use of means, as passive autocatalytic recombiners (PARs), to consume hydrogen. This strategy has been adopted recently in all French PWRs.

In this paper, we propose a methodology to evaluate the impact of PARs on the hydrogen risk in French 900 MWe reactor containment in case of a severe accident and its application to a Level 2 Probabilistic Safety Assessment (PSA-2).

2. Hydrogen Risk Assessment Methodology

The methodology adopted to assess hydrogen risk in the reactor building must take into account the different loads accounting for the impact of hydrogen production, distribution, and mitigation systems. This method uses the following main steps [2].

Step 1. Plant Design. The starting point of any analysis is the selection of the plant and geometrical modeling of the containment. This step aims to well describe the containment shape and volume; which influence hydrogen distribution inside the reactor containment.

Step 2. Selection of Relevant Scenarios. Representative of severe accident sequences and the evaluation of the associated hydrogen production rates and release into the reactor building. These source terms are usually derived from parametric code calculations with best estimates for still uncertain hydrogen production processes.

Step 3. Evaluation of the Containment Atmosphere Conditions. During the accident transient (i.e., temperature, pressure, and gas composition in the different regions and volumes of the containments) accounting for the presence of mitigation systems.

Step 4. Evaluation of the Time Evolution of Flammable Hydrogen-Air-Steam Cloud. The flammability of the containment gas mixture depends on its temperature, pressure, and composition. However, in practice, the point representing the mixture's composition (hydrogen, air, and steam) on the Shapiro diagram [3] (see Figure 1) is used to determine whether the mixture is flammable. In this diagram, the flammability and detonation zones are, respectively, delimited by the exterior and interior curves.

Step 5. Evaluation of the Propensity of a Premixed Flame to Propagate inside the Containment. Under the effect of hydrodynamic instabilities and turbulence (caused primarily by obstacles in the flame's path), an initially laminar deflagration (with a flame velocity around 1 m/s) may accelerate. Fast combustion regimes may also develop, involving rapid deflagration (a few hundred m/s), deflagration-to-detonation transition (DDT) and detonation (over 1000 m/s). These combustion regimes may generate high pressure loads which could endanger the containment integrity.

To define the transition from slow to fast combustion regime, two types of criteria, based on numerous experiments, are considered [2, 4].

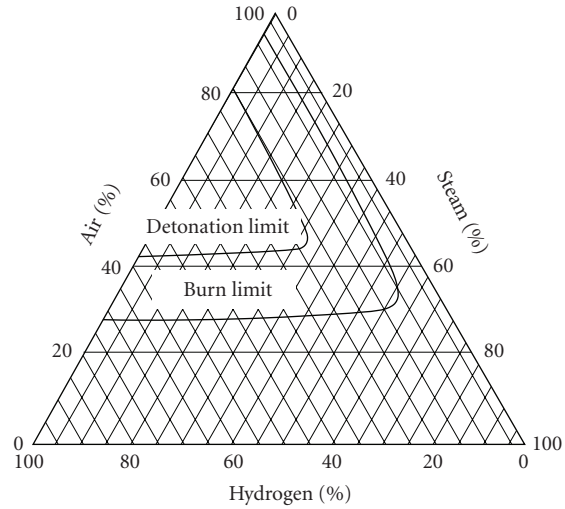

Figure 1: Shapiro diagram for hydrogen-air-steam mixtures.

(i) The "σ" criterion related to flame acceleration. σ stands for the mixture's expansion factor, a ratio of fresh and burnt gas densities at constant pressure. It is an intrinsic property of the mixture.

The critical value σ^* beyond which flame acceleration is possible depends on initial gas composition and temperature and flame stability (see Figure 2).

(ii) Similarly, prerequisite conditions have been defined for characterizing the transition between deflagration and detonation regimes (DDT). They are based on comparing a characteristic dimension of the geometry with detonation cell size λ (see Figure 3).

Flame acceleration and DDT criteria are based on the results of numerous experiments at various scales and in various geometries [5] and are considered as prerequisite criteria, that is, conditions required for the various combustion modes.

Step 6. Evaluation of Pressure and Thermal Loads Generated by Combustion. Two configurations are distinguished.

(i) If flame acceleration criteria are not met: in this case, dynamic pressure loads are excluded, and the pressure load is evaluated by considering adiabatic complete isochoric combustion process.

(ii) If flame acceleration criteria are met: in this case, the induced combustion loads are evaluated using the most appropriate combustion models.

3. Impact of PARs on Hydrogen Risk

In the following, the previous methodology is applied to investigate the PARs impact on hydrogen risk in French 900 MWe reactor containment by considering severe accidents sequences simulated in frame of PSA level 2. Effect of spray actuation and core reflooding is also considered.

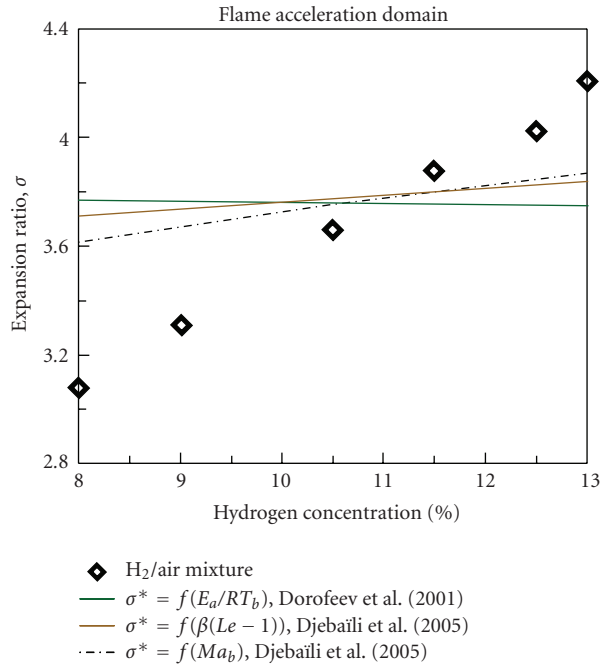

Figure 2: Critical value σ^* as a function of hydrogen concentration.

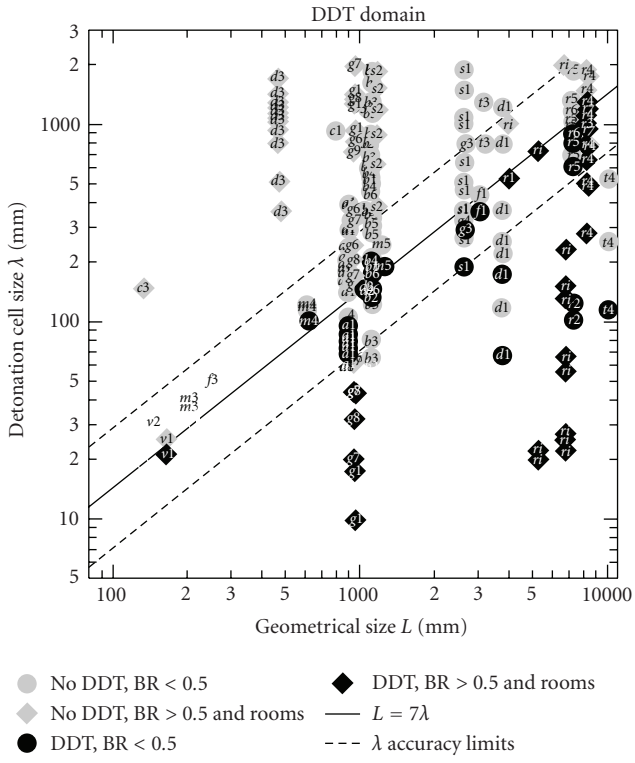

Figure 3: DDT criteria.

All calculations are performed using ASTEC V1.1 Lumped parameter code jointly developed by IRSN and GRS, that is, Gesellschaft für Anlagen- und Reaktorsicherheit mbH and dedicated to the simulation of the whole course of severe accidents in light-water reactors [6].

3.1. Step 1. Plant Design. The reactor containment is modeled by using multicompartment approach (see Figure 4). This model is based on 65 elementary volumes by considering 6 vertical levels, various radials sections, and 3 azimutal sections corresponding to the 3 reactor loops [7].

Moreover, the structure of the casemates surrounding each of the 3 primary loops is described. In addition to elementary volumes and in order to take into account atmosphere wall heat and mass transfer, 450 concrete and steel walls were considered. For gas and liquid transports inside the containment, 270 junctions connecting zones were modeled.

3.2. Step 2. Scenarios Definition. From the analysis of PSA level 1 results, 35 scenarios had been identified as sequences leading to core degradation and hydrogen release inside the reactor containment. Theses core degradation sequences correspond to the following situations:

(i) accidents involving secondary circuit transients,

(ii) accidents involving loss of steam generators feedwater,

(iii) accidents involving steam generator tube ruptures SGTR,

(iv) accidents involving loss of coolant LOCA,

(v) accidents involving loss of electrical power.

Theses sequences lead to different amount of hydrogen with different kinetic of hydrogen release (see Figure 5).

As PARs efficiency is related to the atmosphere composition and thermal hydraulic conditions [8], the analysis of PARs impact on hydrogen risk should take into account several parameters as (pressure, steam, and oxygen concentrations). Nevertheless, the main important effect remains the hydrogen total mass and the kinetic of hydrogen release inside the containment. To take into account those parameters, classification according to hydrogen production rate and hydrogen mass is carried out. The adopted approach distinguishes three levels of hydrogen mass:

(i) *Weak* corresponding to a mass of hydrogen produced lower than 300 kg,

(ii) *Medium* corresponds to a produced hydrogen mass between 300 kg and 550 kg,

(iii) *High* corresponds to a mass of hydrogen produced higher than 550 kg,

and three levels of hydrogen production rate:

(i) *Weak* for H2 production rate lower than 0.1 kg/s,

(ii) *Medium* for H2 production rate between 0.1 kg/s and 0.15 kg/s,

(iii) *High* for H2 production rate higher than 0.15 kg/s.

The combination of the previous criteria leads to 9 types of scenarios as shown in Table 1.

The application of the previous criteria to the various scenarios allowed defining 9 families of accidental scenarios

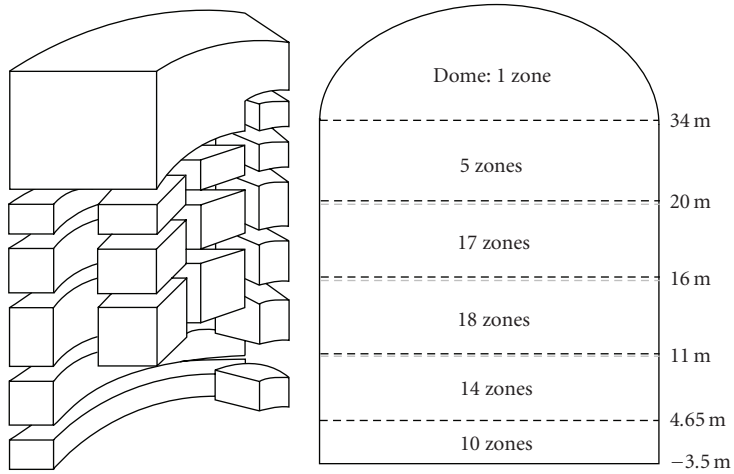

Figure 4: View of PWR 900 Astec nodalisation.

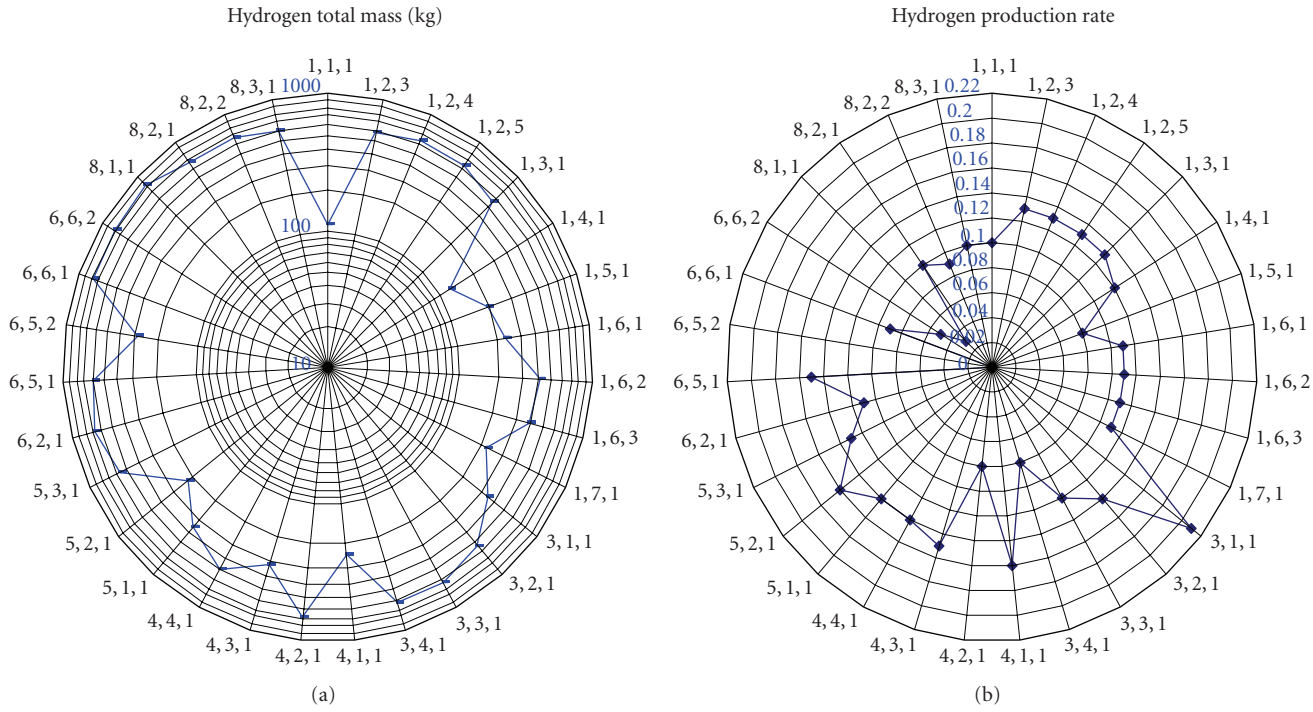

Figure 5: Hydrogen mass and hydrogen production rate for each core degradation sequences.

whose members present the same "behavior" regarding to hydrogen risk. Thus the PARs effect investigation will be limited to these 9 sequences.

In addition and to take into account core reflooding situations, 3 safety injection rates corresponding to 5.5 kg/s, 41.4 kg/s, and 205.6 kg/s are considered. Moreover, spray actuation is considered as soon as gas pressure exceeds 2.4 bars.

3.3. Steps 3 and 4. Time Evolution of Flammable Clouds inside the Containment. The flammable gas time evolution is checked by considering gas mixture in each containment zone at each time in the ternary H2-Air-Steam diagram [3]. At each time, gas composition is represented by a point in the Shapiro diagram. The gas composition time evolution in each zone is then described by curve. Figure 6 shows the gas composition in a zone during the core degradation sequence by considering or not the use of PARs. This figure shows also that the use of PARs decreases the hydrogen concentration in the containment atmosphere and limits the flammable cloud size inside the reactor containment.

Table 1: Families of scenarios.

Families of scenarios	H2 mass	H2 production rate
Type 1	Weak	Weak
Type 2	Weak	medium
Type 3	Weak	High
Type 4	Medium	Weak
Type 5	Medium	medium
Type 6	Medium	High
Type 7	High	Weak
Type 8	High	medium
Type 9	High	High

More generally, the analysis of time evolution of reactor containment atmosphere regarding to PARs effect allows defining three classes of scenarios.

(i) Class 1: constituted of scenarios corresponding to weak productions of hydrogen and to reflooding scenarios with high safety injection rate (205,6 kg/s). For this category, the use of PARs seems to be sufficient to avoid flammable gas formation.

(ii) Class 2: constituted of scenarios corresponding to medium and high productions rate. In these cases, flammable gas mixture is present in certain containment zone during a limited time.

(iii) Class 3: corresponds to reflooding scenarios with safety injection rate of 41.4 kg/s and 5.5 kg/s. In these cases, containment gas atmosphere becomes flammable during reflooding phase.

3.4. Step 5. Flame Acceleration. As for the flammability risk assessment, flame acceleration risk is checked by calculating and comparing the expansion σ factor, corresponding to the gas composition in each zone, to the limit value σ^*, issued from experimental data [4]: situation with σ higher than σ^* could lead to high pressure load in case of combustion.

The analysis of ASTEC results show that the use of PARs leads to low hydrogen concentration and consequently to low σ values. This situation is illustrated in Figure 7 where σ values obtained with and without PARs are compared to the critical values σ^* at time of high hydrogen release for each zone.

As shown in Figure 7, the use of PARs allows to reduce significantly the flame acceleration risk. Nevertheless, the analysis of PARs effect shows that for

(i) class 1, the use of PARs avoids flame acceleration;

(ii) class 2, flame acceleration criterion is satisfied in certain containment zone during a limited time;

(iii) class 3, flame acceleration criterion is satisfied by the reactor containment gas atmosphere during reflooding phase.

Consequently, scenarios from class 1 could not lead to high pressure load in case of combustion. Indeed, scenarios from classes 2 and 3 may endanger the containment integrity in case of combustion if ignition occurs at moment of high hydrogen release.

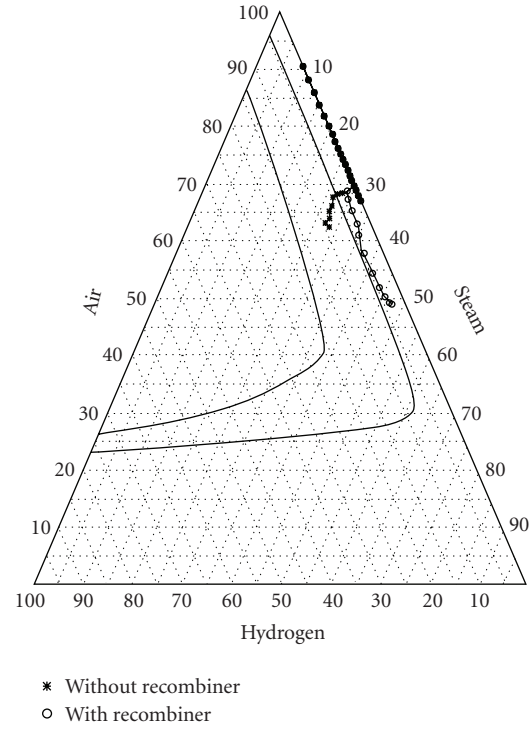

Figure 6: Effect of PARs on gas mixture flammability (with stars: gas composition without PARs; with circle: gas composition with PARs).

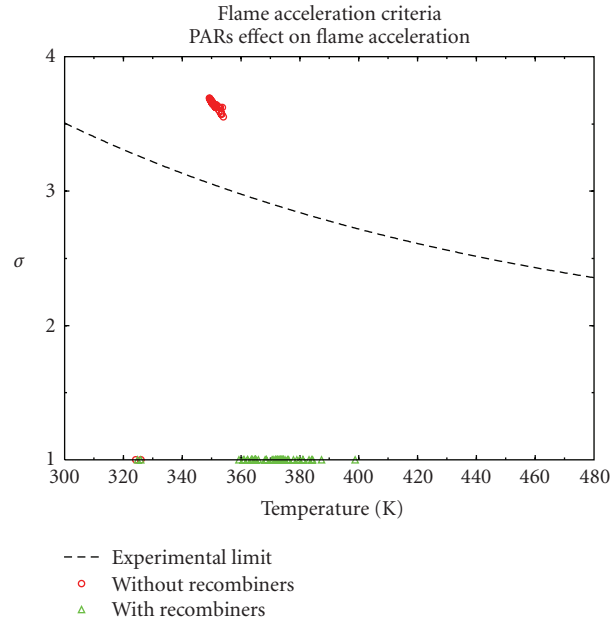

Figure 7: PARs effect on Flame acceleration (in red: gas composition without PARs; in green: gas composition with PARs).

3.5. Step 6. Pressure Loads Evaluation. Before performing combustion calculation, ignition sources have to be defined.

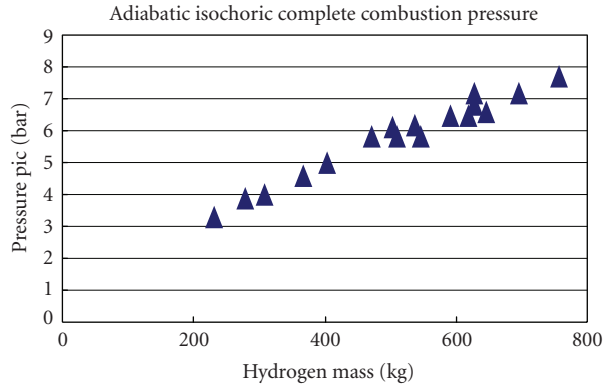

Figure 8: PAICC pressure versus hydrogen mass.

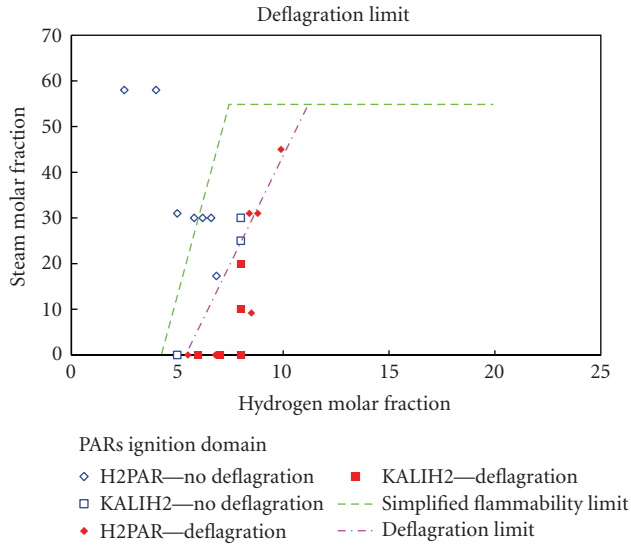

Figure 9: Ignition of SIEMENS PARs.

The ignition must be either predicted mechanistically (self-ignition) or must be postulated with respect to time and location. In this last case, ignition time is usually chosen to induce high pressure load. Figure 8 shows the pressure maximal values obtained by considering adiabatic isochoric complete combustion for different core degradation sequences.

Figure 8 shows also that the "probabilistic" ignition sources could lead to high pressure values beyond the containment pressure design of 6.5 bars. In the framework of PSA level 2 and in order to evaluate "realistic" pressure load, deterministic ignition sources are considered. Due to their hot catalytic sheets, PARs are considered as ignition sources under specific condition (see Figure 9). Indeed, some of the experimental tests performed on KALI H2 and H2PAR [9] show that PARs could ignite the flammable gas mixture. These experimental results show that ignition induced by recombiners occurs for low hydrogen concentrations respecting to the following limits.

These ignition limits correspond to low hydrogen concentration which avoid flame acceleration phenomena. The evaluation of pressure load generated by combustion is then carried out by considering complete, adiabatic and isochoric combustion. Pressure, known as PAICC, thus calculated depends on gas mixture and on the thermodynamic conditions and does not depend on the geometry of the containment. The calculation results show that PAICC does not exceed the containment pressure design.

4. Evaluation of Spraying Effect

Spray system has been activated for the previously selected scenarios. The effect of this activation has been analyzed and shows that, for all scenarios, steam condensation on spray droplets leads to the creation of consequently flammable cloud. Moreover, flame acceleration criteria are satisfied in the whole of the reactor containment. In all cases, scenarios from classes 1 and 2 families behave as scenarios from class 3.

5. Conclusion

This paper presents a methodology for hydrogen risk assessment and its application to evaluate the effect of Passive Autocatalytic Recombiners in framework of Level 2 PSA.

This analysis has shown that the use of recombiners reduces significantly the risk of flame acceleration and transition to detonation. However, the presence of recombiners does not eliminate the risk of flame acceleration which lasts for some specific scenarios and short duration.

These analyses have also shown the beneficial effect of recombiners as igniters. Indeed, based on the experimental data presently available, it seems that ignition induced by recombiners occurs for low hydrogen concentrations, leading to relatively low pressure. These experimental results need however to be corroborated by more detailed experiments and by refined modelling of phenomena occurring in PARs.

References

[1] Research and development with regard to severe accidents in pressurized water reactors: summary and outlook, Tech. Rep. IRSN/2007-083.

[2] P. Royl, H. Rochholz, W. Breitung, J. R. Travis, and G. Necker, "Analysis of steam and hydrogen distributions with PAR mitigation in NPP containments," *Nuclear Engineering and Design*, vol. 202, no. 2-3, pp. 231–248, 2000.

[3] H. F. Coward and G. W. Jones, *Limits of Flammability of Gases and Vapors*, Bulletin 503, Bureau of Mines, United States Government Printing Office, Washington, DC, USA, 1952.

[4] N. Chaumeix-Djeibli, et al., H2 Gradient Effect on Premixed Flame Propagation in a Vertical Facility: ENACCEF ; ICDERS 20 Montréal 2005.

[5] W. Breitung, S. Dorofeev, A. Kotchourko, et al., "Integral large scale experiments on hydrogen combustion for severe accident code validation-HYCOM," *Nuclear Engineering and Design*, vol. 235, no. 2–4, pp. 253–270, 2005.

[6] J.-P. Van Dorsselaere, C. Seropian, P. Chatelard et al., "The ASTEC integral code for severe accident simulation," *Nuclear Technology*, vol. 165, no. 3, pp. 293–307, 2009.

[7] A. Bentaib, et al., "Modèle hydrogène pour l'EPS2 : impact des recombineurs sur la risque hydrogène dans l'enceinte de confinement des REP 900 Mwe—Volume I : synthèse des résultats," Note Technique DPEA / SEAC / 2002-35.

[8] E.-A. Reinecke, A. Bentaib, S. Kelm, W. Jahn, N. Meynet, and C. Caroli, "Open issues in the applicability of recombiner experiments and modelling to reactor simulations," *Progress in Nuclear Energy*, vol. 52, no. 1, pp. 136–147, 2010.

[9] P. Rongier, et al., "Studies of catalytic recombiner performances in H2PAR facility," in *Proceedings of the Cooperative Severe Accident Research Program Meeting (CSARP '97)*, Bethesda, May 1997.

Hindawi Publishing Corporation
Science and Technology of Nuclear Installations
Volume 2010, Article ID 289792, 13 pages
doi:10.1155/2010/289792

Research Article

On the Analysis and Evaluation of Direct Containement Heating with the Multidimensional Multiphase Flow Code MC3D

Renaud Meignen and Tanguy Janin

IRSN, BP17, 92262 Fontenay aux Roses Cedex, France

Correspondence should be addressed to Renaud Meignen, renaud.meignen@irsn.fr

Received 24 April 2009; Accepted 11 September 2009

Academic Editor: Nikola Čavlina

In the course of a postulated severe accident in an NPP, Direct Containment Heating (DCH) may occur after an eventual failure of the vessel. DCH is related to dynamical, thermal, and chemical phenomena involved by the eventual fine fragmentation and dispersal of the corium melt out of the vessel pit. It may threaten the integrity of the containment by pressurization of its atmosphere. Several simplified modellings have been proposed in the past but they require a very strong fitting which renders any extrapolation regarding geometry, material, and scales rather doubtful. With the development of multidimensional multiphase flow computer codes, it is now possible to investigate the phenomenon numerically with more details. We present an analysis of the potential of the MC3D code to support the analysis of this phenomenon, restricting our discussion to the dynamical processes. The analysis is applied to the case of French 1300 MWe PWR reactors for which we derive a correlation for the corium dispersal rate for application in a Probabilistic Safety Analysis (PSA) level 2 study.

1. Introduction

Direct Containment Heating (DCH) is a phenomenon that can potentially happen during a severe accident and may threaten the integrity of the containment by pressurization of its atmosphere. It can occur following a melting of the reactor fuel and its relocation in the bottom of the reactor vessel. Depending on the cooling conditions, the vessel might fail and the melt will be ejected out. If the primary circuit driving pressure is above some threshold, the melt will be, in a second stage, ejected out of the pit, going for a part into some small rooms (e.g., steam generator rooms, called for short hereafter subcompartments) and for the rest directly to the containment dome. If the melt can be oxidized (which is likely), then a very rapid oxidation of a large amount of the melt occurs. The hydrogen produced during this stage may subsequently burn altogether with the pre-existing one. Most of the past studies of this phenomenon were based on geometries of US NPP's (Surry, Zion, etc.). For a good synthesis of these works, the reader can consult a special issue of Nuclear Engineering and Design [1]. Regarding in particular the melt dispersion, several simplified models have been proposed in the past, mainly qualified on US reactor types, and implemented in lumped parameter codes as CONTAIN [2]. However, it is found that all models are highly dependent on the geometry with high variations of the main parameters [3]. Thus the extrapolations to other reactors, other materials, and other scales than those used for the fitting process of the parameters are doubtful. With the development of multidimensional multiphase flow computer codes, it is now possible to investigate the phenomenon numerically with more details, improving thus the comprehension, first, and prediction capabilities, second. At the IRSN, we are using for this purpose the 3-dimensional code MC3D, mainly developed for Fuel Coolant Interaction (FCI) analysis [4, 5].

The current analysis is realized in the frame of the development of a Probabilistic Safety Analysis (PSA) level 2 study on French 1300 MWe reactor. In order to minimize the uncertainties related to the use of unqualified models regarding the specific plant under consideration, it was decided to engage a program including specific experiments and the use of the MC3D code for the understanding and characterization of the dynamical aspects.

A priori, the DCH problem is mainly related to the evaluation of the following physical phenomena:

(i) melt ejection and dispersion to the containment;

(ii) heat transfer from the melt to the containment atmosphere;

(iii) melt oxidation, its energy, and consequences on material properties;

(iv) hydrogen production coming from oxidation by steam;

(v) combustion of the hydrogen (produced and pre-existing).

However, it is important to stress at this stage that this should be considered only as what can be called the "academic" DCH problem. In this viewpoint, the boundary conditions (i.e., the global geometry), are not affected by the phenomenon itself. The break will be supposed to be central and with a constant diameter, although some models exist for the break enlargement due to the melting. The break enlargement is not considered here due to the very high uncertainty regarding the break formation itself (other arguments that support this choice will appear further from the analysis). All in all, this has to be considered as an uncertain parameter. The vessel is supposed to have the shape of an intact one, that is, with no enlargement due to the internal pressurization (which induces the break). Also, the presence of the vessel insulator is not taken into account. The behaviour of this equipment is very uncertain. It should at least loose strongly its mechanical properties but should not disappear. It might then reduce the flow path area to the containment. At first, considering the vessel as undeformed and the vessel insulator as absent could be considered as a conservative point of view. This conclusion is however not totally clear if one considers that a flow path restriction tends to increase the mechanical effort onto the vessel itself and then the mechanical stress onto the attachment points of the vessel. This might involve an important displacement of the vessel that could in turn open some new paths. A second limiting feature of the academic DCH problem is that it considers that no water is present, neither in the pit nor in the vessel (laying over the melt or trapped somewhere in the Reactor Coolant System (RCS)). Both cases are in fact quite unlikely. The presence of water adds a very important additional difficulty. This is not taken into account in this study (neither investigated in the experiments). The impact of remaining water in the RCS was investigated in few CE/CES tests (Calvert Cliffs geometry) [6]. This was possible because in these experiments the melt charge was initially placed in the pit. These tests revealed an important increase of the duration of the vessel pressurization, due to water flashing. However, the overall pressurization was slightly smaller, due to the coejection of water with the melt. This is not sufficient to have firm conclusions since the results should strongly depend on the characteristics of the remaining water (mass, temperature). This effect could in principle be investigated, at least qualitatively, with tools like MC3D.

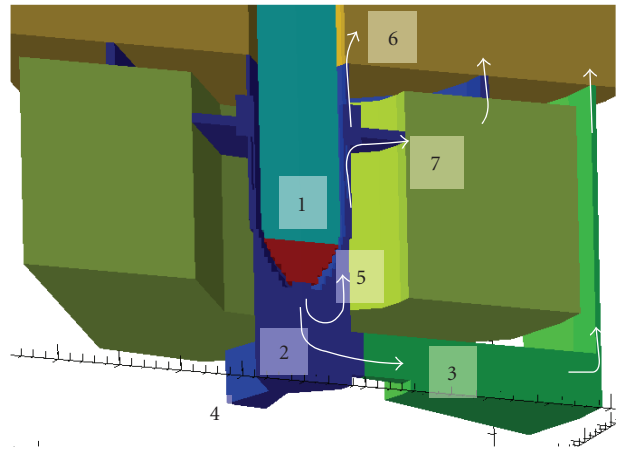

Figure 1: Example of 3D test calculation geometry with a fine mesh, showing the main volumes and flow paths, for the DISCO-F geometry. 1 reactor pressure vessel, 2 reactor cavity, 3 reactor pit access, 4 pit niche, 5 annular space, 6 exit to containment, 7 exit to subcompartments.

2. Experimental Database

The analysis is based on an experimental program investigating the phenomenon with different geometries representative of European reactors such as the EPR (DISCO series, performed by FZK, Germany [7]), the French 1300 MWe P′4 (DISCO-F), VVER, and Konvoï German reactors. A general presentation of the program and the main outcomes can be found in [8]. We will focus our present study on the 1300 MWe P′4 geometry although similar results are available for the EPR geometry.

For the P′4 geometry the scale is 1 : 16th. Figure 1 gives a global sketch of the geometry as represented for a 3D calculation with MC3D. The geometry is complex, 3-dimensional, with an important path section towards the bottom access (path 3), and allows a distribution of the fuel ejected upwards to different spaces: containment dome (path 6) and subcompartments (path 7). A closer view of exit pathways towards the dome and subcompartments is given in Figure 2.

Some of the tests, denoted "2D," were carried out with a simplified geometry with a cylindrical cavity without the access path. The purpose of this simplification is to allow an easier code qualification and analysis. The program comprised:

(i) 10 water-tests called DISCO-F(X), including 2 tests in "2D" geometry;

(ii) 4 cold tests with a heavy metal, made from a gallium alloy, called DISCO-FM(X), of which one is "2D";

(iii) 6 cold tests with a second heavy metal, the Wood's Metal, called DISCO-FW(X), of which 3 are "2D";

(iv) 5 hot integral tests with an alumina-iron thermite, called DISCO-FH(X) with

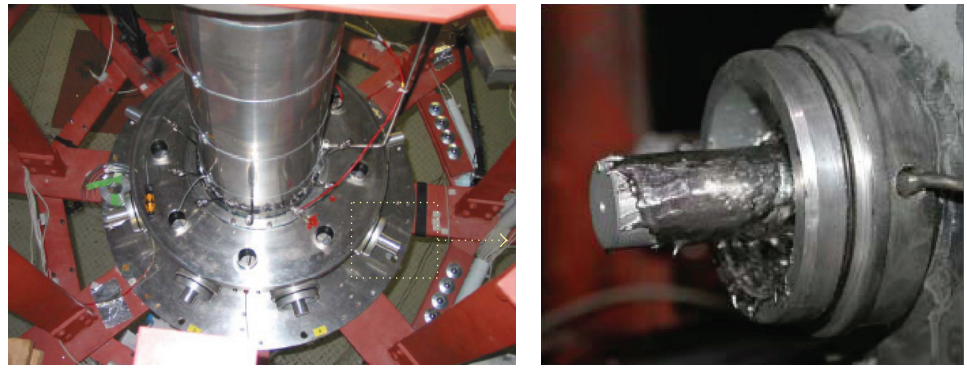

(a) (b)

Figure 2: DISCO-F experimental setup. (a) View from above at the cavity exit holes and the main cooling line stubs during assembly of the test rig. (b) Close view of exit around one cooling line after a test with liquid metal.

(a) 1 test in neutral environment, avoiding chemical effects (FH02),

(b) 1 test in "2D" geometry (FH05).

The pressure differences between the vessel and the pit were varied from 10 to 22 bars approximately. Three diameters of vessel breaks (i.e., vessel outlet nozzle) were used: 30, 45, and 60 mm, corresponding to 0.5, 0.75, and 1 m break diameters at full scale. Note that only tests with a central break were performed for P′4 geometry but previous experiments with EPR geometry showed that this situation was bounding.

In the rest of the paper, we will firstly recall the major characteristics of the MC3D code and show the status of the analysis that has been performed thanks to its use. As MC3D does not treat combustion, we will focus the analysis on the dynamical aspects. Indeed, the dynamical features drives the thermal and chemical phenomena and it is then of first importance to describe this stage accurately.

3. MC3D: Analysis of the Potential and Limitations of the Code to Describe the Main Features of the Phenomenon

MC3D is a computer code devoted to study multiphase and multiconstituent flows in the field of nuclear safety. It is one of the reference tools for the evaluation of Fuel Coolant Interaction (FCI) but it is more generally a Computational Multifluid Dynamics (CMFD) tool that can treat various problems [5]. One of the most important particularities of MC3D is that the fuel is modelled with two fields which allow describing the two possible states of the fuel: either continuous or discontinuous (Figure 3). These two fields are connected by mass transfer constitutive laws (i.e., fragmentation or coalescence). By this way, the drop field is supposed to describe only discontinuous fuel state. The continuous fuel field is modelled with an original Volume of Fluid, Piece Wise Linear Interface Construction (VOF-PLIC) method, avoiding then numerical dispersion (Figure 4).

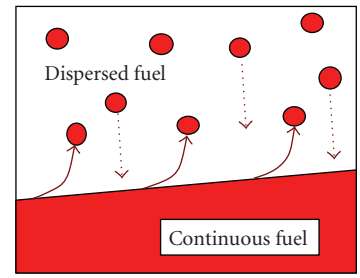

Figure 3: Connections between the continuous and discontinuous fuel fields. Plain arrows: fragmentation; dashed arrows: coalescence towards continuous fuel.

For the DCH evaluations, the fragmentation process is obtained through a model extending the Kelvin-Helmholtz (KH) instability model to multiphase fragmentation, taking into account local velocities. In this model, we write that the volumetric rate of fragmentation of the jet is given by

$$\Gamma_f = N_f c_i, \tag{1}$$

where

$$c_i = \frac{1}{\rho_f + \rho_a}\sqrt{\rho_f \rho_a \left(V_f - V_a\right)^2 - \sigma k\left(\rho_f + \rho_a\right)}\Bigg|_{k=k\max} \tag{2}$$

is the standard instability growth rate of KH model. Index f stands for the continuous fuel, and a stands for the ambient fluid. In a fully local model, the difficulty is to provide

(i) an adequate spatial averaging of the properties in order to limit the effect of mesh size,

(ii) an averaging of the fluid properties and particularly a definition of the ambient fluid.

These numerical aspects cannot be detailed here. Let us simply say that the ambient fluid is related to a mixture formed by liquid water and the gases. Fuel droplets themselves are not taken into account. Then, for DCH simulation, the ambient fluid definition is straightforward since, in general, we do not consider the presence of liquid water.

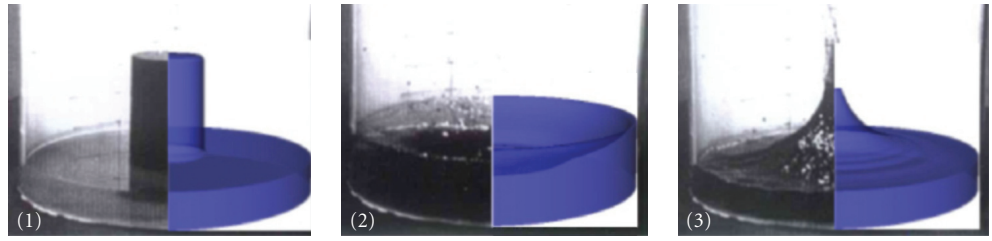

Figure 4: Continuous field slosh test computed by the MC3D code in 2D with a VOF-PLIC approach (the 3D effect is a result of image processing). Each image compares the code visualisation (on the right) with the experiments [9] using water (on the left): (1) initial state of a water cylinder immersed in a shallow basin of water; (2) first maximum at the wall, (3) maximum at the centre after two sloshing movements.

In (1), N_f is called the fragmentation parameter. It is related to the relative height (regarding the wavelength) of the instability when the fragmentation occurs. It also includes eventual nonlinear effects. The expected value stands between 1 and 6. In the calculations, $N_f = 2$ was used, as for FCI evaluations. The wave number corresponding to the maximum growth is given by

$$k_{\max} = \frac{2}{3} \frac{\left(\overline{V_j} - V_a\right)^2}{T} \frac{\rho_f \rho_a}{\rho_f + \rho_a}. \tag{3}$$

In this model, the diameter of the created drops is related to the wavelength λ of the instability so that

$$D_{d,\text{creation}} = N_d \lambda, \tag{4}$$

N_d is a parameter with expected value between 0.1 and 0.5. In calculations, we still use the recommended parameter as for FCI calculations, that is, $N_d = 0.2$.

Coalescence occurs from drop collision with the continuous fuel. Coalescence happens mainly at the impact along a wall.

Moreover, an oxidation model is available. Due to the specific conditions that MC3D has generally to face (high temperature melts, high pressure), the model is however quite simple and parametric. Melt oxidation in such conditions is a particularly complex problem. It is currently under investigation at IRSN in order to improve the code with more predictive constitutive laws in future versions. Currently, we simply set an amount of potential oxidation per surface area of the melt (called capacity), calculated with a transport equation. The oxidation itself occurs at a rate depending on the capacity, the time scale, and the vapour content. Up to now, the approach for this dealing with this problem for DCH evaluations has been mainly heuristic and empirical, based on the experimental evidences of strong and very rapid oxidation. We estimate that some questions regarding the actual characteristics of prototypical corium oxidation are still pending, for example, oxidation level of uranium, as well as the question of scaling. Improvements regarding this issue in codes like MC3D should then give important benefits regarding the understanding and evaluations.

The major key limitation in MC3D is then the evaluation of combustion which is currently not possible. Experiments have shown that this phenomenon drives the essential of the "heating" problem. This means that the treatment of combustion needs a particular attention. However, an important number of situations involve already high containment pressure at the vessel break. The high content of vapour in these cases might inert partially the combustion and then simple thermal heat transfers might play an important role. In the reactor case, oxidation of zirconium will also add an important amount of energy. For the issue of combustion, the treatment up to now has also been mainly empirical. To the knowledge of the authors, only few simulations with dedicated combustion codes were done and failed to describe with high accuracy the characteristics of combustion during a DCH event. Large uncertainties exist due to important energy losses in experiments, particularly if one considers the problem of extrapolating and scaling. However, taking into account the various strong uncertainties and the fact that we are seeking for a practical evaluation for nuclear safety, margins can be taken and conservative approaches might be sufficient. This topic will not then be addressed further in the following of the paper.

Note also that although this could be done quite easily, the code cannot compute friction and heat transfer with structures. In the present application, this should have only a minor impact, particularly at reactor scale.

One of the advantages of the MC3D code is its recognized ability to treat the interaction between the fuel and the water, either for slow mixing, either for steam explosion. It is then possible to combine with the same tool the effect of DCH and FCI. This will be exemplified in Section 8. The qualification of the tool for the specific DCH problem allows us to go far beyond what can be obtained with analytical models with a more comfortable confidence regarding extensions to, for example, different scales and material or different initial conditions as including the effect of the presence of water. Varying the mesh precision allows us to make several kinds of studies. With an intermediate mesh size, we will discuss the flow patterns calculated with the code. With a somewhat rough mesh, one can make a lot of calculations and thus having a statistical treatment to build correlations for application in simplified models for, for example, system codes or PSA studies. In contrast, very fine meshes can allow analysis of particularly complex features of the geometry as the upper part of the annular space where occurs the separation of the melt between the subcompartments and the containment. This last point is however still under

investigation and will not be discussed further in this paper. We will also restrict the discussion to 2D geometries although some 3D situations have been studied with the code. However, the most important features are already present with 2D situations and it is sufficient to focus on this limiting case.

4. Flow Patterns Analyzed with MC3D

4.1. Pure Gas Flow. Investigating the pure gas flow has a limited practical interested. However, this is a necessary step particularly if one intends to build analytical simplified models as for system codes. Indeed, the gas is the carrier fluid and it is important to characterize its flow. It is interesting to notice the existence of a single intense convection roll occupying the whole pit (Figure 5). Then, the definition of a characteristic velocity in the pit (where occurs the entrainment), as required by simple lumped parameter models, is not an easy task. Along the wall, the velocity shows a very strong gradient. On the mean, we find that the upcoming velocity is in the same order as the one at the annular space. The velocity at the break is obviously sonic, but it might be noted that this is not the location of the maximum speed. We obtain a situation which is similar to a Venturi tube with supersonic flow after the contraction.

The vessel depressurization is computed on the basis of an adiabatic flow since no heat transfer is computed between the gas and the vessel. Experiments show that the situation is closer to an isothermal flow. However, the impact on the overall process is very limited. At reactor scale, the impact should be even lower.

4.2. Melt Ejection and Upward Dispersion. The qualification of MC3D regarding the melt and gas ejection out of the vessel have already been discussed in previous analyses [8, 10]. We propose now a visualization for the purpose of illustration and completeness of analysis in Figure 6. At first, the melt flows as an undisturbed jet. Despite the high ejection velocity, the jet fragmentation is limited: due to the small distance between the vessel and the floor in the experiment, the travelling time scale is smaller than the fragmentation time scale. This in fact is not true at full scale: the ejection velocity and then the fragmentation time scale are still the same but the travelling time is increased accordingly to the scale. However, we find that this modification of the flow pattern does not have an important influence on the overall process of dispersion out of the pit. Regarding the impact of the jet with the floor, the code does not (cannot) represent an eventual splashing effect as it was observed in some experiments. However, this splashing does not seem to have a significant effect. More, the effect should also diminish at full scale. Rapidly, a hole is formed inside the melt pool (third picture) and the gas begins to flow out of the vessel with a high velocity. As the gas flows inside the melt, forming first some kind of expanding bubble in the case of large breaks, this one is totally fragmented and dispersed in the pit. However, the drops rapidly hit the floor or the wall and undergo a recoalescence. Before this two-phase flow stage starts, the melt can be accumulated along the wall simply by the effect of inertia. Depending on the vessel pressure, it can either flow back and return on the floor, either be entrained and flow along the wall.

The gas velocity becomes really important only once most of the melt is ejected. During the stage of two-phase flow, the gas velocity is strongly reduced by friction with the dispersed melt. We find that in MC3D calculations, the melt along the wall is really entrained and fragmented only once this essentially single-phase gas flow starts. In MC3D, it is found that the fragmentation mostly occurs as the continuous melt approaches the annular space. It is also seen from Figure 6 that gas flow patterns seen with pure gas flow in Figure 5 are strongly disturbed. We often see the development of two circular rolls (best seen on Figures 8 and 9).

The qualification of the code regarding the experimental results can be shortly discussed with the help of Figure 7 which illustrates the results of a calculation of the test F07 with water as simulant in a 2D geometry (burst pressure = 1.6 MPa, break diameter = 60 mm). There is a mist which is formed in the experimentation due to fragmentation at the edge of the break. This has no identified effect on the dispersion, even for cases with hot simulant. We observe again the formation of a hole inside the jet. This leads to the formation of a kind of pressurized bubble inside the jet. In the present simulation, the bubble breaks just before the jet reaches the floor. This explains why no single-phase liquid flow pattern is detected from the pressure traces in F07. The pictures are taken during the test show that the upward dispersion starts quite lately after about 50–60 milliseconds. For both the calculation and the experiment, we see that the upward ejection begins at approximately the same time as the transition to single-phase flow. This behaviour is confirmed by all MC3D calculations with both the P′4 and EPR geometries. It also confirms the representativity of experiments as CE/CES tests [6] where the melt is initially placed on the pit floor.

4.3. Gas Flow Characteristics during Melt Ejection and Dispersion Steps. Some further characteristics of the gas flow can be qualitatively discussed with the support of Figures 8 and 9. For a characteristic calculation with hot reacting material, both the gas temperature (Figure 8) and the vapour partial pressure (Figure 9) are strongly affected by the fragmentation stage at the break. In this calculation, we set the time scale for melt oxidation at the relatively small value of 10 ms. The real characteristics of thermite oxidation kinetic has not been yet investigated but it is likely that the phenomenon is very rapid due to the high temperature. We however are only seeking here for a qualitative description. As soon as the two-phase flow appears at the break, the gas is strongly heated.

At the experimental scale, the pit is entirely heated at a temperature close to the melt one in a few milliseconds. Meanwhile (but independently in fact) the vapour pressure has mostly disappeared from the pit (Figure 9). The minimum residual value of the vapour partial pressure is due to the limitation of oxidation set in the calculation close to

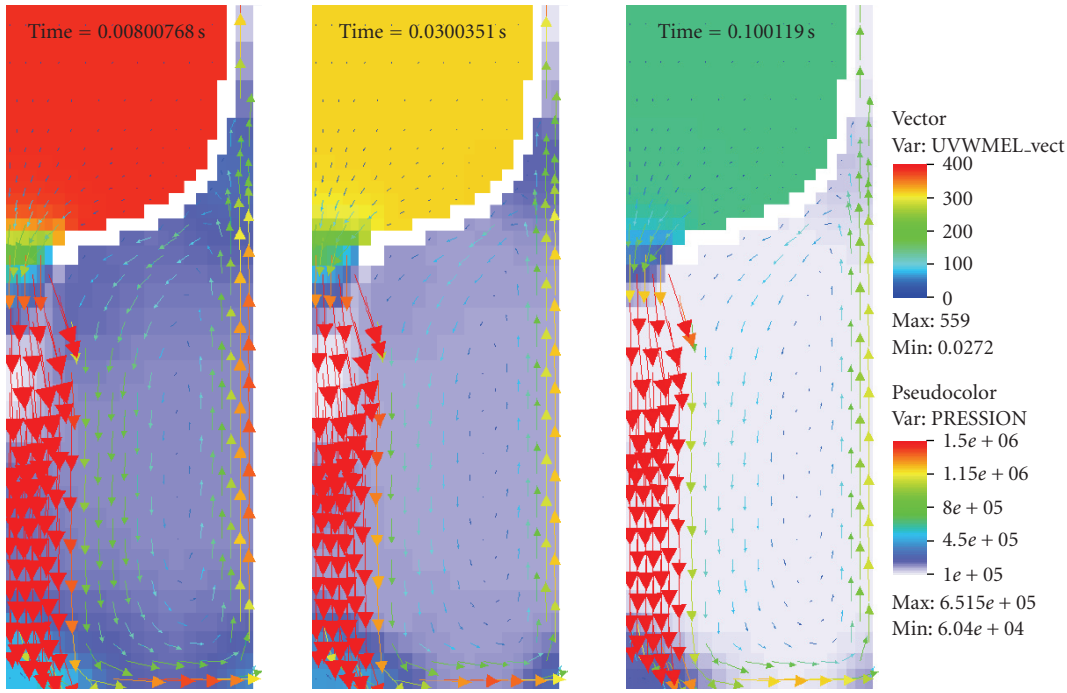

Figure 5: Illustration of pure gas flow computed with MC3D at three different times with DISCO P′4 "2D" geometry (background colour according to pressure).

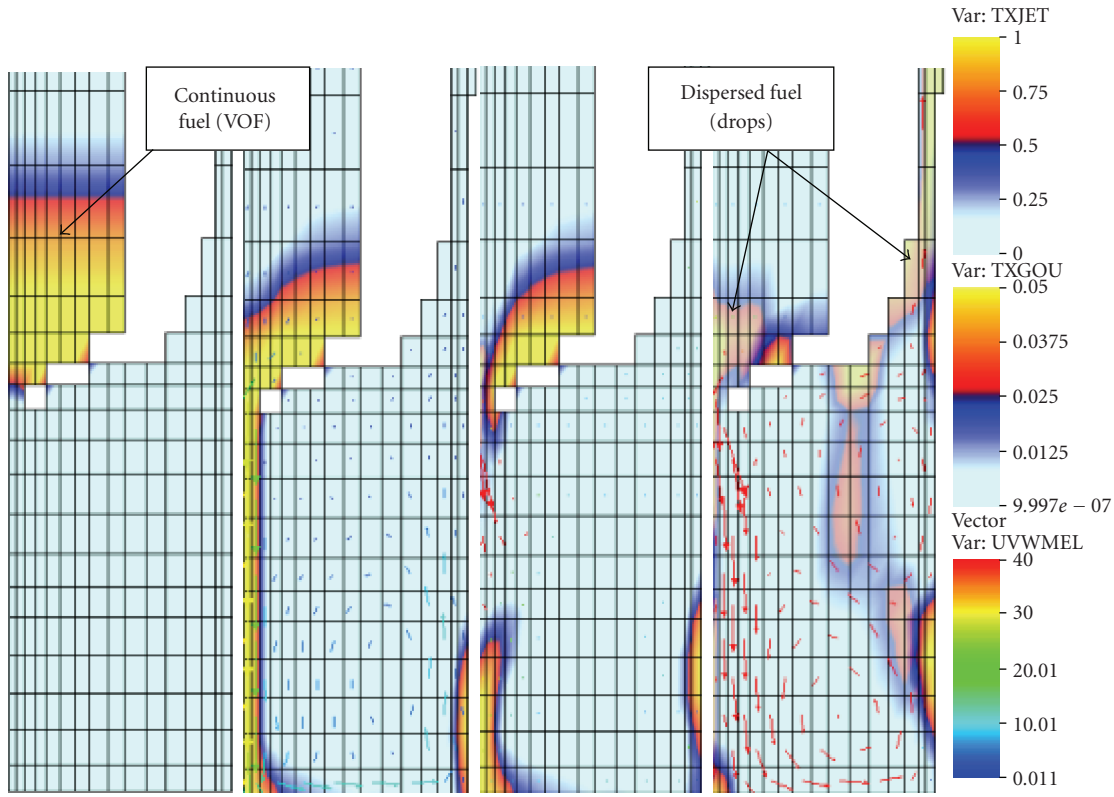

Figure 6: Visualization of melt ejection fragmentation and upward dispersion in a typical simulation of DISCO integral test (P_v = 19 bar, D_b = 30 mm, Al_2O_3-Fe thermite at 2500 K, vessel gas: vapour). Legend: top: continuous fuel field volume fraction, middle: fuel drop volume fraction, bottom: drop velocity (m/s). Frames at times t = 0, 0.08, 0.09, and 0.3 seconds.

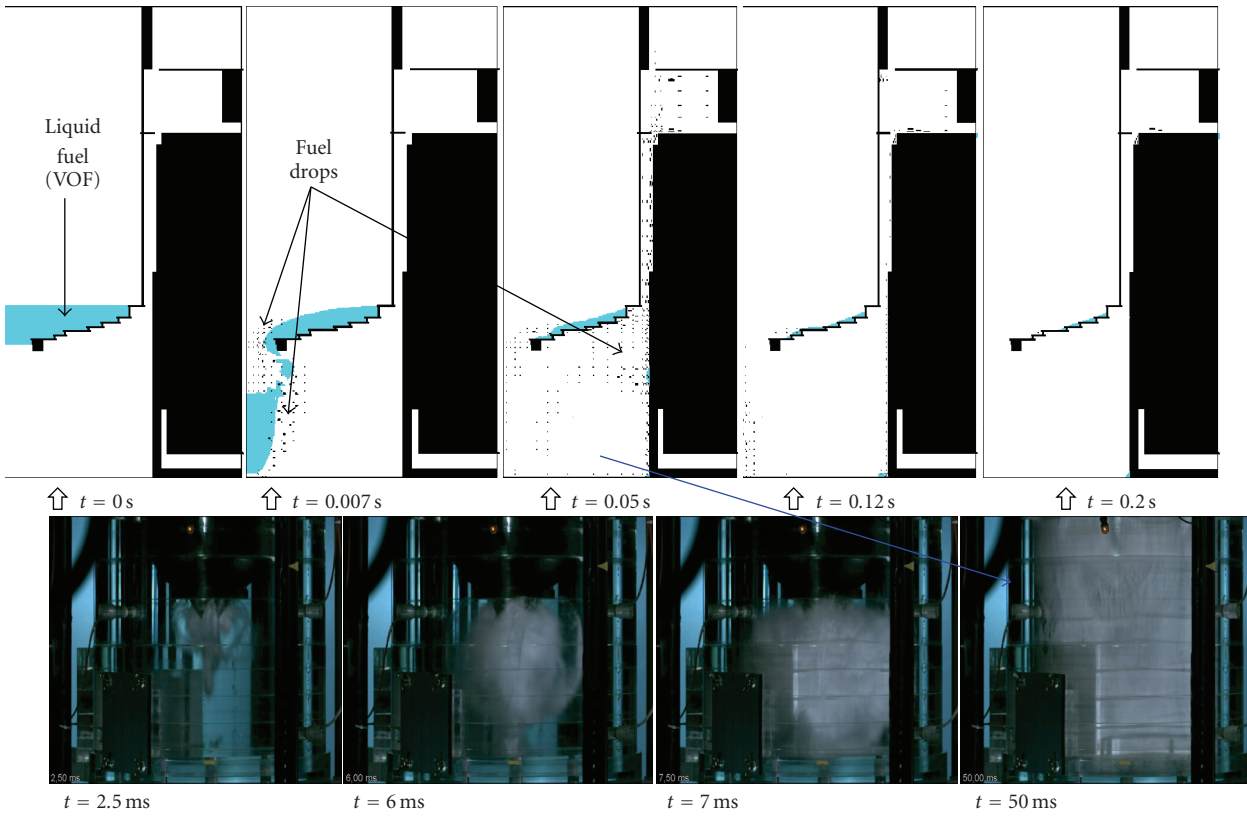

Figure 7: Pictures of the pit during test F07 (bottom) compared with a visualization of flow computed with MC3D (top).

1000 pa. When the flow becomes essentially a single-phase gas flow, then the pit gas starts cooling down and fresh vapour can re-enter in the pit. As the dispersion process occurs mostly during this single-phase gas flow, it is seen that dispersion occurs with very transient conditions regarding the gas properties.

5. Dispersion Correlation

5.1. Method and Limitations. Finding correlations that would work for any case and any geometry has been the subject of work of many researchers in the past (see the important number of correlations in the CONTAIN code). Our purpose is to concentrate on a particular geometry and correlate parameters regarding the initial physical conditions (gas, melt) and the break section. The limited number of experiments makes this task difficult. One of the obvious interests of Computational Fluid Dynamics (CFD) tools (when qualified) is to allow a substitution of the experiments with the calculation. The experiments at our disposal are mainly used to qualify the codes in some particular simulating situations and to verify the correlation. Then we propose a mixed method where we will seek for a correlation with parameters that need to be adjusted thanks to CMFD calculations and validated with experimental results.

At first, we have to admit that, unless using fine 3D meshes, it is necessary to treat the dispersion globally, that is, without taking into account the particular paths to the containment and subcompartments. The particular problem of separation of melt can be investigated only with a different method. Also, the bottom exit path cannot be treated easily unless 3D calculations are performed. Although this is feasible, previous estimations tend to show that the 3D complete geometry behaves similarly to the 2D case [10]: the inceptions of entrainment were found very close and only the maximum dispersed fraction were changed. Then, it is likely that we can use the 2D geometry to build a general correlation that will be calibrated for the 3D case with experimental results and some additional particular 3D calculations. It is also rather clear that we cannot have a very fine precision regarding the maximum possible dispersal. In the code, this depends mostly on the meshing and numerical methods. In the experiment and real reactor case, it depends on local complex geometries particularities that cannot be reproduced.

5.2. Theoretical Analysis. The first idea that comes in mind to correlate the upward dispersion is to relate it with the ability of the gas to entrain melt droplets. The relative terminal velocity of a monodispersed droplet population in an ambient fluid can approximately be given by

$$V \approx V_0(1-\alpha_d) = (1-\alpha_d)\sqrt{\frac{8}{3}\frac{R_d}{C_{d0}}\frac{|\rho_d-\rho_a|}{\rho_c}g}, \quad (5)$$

where the subscript 0 stands for one single droplet.

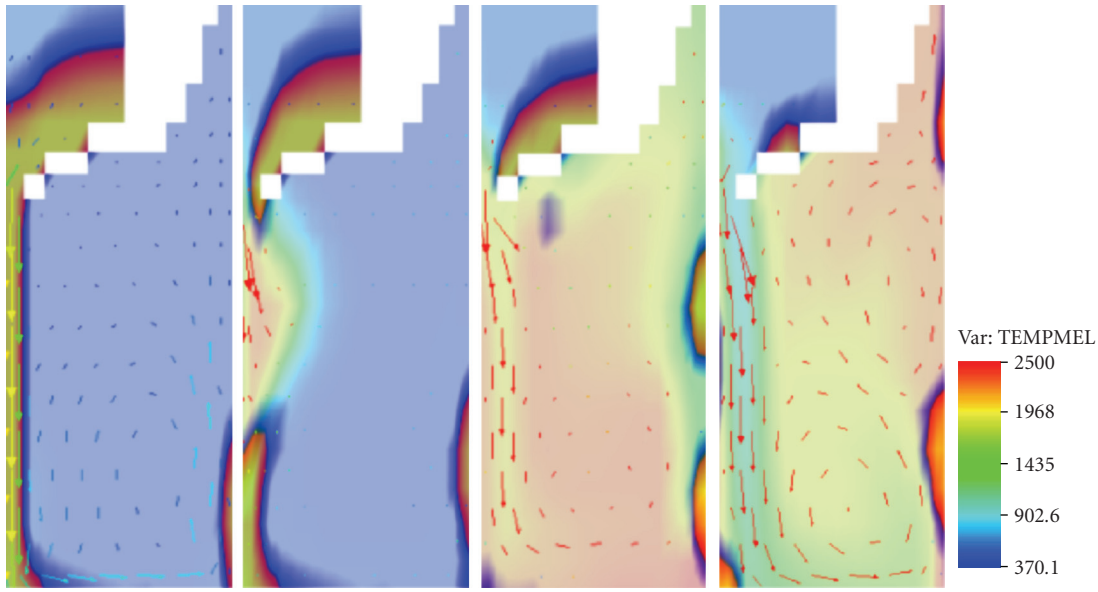

FIGURE 8: Visualization of gas temperature during the phase of melt ejection (same calculation as in Figure 6). Legend: gas temperature (K), see also Figure 6 for continuous melt volume fraction and drop velocity. Frames at times $t = 0.08$, 0.09, 0.15, and 0.3 second.

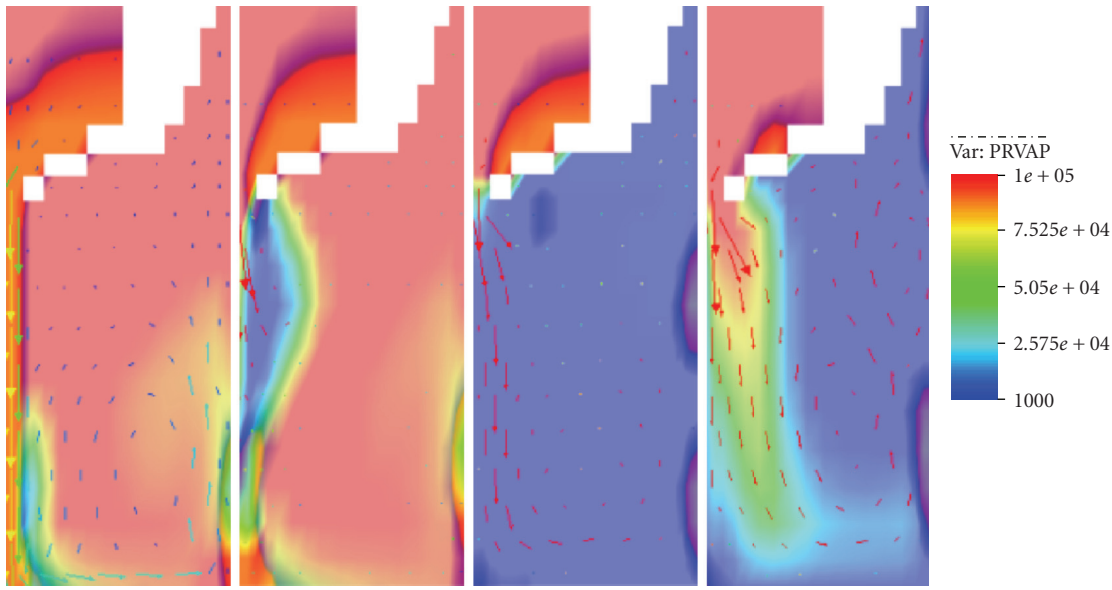

FIGURE 9: Visualization of vapour partial pressure during the phase of melt ejection (same calculation as in Figure 6). Legend: vapour partial pressure (Pa), see also Figure 6 for continuous melt volume fraction and drop velocity. Frames at times as for Figure 8: $t = 0.08$, 0.09, 0.15, and 0.3 second.

On the other hand, the relative flow tends to fragment the drops up to equilibrium. If one single drop is stable for a relative Weber number of, say, 12, it is found experimentally [11] that the mean Weber number of the created drops (relatively to the initial velocity) is lower. More precisely, the drops are not created such that the Weber is equal to the critical one but can be significantly smaller. We will call this number the equilibrium Weber number and take it as an uncertain parameter that should range from 1 to 6. The equilibrium Weber number gives us a second relationship between the velocity and the drop mean diameter:

$$\mathrm{We}_{\mathrm{eq}} = \frac{2\rho_g \Delta v^2 R_d}{\sigma}. \tag{6}$$

In MC3D, the equilibrium Weber number gives its actual limit for secondary fragmentation. Considering only dispersed flow with low drop volume fractions and drop

densities far higher than the ambient one, one has an expression of the relative velocity as

$$\Delta v^2 \approx \sqrt{\frac{4}{3}\frac{\sigma \mathrm{We}_{\mathrm{eq}}}{C_{d0}}\frac{\rho_d}{\rho_a^2}g}. \tag{7}$$

This gives a lower limit for the gas velocity that can lead to melt entrainment. This in fact defines a dimensionless number called the Kutadeladze number:

$$K = \frac{\rho_a v^2}{\sqrt{\sigma \rho_d g}}, \tag{8}$$

and a criteria for entrainement can be expressed as

$$K \geq K_c \equiv \sqrt{\frac{4}{3}\frac{\mathrm{We}_{\mathrm{eq}}}{C_{d0}}}. \tag{9}$$

If the drop diameter is in the inertial range, C_{d0} is about 0.5 and we obtain a critical Kutadeladze of about 3. The Kutadeladze number gives a criterion for inception of entrainment but our purpose is to find a correlation giving the upward dispersion fraction. It is however likely that we can use this number for this purpose. The dispersion is a function of the mass flow rate and thus we will seek for a relation using the square root of the Kutadeladze number, that is,

$$F_d = f\left(\sqrt{K}\right). \tag{10}$$

The problem now is to have a characteristic gas velocity in our system. The fragmentation and entrainment occurs in the reactor pit where no obvious characteristic velocity can be defined. However, it is likely that the velocity along the wall can be related to the velocity in the annular path. Then, for the purpose of a correlation, one can use the annular path velocity as a characteristic velocity to compute the Kutadeladze number. For the case of pure gas flow, all evaluations show that the pressure inside the pit comes very rapidly to equilibrium and the flow is rapidly in a quasisteady state. In that case, the mass flow at the entrance and outlet of the pit are balanced. At the vessel break, the flow is, in all cases of interest, sonic. The classical theory of compressible gas flow gives us the mass flow rate as

$$Q_b = 0.56 A_b P_v \sqrt{\frac{\gamma M_m}{R T_v}}. \tag{11}$$

Then, the velocity in the annular space is

$$v_a = \frac{Q_b}{A_a \rho_a} = 0.56 \frac{A_b}{A_a \rho_a} P_v \sqrt{\frac{\gamma M_m}{R T_v}}. \tag{12}$$

The correlation will then take the form

$$F_d = f\left(0.56 \frac{A_b}{A_a} P_v \sqrt{\frac{\gamma M_m}{R T_v}} (\sigma \rho_d g)^{-1/4} \sqrt{\frac{1}{\rho_a}}\right). \tag{13}$$

In this relation, we identify two difficulties. The first difficulty comes from the influence of the break diameter.

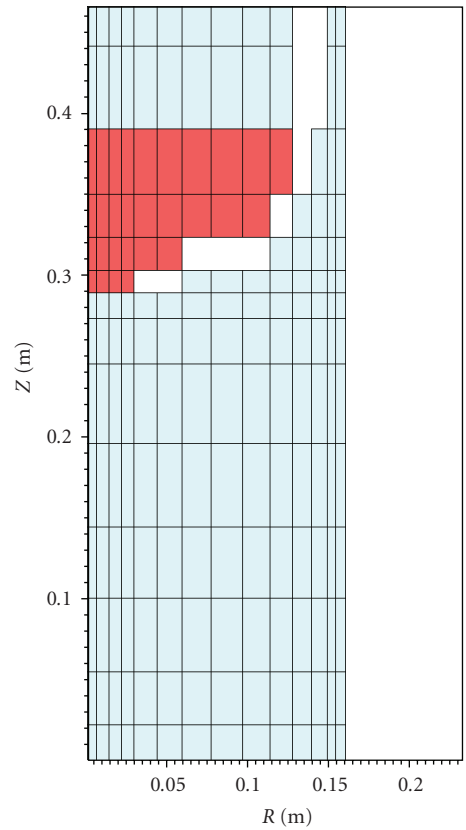

Figure 10: View of the grid used for the evaluation of correlation with MC3D (pit region only, white zone : solid structure, red : corium pool).

A small break will increase the duration of the gas flow, having then an influence on dispersion opposite to the one in (13) (i.e., inversely proportional). Also, for a small break, the two-phase flow stage is longer and there might be an important pressure loss in the vessel during this stage. Then the influence is not so simple. On the overall, the influence should not be linear but rather proportional to A_b^n with a small exponent n. The second difficulty comes from the influence of gas density in the pit. This one is not known a priori and we have seen previously that it should change drastically during the transient.

5.3. Evaluation with MC3D and Comparison to Experimental Data. In order to be able to have a statistical treatment, we use the rough mesh shown in Figure 10, the pit being represented by a 8×15 grid. Such rough mesh has proven to be sufficient to predict the upward dispersion for all tested geometries [10]. Unless indicated, all 2D calculations presented hereafter are done with an equilibrium Weber number of 1. The parameters that have been checked to build the correlation are listed in Table 1 with the range of variation.

Figure 11 shows the influence of break area (scaled with the annular path area). We find that the best fit is obtained with an exponent equal to 1/4 instead of 1, probably due

Table 1: List of parameters checked in the evaluations and range of variation.

Parameters	Minimum value	Maximum value
P_v: vessel pressure (bar)	5	35
T_v: temperature of gas in vessel (K)	380	1000
T_m: temperature of fuel in vessel (K)	(cold) 350	(hot) 2500
D_b: break diameter (mm) => defines area A_b	30	90
ρ_d: fuel density (kg/m^3)	1000	9230
M_m: vessel gas molar mass (g/mol)	(helium) 4	(air) 29
P_0: containment pressure (bar)	1	3
σ: srface tension (N · m^{-1})	(water) 0,07	(thermite) 1
T_0: containment temperature (K)	315	1070

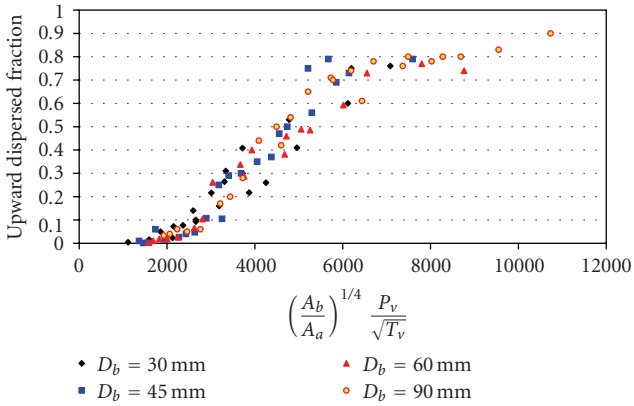

Figure 11: Impact of vessel gas temperature and break diameter on the calculated upward dispersed fraction (all other parameters identical).

to the longer ejection time for small breaks, as expected. The scatter of the data is, as already explained, mostly due to the very rough mesh used. This is a characteristic due to the continuous fuel field numerical treatment (VOF-PLIC), which behaves only approximately with rough meshes. However, in most applications, it is not necessary to have a precise result for a particular situation, but rather a global tendency. On the overall, it is then found that the break diameter is not a very critical parameter, thus limiting the impact of the important uncertainty regarding the break characteristic during a severe accident. We also see on this figure the good correlation with the function $P_v/\sqrt{T_v}$. Then, the temperature inside the vessel is also an important parameter.

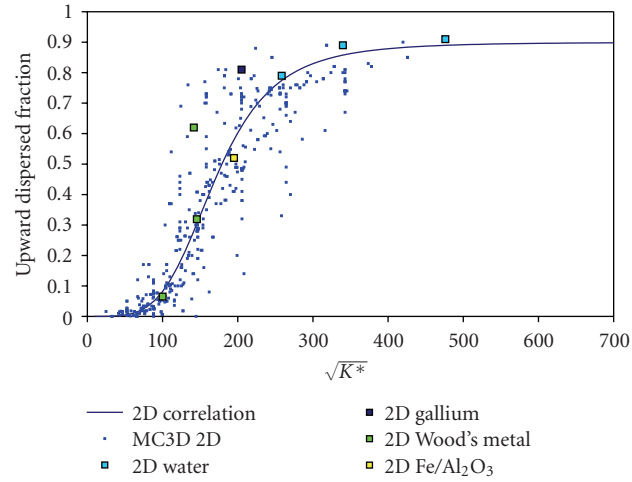

Figure 12: All calculations versus proposed correlation for 2D case, and available 2D experimental data.

The impact of the other parameters not explicitly appearing in (13) (but eventually through the gas density) is found quite mild. We do not see a significant impact of the initial containment pressure (if limited to 3 bars). In contrast, the melt temperature seems to increase noticeably the dispersion. However, in the hot calculations, the combustion effects are not included and it is likely that the increase in containment pressure would lead to a decrease in dispersion. Due to the various uncertainties, it did not seem relevant to include additional parameters in (13) and the gas density was simply changed to a reference density ρ_0 (1 kg/m^3).

The overall result of all the 2-D calculations is plotted in Figure 12 with the available experimental data and the best fit correlation of the form

$$Fd = \frac{Fd_{\max}}{2}\left\{1 + \tanh\left[A^* \log\left(\frac{\sqrt{K^*}}{\sqrt{K^*_{50}}}\right)\right]\right\}, \tag{14}$$

$$\sqrt{K^*} = \left\{0.56\left(\frac{A_b}{A_a}\right)^{1/4} \frac{P_v}{\sqrt{T_v}} \sqrt{\frac{\gamma\, M_m}{R}} \left[\rho_d g \sigma\right]^{-1/4} \frac{1}{\sqrt{\rho_0}}\right\},$$

$$\rho_0 = \text{reference density} = 1\,\text{kg/m}^3. \tag{15}$$

We find, for the "2D" DISCO $P'4$ experimental facility: $\sqrt{K^*_{50}} = 170$, $A = 5$, $F_{d,\max} = 0.9$.

It will be emphasized that the experiments confirms that integral tests behave approximately in the same way as cold tests.

The correlation can now be compared to the experimental 3D data, just changing the maximum dispersion in (14). This is done in Figure 13. In such case, we only modify the maximum dispersion which from experimental results but also MC3D calculations (see [10]), is about 0.6. There is a somewhat important scatter of the data around the correlation. However, considering the very important variations of the physical conditions between a nonreacting water flow and an integral test with chemical reactions,

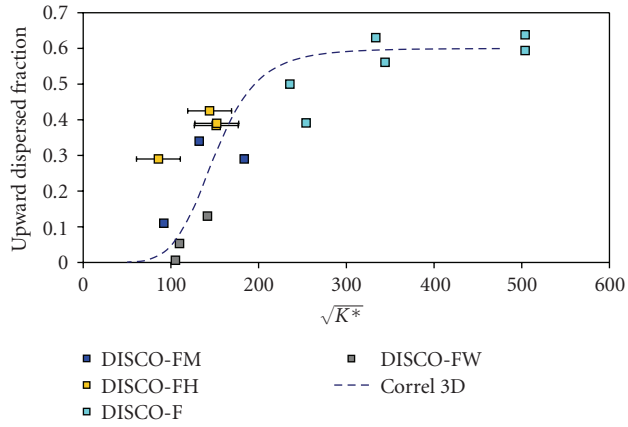

Figure 13: Comparison of the correlation (14) with all 3D available experimental data, same parameters as 2D correlation except maximum dispersion.

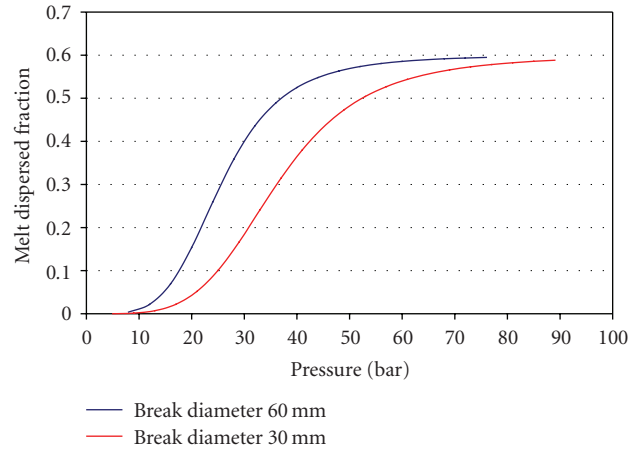

Figure 14: Application of correlation (14) to a case with corium as fuel, and vapor at 550 K in vessel for two break diameters, at the scale of DISCO tests (1/16th).

it can be estimated that the scatter is largely in the uncertainty range of actual conditions during a severe accident and probably of some of the experimental conditions. For the use in a particular problem, it is envisaged to fit more particularly on both the calculations and experimental results (if any) with the particular conditions of consideration. The fit might then be calibrated using corium physical properties, vapour as a driving gas, and high melting temperature.

Nonetheless, with the help of MC3D, it was possible to find a best fit by modifying slightly the influence of melt density (exponent 1/2 instead of 1/4) and suppressing the surface tension. Since no rational can be found for these modifications, and due to the high uncertainty attached to this evaluation, we estimate that correlation (14) is sufficeint for pratical evaluations.

Using the derived correlation, we can now already fix ideas of what can be expected for a representative DCH in a severe accident with however the scale of DISCO tests. This is presented in Figure 14 (see legend for conditions). The inception of entrainment is expected to occur approximately at 20 bars. A full dispersion is obtained at approximately 40 bars with a large break (1 m at full scale) and 60 bars with an intermediate one.

6. Scaling

The scaling is of course a key issue. A large uncertainty can be attached to this problem if one relies only on experimental results and simplified models. The use of CMFD codes as MC3D allows investigating this issue with an increased confidence, although scaling can have an important effect on some specific constitutive laws, particularly when it is obtained mostly with a simple mesh size modification. In the particular case of DCH, the primary fragmentation (i.e., continuous fuel to drops) seems the most critical model regarding mesh sensitivity. However, our evaluations showed a strong sensitivity to the secondary fragmentation model which led us to consider an equilibrium Weber number of the order of the unity. Then, the primary fragmentation model

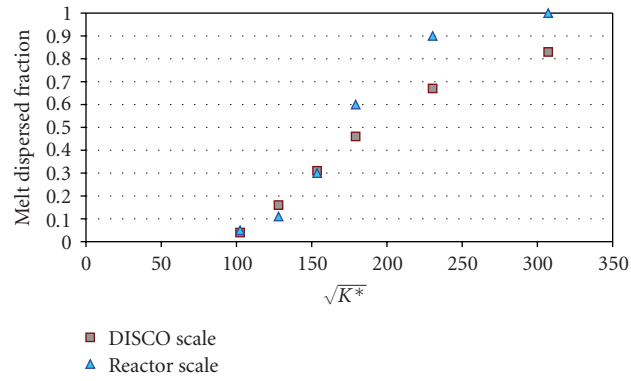

Figure 15: Impact of scaling regarding the upward fuel dispersion estimated with 2D MC3D calculations in cold conditions and heavy metal (Wood's metal).

is expected to have, on the overall, a limited impact. Thus, the impact on scaling on the models is expected also to be limited.

Regarding dispersion, the calculations did not show a noticeable effect regarding the global results of melt dispersion. Some of the flow patterns are different particularly regarding melt ejection. As an example, at full scale, the nearly intact jet issuing the vessel is not visible at full scale. In most cases, the aerodynamic processes of fragmentation have sufficient time to break the jet before hitting the floor. For large break, the two-phase flow also occurs before the melt-bottom contact. Then on the overall, the initial melt fragmentation is more intense. However, due to the recoalescence along wall and floor, there is no really clear effect in the calculations. Figure 15 gives an example of comparison of scaling effect. The dispersion is plotted as a function of the modified Kutadeladze number (see previous section). What has been found from the various trials of calculation at full scale is that the inception of dispersion is not modified. For conditions with strong dispersal, the effect

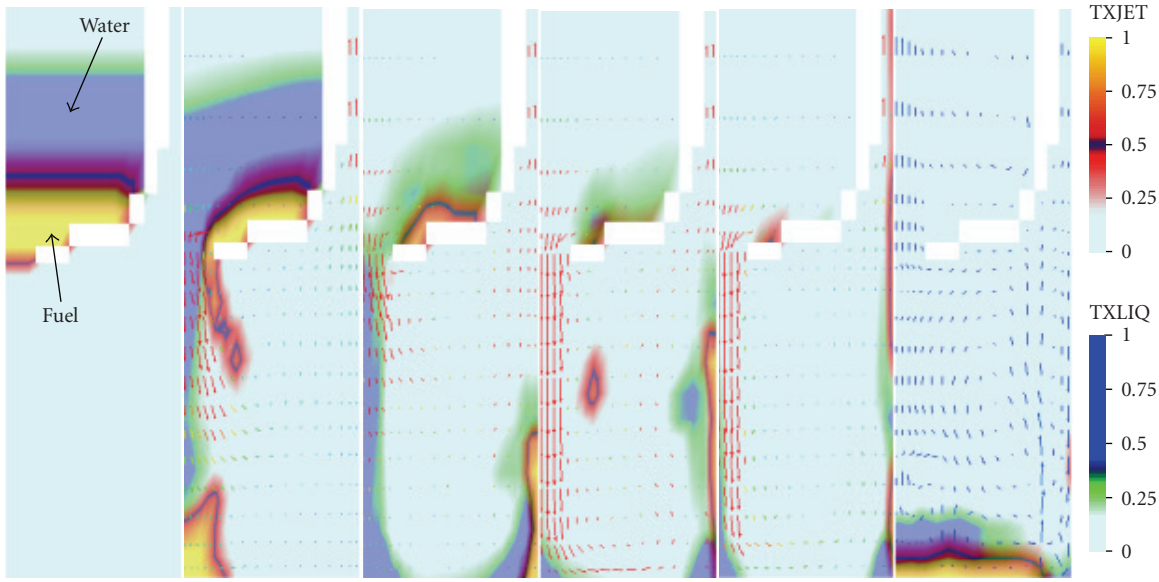

Figure 16: Example of calculation made with a situation where an important mass of saturated water is present in the vessel at the time of failure. $P_v = 7$ bars, geometry as disco FH05 (see, e.g., Figure 6). Frames at times $t = 0, 0.04, 0.12, 0.16, 0.3, 0.75$ seconds.

is not clear and, on the mean, no important effect has been detected.

It should be recalled that MC3D does not compute effects related to the presence of the walls such as friction or heat transfer. At large scale, the impact of wall should be smaller due to a smaller ratio surface/volume. We did not notice important effects at DISCO scale so it is likely that these effects are also minor at reactor scale. On the overall, we conclude that the scaling has no noticeable effect regarding the dispersal processes of the melt.

7. Further Potential Capabilities of MC3D

The "academic" problem of DCH does not take into account the presence of water. However, the probability for presence of water either in the vessel or in the pit is rather high for various reasons. MC3D seems a particularly well-suited code for taking into account the presence of water at least regarding the problem of dispersion. The case of water in the pit is quite easy, as MC3D is already used for the evaluation of Fuel Coolant Interaction in the so-called exvessel situation. This is nothing else, for the code, than a DCH with water in the pit. The case of water in the vessel either just above the melt, either somewhere trapped in the lines of the Reactor Cooling System is more interesting since the flashing might induce a longer pressurization in the pit and then an enhanced dispersion. The case of water lying above the melt has been investigated recently for demonstration purpose and is illustrated in Figure 16.

It is very likely that the water in the vessel will be close to saturation. Then, at the exit from the vessel, a flashing phenomenon will occur, where some part of the water will evaporate quasi-instantaneously. In the example given, the overpressure is only 5 bars, so far below the inception of entrainment without water. Another test with a smaller mass of water and 8 bars as overpressure gives a full dispersion. We find that the flashing increases strongly the pressure in the pit and then the dispersion. In case of large masses of water, there is a large remaining part of water which is expelled together with the melt. This expelled water might inert the combustion and reduce the pressurization. In other situations, the water might flash completely thus avoiding these limiting effects. The impact of water is still under investigation at IRSN.

8. Conclusion and Perspectives for Further Developments

We highlighted the interest of the use of qualified multiphase flow codes as MC3D for the evaluation of the DCH phenomenon during the course of a hypothetical severe accident. Due to the complex geometries of NPPs, this problem has for a long time been faced to the technical difficulties in representing adequately the phenomenon with simplified analytical models. Correlations were largely inspired by experimental results with only restrained applications and weak confidence in extrapolations to real material and real scale.

With the use of the computer code MC3D with relatively rough meshes, we could present a method for developing a dispersion correlation. For each geometry (EPR, large pit reactors), the calculations can be used to calibrate precisely the correlation, as it has been presently done for the case of French P′4 reactors.

For a full evaluation of the phenomenon, one needs a model of combustion. However, even codes dedicated to combustion can have some difficulties to evaluate precisely the phenomenon. Then, despite the progress made and

presented here, we are still faced to a complex problem. In the case of MC3D, it is then envisaged to seek only for a simple model, dedicated to the problem.

Despite this difficulty we have elaborated some patterns of explanation for the dispersion of the melt, we find that 2D and 3D situations might not be so different. We are also able to specify with a good confidence the range of physical conditions for which the dispersion can occur and then propose a range of conditions for which the phenomenon cannot threaten the containment. We can also integrate some supplementary conditions that are usually not taken into account as the presence of water.

Nomenclature

Latin

A:	Section, area (m^2), coefficient in correlation(14)
c_i:	Characteristic velocity of instability ($m \cdot s^{-1}$, (2))
C_d:	Friction coefficient
D:	Diameter (m)
F:	Dispersed fraction
g:	Gravitational constant ($m \cdot s^{-2}$)
k:	Wave number (m^{-1})
K:	Kutateladze number
M:	Molar mass ($kg \cdot mol^{-1}$)
N_f:	Fragmentation parameter(1)
P:	Pressure (pa)
Q:	Mass flow rate ($kg \cdot s^{-1} \cdot m^{-2}$)
R:	Radius (m), gas constant
T:	Temperature
v, V:	Velocity ($m \cdot s^{-1}$)
We:	Weber number

Greek

Γ_f:	Volumetric fragmentation rate ($m \cdot s^{-1}$, (1))
γ:	Adiabatic index
ρ:	Density ($kg \cdot m^{-3}$)
σ:	Surface tension ($N \cdot m^{-1}$ or $J \cdot m^{-2}$)

Subscript

a:	Ambient or annular space
b:	Break
c:	Critical
d:	Drop or dispersed
eq:	Equilibrium
f:	Fuel
v:	Vessel

Acknowledgment

The authors gratefully acknowledge Dr. Leo Meyer from the Forschungszentrum Karlsruhe (FzK) for successfully conducting the DISCO program.

References

[1] T. K. Blanchat and M. D. Allen, "Experiments to investigate DCH phenomena with large-scale models of the Zion and Surry nuclear power plants," *Nuclear Engineering and Design*, vol. 164, no. 1, pp. 147–174, 1996.

[2] K. E. Washington and D. C. Williams, "Direct containment heating models in the CONTAIN code," Tech. Rep. Sand94, UC-610, Sandia National Labs, Albuquerque, NM, USA, 1995.

[3] R. Meignen, S. Mikasser, C. Spengler, and A. Bretault, "Synthesis of analytical activities for direct containment heating," in *Proceedings of the European Review Meeting on Severe Accident Research (ERMSAR '07)*, Karlsruhe, Germany, June 2007.

[4] R. Meignen, D. Plassart, C. Caroli, L. Meyer, and D. Wilhelm, "Direct containment heating at low primary pressure: experimental investigation and multidimensional modelling," in *Proceedings of the 11th International Topical Meeting on Nuclear Reactor Thermal Hydraulics (NURETH '05)*, Avignon, France, October 2005, paper no. 164.

[5] R. Meignen, "Status of the qualification program of the multiphase flow code MC3D," in *Proceedings of the International Congress on Advances in Nuclear Power Plants (ICAPP '05)*, vol. 1, pp. 368–379, Seoul, South Korea, May 2005, paper no. 5081.

[6] K. Blanchat, M. M. Pilch, and M. D. Allen, "Experiments to investigate direct containment heating phenomena with scales models of the calvert cliffs nuclear power Plant," NUREG/CR-6469, SAND96-2289.

[7] L. Meyer and M. G. Gargallo, "Low-pressure corium dispersion experiments with simulant fluids in a scaled annular cavity," *Nuclear Technology*, vol. 141, no. 3, pp. 257–274, 2003.

[8] C. Spengler, L. Meyer, and R. Meignen, "Investigations of direct containment heating in European reactors: database of integral tests and progress in modelling," in *Proceedings of the European Review Meeting on Severe Accident Research (ERMSAR '08)*, Nesseber, Bulgaria, September 2008, paper no. 3-5.

[9] L. Meyer, "Simulation experiments for centralized liquid sloshing motions," KFK 5090, 1992.

[10] S. Mikasser and R. Meignen, "Computation and analysis of the direct containment heating dispersion process with the multiphase flow software MC3D," in *Proceedings of the International Congress on Advances in Nuclear Power Plants (ICAPP '07)*, vol. 3, pp. 1682–1690, Nice, France, May 2007, paper no. 7300.

[11] M. Pilch and C. A. Erdman, "Use of breakup time data and velocity history data to predict the maximum size of stable fragments for acceleration-induced breakup of a liquid drop," *International Journal of Multiphase Flow*, vol. 13, no. 6, pp. 741–757, 1987.

Hindawi Publishing Corporation
Science and Technology of Nuclear Installations
Volume 2010, Article ID 163279, 11 pages
doi:10.1155/2010/163279

Research Article

Influence of Modelling Options in RELAP5/SCDAPSIM and MAAP4 Computer Codes on Core Melt Progression and Reactor Pressure Vessel Integrity

Siniša Šadek,[1] Srđan Špalj,[2] and Bruno Glaser[3]

[1] *Faculty of Electrical Engineering and Computing, University of Zagreb, Unska 3, 10000 Zagreb, Croatia*
[2] *ENCONET d.o.o., Miramarska 20, 10000 Zagreb, Croatia*
[3] *NPP Krško, Engineering Department, Vrbina 12, 8270 Krško, Slovenia*

Correspondence should be addressed to Siniša Šadek, sinisa.sadek@fer.hr

Received 30 April 2009; Accepted 29 August 2009

Academic Editor: Alessandro Petruzzi

RELAP5/SCDAPSIM and MAAP4 are two widely used severe accident computer codes for the integral analysis of the core and the reactor pressure vessel behaviour following the core degradation. The objective of the paper is the comparison of code results obtained by application of different modelling options and the evaluation of influence of thermal hydraulic behaviour of the plant on core damage progression. The analysed transient was postulated station blackout in NPP Krško with a leakage from reactor coolant pump seals. Two groups of calculations were performed where each group had a different break area and, thus, a different leakage rate. Analyses have shown that MAAP4 results were more sensitive to varying thermal hydraulic conditions in the primary system. User-defined parameters had to be carefully selected when the MAAP4 model was developed, in contrast to the RELAP5/SCDAPSIM model where those parameters did not have any significant impact on final results.

1. Introduction

RELAP5/SCDAPSIM and MAAP4 codes are severe accident (SA) analysis codes capable of modelling all important SA phenomena (reactor coolant system response, core material chemical reactions, oxidation, ballooning and rupture of the fuel rod cladding, core heat-up, degradation and relocation to the lower plenum, etc.). The main difference between them is that RELAP5/SCDAPSIM can only model the in-vessel phase of the SA, while MAAP4 is capable to calculate processes in the containment following the release of water, noncondensable gases, and corium from the primary circuit.

RELAP5/SCDAPSIM code [1], designed to predict behaviour of reactor systems during normal and accident conditions, is being developed at Innovative Systems Software (ISS) as part of the international SCDAP Development and Training Program (SDTP). RELAP5/SCDAPSIM uses the publicly available SCDAP/RELAP5 models developed by the US Nuclear Regulatory Commission in combination with proprietary: (a) advanced programming and numerical methods, (b) user options, and (c) models developed by ISS and other members of the SDTP. The code is a combination of RELAP5 code for thermal hydraulics calculation, SCDAP code for severe accident related phenomena, and COUPLE code for a finite element treatment of the reactor pressure vessel (RPV) lower head.

MAAP4 code is an integral system analysis code for assessing severe accidents in light water reactors (LWRs) following large and small break loss of coolant accidents (LOCAs) and transients. The code was developed for Electric Power Research Institute (EPRI) by Fauske and Associates, Inc. [2]. MAAP4 employs simple models for BWRs and PWRs in which the type and number of components and the geometry are predetermined. The user inputs various parameters for each component such as volumes or masses.

MAAP4 version used herein was MAAP4.0.5.

RELAP5/SCDAPSIM is characterized by its detailed, mechanistic models of severe accident phenomena; however, the calculations can be rather time-consuming. RELAP5/SCDAPSIM typically uses on the order of hundreds

of hydrodynamic components to model the primary system. MAAP4 calculations require minimal computation time with simplified geometry models.

Regarding the thermal hydraulic model, RELAP5/SCDAPSIM employs detailed RELAP5/Mod3 nonequilibrium, nonhomogenous, six-equation representation of single and two-phase flows. The presence of boron and noncondensable gases is also simulated using separate equations for each. The robust RELAP5 modelling is clearly superior to the thermal hydraulic model of MAAP4 code. MAAP4 utilizes simplified but fast-running models for thermal hydraulics description using a fixed nodalization of the primary circuit. MAAP4 solves a set of lumped parameter, first-order differential equations for conservation of mass and energy. Differential equations for momentum conservation are not employed because MAAP4 considers momentum balances to be quasisteady which reduces the momentum equations to algebraic equations [3].

The objective of the paper was to evaluate influence of thermal hydraulic conditions on core damage progression and to compare code results by applying different modelling options. The intention was not general validation of codes but the examination of code results for the same specific transient by using qualified input models. The analysed transient was station blackout in NPP Krško with a leakage from reactor coolant pump seals. Two groups of calculations were performed where each group had a different break area. Break flow areas differed by a factor of two. Thereby, a study of influence of coolant discharge rate from the primary system on the core heat-up and melting propagation was possible to be carried out.

2. Code Models for NPP Krško

2.1. RELAP5/SCDAPSIM Model. The RELAP5/SCDAPSIM model of NPP Krško (NEK) was based on the RELAP5/Mod3.3 model [4] and qualified at the steady-state level [5]. That model has been used for many years now at FER (Faculty of Electrical Engineering and Computing), Zagreb, for accident analyses of plant behaviour following large spectrum of initializing events in all modes of operation. NEK RELAP5/Mod3.3 nodalization scheme is shown in Figure 1. Such detailed nodalization was not based solely on the plant geometrical data but it also took into account operating conditions of the plant systems.

For the purpose of simulation of core melt progression, core fuel assemblies were divided in five regions by grouping similarly powered fuel assemblies together; see Figure 2. Furthermore, to apply correct thermal hydraulic boundary conditions for the fuel rods, five thermal hydraulic channels were modelled in a manner that each group of fuel assemblies was put in a separate hydraulic channel.

When a portion of the core has melted, it may occupy completely the flow channel and therefore block the coolant flow in the axial direction. The flow will be then diverted in the radial direction. To enable the coolant to flow also in the radial direction, hydraulic channels in the core were interconnected radially by crossflow junctions.

2.2. MAAP4 Model. The NEK MAAP4 model [6] was used for the development of NEK Severe Accident Management Guidelines (SAMG) and Krško Full Scope Simulator (KFSS) which simulates various severe accident sequences. Krško SAMGs have been developed based on the Krško IPE (Individual Plant Examination) insights, generic WOG SAMGs [7], and plant specific documents [8–10]. MAAP4 code has been used in Krško IPE to determine success criteria for accident sequences.

As already mentioned MAAP4 uses fixed and coarse nodalization that enables fast code execution. Primary system is represented by six water pools and 19 heat sinks. The core is divided into seven concentric radial rings and 13 axial rows. The active fuel region is represented by ten rows; the core support plate, the lower tie plate, and the lower gas plenum are represented by two bottom rows, and the upper tie plate and the upper gas plenum are represented by the top axial row.

All deterministic thermal hydraulic analyses within the NEK IPE project were performed by MAAP3B, Ver. 18 [11]. Since then (end of 1994) that analysis tool has been further improved and new versions have been issued. The version MAAP4.0.5 was used in the presented analyses. MAAP3B was revised to include major model improvements in areas of the core heat-up, lower plenum phenomenology, corium-concrete interactions, containment and auxiliary building thermal hydraulics, and hydrogen combustion. Furthermore, new models were added to characterize actions that could stop the accident, that is, the in-vessel and the ex-vessel cooling. The mathematical solution techniques were implemented to maintain a quick-running code suitable for extensive accident screening and parameter sensitivity applications. As a part of the development, the code underwent a complete design review.

3. Analysis and Results

3.1. Description of the Scenario. The analyzed accident was station blackout (SBO) with a leakage from the reactor coolant system (RCS) through reactor coolant pump (RCP) seals following their degradation. It was assumed that off-site and on-site (emergency diesel generators) AC power was unavailable. Therefore, the primary system coolant inventory was decreasing due to the unavailability of the high-pressure (HPSI) and the low-pressure safety injection (LPSI) flow. Water was injected only from the accumulators because their operation did not depend on the availability of electrical power. Steam generators (SGs) acted as a heat sink since the turbine driven auxiliary feedwater (TD AFW) pump delivered water to SGs. TD AFW flow was controlled in a manner to maintain the SG narrow range level between 10% and 50%. Those values were in compliance with ECA-0.0 "Loss of all AC power" procedure [12].

Two groups of calculations were performed (Table 1) where each group had a different break area and, thus, a different leakage rate from the RCS. For the first group, the break area was taken from the WOG 2000 RCP seal leakage model [13]. In WOG 2000 model, series of discharge

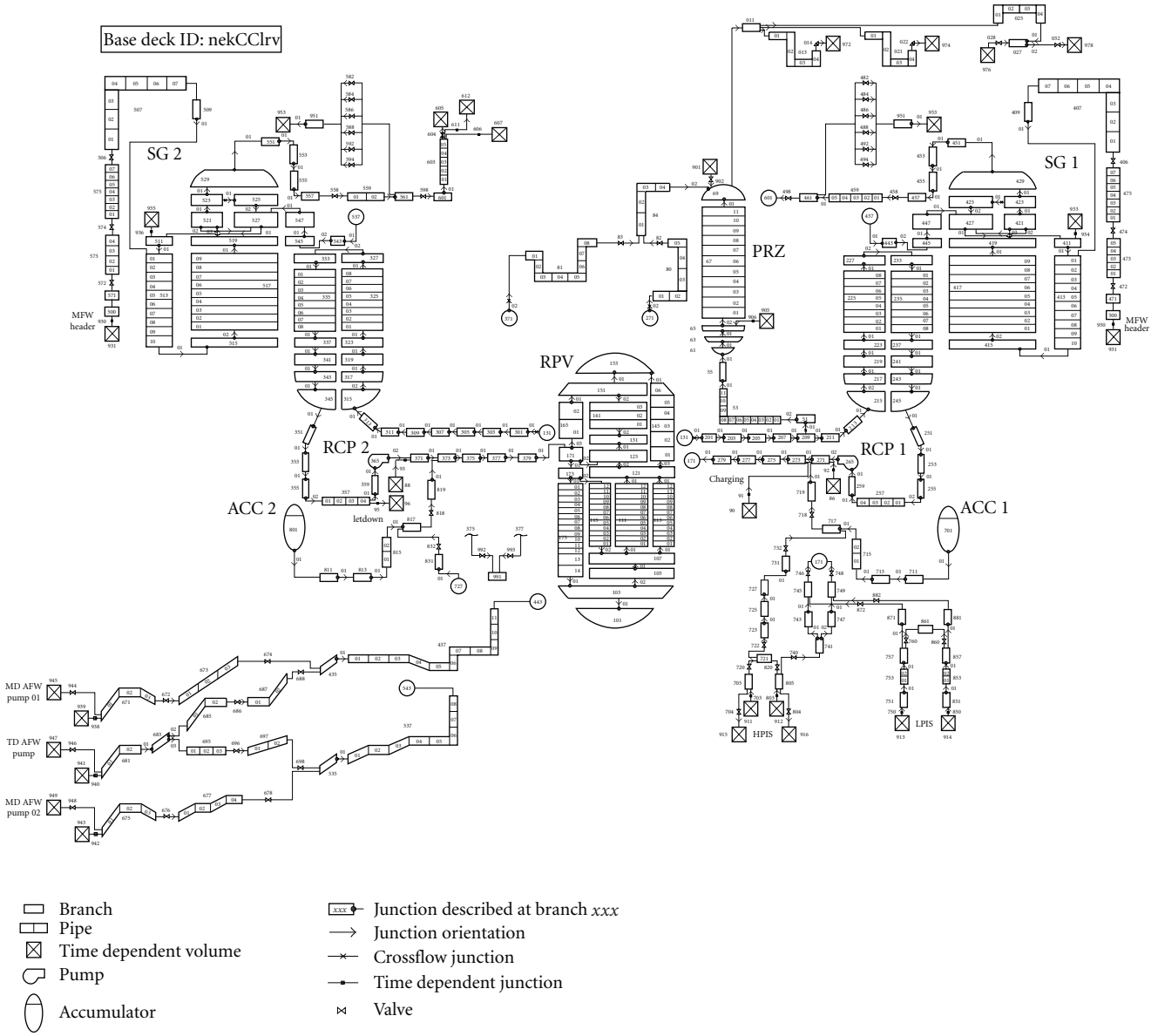

Figure 1: NEK RELAP5/Mod3.3 nodalization scheme.

rates with their respective probabilities were defined. For the presented case, the scenario with the highest leakage rate was chosen: the break area was 10^{-5} m^2 for the first 780 seconds and it increased afterwards to $2.5 \cdot 10^{-4}$ m^2. For the second group, the break area was two times higher ($5 \cdot 10^{-4}$ m^2) but it remained constant throughout the transient. The reason for performing calculations with different break flow areas was to check the influence of thermal hydraulic conditions on accident progression. The smaller break area meant slower depressurization of the RCS and later actuation of the accumulators, thus, the earlier core dryout. The larger break area meant an earlier loss of RCS coolant which would force accumulators' actuation in the earlier phase of the accident. The specific differences between those two cases will be discussed in separate sections.

Table 1: RCP break area for the two groups of analyzed cases.

	Break area
Group 1	0–780 s: 10^{-5} m^2
	>780 s: $2.5 \cdot 10^{-4}$ m^2
Group 2	$5 \cdot 10^{-4}$ m^2

3.2. Modelling of the Hot Leg Natural Circulation. After the hot legs have been voided and prior to the loop seal clearing, a countercurrent natural circulation between the reactor vessel, hot legs, and steam generator U-tubes may develop [14]. Superheated vapour enters the top of the hot leg displacing saturated vapour, which then flows back to the reactor vessel along the bottom of the hot leg. When

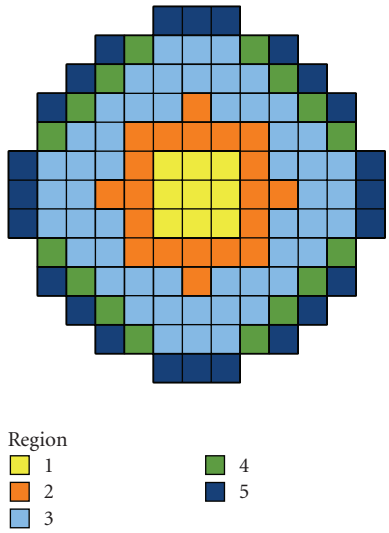

Figure 2: Radial cross-section of the NEK core.

hotter vapour enters the steam generator inlet plenum, it will rise toward the steam generator U-tubes. Vapour enters some of the tubes, displacing cooler steam that was in the tubes. Displaced vapour enters the outlet plenum, then reenters other steam generator tubes, forcing vapour into the inlet plenum. A density gradient is thus established between the tubes which supports the natural circulation. Once the loop seals have cleared, the natural circulation will be terminated.

Hot leg countercurrent flow can affect the structural integrity of the RCS piping. Heating of the pipes and steam generator tubes may lead to melting and creep rupture failure of those components.

Hot leg natural circulation model is an integral part of the MAAP4 code and no specific rearrangement of the input deck is needed to invoke that model. On the other hand, to allow the hot leg countercurrent flow in the RELAP5/SCDAPSIM code, the primary system should be renodalized in a manner to split the hot legs and U-tubes as shown in Figure 3. In addition, the loss coefficients need to be adjusted to correctly simulate mixing in the SG inlet plenum. Preliminary calculations with the new model did not reveal any increase of the creep failure probability of the RCS piping, contrary to the findings of MAAP4 calculations. In the accident with a high leakage rate from the RCS, the loop seals will clear early during the transient; so the impact of the hot leg natural circulation will not be so significant. Nevertheless, in MAAP4 calculations the hot leg pipe creep failure did occur; so this phenomenon cannot be ruled out. MAAP4 predicted high RCS piping temperatures (1300 K) which were the direct cause for the pipe failure. RELAP5/SCDAPSIM piping temperatures were lower (650 K), and so the pipes remained intact.

Taking this into account, two different MAAP4 calculations were performed, one with the hot leg creep failure and one without it. That was necessary in order to make correct comparison between the two codes.

3.3. Group 1 Cases

3.3.1. MAAP4 Calculation. Two MAAP4 calculations were performed: one that takes into account and the other that does not take into account the creep rupture of the hot leg piping. Those two calculations were performed to examine the influence of the hot leg piping failure on the core damage progression and to make a comparison with RELAP5/SCDAPSIM results. Namely, contrary to MAAP4 calculation, RELAP5/SCDAPSIM did not calculate the creep failure of the hot leg; so to compare correctly the two codes, the creep failure had to be turned off in the MAAP4 calculation.

Hot leg creep failure at 10300 seconds caused primary system pressure to decrease rapidly (Figure 4). When pressure dropped to 5 MPa, accumulators started to inject water in the RCS. In the case of no hot leg creep failure, accumulators gradually injected water in small intervals because the primary system depressurized at a slower rate. More water was injected in the core when the hot leg failed because all water inventory from the accumulators was discharged into the RCS. Collapsed water level in the RPV is shown in Figure 5. After the breach of the hot leg, water level increased instantly providing higher rate of heat removal from the core and its supporting structures.

Figure 6 shows the core maximum temperature for the two cases. The core started to melt in the center and later the process of melting progressed toward the core baffle. Once the core baffle failed, corium slumped through the bypass region between the core baffle and the core barrel in the RPV lower head. In the case with no hot leg creep rupture the core baffle failed at 11500 seconds, and when the hot leg rupture was taken into account the baffle failed at 16700 seconds. Accordingly, the RPV wall failed later in the second case.

Although the hot leg failure did not have almost any influence on the maximum core temperature, the structures at the core periphery for the case with the creep failure were much better cooled, their temperatures were lower, and so the core baffle failed later.

3.3.2. Comparison between MAAP4 and RELAP5/SCDAPSIM Calculation. Figures 7–10 show different variables as calculated by the two codes. MAAP4 calculation did not take into account the possibility of the hot leg creep rupture in order to be consistent with RELAP5/SCDAPSIM calculation.

A good agreement in the primary system pressure (Figure 7) prior to accumulator actuation between the two codes is apparent which meant that both codes calculated the same rate of coolant discharge from the RCS. Boiling of water injected from the accumulators caused significant increase of pressure as calculated by RELAP5/SCDAPSIM. That pressure increase terminated further water injections for the next 3000 s and left the core dry. MAAP4 calculation did not show such behaviour of the RCS. Pressure slightly oscillated around 4 MPa, accumulators were more or less active all the time, and the bottom part of the core was covered as long as water was injected into the reactor vessel (Figure 8).

Core maximum temperature (Figure 9) was also pretty well reproduced. A larger discrepancy was observed in

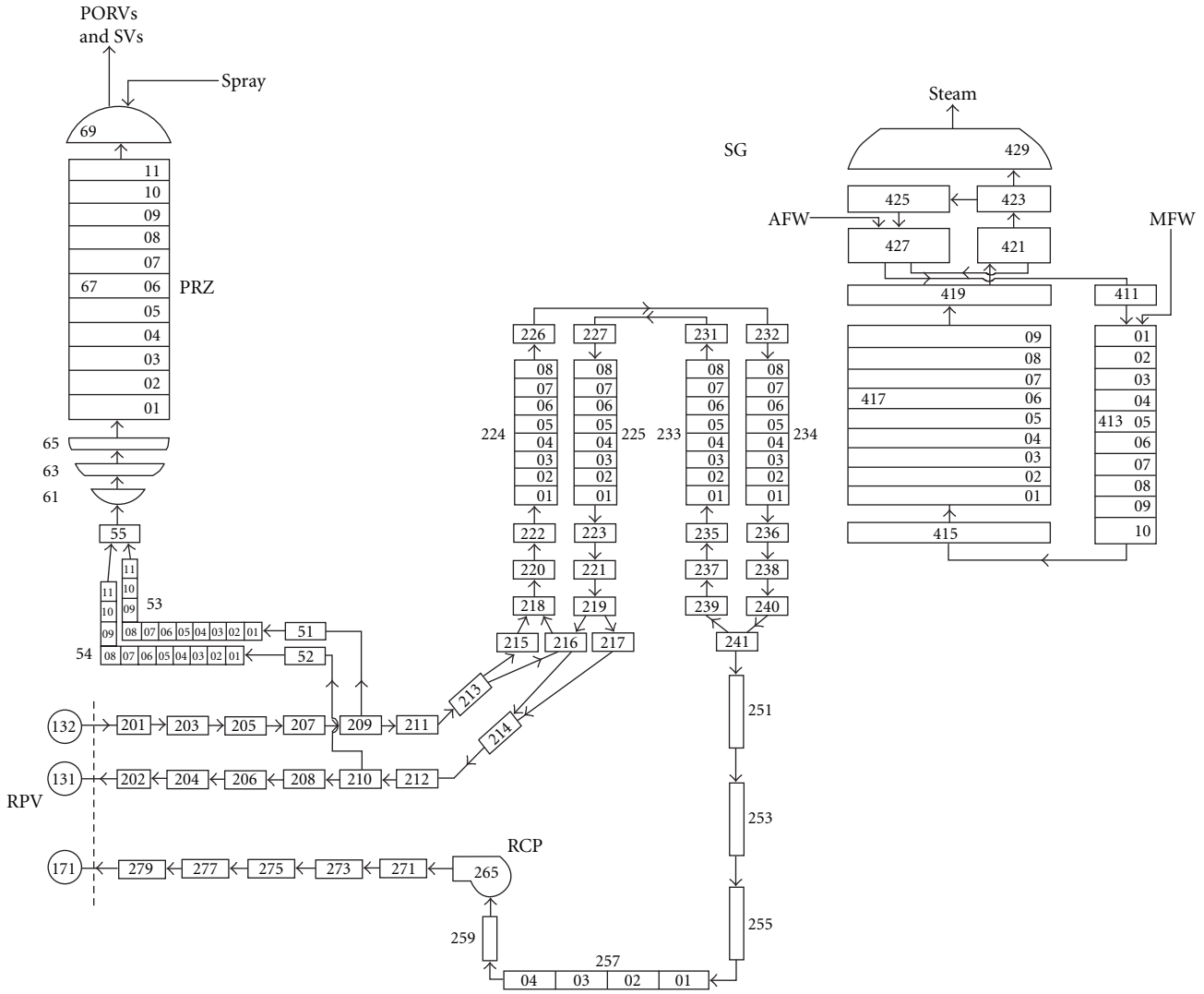

Figure 3: RELAP5/SCDAPSIM nodalization for modelling natural circulation.

Table 2: Composition of molten material in the reactor vessel lower head, Group 1.

Material	UO_2 [kg]	ZrO_2 [kg]	Zr [kg]	Stainless steel [kg]
RELAP5/SCDAPSIM	22800	3100	2200	3000
MAAP4	120	320	220	0

Table 3: Time of the core baffle and the reactor vessel failure, Group 1.

Parameter	Time of the core baffle failure [s]	Time of the RPV failure [s]
RELAP5/SCDAPSIM	9300	9500
MAAP4	11500	19900

the hydrogen production rate, although final amount of produced hydrogen differed by less than 10% (Figure 10). Most of hydrogen was produced in the period of initial core dryout (8000 s–9000 s) which was well reproduced by both codes.

Composition of molten material in the RPV lower head shortly after the baffle failure and material relocation

is shown in Table 2.

Time of the core baffle failure and the RPV failure is shown in Table 3.

Following the core baffle failure, all molten material from the core slumped to the lower head as calculated by RELAP5/SCDAPSIM. MAAP4 did not predict any major slumping until after the stoppage of water injection at 16500 seconds. Throughout that period integrity of core support structures and the crust surrounding molten corium was maintained by continuous water/steam flow. Therefore, only small amount of material was relocated to the lower

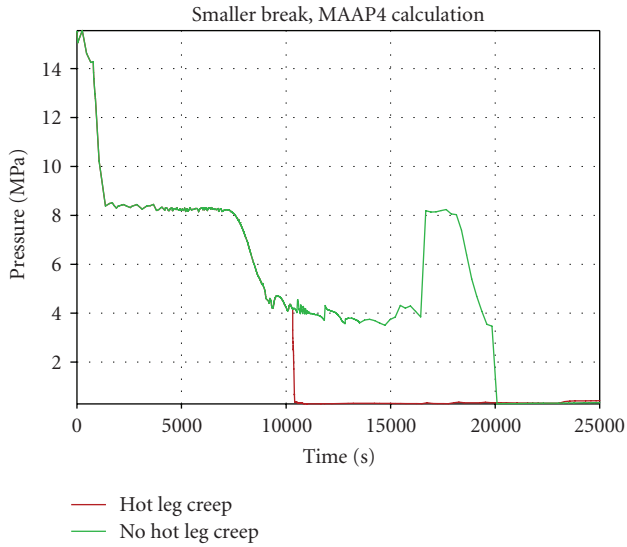

Figure 4: RCS pressure, MAAP4 calculation, Group 1.

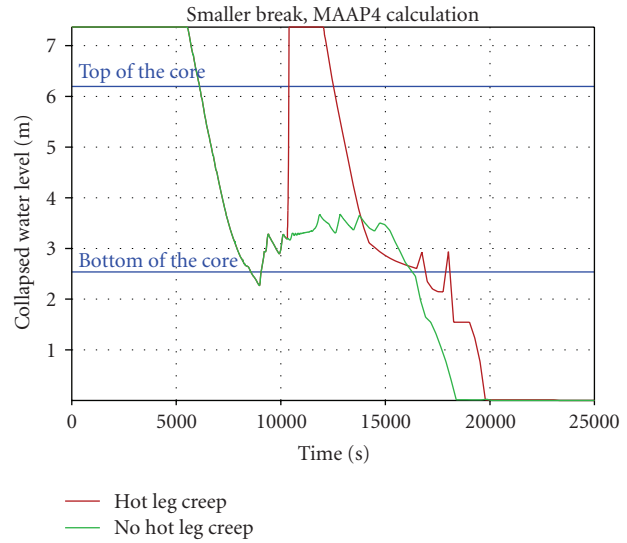

Figure 5: Collapsed water level in the reactor vessel, MAAP4 calculation, Group 1.

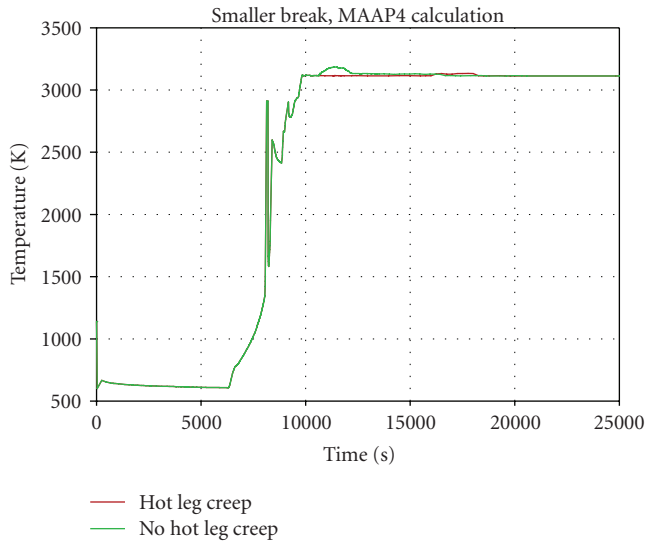

Figure 6: Core maximum temperature, MAAP4 calculation, Group 1.

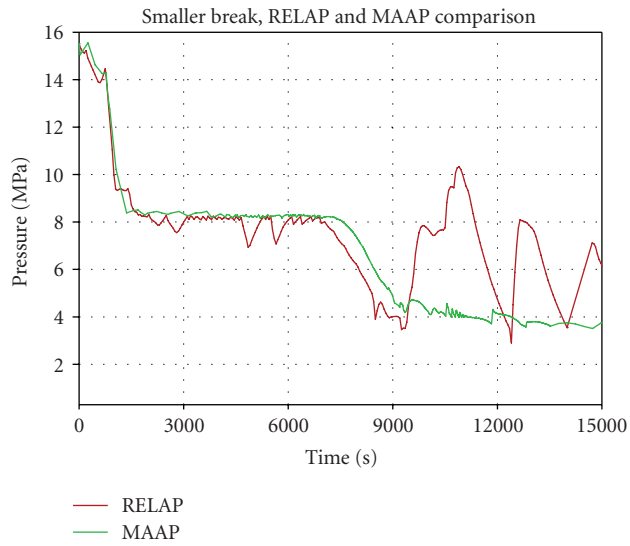

Figure 7: RCS pressure, Group 1.

head after the initial breach of corium through the core baffle. In the initial melting phase, there was more ZrO_2 melted than UO_2 because ZrO_2 has lower melting temperature; so more ZrO_2 slumped to the lower head. As the degradation process continued, mass of molten UO_2 became higher than mass of molten ZrO_2 due to its larger core inventory.

RELAP5/SCDAPSIM calculated earlier core degradation than MAAP4 code. The reason for that discrepancy was the difference in prediction of thermal hydraulic behaviour of the primary system as it had been already discussed. Another reason was the way how codes handle the core degradation process. RELAP5/SCDAPSIM uses very detailed models based on phase diagrams to calculate temperature and quantity of reacted materials. MAAP4 uses more general models of conservation of mass and energy for different materials and structures whose results depend strongly on selection of user-defined parameters.

RPV lower plenum temperature distribution was calculated using on one hand the COUPLE code, a two-dimensional, finite element heat conduction code incorporated in the RELAP5/SCDAPSIM code and, on the other hand, a much simpler MAAP4 RPV lower head model. The COUPLE model of the NEK lower head is shown in Figure 11.

Time of the RPV failure was evaluated using Larson-Miller parameter model [15] for the creep rupture which is incorporated in both codes. It can be seen from Table 3 that the timing of the RPV wall failure differed in order of magnitude for the two codes. The reason was the difference in the application of the creep rupture model [16]. The creep

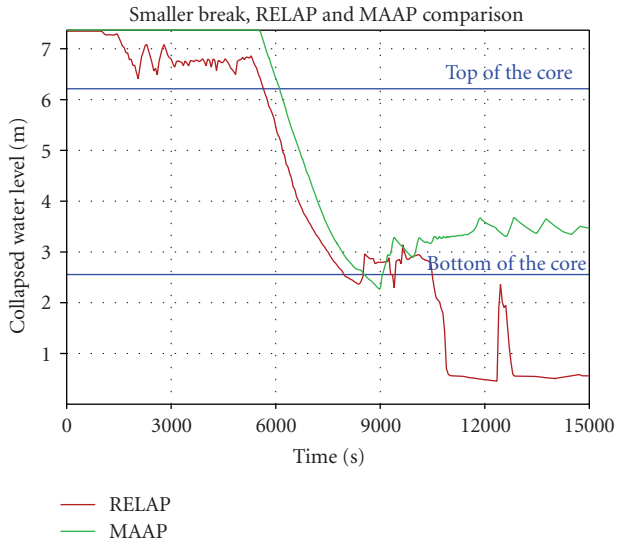

Figure 8: Collapsed water level in the reactor vessel, Group 1.

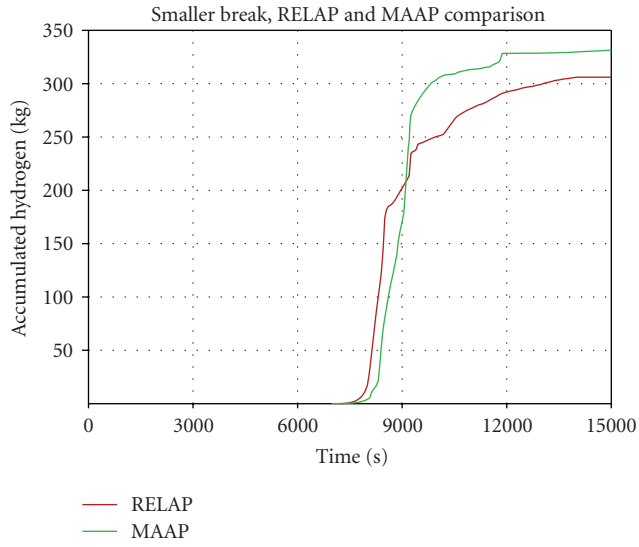

Figure 10: Mass of accumulated hydrogen, Group 1.

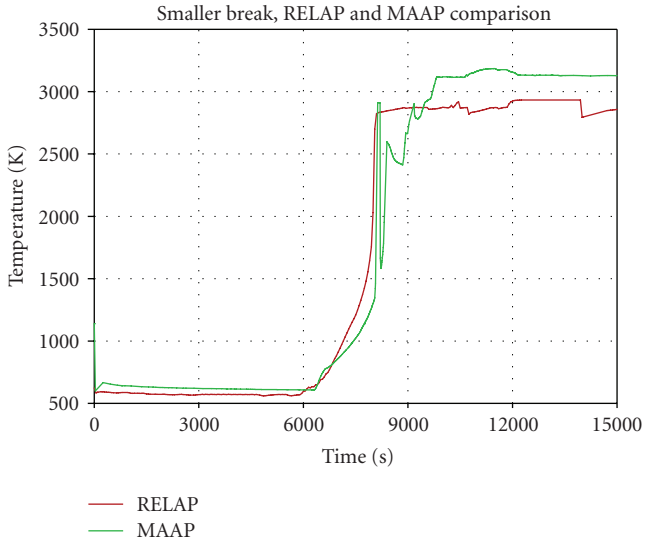

Figure 9: Core maximum temperature, Group 1.

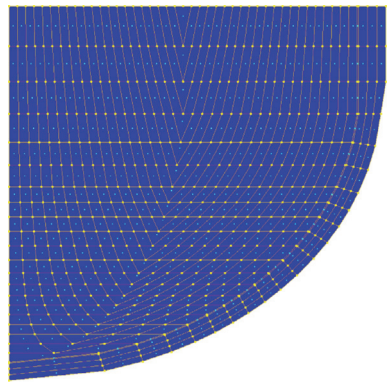

Figure 11: COUPLE model of the NEK RPV lower head.

rupture in RELAP5/SCDAPSIM was calculated using the average wall temperature, while in MAAP4 the creep damage term was evaluated at each temperature node. Each of these two approaches had its advantages and disadvantages, but in the scope of the presented analysis, it was not so essential to correctly calculate time of the RPV failure. It was more important to give the answer to the question: "will the RPV resist molten corium attack or not?" Since in the analyzed case no SI was available and no cavity flooding was provided, RPV finally failed opening a path for fission products to escape into the containment.

3.4. Group 2 Cases

3.4.1. MAAP4 Calculation. Similar to Group 1 cases, two MAAP4 calculations were performed: one that takes into

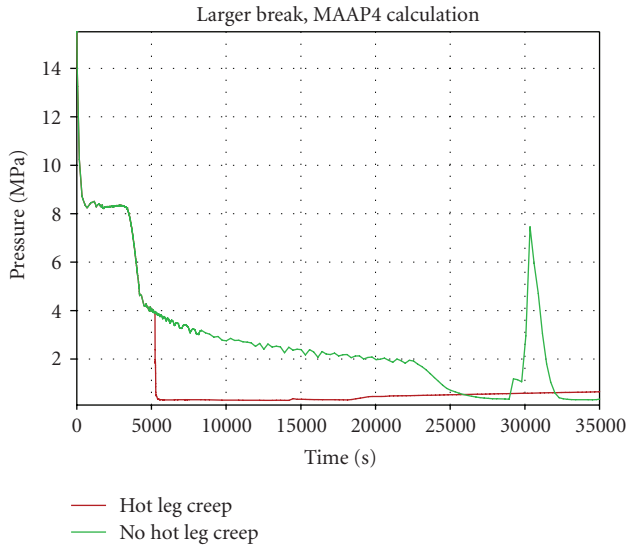

Figure 12: RCS pressure, MAAP4 calculation, Group 2.

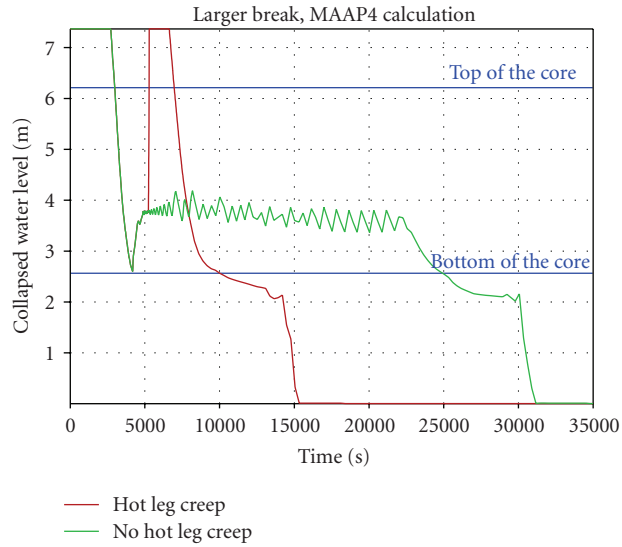

Figure 13: Collapsed water level in the reactor vessel, MAAP4 calculation, Group 2.

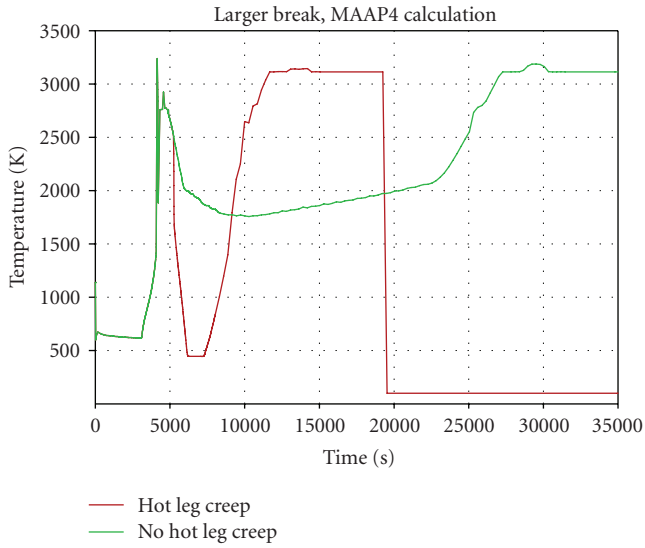

Figure 14: Core maximum temperature, MAAP4 calculation, Group 2.

account the creep rupture and the other that does not take into account the creep rupture of the hot leg piping.

Hot leg failed due to creep at 5200 seconds, 5000 seconds earlier than in the case with a smaller break. Accumulators were actuated prior to the hot leg failure and continuously injected water afterwards. Hot leg break caused primary system pressure to decrease rapidly (Figure 12). The consequence was that accumulators drained out almost immediately. In the short term that was positive because injection of a large amount of water forced the core temperature to decrease. On the other hand, in the longer term, there was no more water available for core quenching once the temperature increased again. In the case of no hot leg creep failure, accumulators gradually injected water,

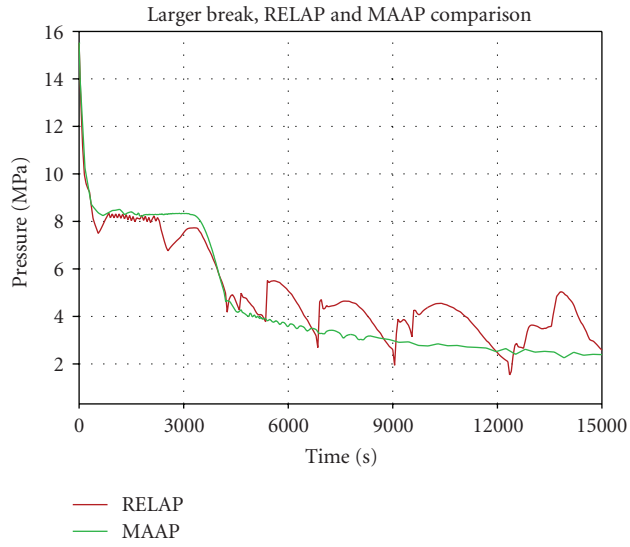

Figure 15: RCS pressure, Group 2.

but contrary to the calculation with the smaller break area, they injected more water which was enough to prevent the core temperature to increase above the $UO_2 - ZrO_2$ eutectic temperature for more than seven hours. The higher water injection rate was due to the larger pressure drop in the RCS.

Looking at Figures 13 and 14, it can be seen that continuous water injection from the safety systems at a high rate is enough to keep the core covered and its temperature at a low value although there is a large break on the RCS piping.

For the reasons explained above, in the case with no hot leg creep rupture, the core baffle failed at 29000 seconds and when the hot leg rupture was taken into account, the baffle failed at 13100 seconds. Although the analyzed transients were not representative for the real plant situations, they showed that thermal hydraulic phenomena dictate the SA progression. Correct thermal hydraulic modelling of the plant systems is therefore essential for an SA simulation, especially in the longer term.

3.4.2. Comparison between MAAP4 and RELAP5/SCDAPSIM Calculation. Comparing to the case with the smaller break area, discrepancy between the results was more pronounced. Whereas the calculated RCS pressure (Figure 15) was similar for the two codes, the water level in the reactor vessel (Figure 16), the core maximum temperature (Figure 17) and produced hydrogen (Figure 18) varied significantly.

The core dried out in approximately one hour (Figure 16). At the same time, RCS pressure dropped to 5 MPa and the accumulators started to operate. RELAP5/SCDAPSIM predicted that the core was quenched for the next 3000 seconds. Injection of water in the hot core at 6800 seconds resulted in the high oxidation rate and the immediate jump in the temperature (Figure 17). MAAP4 results show that the first time when the accumulators were actuated, the core was immediately overheated due to oxidation (Figures 17 and 18). It is interesting to notice that all hydrogen was produced during that period as calculated

Table 4: Composition of molten material in the reactor vessel lower head, Group 2.

Material	UO_2 [kg]	ZrO_2 [kg]	Zr [kg]	Stainless steel [kg]
RELAP5/SCDAPSIM	12300	460	1300	1500
MAAP4	35500	8100	2600	4200

Table 5: Time of the core baffle and the reactor vessel failure, Group 2.

Parameter	Time of the core baffle failure [s]	Time of the RPV failure [s]
RELAP5/SCDAPSIM	9600	9800
MAAP4	29000	34600

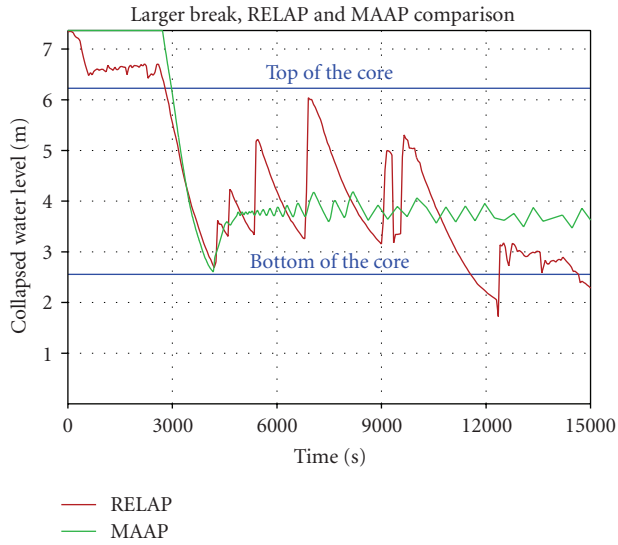

Figure 16: Collapsed water level in the reactor vessel, Group 2.

by MAAP4, while RELAP5/SCDAPSIM predicted release of hydrogen any time when there was water injected into the core.

As calculated by MAAP4, energy released during oxidation accumulated mostly in the core material and, therefore, the core temperature rose swiftly. Amount of the oxidation energy transferred to fluid was very small compared to total released energy; thus, it did not affect the RCS pressure (Figure 15). After the oxidation escalation and increase of the core temperature to more than 3000 K, MAAP4 calculated successful quenching of the core. Decrease of temperature prevented any significant core damage. On the other hand, when the core temperature reached ~2800 K in the RELAP5/SCDAPSIM calculation, no quenching onward was possible. The core started to melt and the process of core degradation proceeded rapidly with no possibility for stopping it.

The heat released due to oxidation in MAAP4 calculation in the short period when the accumulators were turned on was later successfully removed. RELAP5/SCDAPSIM calculated that the energy accumulated in the fuel due to oxidation was too high to be removed by water injected from the accumulators only. The emergency core cooling system (ECCS) is therefore necessary to be operable in order to prevent core damage when looking the RELAP5/SCDAPSIM results. On contrary, MAAP4 results indicate that water from the accumulators is enough to cool the core and that SI pumps are not needed in the early phase of an accident.

Composition of molten material in the RPV lower head shortly after the baffle failure and material relocation is shown in Table 4.

Time of the core baffle failure and the RPV failure is shown in Table 5.

Results in those two tables are reasonable taking into account previous discussion. There is a difference in MAAP4 results comparing to the case with a smaller break. In that former case MAAP4 predicted that only a few hundred kilograms of molten material would relocate to the lower head. Now, when the baffle failed, more than 60% of the total core inventory was removed from the core. The reason was that there was no more water injected to the vessel at 29000 seconds when the slumping began. The integrity of core support structures and the crust surrounding molten corium could not be maintained by flow of water.

Figure 19 shows the temperature of the RPV lower head wall after molten material slumped to the lower plenum. MAAP4 predicted that temperature would rise at a much higher rate than RELAP5/SCDAPSIM. In order to check those findings, an additional calculation was made by using commercial FEM code ANSYS. The results were similar to RELAP5/SCDAPSIM results. That is not so unusual since RELAP5/SCDAPSIM uses FEM model as well to simulate lower head thermal response. Correct temperature distribution through the RPV wall is essential when performing detailed structural analyses. Present FEM codes allow such 3D analyses and RELAP5/SCDAPSIM results could be used as boundary conditions for those calculations.

There are many reasons for large differences in the results of the two codes. First of all, models included in codes are different: not only thermal hydraulic models but also models that simulate core damage progression. RELAP5/SCDAPSIM is a mechanistic code, while MAAP4 is a parametric code that uses more phenomenological models. The analyzed transient was quite demanding and necessitated careful preparation of the input data and initial and boundary conditions. Due to those reasons, the uncertainties of the input data were not taken into account because the differences between code predictions could not be covered by the uncertainties only.

3.5. Influence of User-Selected Parameters. Severe accident codes generally use a large set of user-defined parameters to cover uncertainties in the analytical description of SA processes. MAAP4 code is regarded as a parametric code because its results rely on proper selection of many of parameters describing phenomena starting from an early stage of core degradation to the late stage of containment fission products behaviour. RELAP5/SCDAPSIM code utilizes

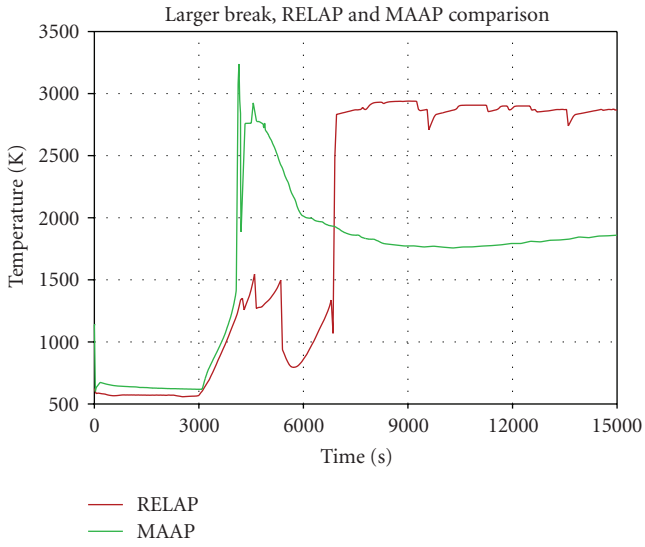

Figure 17: Core maximum temperature, Group 2.

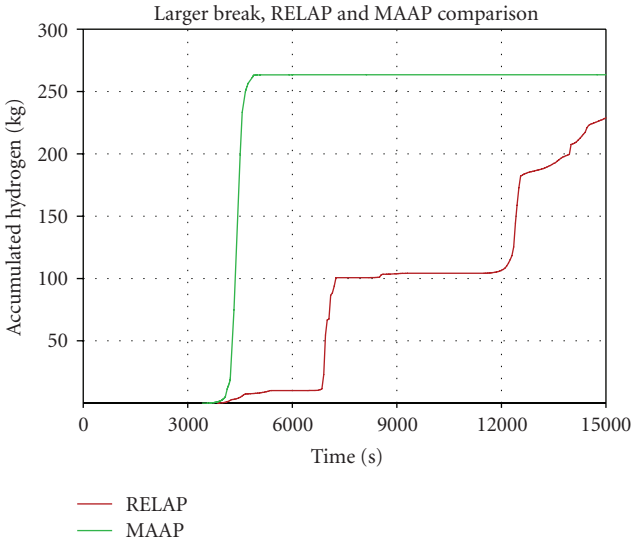

Figure 18: Mass of accumulated hydrogen, Group 2.

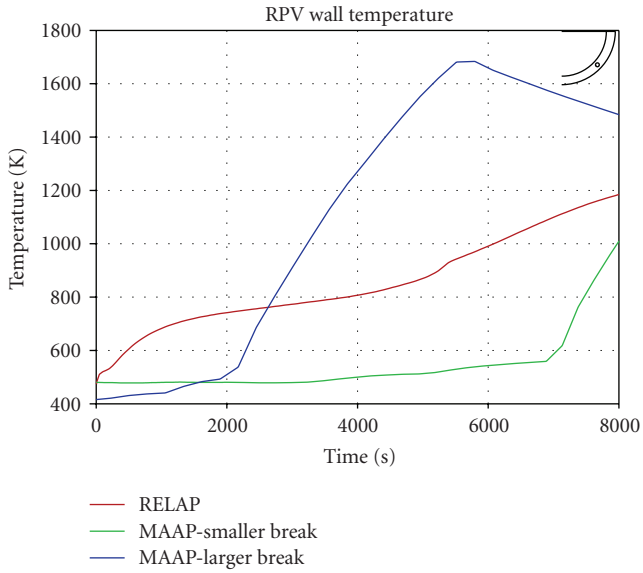

Figure 19: Temperature of the wall of the RPV lower head after relocation of molten material (the red dot on the figure in the upper right corner represents the position at the RPV wall where the temperature was calculated).

more mechanistic models and user-defined parameters are primarily used in sensitivity calculations.

There are a large variety of user-defined parameters in MAAP4 code which significantly influence the results. For example, there is a set of parameters used in modelling the failure of the oxide shell on the outside cladding surface. By changing values of some of those parameters, the melt progression inside the core could be altered. Another set of input data that was tested was the set of parameters used in simulation of debris jet interaction with the water pool in the lower plenum. That set of data had a big impact on thermal behaviour of the wall of the RPV lower head. The last issue that was tested was the stratification of molten material in the lower head. Surprisingly, whatever corium configuration was chosen ((1) oxidic melt + metallic melt + particulate debris, (2) mixed melt + particulate debris, (3) mixed melt without any solid debris), there was almost no influence on RPV wall temperatures. Thus, in the case of stratification of molten material, no heat focussing effect by the molten metal layer was calculated to occur.

Influence of few RELAP5/SCDAPSIM parameters was also tested, and it was found that their influence on core degradation kinetics and the timing of the lower head failure was negligible. Nevertheless, the user influence on RELAP5/SCDAPSIM results cannot be ruled out because correct modelling requires a qualified and experienced user with the good knowledge of plant systems and their interconnections.

4. Conclusion

Capabilities of RELAP5/SCDAPSIM and MAAP4 codes in simulating in-core severe accident progression were compared, focussing on influence of thermal hydraulics and selection of user-defined parameters. The input decks for both codes were prepared taking into account the actual geometric and operational data of NPP Krško making them qualified for a comprehensive and systematic analysis.

The correct prediction of RCS thermal hydraulic behaviour is important for the later SA progression. Oxidation rate and removal of heat from the core are dictated by the availability of coolant; thus, production of hydrogen and core heat-up and degradation depend primarily on RCS thermal hydraulics. Calculations have shown that MAAP4 results are more sensitive to variations of the RCS pressure and the coolant discharge rate from the break. Increase of the break area substantially affected the timing of both core melt process and the failure of the RPV lower head. RELAP5/SCDAPSIM, on contrary, regardless the size of the

break area, predicted RPV damage almost at the same time, meaning that in the case of a large break, whatever the size of the break actually was, the core would lose its geometry early during the transient unless mitigation measures are undertaken before.

A number of user-defined parameters, especially in MAAP4 code, have to be entered during preparation of an input deck. While in RELAP5/SCDAPSIM code those parameters are used only in sensitivity calculations, in MAAP4 code their selection could significantly alter the results. The solution is to use values of the parameters recommended by MAAP4 developers or ones which are experimentally measured and confirmed.

The comparison between the codes showed not only some similar trends but also large disagreements in the obtained results. Code validation against plant and experimental data is therefore a necessary tool in testing code's accuracy. Nevertheless, both codes showed capability of modelling complex interactions between core materials and overall core behaviour during harsh severe accident conditions.

References

[1] SCDAP/RELAP5 Development Team, "SCDAP/RELAP5/MOD3.2 Code Manuals, Vols. 1 to 5, NUREG/CR-6150, INEL-96/0422, Rev. 1," INEEL, Idaho Falls, Idaho, USA, 1997.

[2] Fauske and Associates, Inc., "MAAP4—Modular Accident Analysis Program for LWR Power Plants, Vols. 1 to 3," prepared for Electric Power Research Institute, 1994.

[3] K. Vierow, Y. Liao, J. Johnson, M. Kenton, and R. Gauntt, "Severe accident analysis of a PWR station blackout with the MELCOR, MAAP4 and SCDAP/RELAP5 codes," *Nuclear Engineering and Design*, vol. 234, no. 1–3, pp. 129–145, 2004.

[4] D. Grgić, et al., "NEK RELAP5/MOD3.3 Nodalization Notebook (2000 MWt and new SGs)," NEK ESD TR 09/03, 2003.

[5] T. Bajs, V. Benčik, and S. Šadek, "NEK RELAP5/MOD3.3 Steady-State and On-Transient Qualification Report (Based on NEK ESD TR09/03)," NEK ESD TR 10/03, 2003.

[6] T. Bilić-Zabric and B. Glaser, "Krško MAAP Nodalization Notebook," NEK ESD TR02/00, 2000.

[7] WOG Program MUHP-2310, "Severe Accident Management Guidance," Westinghouse Electric Corporation, 1994.

[8] "Krško Individual Plant Examination Level 2," WENX-95-24, Westinghouse Electric Corporation, 1995.

[9] T. Bilić-Zabric and I. Bašić, "NEK Plant Specific SAMG Strategies," NEK ESD TR22/00, Rev. 1, 2002.

[10] T. Bilić-Zabric and I. Bašić, "Krško Severe Accident Management—Setpoint Calculation," NEK ESD TR23/00, Rev. 1, 2002.

[11] T. Bilić-Zabric, I. Bašić, and J. Špiler, "Hydrogen behaviour in PWR containment evaluated with MAAP4.0.5," in *Proceedings of the 5th International Conference on Nuclear Option in Countries with Small and Medium Electricity Grids*, pp. S4-4.1–S4-4.10, Dubrovnik, Croatia, 2004.

[12] NEK EOP-3.5, ECA-0.0, "Loss of all AC Power, Rev. 11," 2002.

[13] "WOG 2000 Reactor Coolant Pump Seal Leakage Model for Westinghouse PWRs," WCAP-15603, Rev. 1-A, 2003.

[14] "Natural Circulation in Water Cooled Nuclear Power Plants, Phenomena, Models and Methodology for System Reliability Assessments," IAEA-TECDOC-1474, 2005.

[15] F. R. Larson and J. Miller, "A time temperature relationship for rupture and creep stress," *Transactions of the ASME*, pp. 765–775, 1952.

[16] K.-I. Ahn and D.-H. Kim, "A state-of-the-art review of the reactor lower head models employed in three representative U.S. severe accident codes," *Progress in Nuclear Energy*, vol. 42, no. 3, pp. 361–382, 2003.

Hindawi Publishing Corporation
Science and Technology of Nuclear Installations
Volume 2010, Article ID 219294, 9 pages
doi:10.1155/2010/219294

Research Article

Main Results of Phase IV BEMUSE Project: Simulation of LBLOCA in an NPP

M. Pérez,[1] F. Reventós,[1] L. Batet,[1] R. Pericas,[1] I. Toth,[2] P. Bazin,[3] A. de Crécy,[3] P. Germain,[3] S. Borisov,[4] H. Glaeser,[5] T. Skorek,[5] J. Joucla,[6] P. Probst,[6] A. Ui,[7] B. Chung,[8] D. Y. Oh,[9] M. Kyncl,[10] R. Pernica,[10] A. Manera,[11] F. D'Auria,[12] A. Petruzzi,[12] and A. Del Nevo[12]

[1] *Technical University of Catalonia (UPC), Diagonal 647, 08028 Barcelona, Spain*
[2] *Atomic Energy Research Institute, Hungary*
[3] *Commissariat à l'Energie Atomique, France*
[4] *EDO Guidropress, Russia*
[5] *Gesellschaft für Anlagen- und Reaktorsicherheit, Germany*
[6] *Institut de Radioprotection et de Sûreté Nucléaire, France*
[7] *Japan Nuclear Energy Safety, Japan*
[8] *Korea Atomic Energy Research Institute, South Korea*
[9] *Korean Institute of Nuclear Safety, South Korea*
[10] *Nuclear Research Institute, Czech Republic*
[11] *Paul Scherrer Institute, Switzerland*
[12] *University of Pisa, Italy*

Correspondence should be addressed to F. Reventós, francesc.reventos@upc.edu

Received 19 June 2009; Accepted 6 January 2010

Academic Editor: Michel Giot

Phase IV of BEMUSE Program is a necessary step for a subsequent uncertainty analysis. It includes the simulation of the reference scenario and a sensitivity study. The scenario is a LBLOCA and the reference plant is Zion 1 NPP, a 4 loop PWR unit. Thirteen participants coming from ten different countries have taken part in the exercise. The BEMUSE (Best Estimate Methods plus Uncertainty and Sensitivity Evaluation) Program has been promoted by the Working Group on Accident Management and Analysis (WGAMA) and endorsed by the Committee on the Safety of Nuclear Installations (CSNI). The paper presents the results of the calculations performed by participants and emphasizes its usefulness for future uncertainty evaluation, to be performed in next phase. The objectives of the activity are basically to simulate the LBLOCA reproducing the phenomena associated to the scenario and also to build a common, well-known, basis for the future comparison of uncertainty evaluation results among different methodologies and codes. The sensitivity calculations performed by participants are also presented. They allow studying the influence of different parameters such as material properties or initial and boundary conditions, upon the behaviour of the most relevant parameters related to the scenario.

1. Introduction

Models and codes are an approximation of the real physical behaviour occurring during a hypothetical transient, and the data used to build these models are also known with certain accuracy. Therefore, code predictions areuncertain. The BEMUSE programme is focussed on the application of uncertainty methodologies to large break LOCAs. This introduction deals with some background considerations and establishes the objectives of the programme along with its steps and phases.

1.1. Background. One of the goals of computer code models of Nuclear Power Plants (NPP) is to demonstrate that these are designed to respond safely at postulated accidents. To deal with uncertainties, the analyses can either use conservative or best-estimate (BE) codes.

(i) The conservative codes contain assumptions to try to cover unknown uncertainties. These assumptions are often unphysical and lead to predictions that could be worse than reality.

(ii) BE codes are designed to model all the relevant processes in a physically realistic manner. A calculation with a BE code is then considered the best approach of what is more likely to occur. In any case, it is necessary to evaluate the uncertainty of the estimation.

The reasons and motivation for using BE codes have been explained in many occasions [1–3]. The OECD BEMUSE started with the aim of achieving a deeper understanding of such methods [4].

1.2. Objectives. The BEMUSE programme is focussed on the application of uncertainty methodologies to large break LOCAs. The objectives of this programme are the following:

(i) to evaluate the practicability, quality, and reliability of best-estimate methods including uncertainty evaluations in applications relevant to nuclear reactor safety,

(ii) to develop common understanding,

(iii) to promote/facilitate their use by the regulator bodies and the industry.

Using the same codes and similar methods should allow comparing the potential important uncertain parameters, and the effects of different modelling for uncertainties can be evaluated. Therefore, the assessment of each methodology by comparison with experimental data is also one of the purposes of the programme.

1.3. Steps and Phases. The BEMUSE program is divided into two steps. The first step is to perform an uncertainty and sensitivity analysis of LOFT L2-5 test calculations and the second is to perform this analysis for an NPP-LBLOCA.

Each of these two steps is made up of three phases.

(i) First step (Phases I, II, and III):

  (a) Phase I: presentation a priori of the uncertainty evaluation methodology to be used (lead organisation: IRSN),

  (b) Phase II: reanalysis of the ISP-13 exercise, post-test of LOFT L2-5 test (lead organisation: University of Pisa),

  (c) Phase III: uncertainty evaluation of the L2-5 test calculations (lead organisation: CEA).

(ii) Second step (Phases IV, V, and VI):

  (a) Phase IV: best-estimate analysis of an NPP-LBLOCA (lead organisation: UPC),

  (b) Phase V: uncertainty evaluation of the NPP-LBLOCA (lead organisation: UPC),

  (c) Phase VI: status report, conclusions, and recommendations (lead organisation: GRS).

2. Lessons Learned from Previous Phases

Participants to Phase II achieved significant results. Almost all performed calculations appear qualified against the fixed criteria and few mismatches between results and acceptability thresholds have been characterized. Dispersion bands of results appear substantially less than years ago in ISP-13. Modelling techniques used by participants are the most fruitful outcome of phase II to be used in phase IV analysis.

The Input/Output Specification of Phase IV has been prepared by the coordinator team taking into account achievements and recommendations basically of Phase II but also of phases I and III.

3. Phase IV Scope and Objectives

The scope of Phase IV of BEMUSE programme is the simulation of an LB-LOCA in a Nuclear Power Plant using experience gained in previous Phase II [5]. Calculation results will be the basis for uncertainty evaluation, to be performed in next phase.

The objectives of the activity are

(i) to simulate an LB-LOCA reproducing the phenomena associated to the scenario,

(ii) to have a common, well-documented basis for the execution of the uncertainty evaluation step in Phase V.

4. Plant and Scenario

The selected plant was Zion Station, a dual-reactor nuclear power plant operated and owned by the Commonwealth Edison network. No other options were available. This power generating station is located in the extreme eastern portion of the city of Zion, Lake County, Illinois. It is approximately 40 direct-line miles north of Chicago, Illinois and 42 miles south of Milwaukee, Wisconsin.

The main features of the plant are

(i) 4 loops,

(ii) pressurized water reactor,

(iii) westinghouse design,

(iv) net Output: 1040 MWe,

(v) thermal power 3250 MWth,

(vi) permanently shut down,

(vii) date started: June 1973,

(viii) date closed: January 1998.

The Steady-State conditions are summarized in Table 1

The scenario is a cold leg Large Break LOCA in double guillotine without HPIS. The following statements specify the scenario description:

(i) LPIS injection with a pressure set point of 1.42 MPa (driven by a flow-pressure table),

(ii) accumulators injection with a pressure set point of 4.14 MPa,

Table 1: Steady-State main parameters.

Parameter	Steady-State value
Power (MW)	3250.0
Pressure in cold leg (MPa)	15.8
Pressure in hot leg (MPa)	15.5
Pressurizer level (m)	8.8
Core outlet temperature (K)	603.0
Primary coolant flow (kg/s)	17357.0
Secondary pressure (MPa)	6.7
Steam generator's downcomer level (m)	12.2
Feed water flow per loop (kg/s)	439.2
Accumulator pressure (MPa)	4.14
Accumulator gas volume per tank (m^3)	15.1
Accumulator liquid volume per tank (m^3)	23.8
Reactor coolant pump's velocity (rad/s)	120.06

Table 2: Time sequence of imposed events.

Event	Time (s)
Break	0.0
SCRAM	0.0
Reactor coolant pumps trip	0.0
Steam line isolation	10.0
Feed water isolation	20.0
HPIS	NO

(iii) containment pressure imposed as a function of time after the break,

(iv) reactor coolant pumps velocity imposed as a function of time after the break (see Table 2.)

All the information needed to carry out Phase IV calculations was organized by the coordinator as the "BEMUSE Phase IV Input Specification" [5] and distributed among participants. The specification includes information on:

(i) decay power multiplier,

(ii) LPIS pressure-flow curve,

(iii) containment pressure,

(iv) pump velocity for primary coolant pumps in intact loops,

(v) pump velocity for primary coolant pumps in broken loops.

All the available details related to the plant lay-out were also included in the specification.

It is important to point out that, as the plant was in permanently shutdown condition from 1998, no detailed information could be made available if needed during the development of the project. In order to work out this problem along with plant parameters, the main features of the LBLOCA scenario were specified in order to ensure common initial and boundary conditions.

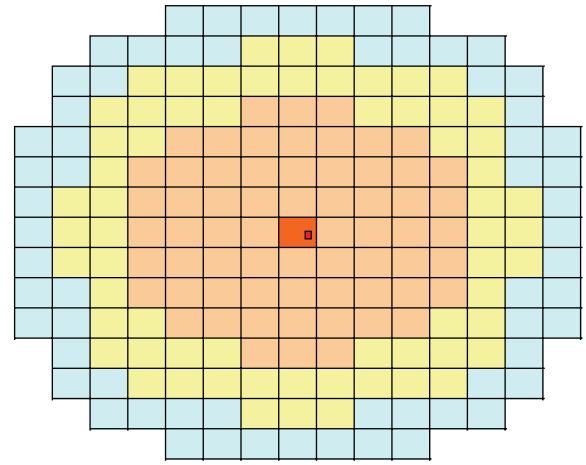

FA	Rods per FA = 204	Fuel rods
64	Peripheral channel	13056
64	Average channel	13056
64	Hot channel	13056
1	Hot FA in hot channel	203
1Rod	Hot rod in hot FA	1
193	Total	39372

Figure 1: Core heat structures.

5. Codes and Nodalizations

Table 3 shows the features of codes and nodalizations used by each participant. The table includes

(i) number of hydraulic nodes,

(ii) number of mesh points for the heat structures,

(iii) number of core channels (not including the bypass channel),

(iv) number of axial core nodes per channel.

Five active heat structures were nodalized simulating the fuel elements. Figure 1 shows a sketch of core heat structures zones, listed below:

Zone 1: average fuel rods in peripheral channels,

Zone 2: average fuel rods in average channels,

Zone 3: average fuel rods in hot channels,

Zone 4: hot fuel assembly in hot channel,

Zone 5: hot rod in hot fuel assembly.

Figures 2 and 3 show the sketch of two different nodalization schemes used by two different participants.

The most relevant differences among the nodalizations used are the core vessel detail and the fuel rods. Core vessels have been modelled using one dimensional and three dimensional codes. In each particular case, the resulting flow distribution, ECCS bypass, and the behaviour of liquid in the upper head, among others, significantly explain the

Table 3: Nodalization resources used by each participant.

Participant	Code's name	Hydraulic nodes	Mesh points (heat structures)	Core channels (core channels)	Axial active core nodes per channel
AEKI	ATHLET 2.0A	580	1839	2	18
CEA	CATHARE V2.5 1 mod.3.1	NS	NS	NS	NS
EDO	Tech-M-97	87	811	5	12(*)
GRS	ATHLET 2.1A	395	526	2	18
IRSN	CATHARE2 V2.5_1 mod5.1	NS	NS	NS	NS
JNES	TRACE ver4.05	743	10660	16	42
KAERI	MARS 3.1	1116	NS	3	18
KINS	RELAP5/MOD3.3	280	2193	2	18
NRI-1	RELAP5/MOD3.3	306	2055	4	18
PSI	TRACE5.0rc3	908	5117	5	18
UNIPI-1	RELAP/MOD3.2	NS	NS	NS	NS
UNIPI-2	CATHARE2 V2.5 1	79	12017	5	21
UPC	RELAP5/MOD3.3	305	2193	2	18

(*) The fuel path is simulated by 10 axial nodes.

diversion of results. Among one-dimensional codes, an influent feature in nodalization is the use or the availability of cross-flow junctions between the core channels and between the downcomer pipes. Related to fuel rods, one participant simulated the oxidation of the cladding while the others did not compute it.

The specifications document for BEMUSE phase IV devoted a whole section [5, Section 3] to list a number of requirements and recommendations for nodalization performance with the aim to have a common basis for comparison. Among them

(i) some initial conditions,

(ii) some nodalization characteristics (core, downcomer, lower plenum, and the break itself),

(iii) the use of code options (reflood and CCFL).

The level at which each participant followed the recommended procedures strongly affects the dispersion of the results.

6. Main Results

The nodalization development and the steady-state results were compared among participants in a systematic way. Figure 4 shows a piece of information related to the complete comparison. The example is the normalized pressure drop curve which is quite acceptable. Most of the participants manage to reproduce the reference curve. Some of the differences are due to the small changes performed by participants after the reference curve was supplied. These small changes (like those related to resplitting the downcomer from 2 to 4 pipes in the coordinators case) produced only small deviations in the comparative plot but came up with some improvements in the reference case.

The comparison of participant results for the reference case has also been performed in a systematic way which includes

(i) calculated sequence of events,

(ii) time trends,

(iii) relevant Thermalhydraulic Aspects (RTA),

(iv) comments on similarities and discrepancies found among the different groups.

All this information can be found in detail in Phase IV report. Among the 25 compared time trends, the most significant have been selected and are shown below in Figures 5–10. Figure 5 shows time trend of the intact loop 1 pressure in hot leg. A zoom-in figure has been chosen in order to show the cause of the different behaviour observed in accumulators' injection. Although this difference in time is only about 5 or 6 seconds between the most extreme predictions, it helps understanding other important aspects like the differences in accumulators' pressure or in integral break mass flow that appear respectively in Figures 6 and 7.

Most of the events related to the scenario are strongly dependent on primary pressure time trend. Despite of the dispersion shown in some of the Figures, some events are predicted in a consistent way by participants among these:

(i) subcooled blowdown ended,

(ii) cladding temperature initially deviated from saturation (DNB in core),

(iii) pressurizer emptied,

(iv) accumulator injection initiated,

(v) LPIS injection initiated.

Events related to the partial top-down rewet need some explanation. After analyzing the corresponding Figures, despite of a nonnegligible dispersion, the shape of the curves shows some consistency. All participants predict a first PCT, a temperature decrease (at the initiation of the partial rewet), and a further temperature increase (at the end of the partial rewet). These events are not so clearly shown when participants are asked to define a time quantity related to

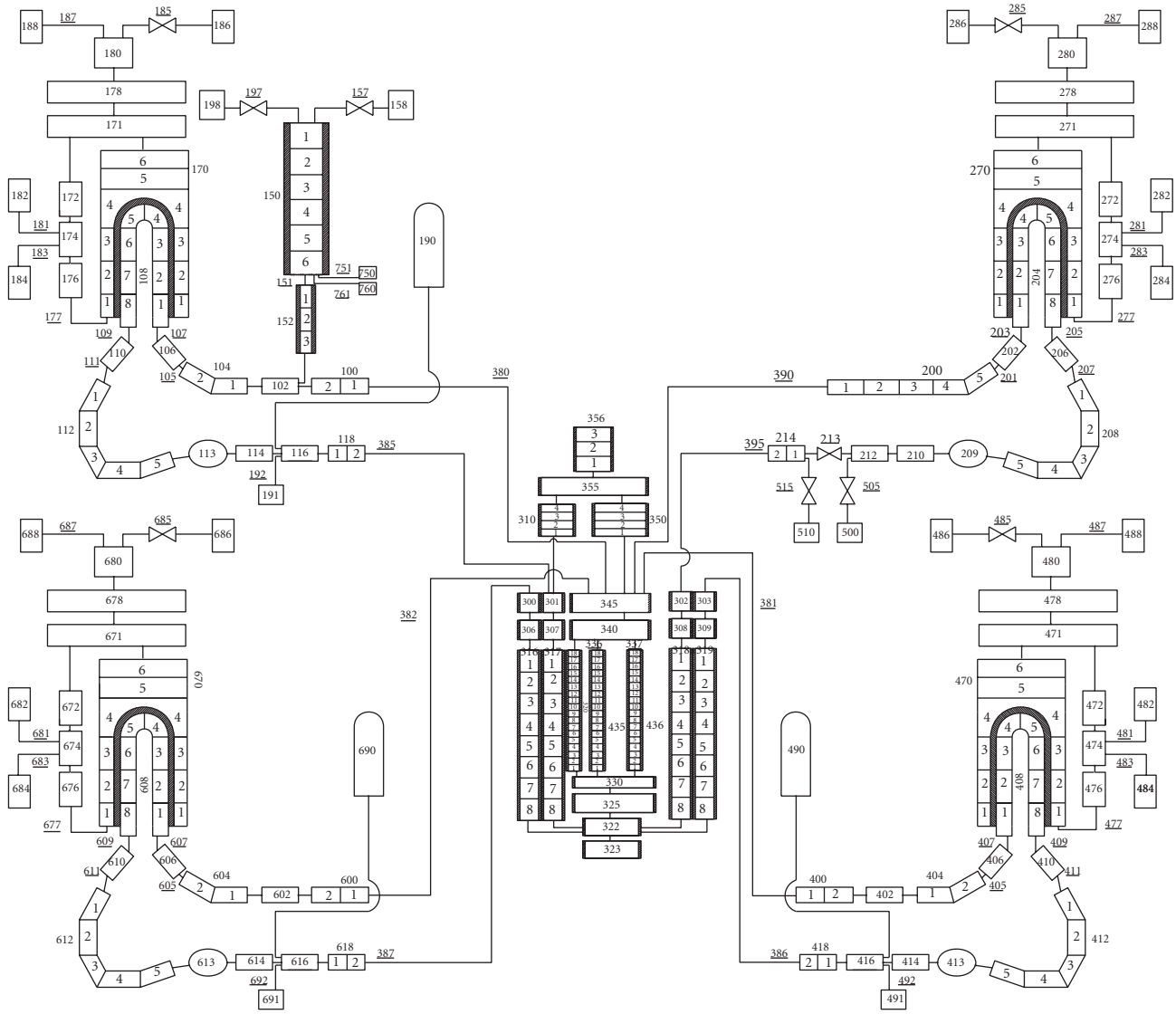

Figure 2: Example of 1-D Relap5 nodalization scheme used by UPC.

each event but there is a general agreement on the shape of the curves. Clearly the time trend analysis (instead of the simple comparison of the time of occurrence of the events) is the best way to show the discrepancies and similarities among results.

A similar comment can be made regarding accumulator behaviour. Despite that injection initiation is consistently predicted by participants and properly shown in Figure 8, the prediction of accumulators emptying shows some dispersion. As it is a phenomenon depending on intact leg pressure, pressure error and cumulative time error have a strong effect on the occurrence of the event and dispersion increases.

Finally, the core thermal behaviour, and mainly the full quench, is another event needed of clarification. Figure 10 is maybe the best information for discussion that has some comments involving code effect. The spread of results for the first PCT and for the second is not so high (roughly 200 K for each peak). The lowest of PCT has been obtained by KAERI (1159.1 K) and highest of PCT by EDO "GUIDROPRESS" (1326.15 K). Difference between lowest and highest of PCT for RELAP users is about 100 K, for CATHARE and ATHLET users is about 40 K, and for TRACE users is 20 K. Eight participants predicted the time of PCT between 40 s and 60 s except for NRI-1, CEA, GRS, JNES, and IRSN. These participants predicted more early the time of PCT (about 10 s). The major differences between results come with the reflooding behaviour and mainly its duration. Concerning this aspect, among the 13 participants, 8 of them show a medium reflood duration (total core quench obtained between 160 and 250 s), 3 other computations show a long reflood duration (total core quench between 320 to 420 s), and the other 2 show a kind of slow cladding temperature decrease in which it is difficult to establish the time of full quench.

It is clear that dispersion bands exist but it is also clear that the effort of explaining the reasons of such dispersion is a valuable outcome from this phase. The outcome of BEMUSE

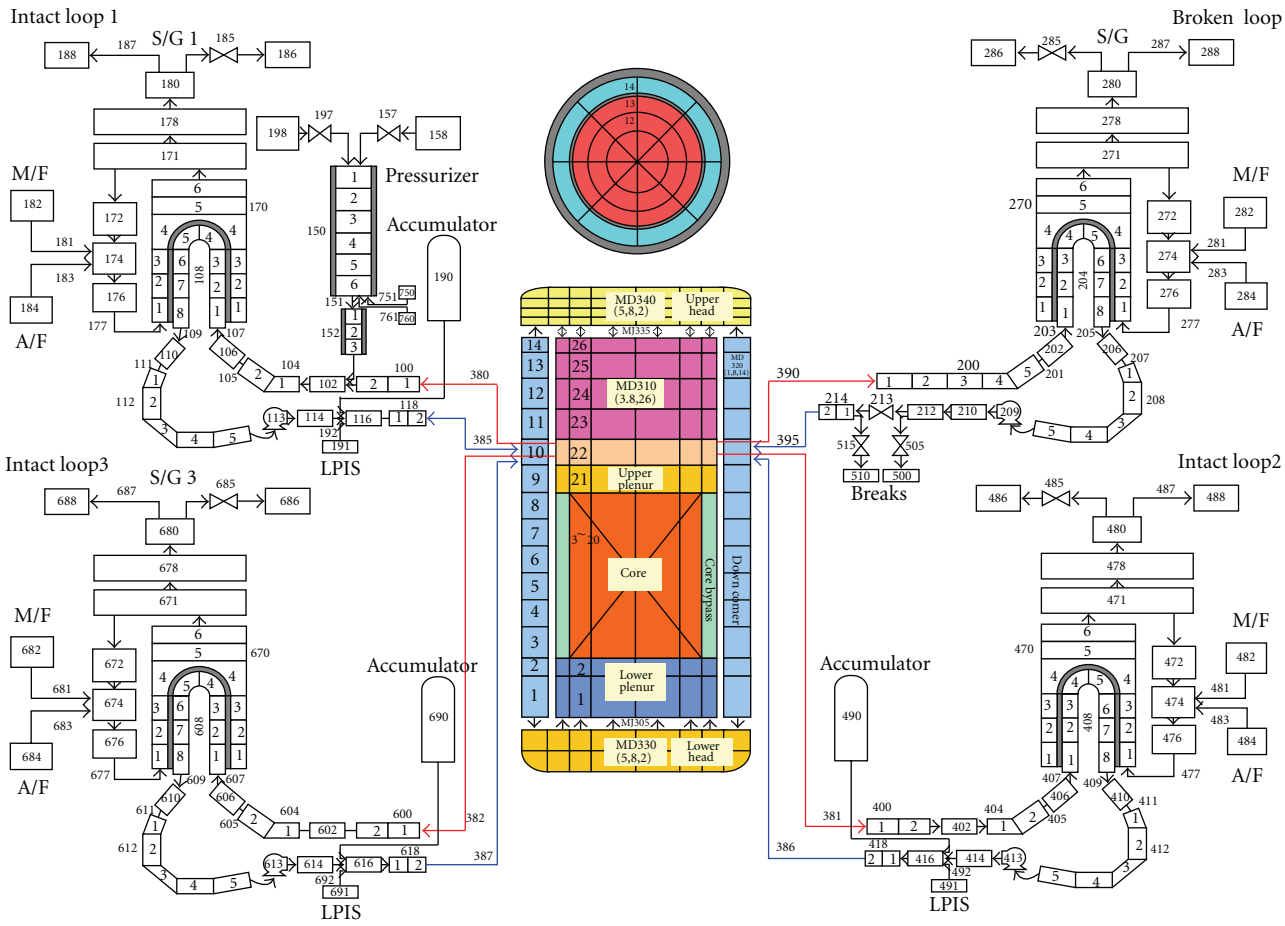

Figure 3: Example of 3-D MARS vessel nodalization scheme used by KAERI.

Phase IV is also helpful to understand the nuances existing inside the user effect. The discussion on the point related to the full quench has been useful to clarify the "border" between user effect and code effect. Figure 11 enlights these considerations putting together CATHARE and RELAP5 calculations results for this particular aspect. Despite the consistency of both groups of calculations, some code effect appears. This point is a minor result of Phase IV detected within the programme although it cannot be solved in its framework.

7. Sensitivity Calculations

Different sensitivity calculations were performed in Phase IV with the aim of helping to prepare the following Phase V of BEMUSE project. The results can be used by participants individually either when deciding which parameters are to be included in their respective uncertainty analysis or after running the uncertainty calculations (for those participants using methods based on Wilks' formula) when deciding whether to accept or to put in question the results of the sensitivity analysis postcalculation.

In order to provide the reader with a better sight of the sensitivity analysis results, the values for ΔPCT and for Δ*REFLOOD* given by all participants have been averaged. As reasonable ranges of variation have been assumed for the input parameters, ΔPCT and Δ*REFLOOD* values provide a good measure of the influence that these input parameters can have on the calculation results.

Figure 12 is devoted to illustrate quantitatively the usefulness of sensitivity results as an example for ΔPCT. It shows the mean impact on ΔPCT in °K when the sensitivity input parameter changes from its lower to its upper value. The Figure includes the standard deviation of the ranges found by participants. For the ΔPCT, participants in average have found that the most influential parameters are those related to the energy stored in the fuel elements (i.e., fuel and gap conductivity, power—before and after the scram,

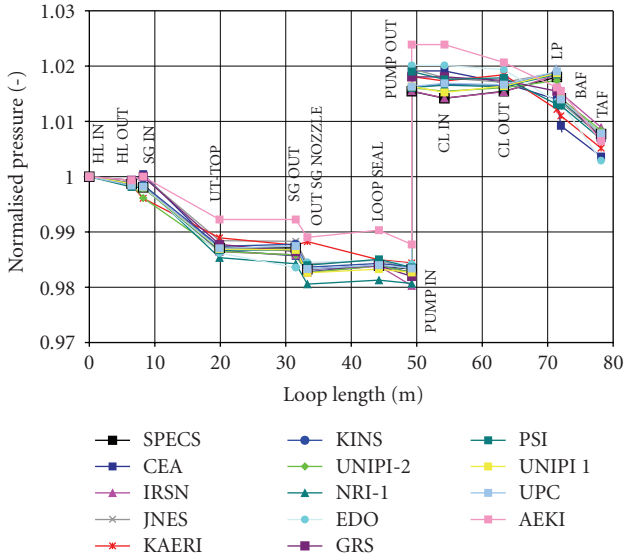

Figure 4: Normalized pressure curve along the loop.

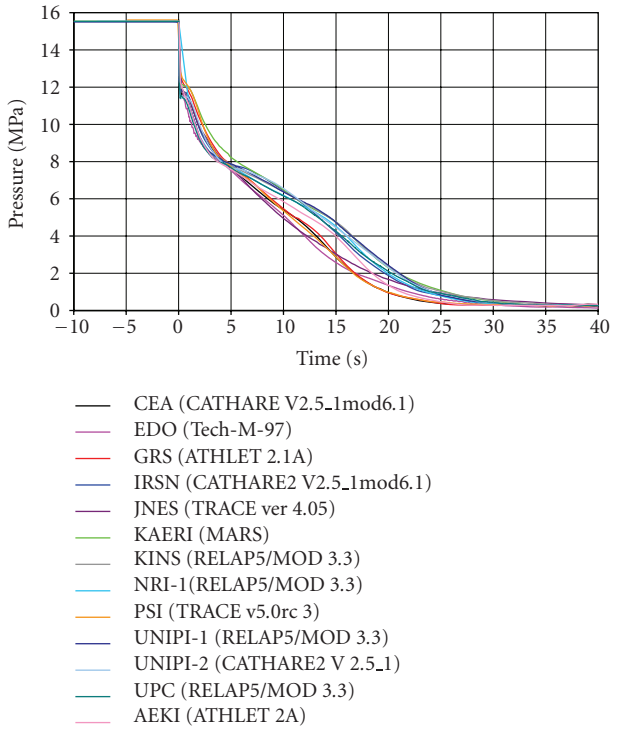

Figure 5: Time trends of intact loop 1 pressure in hot leg.

and fuel dimensions) and, among them, fuel conductivity, radial power factor (hot rod power), and fuel dimensions. The parameters in Figure 12 are the following: s1-fuel conductivity, s2-gap conductivity, s3-power after scram, s4-power before scram, s5-hot rod power, s6-LPIS delay, s7-accumulator liquid volume, s8-accumulator pressure, s9-containment pressure, and s10-hot/cold conditions for pellet radius.

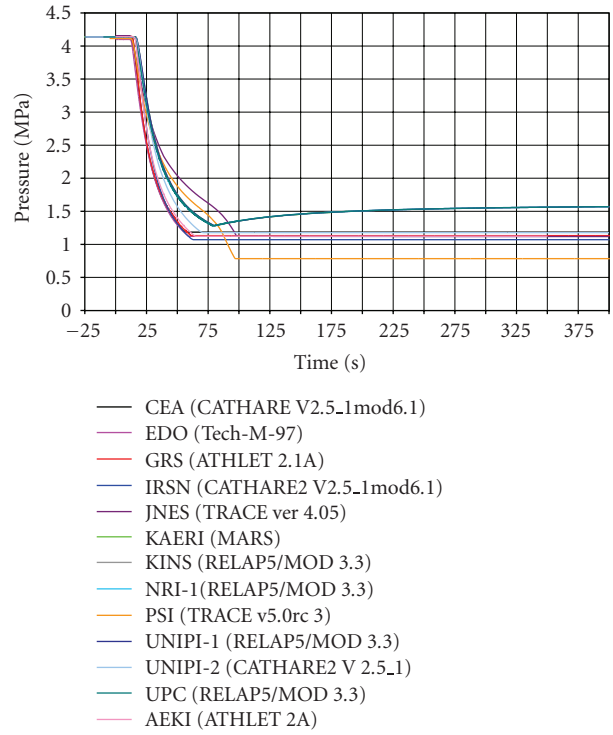

Figure 6: Time trends of accumulator 1 pressure.

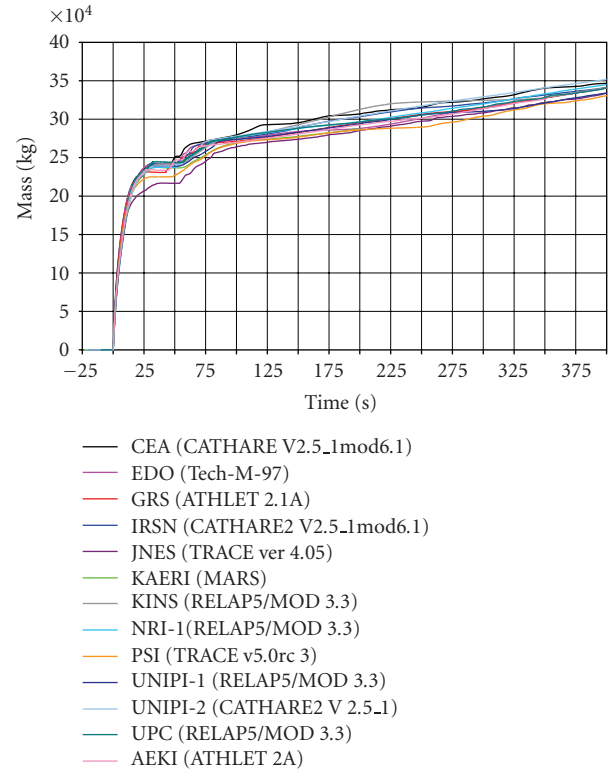

Figure 7: Time trends of integral break mass flow.

Regarding the Δ*REFLOOD*, the *average participant* has encountered that the parameters having more influence in the time of reflood are containment pressure, power after

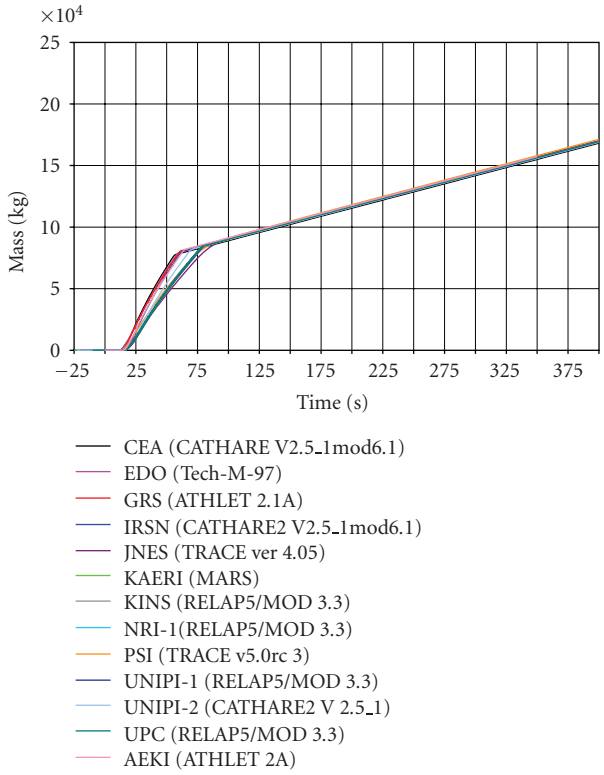

Figure 8: Time trends of ECCS integral mass flow.

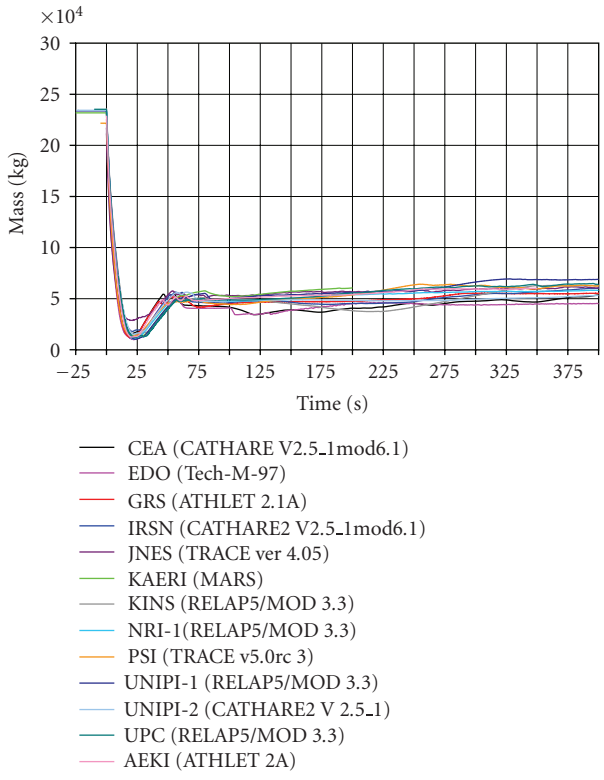

Figure 9: Time trends of primary system mass (including pressurizer).

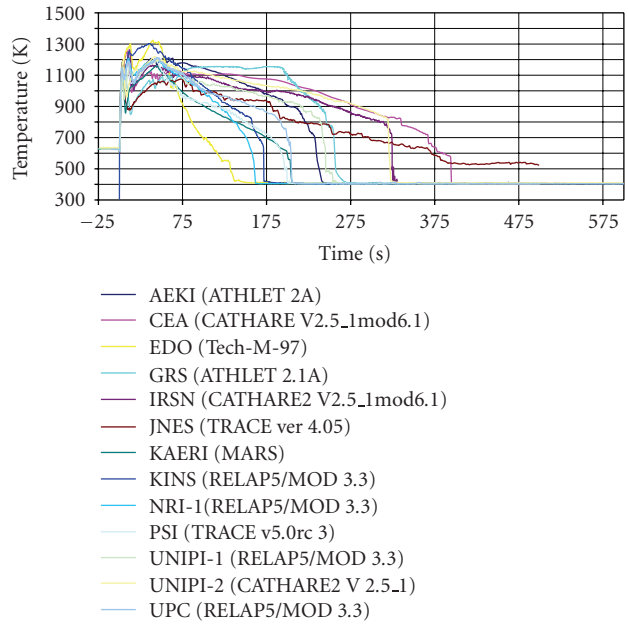

Figure 10: Time trends of maximum cladding temperature.

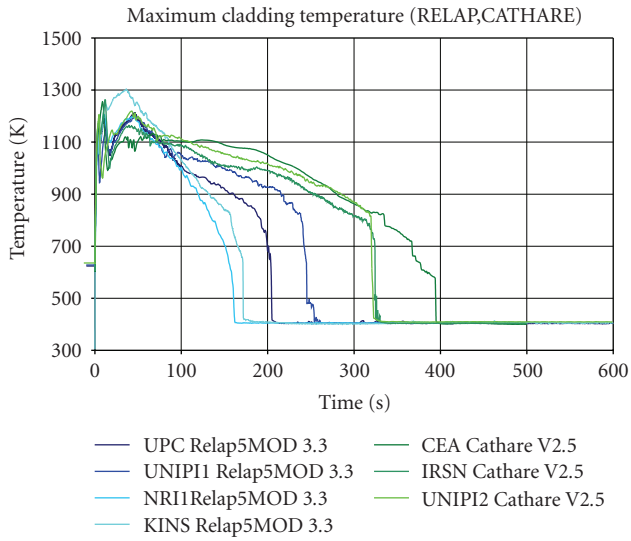

Figure 11: Calculated hot rod temperature/Code effect considerations.

scram (decay power), radial power factor (hot rod power), power before scram (steady state power), and volume of liquid in accumulators.

The sensitivity study performed in Phase IV has proved to be useful in order to set up the Specification for Phase V.

8. Conclusions

Conclusions can be summarized as follows:

(i) all participants managed to simulate the scenario and predict the main parameters with credible consistency;

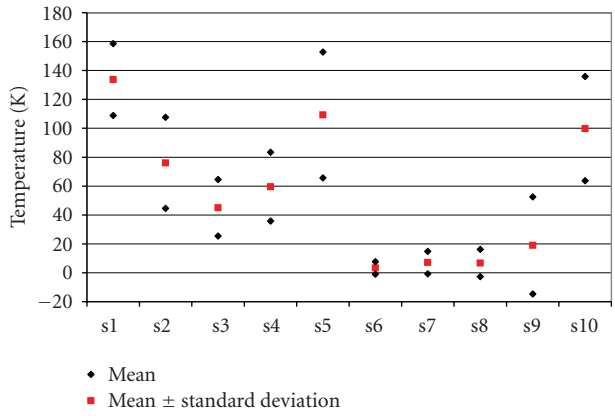

Figure 12: Sensitivities mean ΔPCT values—Scalar parameters.

(ii) maximum values of PCT predicted by participants are quite close one each other;

(iii) PCT time trends and timing of complete core rewet still show some disagreements;

(iv) a database, including comparative tables and plots has been produced. This database is suitable for providing the explanations needed for the following phases.

About the announced difficulty of dealing with a plant that was in permanent shutdown condition from 1998, one can conclude that the participants in the exercise managed to work it out. Although no detailed information could be made available during the development of the project, the specification itself and further contacts among participants were sufficient to reach a suitable definition of common initial and boundary conditions.

The final calculation results had a credible consistency and are considered a good basis for the comparison work of next phase of the project, in which uncertainty bands will be calculated.

Phase IV results are a step forward that contributes to the general goals of BEMUSE project.

Acronyms

AEKI: Atomic Energy Research Institute
BE: Best estimate
BEMUSE: Best Estimate Methods plus Uncertainty and Sensitivity Evaluation
CCFL: Counter current flow limit
CEA: Commissariat à l'Energie Atomique
CSNI: Committee on the Safety of Nuclear Installations
DNB: Departure from nucleate boiling
ECCS: Emergency core cooling
EDO: EDO Guidropress
FA: Fuel assembly
GRS: Gesselschaft fÄur Anlagen und Reaktorsicherheit
HPIS: High-Pressure injection system
IRSN: Institut de Radioprotection et de Sûreté Nucléaire
ISP: International standard problem
JNES: Japan Nuclear Energy Safety
KAERI: Korea Atomic Energy Research Institute
KINS: Korean Institute of Nuclear Safety
LBLOCA: Large break loss of coolant accident
LOCA: Loss of coolant accident
LOFT: Loss of fluid test
LPIS: Low-pressure injection system
NEA: Nuclear Energy Agency
NPP: Nuclear Power Plant
NRI: Nuclear Research Institute
OECD: Organization for Economic Cooperation and Development
PCT: Peak cladding temperature
PSI: Paul Scherrer Institute
PWR: Pressurized water reactor
RTA: Relevant thermalhydraulic aspects
UNIPI: University of Pisa
UPC: Universitat Politècnica de Catalunya
WGAMA: Working Group on Accident Management and Analysis
ΔPCT: Delta PCT
ΔREFLOOD: Delta time of reflood.

Acknowledgments

This paper contains results produced within an OECD-NEA BEMUSE Project. The authors are grateful to OECD-NEA. The authors are also grateful to the Spanish Nuclear Safety Council (Consejo de Seguridad Nuclear) for funding UPC's participation in the project.

References

[1] NUREG/CR-5249, "Quantifying Reactor Safety Margins—Application of CSAU to a LBLOCA," December 1989.

[2] G. E. Wilson, et al., "Quantifying reactor safety margins—part 2: characterization of important contributors to uncertainty," *Nuclear Engineering and Design*, vol. 119, pp. 17–31, 1990.

[3] W. Wulff, et al., "Quantifying reactor safety margins—part 3: assessment and ranging of parameters," *Nuclear Engineering and Design*, vol. 119, pp. 33–65, 1990.

[4] "Best-Estimate Methods (Including Uncertainty Methods and Evaluation) Qualification and Application," First Meeting of the Programme Committee NEA/SEN/SIN/AMA(2003)8, Issy-les-Moulineaux, France, February 2003.

[5] M. Pérez,, F. Reventos, L. Batet, and R. Pericas, "Phase 4 of BEMUSE Programme: Simulation of a LB-LOCA in ZION Nuclear Power Plant. Input and Output Specifications," UPC Report, Barcelona, Spain, July 2007.

Hindawi Publishing Corporation
Science and Technology of Nuclear Installations
Volume 2010, Article ID 646971, 7 pages
doi:10.1155/2010/646971

Review Article

Fuel R&D Needs and Strategy towards a Revision of Acceptance Criteria

François Barré, Claude Grandjean, Marc Petit, and Jean-Claude Micaelli

Institut de Radioprotection et de Sûreté Nucléaire (IRSN), Direction de Prévention des Accidents Majeurs, BP3, 13115 Saint-Paul lez Durance Cedex, France

Correspondence should be addressed to François Barré, francois.barre@irsn.fr

Received 5 May 2009; Accepted 30 December 2009

Academic Editor: Nikola Čavlina

The study of fuel behaviour under accidental conditions is a major concern in the safety analysis of the Pressurised Water Reactors. The consequences of Design Basis Accidents, such as Loss of Coolant Accident and Reactivity Initiated Accident, have to be quantified in comparison to the safety criteria. Those criteria have been established in the 1970s on the basis of experiments performed with fresh or low irradiated fuel. Starting in the 1990s, the increased industrial competition and constraints led utilities to use fuel in more and more aggressive conditions (higher discharge burnup, higher power, load follow, etc.) and create incentive conditions for the development of advanced fuel designs with improved performance (new fuel types with additives, cladding material with better resistance to corrosion, etc.). These long anticipated developments involved the need for new investigations of irradiated fuel behaviour in order to check the adequacy of the current criteria, evaluate the safety margins, provide new technical bases for modelling and allow an evolution of these criteria. Such an evolution is presently under discussion in France and several other countries, in view of a revision in the next coming years. For this purpose, a R&D strategy has been defined at IRSN.

1. Industrial Context

The economic context is increasingly demanding for the utilities who, in order to keep competitive, have to produce the cheapest possible KWh while retaining sufficient flexibility to adjust the energy produced to the demand. The response of nuclear reactor operators is to increase reactor power, the cycle length (and thus discharge burnup), and the fuel enrichment. Applying flexible operating modes involve power variations imposing high stresses on the fuel which must be taken into account when considering changes in Safety Assessment.

Fuel rods are therefore subjected to increasing mechanical, thermal and chemical stresses in the new fuel management procedures, while having to satisfy the following contradictory requirements:

(i) reliability, to avoid degrading the operating conditions (e.g., few manufacturing defects, low deformation of assemblies, etc.),

(ii) robustness, to withstand the contingencies of the operating conditions (e.g., low corrosion),

(iii) high performance, to provide margins that can be used in operation (sufficiently high PCI limit; proper behaviour in accident conditions: RIA, LOCA, etc.).

Furthermore, fuel elements are complex objects, the design of which requires an in-depth knowledge of coupled phenomena (neutronics, thermohydraulic, thermomechanical, chemical) that are very difficult to separate out. To ensure the reliability and robustness of a new fuel element, to predict its performance (in particular, from a safety point of view, its behaviour in accidental conditions), it is therefore necessary to make use of simulation duly validated by experiment, including integral tests which may reveal previously unknown phenomena.

In addition, the number of fuel rods under operation in the world is very high and the probability to have defect rods or unknown phenomena is nonnegligible. For example, in France, the utility EDF manages more than 10,000 irradiated assemblies, representing about 2.7 million fuel rods, which are loaded in NPP reactor cores, exposed to a harsh environment (high temperature: 300°C for the

coolant, high flow velocity, aggressive chemistry: borated, lithiated fluid) over periods of up to six years.

In the current increasingly competitive context, the utilities clearly indicate that, for PWR presently under operation, there is a constant need to improve fuel performance and develop innovative products for a more efficient use of fuel at a time when the uranium market will be under pressure, so as to minimize the quantity of waste, to increase unit power and cycle length, and so forth.

It is planned to reinforce R&D on fuel for a continued improvement of the present products and optimization of their management and, in the long term, to design new fuel elements that represent a real break with today's current concepts. Substantial evolution of present technologies has been developed for an increase in robustness and performance, for example, a constant upgrading of the fuel matrices (UO2, MOX, etc.), a general use of consumable poisons, the introduction of doped pellets, and also continuous cladding evolution, with the introduction of M5, optimized ZIRLO, MDA, etc. New generation of products for the PWRs is under preparation.

Moreover, all operators are going to both diversify their fuel supply by calling upon manufacturers that are developing different technologies and benefit from progress made in fuel element design.

Thus, the diversity in fuel supply and in the operation of the various units means that a very large number of initial states and responses to various stresses in incident and accident conditions have to be taken into account in accident studies, the evolution of acceptance criteria, and available methodologies for safety demonstration.

2. Safety Needs

Safety demonstrations for pressurised water reactors are deterministic, supplemented by a probabilistic approach. The deterministic method is based on analysing postulated initiating events, which can be grouped to define a limited number of operating transients and design-basis incidents and accidents, which constitute the design-basis operating conditions. The studies of design-basis operating conditions must demonstrate compliance with safety requirements involving the first safety barrier that is the fuel cladding. As part of the safety demonstration, the safety requirements are developed into decoupling criteria (improperly referred to as safety acceptance criteria).

The objective is to guarantee a proper behaviour of the first barrier, in all conditions, including extended periods of operation, incidental situations, low-probability extreme accident conditions such as loss-of-coolant accidents (LOCAs) or reactivity-initiated accidents (RIAs). For such conditions the utility has to demonstrate the possibility of keeping the nuclear reaction under control, ensuring the short-term and long-term core cooling and a limited extend of cladding degradation, this last one being the first safety barrier.

In this respect, a safety baseline is used which defines the fuel operating conditions, the phenomena to be taken into account in normal operation or in incident or accident conditions, the computing methodologies and tools to be used for safety demonstration, and of course the acceptance criteria to be met. IRSN must make sure that this safety baseline is relevant (if necessary pressing for changes) and that the criteria are met, and must also assess the operating margins during reactor operation.

Expert assessment of fuel is an excessively difficult field, first because of the complexity of the physics (multidisciplinary), the mechanisms of which are difficult to separate out and subjected to very varied boundary conditions (large number of external stresses). The difficulties are also technological, because of a large variety of technologies (constantly evolving field), a growing diversity and change in the operating conditions (leading to diversity of changes in the fuel while it is in the reactor), and the diversity of incident and accident conditions to be taken into account over the whole downstream fuel cycle.

Furthermore, the utility, in its concern for economic profitability and therefore always getting the most out of the fuel, is led to use ever-more-sophisticated methods and arguments in order to demonstrate compliance with the safety baselines.

Thus Safety Assessment should be based on a well-thought-out simulation/experimentation R&D strategy, including in-pile integral testing. The IRSN has to conduct such a major R&D programme, so as to be in a position to validate products, assessment methodologies, and operating conditions. One reason is that Technical Support Organisation (TSO), such as IRSN, should be leader in the investigation of accidental situations. They must also develop generic knowledge and computing tools because of the diversity of situations that will have to be assessed (technologies, operation, etc.), have their own computing tools and methodologies in order to ensure the independence of their judgement, and provide high-level skills training for expert assessment.

In this paper we focus on the R&D needs towards a revision of acceptance criteria and the evolution of methodologies used for the safety assessment for LOCA and RIA.

3. R&D Strategy for Revisiting Loss of Coolant Accidents (LOCAs); The CYCLADES Project

The LOCA results from a break in the primary circuit that leads to the depressurisation of the primary system with power decrease to its residual level and water reflooding. As a consequence, the core fuel rods undergo the following evolution: clad temperature increase and dry-out, transfer of the stored energy from the fuel to the clad, clad ballooning with possible contact with the neighbouring rods, burst failure around 800°C and fuel relocation inside the ballooned zone; beyond this phase, oxidation of the cladding will occur at high temperature leading to a significant clad embrittlement before quenching due to reflooding water.

The LOCA is a Design-basis accident (DBA) used for the design of the safety emergency cooling systems and the limitation of the power at the hottest point in the core during normal operation. The safety principle is that the coolability

of the core has to be preserved. The associated safety requirements are to ensure the resistance of the fuel rods upon quench and postquench loads and to maintain a coolable geometry in the core. These requirements are formalised in safety criteria, associated with limit values, mainly expressed through a maximum cladding temperature (PCT) and an equivalent cladding reacted ratio (ECR) (ECR is the ratio of the cladding thickness equivalently transformed into ZrO_2 by oxidation over the initial clad thickness, taking into account possible thinning during clad ballooning) with the aim of ensuring a residual ductility of the cladding for maintaining core coolability capability on short- and long-term duration. In France as in the U.S., the current limits are 1204°C on PCT and 17% on ECR. These LOCA acceptance criteria are issued from a long process in the United States (Ergen Task force in 1967, Interim Acceptance Criteria for ECCS in 1971, then ECCS Rule-making Hearing in 1972-1973). Since they were established, the evolution of fuel operating conditions and fuel technologies leads the international community to review the technical basis to reassess these criteria and their limit values.

In order to prepare acceptance criteria reassessment, IRSN recently conducted an extensive Start-of-the-Art–Review relative to fuel behaviour under LOCA conditions, covering the aspects of clad ballooning and flow blockage, coolability of partially blocked assemblies, clad oxidation, and clad resistance to quench and postquench loads [1–3]. Additionally, a review of existing computation tools devoted to the calculation of fuel behaviour under LOCA was performed. Together with the outcomes from the recent results from experimental program, this leads to summarising the main pending questions relative to fuel behaviour under LOCA in the three following topics:

(i) the cladding embrittlement, to address the loss of cladding integrity upon quench and postquench loads,

(ii) the relocation of fuel in the ballooning parts of the fuel rods,

(iii) the flow blockage by ballooning rods and its coolability.

IRSN considers important that these questions be solved to guarantee core coolability in a postulated LOCA transient and has launched an R&D project, named CYLCADES, to investigate them.

3.1. Cladding Embrittlement. The effects of both alloy composition and burnup on cladding embrittlement were extensively studied [3, 4] but questions still remain to properly understand physical phenomena and to ensure a correct prediction of the behaviour of future cladding alloys. Some of the hydrogen that is liberated in the corrosion process enters the cladding during normal operation. The hydrogen was found to produce a strong effect on the embrittlement of the cladding, but the effect is indirect. Hydrogen mainly acts as a catalyst while oxygen, which diffuses into the cladding metal during a LOCA transient, and is the direct cause of embrittlement. Oxygen from the oxide fuel pellets was found to enter the cladding from the inner side in high-burnup fuel in addition to the oxygen that enters from the oxide layer on the outer side of the cladding. Under conditions that might occur during a small-break LOCA, the accumulating oxide on the surface of the cladding can break up and was found to let large amounts of hydrogen into the cladding during the LOCA transient, thus exacerbating the embrittlement process. The current work also confirmed an older finding that, if rupture occurs during a LOCA transient, large amounts of hydrogen can enter the cladding from the inside near the rupture location.

Postquench ductility, a commonly used parameter in the past as the basis of safety criteria, appears as an inappropriate parameter to define an embrittlement threshold, since no practical limit can be derived to ensure ductility retention in the cladding balloon. However, the results from ANL 4-point bending tests [5] at room temperature on unirradiated samples after integral testing suggest that, below some oxidation limit, the rod cladding would resist fragmentation when subjected to quench and postquench loads.

A strength-based approach addressing the structural response of the whole cladding, instead of a ductility approach, might provide an acceptable alternative. IRSN has proposed a two-step R&D strategy to address those questions.

The first step is to quantify a relevant embrittlement threshold. The first important item is to identify and quantify mechanical loads that should be supported by fuel rods during quench and post-quench phases of LOCA transients. This will be informed through from numerical simulations in bundle geometry. It is a necessary challenge. Afterwards, appropriate structural response tests, taking into account bounding mechanical loads (quench under controlled loading, impact tests, etc.) to determine embrittlement threshold, should be defined. Finally, it is necessary to carry out Finite Element calculations with typical cladding geometry and properties to verify that the experimental domain covered by this type of tests is adequate. This step may require appropriate analytical experimental tests to characterise the evolution of clad properties, in particular at the location of the balloons.

The second step is to select the most appropriate parameter characterising the oxidation and hydriding amount on which to correlate embrittlement, so as to find out an alternative to the ECR. It is based on the previous work from early investigators ([6–9], etc.). At that time, research programs and calculation tools were not ready to make successful these attempts. Based on the one hand on this previous work and on the other hand on recent important research results obtained at ANL [4], CEA [10], or JAEA [11], IRSN considers that an embrittlement threshold based on residual thickness of prior β-Zr layer with low oxygen content as function of H content should be more appropriate. In this respect, IRSN has been developing an R&D program which consists in a computer code development (diffusion code DIFFOX), with the support of specific tests and experimental techniques (IRSN MARGO-R tests), which makes possible to correctly evaluate the thickness of the β layer and the oxygen distribution in this layer [12].

3.2. Axial Fuel Relocation. During normal operation, oxide fuel pellets develop many cracks because of thermal stresses. After clad ballooning and burst, some fragmented fuel particles located above the ballooned region of a fuel rod will thus relocate into the enlarged volume of the balloon under the influence of gravity and pressure differences. This effect was first noticed in 1980 in reactor tests in the United States (PBF/LOC tests, INEL, [13]), Germany (FR-2 tests, KFK, Karb 83), and France (FLASH-5 tests, Bruet 92), and recent integral tests at Argonne National Laboratory (ANL) and the Halden Reactor Project in Norway (IFA-650 test series) have confirmed it. The consequence of fuel relocation is an increase in heat generation in the ballooned region together with a reduction of the thermal resistance between fuel and cladding, which may increase the cladding temperature and oxidation compared with an undeformed length of the fuel rod.

The strategy proposed by the IRSN is to carry out integral tests with different cladding, different types of fuel pellets, and different burn-ups, in particular to actively support the on-going OECD program performed in the Halden reactor (IFA-650 test series) and to consider complementary tests in the Halden reactor or the Cabri reactor (with the use of the hodoscope which allows to analyse precisely the fuel relocation without moving the rods). A consistent and sound interpretation of this large range of older and recent tests has to be performed and will be supported by laboratory studies to understand the basic mechanisms of fuel fragments slumping and accumulation in a cladding balloon and then to model fuel fragmentation as function of fuel types, burn-up, and power load history. Then, in the calculation tools, balloon filling ratio should be given as a function of fuel rod characteristics.

3.3. Flow Blockage and Its Coolability

3.3.1. Flow Blockage Characteristics. The question of the cumulative effects of irradiation, which homogenize the azimuthal temperature distribution in the fuel rod cladding, and of the bundle size on the main characteristics of the blockage (maximum flow restriction ratio, axial extent) has been under investigation for a long time and several programmes have been devoted to it (see [1]). Based on a comparison of the burst strains obtained in ORNL Single rod/ Multirod tests and in PBF-LOC tests with fresh rods/irradiated rods, one of the major conclusions of the past R&D programmes was provided by INEL, which recommended to perform in-pile bundle tests of sufficient bundle size with irradiated rods [13].

However, such a strategy might lead to significant costs; indeed, a short series of in-pile integral bundle tests could close the issue for a given fuel but let it open for another type of fuel; in addition, in-pile experimental facilities for testing with large size bundles are more and more difficult to find (PHEBUS reactor has been recently shutdown!).

A simulation strategy based on the use of a detailed and well assessed code is proposed by IRSN. For this purpose, with the support of EDF, IRSN is developing the DRACCAR code [14] which is a multirod 3D thermomechanics code, with mechanical and thermal interactions between rods, coupled with subchannel type two-phase flow codes. DRACCAR code has to be rigorously assessed prior to reactor applications. The model validation will be based on the results of existing experimental programmes and additional in-pile tests with single irradiated fuel rods in a well instrumented prototypical environment; these tests could be performed in the Cabri reactor and could possibly be complemented by "small" bundle tests. This can be supported, if necessary, by more analytical out-of-pile tests focusing on clad-to-clad thermomechanical interactions and balloon axial extension.

3.3.2. Flow Blockage Coolability. IRSN has carried out a state-of-the-art review of the main experimental programmes related to the question of the coolability of blocked regions in a rod bundle after ballooning in a LOCA, such as the FEBA, SEFLEX, THETIS, ACHILLES, CEGB, and FLECHT-SEASET programmes [2], as well as of several analytical developments performed in association with these experimental programmes. The conclusions drawn from these results were used to improve our understanding of the physical phenomena governing the behaviour of a partially blocked rod array during a LOCA reflood scenario and to evaluate the limits of blockage coolability under the most severe geometric (blockage ratio and length) and thermo-hydraulic conditions. However, it is important to underline that these results were obtained in out-of-pile experiments performed with electrically heated fuel rod simulators with a large gap between the heaters and the ballooned cladding. These experiments promote the cladding coolability because it is separated from the heat source by a wide gap, which is not representative of the situation with fragmented fuel accumulated in the cladding balloons (fuel relocation), as was observed during all in-pile tests with irradiated fuel rods. The impact of fuel relocation upon blockage coolability therefore remains to be investigated.

It is necessary to perform out-of-pile experiments with a partially blocked full-length bundle, with realistic simulation of fuel relocation in the balloons, in view of updating the upper bound value of maximum blockage remaining coolable. It can be supported by some more analytical tests addressing basic phenomena (droplet impact and fragmentation, heat transfer on balloon walls, flow redistribution, etc.) to reach a better understanding of the leading phenomena and to select the most appropriate form of heat transfer correlations for the DRACCAR code.

4. R&D Strategy for Revisiting Reactivity Initiated Accident (RIA)

The postulated reactivity initiated accident results from the failure of the drive mechanism of a control rod cluster made of absorber rods regulating the nuclear reaction. This failure causes the ejection of the control rod cluster due to pressure difference (around 150b) between reactor cooling system and containment and leads to reactivity insertion. This accident generates a fast power transient (in some tens

of milliseconds) with significant energy injection in the fuel rods neighbouring the ejected control rod assembly, and raises the following questions.

(i) Do the fuel rods fail and what are the rod failure conditions for the various fuel types, operating conditions experienced by the fuel rod, and burnup levels?

(ii) Does ejection of solid fuel particles into the coolant occur after rod failure?

(iii) If fuel is ejected, could the fuel-coolant thermal interaction propagate the accident to the neighbouring rods and jeopardize the core cooling capability?

RIA is a DBA; the safety principle is the preservation of core coolability. The associated safety requirements are defined in order to limit the fuel pellets melting and the number of fuel rods affected by boiling crisis and to avoid fuel dispersion in the primary coolant. The associated current safety criteria for RIA have been formulated in the 1970s on the basis of the available experimental database (from SPERT, PBF, and early NSRR experiments) that was restricted to fresh or slightly irradiated UO2 fuels (up to 30 GWd/tU for UO2 fuel) and with cladding and fuel technologies which are no more currently in operation. However, the clear evidence of specific aspects of highly irradiated fuel that could affect the transient rod behaviour during a RIA and the lack of data on irradiated MOX fuel, created the need to both verify and/or adjust the current safety criteria and to evaluate the corresponding margins. As a result, various organizations in most countries operating reactors [15–17] are assessing the RIA limits that apply to current and future fuels, in terms of component materials as well as burn-up.

Indeed, several CABRI REP tests (Na-1 to Na-12) on UO_2 and MOX rods with zircaloy-4 cladding were carried out by IRSN between 1993 and 2000 in the sodium loop of the CABRI reactor. The test results revealed rod failures for enthalpy values less than the SPERT failure threshold of 140 cal/g for irradiated fuels. These CABRI tests clearly showed the need to define new criteria for irradiated fuel [18]. Most countries that operate reactors decided that the RIA criteria were in need of changes and are cofinancing experimental programmes to generate fuel behaviour data. This primarily concerns the CIP programme (IRSN) [19] and the ALPS programme (JAEA) [20].

4.1. The IRSN Strategy. In order to be able to give relevant technical advice on revising the RIA criteria, the IRSN felt it is necessary to develop its own methodology for deriving RIA safety limits. Indeed, developing a methodology call for a thorough understanding of the physical mechanisms involved in each phase of an RIA, supported by interpretation of the experimental database, developing computing codes, identifying the relevant parameters using the above methodology. All those aspects are required for an accurate assessment of the safety criteria and methodologies proposed by the utilities.

Taking into account these considerations, as well as the continuous fuel evolutions, the complex and intimately coupled phenomena under transients, IRSN, develops an R&D strategy which aims at getting physical bases for establishing new safety criteria. The approach consists of

(i) the development of the SCANAIR computational tool dedicated to the description of the global fuel rod behaviour in reactor conditions; it has to be validated on the available tests for valuable prediction capability and for use in supporting expertise studies,

(ii) the acquisition of the necessary knowledge and identification of the main phenomena, through in-pile testing programs in which consequences of a fast power transient applied to an industrial irradiated fuel rod (single) can be studied under representative reactor conditions (nuclear heating, coolant temperature, thermo-mechanical loading, etc.) up to rod failure and postfailure events, taking into account the intimately coupled phenomena;

(iii) the performance of separate effect tests programs aiming at the back-up of the SCANAIR development and at improvement of the understanding of some parts of the phenomenology; for instance, the Prometra program for mechanical characterisation of the Zr-4 and advanced claddings Zirlo and M5 [21], the Patricia program for the study of clad to coolant heat transfer under fast transient [22], the fission gas dynamic (FGD) program under preparation within cooperation with JAEA;

(iv) the development of a more detailed modeling with a multiscale approach when possible, allowing confirmation of the necessarily simplified models implemented in the reactor computational tool.

4.2. In-Pile Experiments. The main outcomes of the Cabri REP-Na program, conducted by the IRSN in 1992–2002 with the support of EDF, was the role of hydrides in the risk of rupture, the contribution of fission gases at the grain boundaries, the importance of oxide layer spalling, and above all the need to update the current safety criteria, which are no longer appropriate for present operation conditions. The Cabri International Program conducted by IRSN, launched in 2002, under OECD auspices with a broad international cooperation and partnership of EDF, will be carried out in the renewed facility under typical pressurised water reactor conditions. The main objectives are to address the pending questions relative to the fuel rod behaviour over the whole transient, the occurrence of boiling crisis and its consequences on rod failure with high clad temperature, high coolant and rod internal pressures and fission gas loading, and the postfailure phenomena (fuel ejection, fuel-coolant interaction with finely fragmented solid fuel, thermal to mechanical energy conversion). The capability of the CABRI reactor with typical PWR conditions and its versatility will allow exploring the influence of the pulse width on the phenomena as well as the effect of advanced fuel microstructures for UO2 and MOX.

Today the IRSN is moving towards "analytical" safety criteria [23, 24]; implementation of which is based on more detailed understanding of the physical phenomena involved (e.g., the different clad failure modes of hydrided claddings). Same kinds of approaches are developed by EDF and EPRI [24]. Studies in progress at present, in particular at the IRSN, suggest that the study of the zero power RIA is not necessarily conservative for all cases and that conditions at intermediate power must be considered. The Cabri REP-Na and CIP0 programmes have shown that the tests were very complex and could not be used in a binary manner (failed/not failed). Their interpretation necessitates analytical tests, upstream research, use of complex simulation tools, and understanding of coupled basic phenomena (mechanics, materials, thermochemistry). No consensus has been reached on the interpretation of some tests in the REP-Na programme, and comparison with the NSSR tests rises up new questions, for example, the effect of initial test temperature. Lastly, the criteria as conceived for the binary failed/not failed approach would necessitate thorough RIA tests on all types of fuel, cladding, and burnup and having experienced all types of transient during life in a reactor, which is not achievable. A simulation approach must therefore be considered in order to extrapolate to actual rods under reactor conditions, but validated by a broader range of RIA tests and analytical tests. Changes in the safety baseline, like fuel technologies, lead inevitably to consideration of new programmes after CIP, taking up a clear position in favour of a simulation approach.

The objectives of future programmes in Cabri will be to validate the new analytical safety criteria, to test rods with new fuel rod technologies, to explore accident conditions not yet investigated.

Tests at zero initial power must therefore be considered, updating the concept (and the instrumentation) to give a better response to the following current approaches:

(i) more analytical tests, on lengths of moderate size prepared from a given rod stage, scanning physical parameters, for example, different deposited energies; tests on defective rods for more specific study of fuel ejection conditions and consequences might be considered;

(ii) tests to explore other types of pulse insofar as late injected energy could have a strong influence on behaviour after departure from nucleate boiling;

(iii) RIA tests similar to those of the CIP programme (full length in particular) on new fuel rods (changes in cladding, fuels, etc.); potential needs include changes in fuels (additives, pellet geometries), high burnup (>45 GWd/t) gadolinium-containing rods, VVER fuels, new products to counter PCI (short pellets), and so forth.

In parallel, it is also necessary to explore the cases at intermediate powers which are not covered by the transients at zero power.

5. Conclusion

The increased industrial competition and constraints result in more aggressive conditions for the fuel (higher burnup, higher power, load follow, etc.) and create incentive conditions for the development of advanced fuel designs with improved performance (new fuel types with additives, cladding material with better resistance to corrosion, etc.). This situation involved the need for new investigations of irradiated fuel behaviour under reference accidents in order to check the adequacy of the current criteria, evaluate the safety margins, provide new technical bases for modelling, and allow an evolution of these criteria. Safety Assessment should be based on a well-thought-out simulation/experimentation R&D strategy, including in-pile integral experiment. Technical Support Organisation (TSO), such as IRSN, should be leader in the investigation of accidental situations. They must also develop generic knowledge and computing tools because of the diversity of situations that will have to be assessed (technologies, operation, etc.). They have to get their own computing tools and methodologies in order to ensure the independence of their judgement and provide high-level skills training for expert assessment.

The IRSN is proposing an R&D programme, in the framework of international collaboration, in particular with TSOs, so as to be in a position to validate products, assessment methodologies, and operating conditions.

In this paper we focused on the R&D program proposed by IRSN in the context of a revision of acceptance criteria and the evolution of methodologies used for the safety assessment for LOCA and RIA.

In supporting evolution of LOCA criteria, IRSN is developing the CYCLADES program which adresses the main following topics.

(i) The analysis of cladding embrittlement with integral experiments taking into account bounding mechanical loads and the analysis of most appropriate parameters to characterise hydriring and oxidation of the cladding.

(ii) The axial fuel relocation, in developping experimental programs in Halden and CABRI reactors.

(iii) The coolability of flow blockage with a program of out-of-ile coolability experiments and single rod flow blockage experiments in CABRI reactors.

Concerning RIA, the IRSN strategy is based on mechanical tests on claddings, the forthcoming CIP and complementary programs on CABRI adressing postboiling crisis ruptures, fuel coolant interactions, and radiological releases.

All these programs are linked with a simulation strategy for extrapollation to reactor conditions.

References

[1] C. Grandjean, "A state of the art review of past programs devoted to fuel behaviour under LOCA conditions—part 1: clad swelling and rupture; assembly flow blockage," IRSN/DPAM/SEMCA 2005-313, http://net-science.irsn.org/.

[2] C. Grandjean, "A state of the art review of past programs devoted to fuel behaviour under LOCA conditions—part 2: impact of clad swelling upon assembly cooling," IRSN/DPAM/SEMCA 2006-183, http://net-science.irsn.org/.

[3] C. Grandjean and G. Hache, "A state of the art review of past programs devoted to fuel behaviour under LOCA conditions—part 3; cladding oxidation, resistance to quench and post quench loads," IRSN/DPAM/SEMCA 2008-093, http://net-science.irsn.org/.

[4] M. Billone, Y. Yan, T. Burtseva, and R. Daum, "Cladding embrittlement during postulated loss of coolant accidents," Tech. Rep. NUREG/CR-6967/ ANL-07/04, Argonne National Laboratory, Argonne, Ill, USA, 2007.

[5] M.C. Billone, Y. Yan, and T. Burtseva, "Overview of ANL LOCA programs," in *Proceedings of the ANL LOCA Program Review Meeting*, Argonne National Laboratory, Argonne, Ill, USA, October 2007.

[6] D. O. Hobson, "Ductile-brittle behaviour of Zry fuel cladding," in *Proceedings of the Topical Meeting on Water Reactor Safety*, Salt Lake City, Utah, USA, March 1973.

[7] R. E. Pawel, "Oxygen diffusion in beta zircaloy during steam oxidation," *Journal of Nuclear Materials*, vol. 50, no. 3, pp. 247–258, 1974.

[8] A. Sawatzky, "A proposed criterion for the oxygen embrittlement of Zircaloy 4fuel cladding, zirconium in the nuclear industry," *ASTM STP*, vol. 681, pp. 479–496, 1979.

[9] H. M. Chung and T. F. Kassner, "Embritttlement criteria for Zircaloy Fuel Cladding applicable to accident situations in Light Water reactors," *Summary Report*, no. NUREG/CR-1344, ANL-7948, January 1980.

[10] J. C. Brachet, et al., "Overview of CEA analytical studies on the cladding behaviour during and after prototypical LOCA transients," in *Proceedings of the OECD Ad-Hoc LOCA Meeting*, Paris, France, June 2006.

[11] F. Nagase, M. Tanimoto, and H. Uetsuka, "Study on high burnup fuel behaviour under a LOCA condition at JAERI," in *Proceedings of the IAEA Technical Committee Meeting on Fuel Behaviour under Transient and LOCA Conditions*, Halden, Norway, September 2001.

[12] C. Grandjean and L. Belovski, "Oxidation of Zircaloy under LOCA conditions; development of the diffusion code DIFFOX 1.1," in *Proceedings of the ANL LOCA Program Review Meeting*, Argonne National Laboratory, Argonne, Ill, USA, October 2007.

[13] J. M. Broughton, et al., "PBF Loca tests," fuel behaviour report NUREG/CR-3184, EGG-2244, 1983.

[14] G. Repetto, F. Jacq, F. Barré, F. Lamare, and J. M. Ricaud, "DRACCAR, a new 3D thermal mechanical computer code to simulate LOCA transients on Nuclear Power Plants," in *Proceedings of the International Congress on Advances in Nuclear Power Plants (ICAPP '09)*, Tokyo, Japan, May 2009.

[15] R. Landry, "Technical and regulatory basis for the reactivity Initiated accident interim acceptance criteria and guidance," Memorendum ML070220400, January 2007.

[16] L. O. Jernkvist, et al., "Assessment of core failure limits for LWRs under RIA," SKI Report 2005-16.

[17] M. T. Del Barrio and L. E. Herranz, "Failure criteria of a fuel rod during RIA," CIEMAT Report DFN/SN-03/OP-02, 2002.

[18] J. Papin, et al., "Summary and interpretation of the CABRI REP-Na Program," *Nuclear Technology*, vol. 157, no. 3, pp. 230–250, 2007.

[19] J. Papin, M. Petit, C. Grandjean, and V. Georgenthum, "IRSN R&D studies in high burn up fuel behaviour under RIA and LOCA conditions," in *Proceedings of the Top Fuel Conference*, Salamanca, Spain, October 2006.

[20] T. Fuketa, et al., "Behaviour of high burnup PWR fuels during simulated reactivity initiated accident conditions," in *Proceedings of the Top Fuel Conference*, Salamanca, Spain, October 2006.

[21] B. Cazalis, J. Desquines, C. Poussard, et al., "The PROMETRA program: fuel cladding mechanical behavior under high strain rate," *Nuclear Technology*, vol. 157, no. 3, pp. 215–229, 2007.

[22] V. Bessiron, "Modelling of clad-to-coolant heat transfer for RIA applications," *Journal of Nuclear Science and Technology*, vol. 44, no. 2, pp. 211–221, 2007.

[23] C. Sartoris, A. Taisne, M. Petit, F. Barré, and O. Marchand, "A consistent approach to assess safety criteria for reactivity initiated accidents," *Nuclear Engineering and Design*, vol. 240, no. 1, pp. 57–70, 2010.

[24] "Nuclear fuel behaviour during reactivity initiated accidents," in *Proceedings of the OECD/NEA Workshop*, Paris, France, September 2009.

Hindawi Publishing Corporation
Science and Technology of Nuclear Installations
Volume 2010, Article ID 457094, 11 pages
doi:10.1155/2010/457094

Research Article

CATHARE Multi-1D Modeling of Coolant Mixing in VVER-1000 for RIA Analysis

I. Spasov,[1] J. Donov,[1] N. P. Kolev,[1] and L. Sabotinov[2]

[1] *Institute for Nuclear Research and Nuclear Energy, Tsarigradsko Chaussee 72, 1784 Sofia, Bulgaria*
[2] *Institute de Radioprotection et Surete Nucleaire, 92262 Fontenay-aux-Roses, France*

Correspondence should be addressed to N. P. Kolev, npkolev@abv.bg

Received 25 April 2009; Accepted 25 October 2009

Academic Editor: Alessandro Petruzzi

The paper presents validation results for multichannel vessel thermal-hydraulic models in CATHARE used in coupled 3D neutronic/thermal hydraulic calculations. The mixing is modeled with cross flows governed by local pressure drops. The test cases are from the OECD VVER-1000 coolant transient benchmark (V1000CT) and include asymmetric vessel flow transients and main steam line break (MSLB) transients. Plant data from flow mixing experiments are available for comparison. Sufficient mesh refinement with up to 24 sectors in the vessel is considered for acceptable resolution. The results demonstrate the applicability of such validated thermal-hydraulic models to MSLB scenarios involving thermal mixing, azimuthal flow rotation, and primary pump trip. An acceptable trade-off between accuracy and computational efficiency can be obtained.

1. Introduction

This work is motivated by the need for improved single-phase vessel mixing models in system codes that are able to properly represent local effects in reactivity insertion accidents. The study has been performed in Phase 2 of the OECD VVER-1000 coolant transient benchmarks labelled V1000CT-2 [1, 2]. These benchmarks provide a consistent approach to the testing of coupled neutronic/thermal-hydraulic codes. Separate exercises are devoted to stand-alone testing of thermal hydraulic and core physics models. Then the validated models are tested in coupled code simulation of asymmetric MSLB transients.

The V1000CT-2 vessel mixing benchmark [1] is based on a steam generator isolation experiment during the plant commissioning phase of Kozloduy-6 in Bulgaria. Local and integral plant data are available for comparison. The objective of this benchmark is to test the capability of system and CFD codes to represent in-vessel thermal hydraulics. The purpose of the V1000CT-2 MSLB benchmark is to test the core neutronics and coupled N/TH calculations. This paper presents results of thermal-hydraulic calculations with CATHARE [3] for the VVER-1000 coolant mixing and MSLB benchmarks.

2. The VVER-1000 Reactor

The reference plant is Kozloduy-6 with a VVER-1000 V320 in Bulgaria. This is a four-loop pressurized water reactor with horizontal steam generators (SGs). The steam is supplied to a 1000 MWe turbine. The core is of open type and contains 163 hexagonal fuel assemblies, each of which has 312 fuel rods, 18 guide channels for control rods, and a central instrumentation tube. The fuel pins are arranged in triangular grid. The geometry of the reactor pressure vessel is shown in Figure 1. See [1] for details.

The flow in the lower part of the vessel is throttled through the perforated barrel bottom (1344 holes) and the perforated fuel support columns serving as flow distributors. The support columns are welded at the core support plate so that no flow passes around the support columns. The primary coolant flows through the slots, upward through the support columns, and into the fuel assemblies. The flow through the core region consists of flow through the heated part and 2.9% bypass flow of which 2.2% is through the control rod guide channels and water holes.

At the upper core plate most of the fuel assembly heads are connected to guide tubes located in the upper plenum to protect the control rods and instrumentation

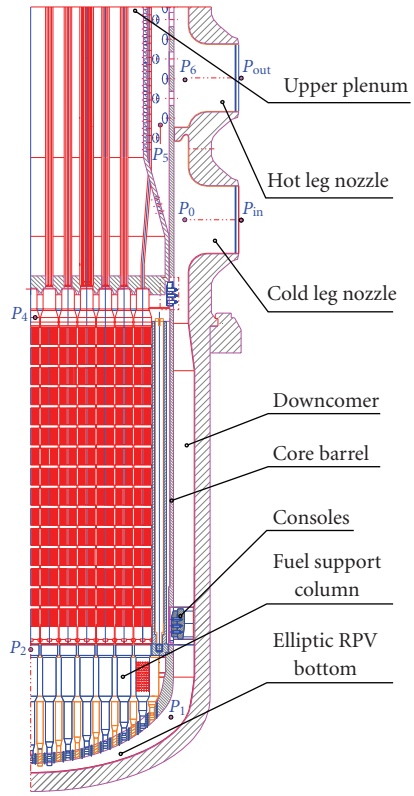

Figure 1: VVER-1000 reactor pressure vessel and internals.

cables from mechanical impacts. The bulk flow to the upper plenum passes mainly through the holes of the upper plate around the guide tubes. The bypass flow through the guide tubes is about 1% of the total because of the small flow area of the available orifices (see [1]). The outlets of ninety five assemblies are equipped with thermocouples located eccentrically in the upper part of the assembly head. Because of construction peculiarities there is a quasi-stagnation flow at the location of the thermocouples. The cooler jets through the control rod guide channels cause the measured temperature to be somewhat lower than the real coolant temperature at the end of the heated part. This should be taken into account when comparing with computations, or estimated core inlet temperatures can be used for comparison.

The flow in the upper plenum passes upwards, then through the perforated walls of the support ring and the core barrel to the vessel outlet.

3. Test Cases

3.1. Calculation of the Kozloduy-6 Vessel Mixing Experiment. The Kozloduy-6 SG isolation problem at 9.36% nominal power and the corresponding vessel mixing was chosen as reference problem of the OECD V1000CT-2 Benchmark, Exercise 1 [1]. The benchmark provides a validation test of the vessel thermal hydraulics in case of loop temperature and flow disturbances with all main coolant pumps (MCPs) in operation. It is relevant to the initial part of VVER-1000 MSLB scenarios from hot full power. The test problem is considered as pure thermal hydraulic problem because the moderator temperature reactivity coefficient was close to zero and the relative power distribution was approximately constant during the transient.

The mixing experiment was initiated by disturbing loop no. 1. It includes three states: a stabilized initial state, a transient state, and a stabilized final state. These states are briefly described below. After the stabilization of the core outlet temperature and the pressure, the experiment was repeated for loop no. 2. The transient caused by disturbing loop no. 1 is selected for the coolant mixing analysis and the data of the second experiment is used indirectly to support the analysis.

3.1.1. Initial State. The reactor is at the beginning of Cycle 1 and the power is 9.36% of the nominal. All four MCPs and four SGs are in operation. The pressure above the core is 15.59 MPa, close to the nominal value of 15.7MPa. The coolant temperature at the reactor inlet is 268.6°C and the boron acid concentration is 7.2 g/kg (the coolant temperature reactivity coefficient is zero near 7.5 g/kg). For this initial state, the fuel assembly temperature rise $\delta T_{k,\mathrm{rel}} k$ = 1,95 in 95 instrumented assemblies was calculated from measured cold leg and assembly outlet temperatures. The measured data and the 60-degree rotational symmetry of the fresh fuel core were used to estimate the heat up for assemblies without temperature control, so that the full core temperature rise distribution was obtained.

3.1.2. Transient. A transient was initiated by closing the steam isolation valve of SG-1 and isolating SG-1 from feed water. The pressure in SG-1 started to increase and stabilized at 6.47 MPa in about 20 minutes. The main steam header pressure was maintained approximately constant during the transient by operating the steam dump to condenser in pressure control mode. The coolant temperature in the cold and hot legs of loop no. 1 rose by approximately 13.5°C and the mass flow rate decreased by about 3.4%. The mass flow rate through the reactor decreased by about 1%. At 90 seconds after the disturbance, the temperature of cold leg no. 1 exceeded that of the hot leg. The difference stabilized to 0.6–0.8°C in about 20 minutes. The reactor power changed 0.16% calculated from primary circuit energy balance. The initially symmetric core power distribution did not change significantly.

3.1.3. Final State. For the analysis presented here, the stabilized state of the experiment 30 minutes after the separation of the SG-1 is considered as "final state." The core inlet temperatures were calculated from the measured core outlet temperatures and the estimated assembly by assembly temperature rise δT_k, k = 1,163 for the initial state, where k is the assembly number. The $\delta T_{k,\mathrm{rel}}$ distribution was assumed constant during the transient due to the approximately constant normalized core power distribution.

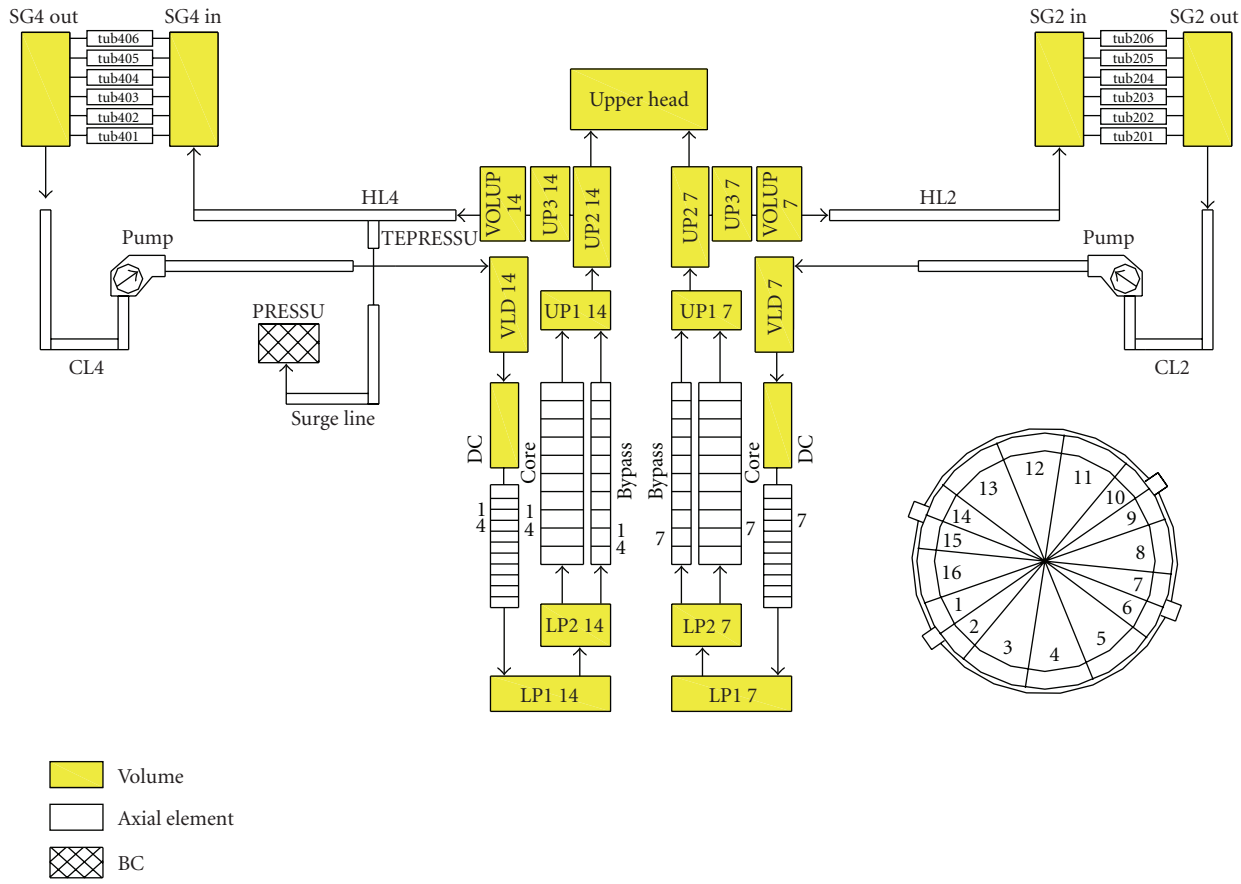

Figure 2: Primary circuit nodalization scheme (2 of 16 vessel channels are shown).

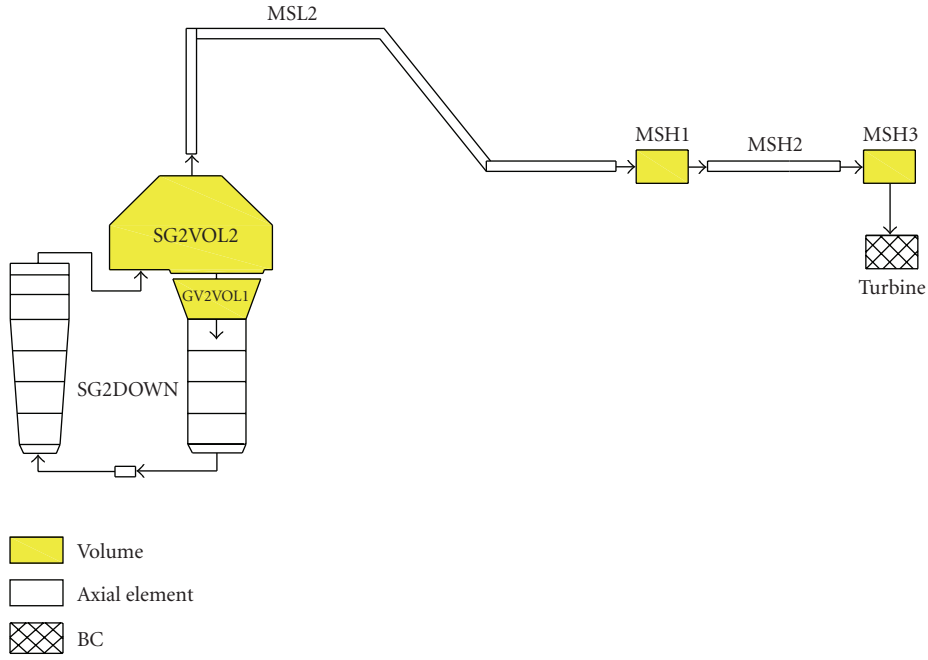

Figure 3: Secondary circuit nodalization scheme (SG-2 and steam line 2 are shown).

Table 1: Initial state.

Parameter	Plant data	Cathare 12 sectors	Cathare 16 sectors	Cathare 24 sectors	Uncertainty
Core power, MW	281	281	281	281	± 60
Pressure above the core, MPa	15.59	15.608	15.605	15.605	± 0.3
Cold leg no. 1 coolant temp, K	541.75	541.75 (BC)	541.75 (BC)	541.75 (BC)	± 1.5
Cold leg no. 2 coolant temp, K	541.85	541.85 (BC)	541.85 (BC)	541.85 (BC)	± 1.5
Cold leg no. 3 coolant temp, K	541.75	541.75 (BC)	541.75 (BC)	541.75 (BC)	± 1.5
Cold leg no. 4 coolant temp, K	541.75	541.75 (BC)	541.75 (BC)	541.75 (BC)	± 1.5
Mass flow rate 1, kg/s	4737	4737	4737	4737	± 200
Mass flow rate 2, kg/s	4718	4717.9	4718	4718	± 200
Mass flow rate 3, kg/s	4682	4682	4682	4682	± 200
Mass flow rate 4, kg/s	4834	4834	4833.8	4833.9	± 200
Reactor mass flow rate, kg/s	18971	18971	18971	18971	± 800
Hot leg no. 1 coolant temp, K	545	544.76	544.66	544.65	± 1.5
Hot leg no. 2 coolant temp, K	545.9	544.70	544.68	544.68	± 1.5
Hot leg no. 3 coolant temp, K	544.9	544.71	544.70	544.71	± 1.5
Hot leg no. 4 coolant temp, K	545	544.84	544.84	544.83	± 1.5
Reactor pressure drop, MPa	0.418	0.417	0.418	0.418	± 0.043

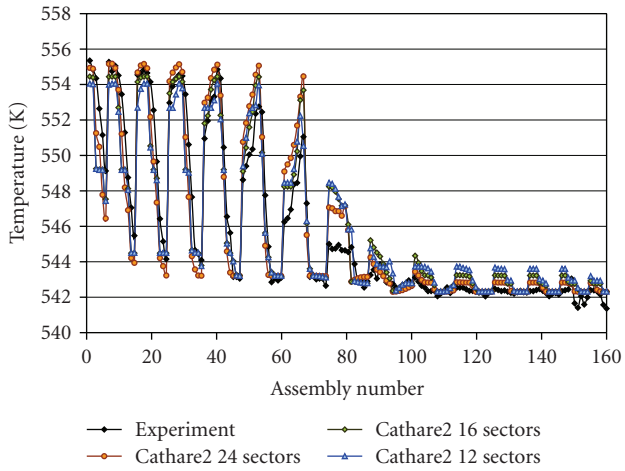

Figure 4: Kozloduy-6 flow mixing test: assembly by assembly core inlet temperatures.

For this analysis the benchmark problem was run with vessel boundary conditions from the V1000CT-2 benchmark specifications. The task is to calculate the coolant parameters at fuel assembly inlets and at the reactor outlets. Measured hot leg temperatures and estimated assembly inlet temperatures were used as reference.

3.2. VVER-1000 MSLB Problem. Two scenarios are defined for the purposes of OECD V1000CT-2 benchmark [2]. The first is close to the current licensing practice while the second is a pessimistic scenario derived from Scenario 1 by assuming that all main coolant pumps remain in operation and the scram worth is reduced through adjustment of the cross sections.

3.2.1. MSLB Scenario 1. Large MSLB between the SG and the steam isolation valve (SIV) without loss of off-site power.

The analysed transient is initiated by a main steam line break in a VVER-1000 between the SG and SIV, outside the containment.

One of the major concerns for this case is the possible return to power and criticality after reactor scram due to overcooling. Because of this concern, the main objective of the study is to clarify the local 3D feedback effects depending on the vessel mixing.

A burnt fuel loading with three-year fuel assemblies is considered. The reactor is at the end of cycle (EOC) and the initial hot full power (HFP) conditions are chosen consistent with the above objective. The SG water inventory is about the possible maximum at HFP. Following the break and the scram signal, one of the most reactive peripheral control assemblies remains stuck out of the core and is assumed to be in the affected sector.

A mechanical failure of the large feed water regulating valve in the broken line is assumed. At the time of the steam line rupture the valve starts to open from about 70% to 100% and then remains stuck in the open position. The main feed water flow to the faulted SG is terminated by closure of the feed water block valve in 52 seconds. The mass of feed water in the piping between the isolation valve and the affected SG, estimated to about 8000 kg, also contributes to the overcooling.

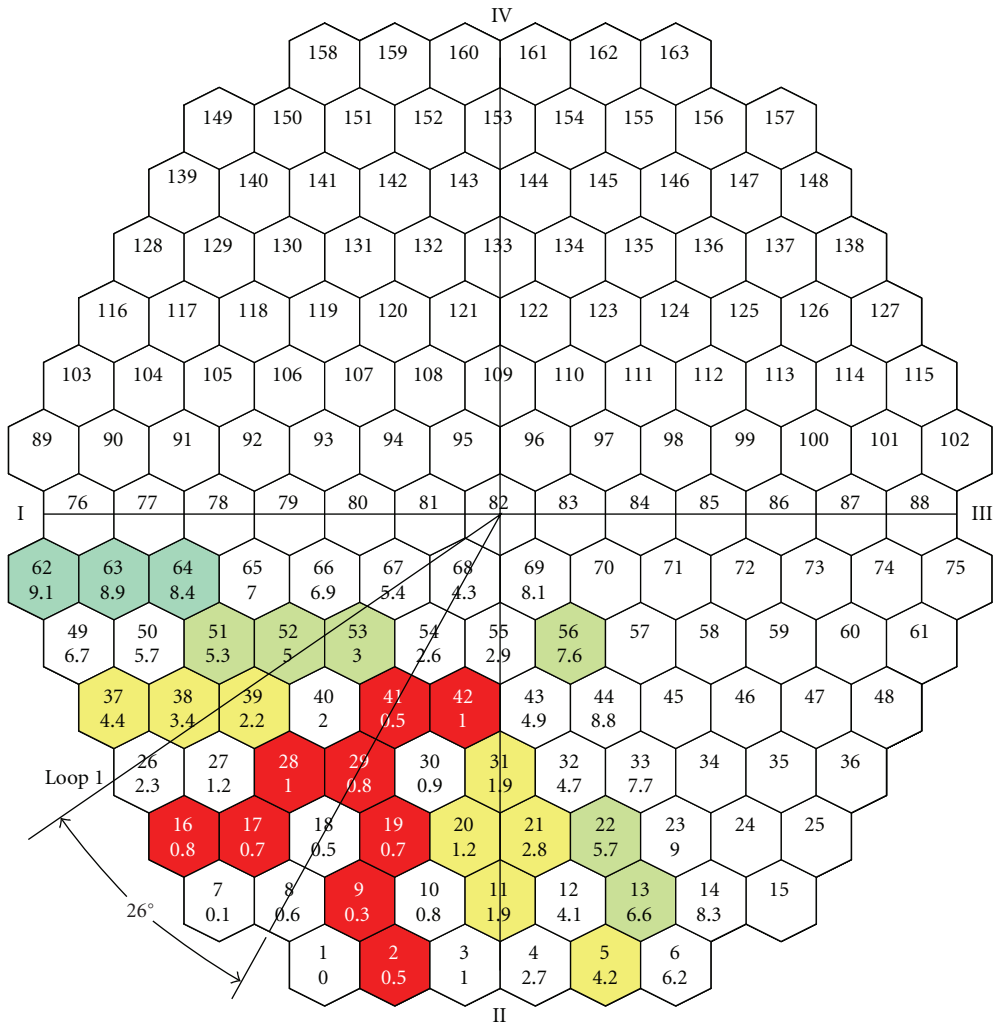

Figure 5: Plant data: estimated temperature differences (K) from cold leg no. 1 to the assembly inlets and angular turn of the loop no. 1 flow centre.

For benchmark purposes the feed-water temperature is conservatively fixed to 160°C to the broken SG and 170°C to the intact ones. In case of high-pressure safety injection operation no credit is taken for the negative reactivity insertion from the boron addition. Other major assumptions are that off-site electric power is available, and the MCPs of the faulted loop trips and the other MCP run normally during the transient.

3.2.2. MSLB Scenario 2. Large MSLB upstream of SIV without loss of off-site power and with all MCP in operation.

This is a pessimistic case derived from Scenario 1 by assuming that the MCP in the faulted loop fails to trip on signal and all reactor coolant pumps remain in operation. The scram worth is additionally reduced through adjustment of the cross sections.

For the present analysis, Exercise 2 was considered which consists of separate core-vessel calculation with given pre-calculated vessel MSLB boundary conditions. The reported results were obtained with validated multichannel vessel models and point kinetics.

4. Cathare2 VVER-1000 Model

The considered vessel thermal-hydraulic model [4–6] is multi-1D with cross-flow. For the purposes of this analysis the RPV thermal-hydraulics is described by 12-, 16-, or 24-sector vessel models. The testing includes separate effects (from vessel inlet to the fuel assembly inlets), component scale (vessel with boundary conditions), and full system simulation. The main features of the TH model are summarized as follows.

4.1. Cathare Nodalization Scheme. We have the following

(i) multi-1D channel vessel model with N sectors (N = 12, 16, or 24) all the way from the inlet to the outlet. each sector is one main channel, and there is no radial subdivision,

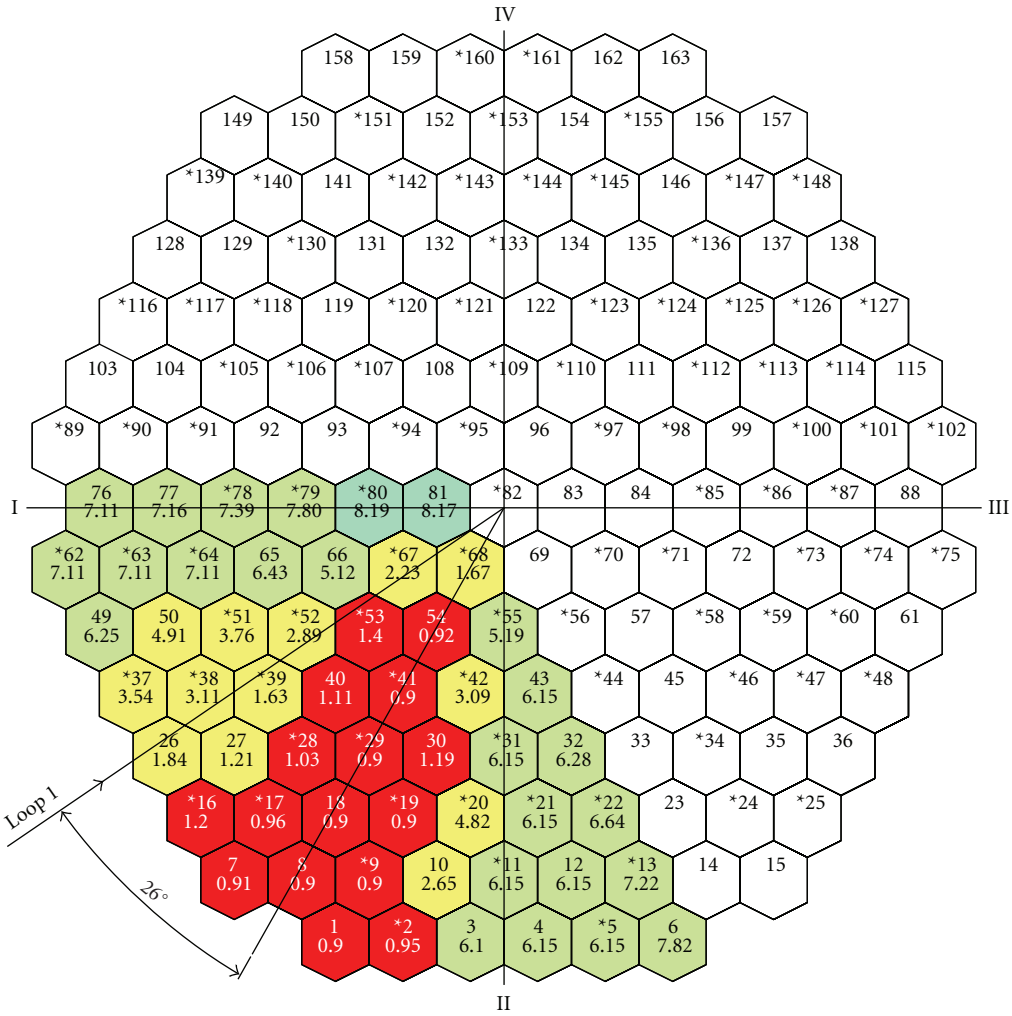

Figure 6: CATHARE 16-sector vessel model: angular turn of the loop no. 1 flow centre.

(ii) vessel inlet zone modeled with N volumes,

(iii) down-comer modelled with $N \times 2$ volumes and N axial elements,

(iv) lower plenum modeled with 2 layers $\times$ N volumes,

(v) core with N main and N bypass channels,

(vi) ten axial nodes in the core,

(vii) upper plenum (shielding tubes zone) with 2 layers $\times$ N volumes,

(viii) upper plenum (annular zone) with N volumes,

(ix) upper plenum (outlet zone) with N volumes,

(x) upper head modelled with one volume,

(xi) four-loop system model,

(xii) SG tube bundle primary side modelled with 6 layers and 10 axial nodes,

(xiii) one-volume pressurizer model,

(xiv) steam generator (SG) secondary side modelled with an axial component both for the down-comer and riser and two volumes for the upper part of the vessel,

(xv) four main steam lines connected through the main steam header.

The elements of the pressure vessel and primary circuit models are schematically shown on Figures 2 and 3.

4.2. Vessel Mixing Model. The vessel mixing is modelled through cross-flow between the parallel channels and is governed by local pressure drops. Cross-flow is modelled with horizontal junctions and vertical (diagonal) junctions connecting donor cells at a given elevation to receptor cells in the neighbour sectors, at a higher elevation. The model is implemented by the user using the utilities of the code through the input file. Tuning was applied only in the initial steady state, through adjustment of the flow resistance in horizontal cross-flow junctions and the flow area in diagonal junctions. Horizontal junctions were specified in the vessel inlet ring and in the upper part of the down-comer below

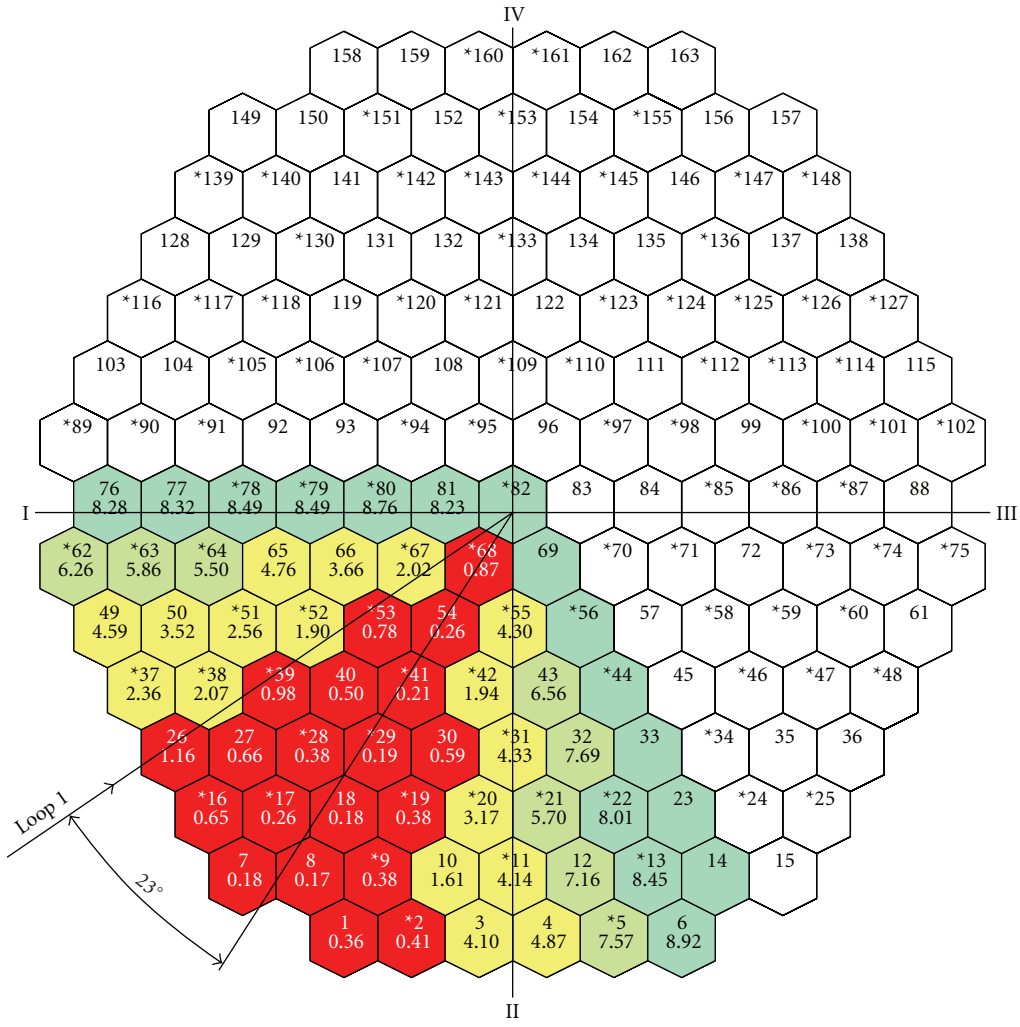

Figure 7: CATHARE 24-sector vessel model: angular turn of the loop no. 1 flow centre.

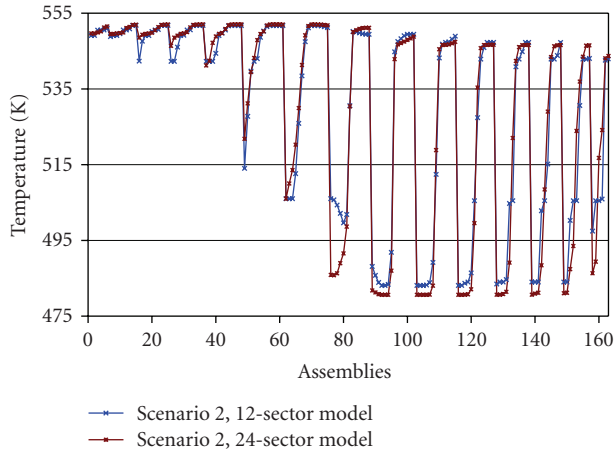

Figure 8: Snapshot for MSLB Scenario 2 at highest return to power: assembly by assembly core inlet temperatures for different angular meshes.

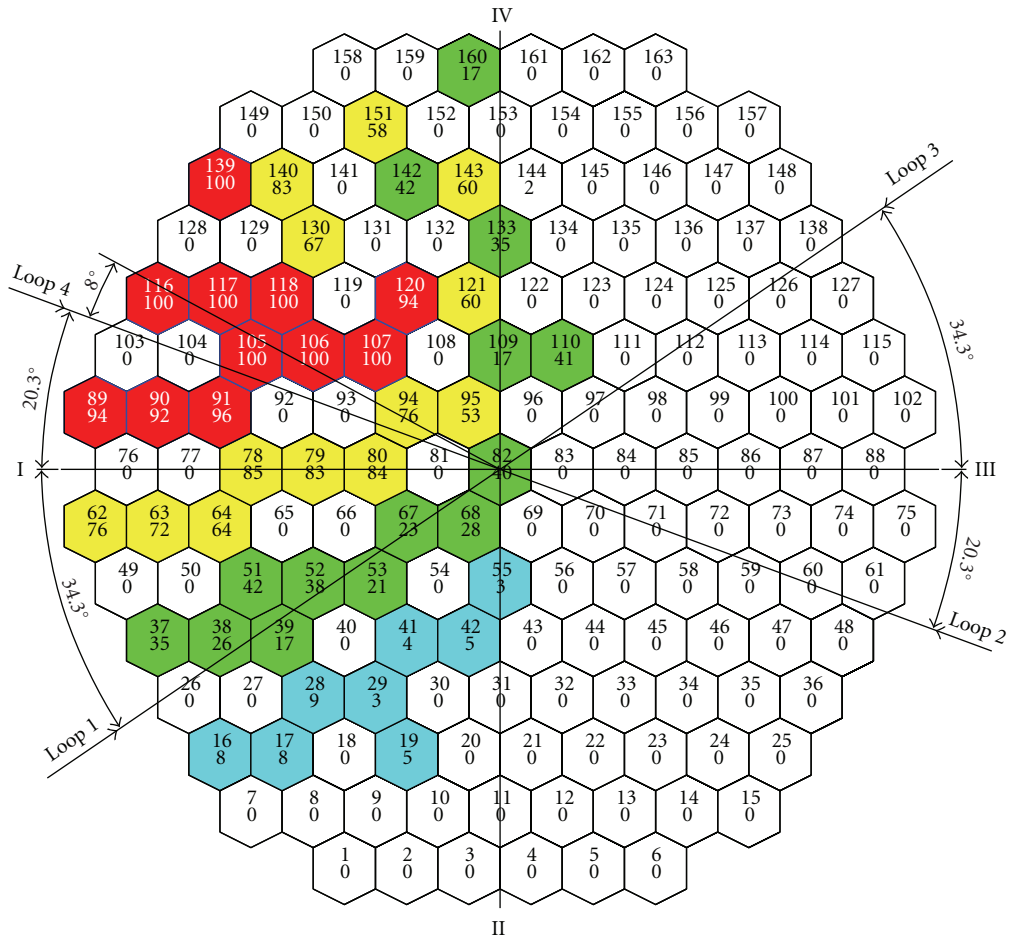

Figure 9: Kozloduy-6 vessel mixing experiment: assembly outlet data for loop-to-assembly mixing coefficients, and zone of minimal mixing and angular turn of the flow centre for loop no. 4.

the diffuser, as well as in the annular zones of the upper plenum and the outlet ring. Vertical junctions were used to a limited extent, with small relative flow area and in the lower and upper plenums only. Plant data from [1] were used to validate the multi-1D vessel mixing model.

The assembly by assembly temperature and flow distributions at the core inlet were obtained from the corresponding channel parameters through an appropriate mapping scheme. The temperature at the boundary between two sectors was taken as the weighted average of the two sector temperatures. This yields 88 inlet temperatures for the 12-sector model and 154 ones for the 24-sector model.

5. Results

5.1. Simulation of the Kozloduy-6 Flow Mixing Experiment. CATHARE multichannel-calculated results for the initial and final states are given in Tables 1 and 2. A good match of the reference states is achieved. In the discussion to follow we will consider the final asymmetric state.

Figure 4 shows the computed assembly-by-assembly core inlet temperatures in comparison with the plant-estimated data. Good overall agreement is displayed, with maximum deviations within a few K. Figure 5 illustrates the experimentally observed angular turn of the loop flow centre. In the present study the loop flow centre is defined as the centre line of the zone of minimal mixing. This zone is formed of assemblies where the temperature difference between the disturbed cold leg and each assembly inlet is $\leq$1.2 K. Figures 6 and 7 show the computed angular turn of loop no. 1 flow. The results agree well with the plant data.

The code-to-experiment comparison illustrates the effects of azimuthal mesh refinement on the prediction of assembly inlet temperatures and the angular turn of the loop flow centres as well as the vessel outlet temperatures. Although radial refinement is not considered in this study, the results are quite reasonable due to the use of appropriate mapping schemes at the core inlet. The results show that for 16 or more azimuth meshes the computed angular shift of the loop flow centre with respect to the loop axis is in

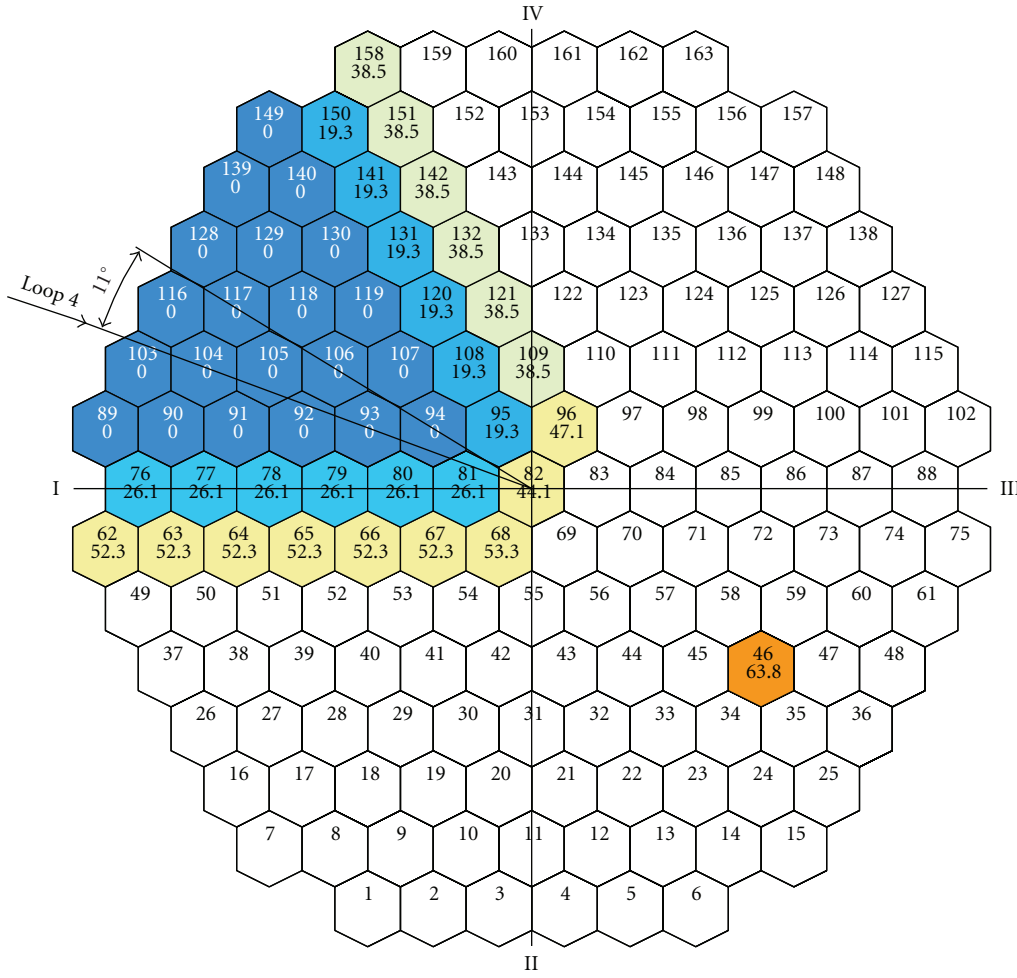

Figure 10: MSLB Scenario 2 with stuck rods no. 117 and no. 140: CATHARE 12-sector calculated angular turn of loop no. 4 flow centre.

Table 2: Final state.

Parameter	Plant data	Cathare 12 sectors	Cathare16 sectors	Cathare 24 sectors	Uncertainty
Core power, MW	286	286	286	286	± 60
Pressure above the core, MPa	15.593	15.584	15.585	15.585	± 0.3
Cold leg no. 1 coolant temp, K	555.35	555.35 (BC)	555.35 (BC)	555.35 (BC)	± 1.5
Cold leg no. 2 coolant temp, K	543.05	543.05 (BC)	543.05 (BC)	543.05 (BC)	± 1.5
Cold leg no. 3 coolant temp, K	542.15	542.15 (BC)	542.15 (BC)	542.15 (BC)	± 1.5
Cold leg no. 4 coolant temp, K	542.35	542.35 (BC)	542.35 (BC)	542.35 (BC)	± 1.5
Mass flow rate 1, kg/s	4566	4569.8	4567.4	4567.5	± 200
Mass flow rate 2, kg/s	4676	4677.0	4676.2	4676.2	± 200
Mass flow rate 3, kg/s	4669	4668.2	4668.2	4668.2	± 200
Mass flow rate 4, kg/s	4819	4818.2	4818.2	4818.2	± 200
Reactor mass flow rate, kg/s	18730	18733.2	18729.9	18730	± 800
Hot leg no. 1 coolant temp, K	554.85	554.49	554.64	555.24	± 1.5
Hot leg no. 2 coolant temp, K	548.15	548.19	548.55	547.54	± 1.5
Hot leg no. 3 coolant temp, K	545.75	545.54	545.53	545.48	± 1.5
Hot leg no. 4 coolant temp, K	546.45	546.92	546.44	546.89	± 1.5
Reactor pressure drop, MPa	0.419	0.410	0.411	0.411	± 0.043

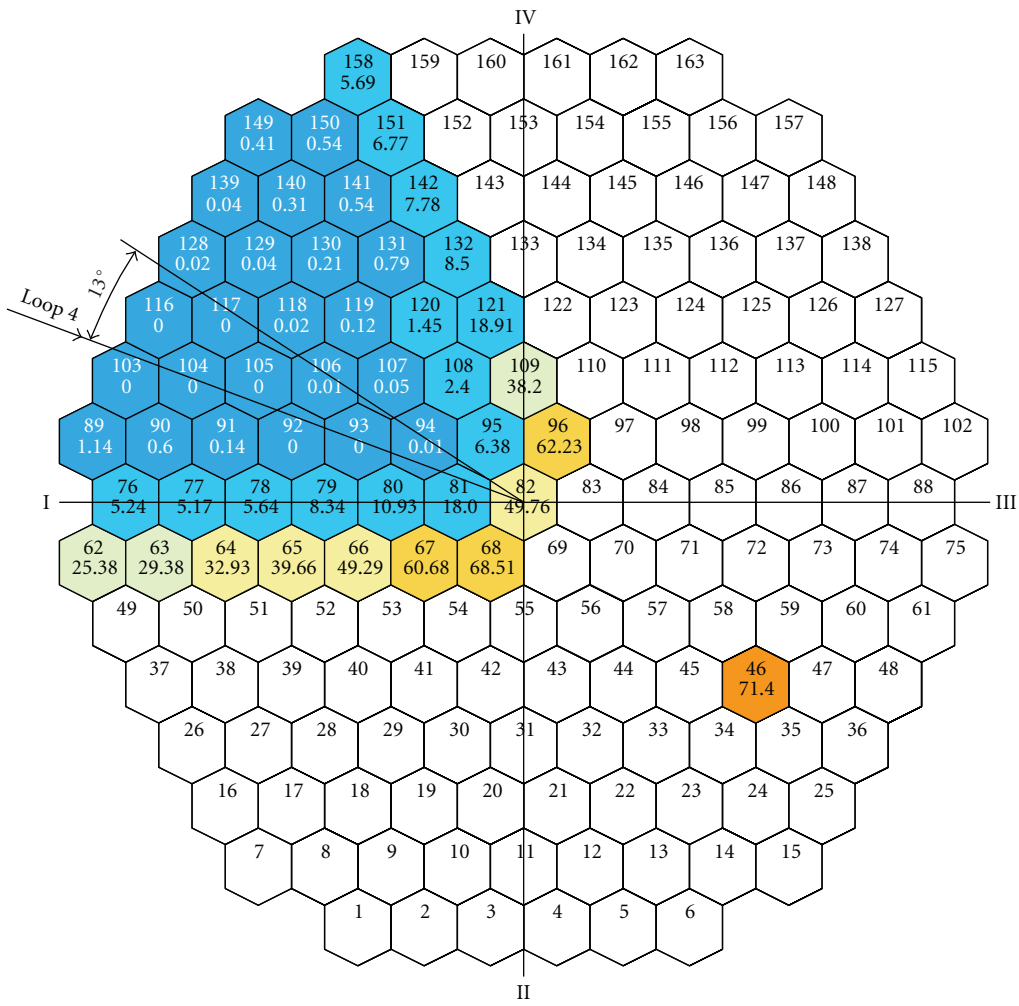

Figure 11: MSLB Scenario 2 with stuck rods no. 117 and no. 140. CATHARE 24-sector calculated angular turn of loop no. 4 flow centre.

good agreement with the plant data. The maximal deviations between the computed assembly inlet temperatures and plant estimated data are 3.41 K for 24 azimuth sectors, 4.88 K for 16 sectors, and 5.01 K for the 12-sector model. The average in modulus deviations are 0.94 K for 24 sectors, 0.92 K for 16 sectors and 0.92 K for 12 sectors.

5.2. MSLB Mixing Calculations. Figure 8 shows a CATHARE-CATHARE comparison of assembly inlet temperatures for Scenario 2 at the highest return to power illustrating the effect of angular mesh refinement.

Plant-estimated data for the angular turn of loop no. 4 flow [1] shown in Figure 9 can be used for qualitative comparison of the computed angles, displayed in Figures 10 and 11. The angular turn in Figure 9 is estimated in terms of loop-to-assembly outlet mixing coefficients Cnk (%), defined as the ratio of flow from loop n into assembly k to the total flow through assembly k. The zone of minimal mixing is formed by assemblies with 90% $< C_{nk} <$ 100% (approximately equivalent to δT_{nk} <1.2 K). Reasonable agreement is observed when using validated multichannel models with cross-flow.

The results in Figures 10 and 11 show that the validated multichannel vessel mixing models are applicable to the analysis of the initial phase of MSLB transients. The maximal errors can be reduced by further azimuthal and radial mesh refinement. The performance of the vessel mixing models in case of flow reversal in the affected loop is subject of a separate study.

6. Conclusions

Computationally efficient multichannel vessel models with cross flow can produce reasonable flow mixing results for asymmetric transients with sector formation.

A minimum of 12–16 azimuth sectors is required for acceptable accuracy such that the maximal errors in assembly inlet temperatures are in the order of a few K.

The results are of practical value for current safety analyses with system codes because of the strong impact of vessel mixing on the 3D core dynamics.

Acknowledgment

This study was carried out by using CATHARE2 V2.5 developed by CEA, EDF, AREVA NP, and IRSN.

References

[1] N. P. Kolev, S. Aniel, E. Royer, U. Bieder, D. Popov, and Ts. Topalov, "VVER-1000 Coolant Transient Benchmark (V1000CT-2): Specifications of the VVER-1000 vessel mixing problems," OECD NEA/NSC/DOC(2004)6; Rev.1, 2006, http://www.nea.fr/html/science/egrsltb/v1000ct/index.html.

[2] N. P. Kolev, et al., "VVER-1000 Coolant Transient Benchmark (V1000CT-2 Vol.2): Specifications of the VVER-1000 MSLB problem," OECD NEA/NSC/DOC(2006), http://www.nea.fr/html/science/egrsltb/v1000ct/index.html.

[3] CATHARE 2.5 Manuals, CEA Grenoble, 2006.

[4] N. P. Kolev, N. Petrov, L. Sabotinov, S. Nikonov, and J. Donov, "Validation cases of CATHARE2 for VVER-1000 main steam line break analysis," *Journal of Power and Energy Systems*, vol. 2, no. 2, pp. 512–521, 2008.

[5] I. Spasov, J. Donov, S. Stoyanov, and N. P. Kolev, "CATHARE multi-channel calculation of the coolant mixing in VVER-1000," Annual Report, TU-Sofia, 2008.

[6] N. P. Kolev, I. Spasov, and E. Royer, "VVER-1000 Coolant Transient Benchmark (V1000CT-2 Vol.3): Summary results of Exercise 1 on Vessel Mixing Simulation" NEA/NSC/ DOC(2009)," http://www.nea.fr/html/science/egrsltb/v1000ct/index.html.

Hindawi Publishing Corporation
Science and Technology of Nuclear Installations
Volume 2010, Article ID 470794, 14 pages
doi:10.1155/2010/470794

Research Article

Investigation of a Coolant Mixing Phenomena within the Reactor Pressure Vessel of a VVER-1000 Reactor with Different Simulation Tools

V. Sánchez,[1] W. Jaeger,[1] M. Boettcher,[1] and B. Truong[2]

[1] *Forschungzentrum Karlsruhe GmbH (FZK), Institute of Neutron Physics and Reactor Technology (INR), Hermann-von-Helmholtz-Platz 1, 76344 Eggenstein-Leopoldshafen, Germany*
[2] *Massaschusetts Institute of Technology, 77 Massachusetts Avenue, 24-215, Cambridge, MA 02139-4307, USA*

Correspondence should be addressed to V. Sánchez, victor.sanchez@inr.fzk.de

Received 19 May 2009; Accepted 4 October 2009

Academic Editor: Dubravko Pevec

The Institute of Neutron Physics and Reactor Technology (INR) is involved in the qualification of coupled codes for reactor safety evaluations, aiming to improve their prediction capability and acceptability. In the frame of the VVER-1000 Coolant Transient Benchmark Phase 1, RELAP5/PARCS has been extensively assessed. Phase 2 of this benchmark was focused on both multidimensional thermal hydraulic phenomena and core physics. Plant data will be used to qualify the 3D models of TRACE and RELAP5/CFX, which were coupled for this purpose. The developed multidimensional models of the VVER-1000 reactor pressure vessel (RPV) as well as the performed calculations will be described in detail. The predicted results are in good agreement with experimental data. It was demonstrated that the chosen 3D nodalization of the RPV is adequate for the description of the coolant mixing phenomena in a VVER-1000 reactor. Even though only a 3D coarse nodalization is used in TRACE, the integral results are comparable to those obtained by RELAP5/CFX.

1. Introduction

The qualification of thermal hydraulic system codes is an important prerequisite for the use of best-estimate codes to assess the safety features of nuclear power plants. In the last years, many best-estimate codes were improved by the implementation of three-dimensional thermal hydraulic (3D) models, at least for the reactor pressure vessel. Good examples of such codes are RELAP5-3D [1], TRAC-B/P [2], CATHARE-3D [3], ATHLET-FLUBOX [4], and TRACE [5]. In TRACE, a 3D vessel model in both cartesian and cylindrical geometry is available. Since these system codes are coupled to 3D neutron kinetic codes, powerful multidimensional tools like RELAP5/NESTLE, CATHARE/CRONOS2, and TRACE/PARCS arise which can be used to analyze transients with strong, nonuniform power perturbations.

The main goal of this analysis is to evaluate the prediction capabilities of the multidimensional thermal hydraulic models of TRACE by comparing calculated results with both experimental plant data and with an RELAP5/CFX-coupled simulation using a rather coarse azimuthal TRACE nodalization since it is the first attempt to validate the 3D vessel model. The test data are related to the coolant mixing phenomena within the RPV of a VVER-1000 reactor, which was distributed by the VVER-1000 Coolant Transient Phase 2 benchmark team [6]. It is an excellent opportunity to qualify the 3D models of TRACE. These investigations are restricted to the first exercise of the benchmark phase.

One option is to describe the coolant mixing by 1D system codes, where the downcomer is subdivided into several parallel channels that are connected to each other at each axial elevation by cross flow. In such approach, the appropriate form loss coefficients at the cross connections are needed. However, their derivations are not trivial and depend on the user's experience and engineering judgment. On the contrary, the 3D models of codes like TRACE solve the fluid dynamics equations in three directions and no additional effort is necessary to obtain the right cross flow among the azimuthal sectors or rings. In addition, the CPU time of coarse mesh 3D thermal hydraulic models increases with

Table 1: Main parameter of the VVER-1000 core.

Parameter	Value
Pellet diameter, mm	7.56
Central void diameter, mm	1.4
Clad diameter (outside), mm	9.1
Clad wall thickness, mm	0.69
Fuel rod total length, mm	3837
Fuel rod active length (cold state), mm	3530
Fuel rod active length (hot state), mm	3550
Fuel rod pitch, mm	12.75
Fuel rod grid	Triangular
Number of guide tubes	18
Guide tube diameter (outside), mm	12.6
Guide tube diameter (inside), mm	11.0
Number of fuel pins	312
Number of water rods/assembly	1
Water rod diameter (outside), mm	11.2
Water rod diameter (inside), mm	9.6
FA wrench size, mm	234
FA pitch, mm	236

the increase of the 3D nodes, that is, there is a limitation for the refinement of the 3D domain.

The development of coarse mesh 3D thermal hydraulic models for a complete reactor pressure vessel is very challenging since a proper strategy needs to be developed for the discretization of the computational domain in axial levels, radial rings, and azimuthal sectors. To do so, the constructive peculiarities of the main flow paths such as the downcomer, lower plenum, core, and upper plenum must be taken into account.

The modeling efforts for this analysis will be described in the following chapters. The test conditions and measured data as well as the results obtained with the different thermal hydraulic codes will be presented and discussed hereafter.

2. Peculiarities of the VVER-1000 Reactor

The VVER-1000 is a Russian type pressurized water reactor (PWR), operated at around 15.5 MPa. It is a four loop plant with horizontal steam generators (SGs). The fuel pins are arranged in hexagonal fuel assemblies (FAs) with a central hole instead of square FA found in most western type reactors. In the benchmark specifications [6] geometrical specifications and operational conditions are given so that the development of the models for the computer simulations is possible. In Table 1, some important data of the VVER-1000 plant are summarized [6].

Regarding the foreseen investigations, it has to be noted that the constructive peculiarities of the RPV in-vessel structures are an additional challenge for the development of a detailed 3D model, especially for codes like CFX [7] and TRACE. Figure 1 shows the constructive peculiarities of the lower and the upper plenum of the VVER-1000 RPV, which is more complex than that of Western type PWR. The description of the relevant flow patterns within the RPV needs special considerations regarding the axial, radial, and azimuthal direction. Since the envisaged investigations dealing with asymmetrical heat-up of the primary system due to the perturbation in one of the four loops, it is important to note that in the case of the VVER-1000 reactor, the four loops are not symmetrically arranged, has indicated in Figure 2. This peculiarity will influence the multidimensional flow conditions and it represents an additional challenge for the model developers.

The constructive design of the VVER-1000 RPV internals represents a real challenge for the development of a 3D RPV model. The most challenging aspects are summarized as follows:

(1) lower plenum: radial core barrel elliptical bottom, support columns (hallow with perforation of different size),

(2) core design: fuel assemblies and fuel pin arrangement,

(3) upper grid plate with upper perforated fuel assembly head,

(4) upper plenum: inner perforated cylinder (lower part: conic) and outer perforated cylinder.

In Figure 3, the complex flow path along the lower plenum is depicted. There, the coolant has to pass first through the 163 holes of the core barrel elliptical bottom. Then, it flows upwards, along the support columns, and enters through the perforated support columns upper part. Finally, it flows through the lower core support plate into the fuel assembly.

A further challenge is the fuel pin arrangement in the core regarding the azimuthal and radial nodalization. Assumptions and engineering judgment have to be made to estimate the main thermal hydraulic parameters at the cell faces; see Figure 4. Especially the evaluation of the following input deck parameters is crucial: (1) cell volume liquid-to-solid ratio, (2) flow area fraction, (3) hydraulic diameter, and (4) additional form loss coefficient. Furthermore, the peculiarities of the upper end of the fuel assembly and the upper grid plate, Figure 5, result in complicated flow path through the perforated, conical part of the fuel assembly head, and finally through the upper core support plate. The upper plenum is characterized by two concentric cylinders with perforations, through which the coolant has to pass, shown in Figure 6. The presence of the guide tubes makes the flow more complex. The coolant, leaving the core, flows through the perforated part of the inner ring and then through the perforated core barrel.

3. Short Description of the Numerical Tools

For the investigation of the coolant mixing that occurred during the heat-up test at the Kozloduy nuclear power plant, the system code TRACE and the offline coupled RELAP5/CFX are used. TRACE [5] (TRAC/RELAP Advanced Computational Engine) is being developed by Los Alamos National Laboratory (LANL) and the Pennsylvania State University. TRACE is a multidimensional, two-phase

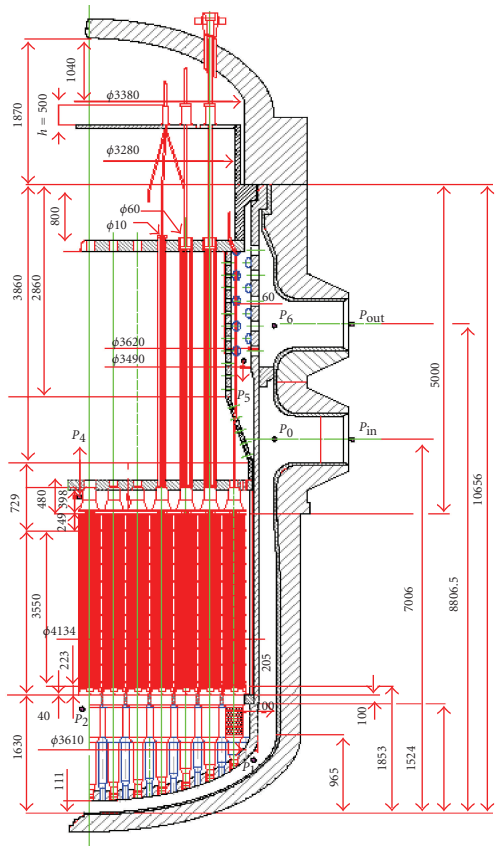

Figure 1: The RPV of the VVER-1000 reactor with the constructive peculiarities.

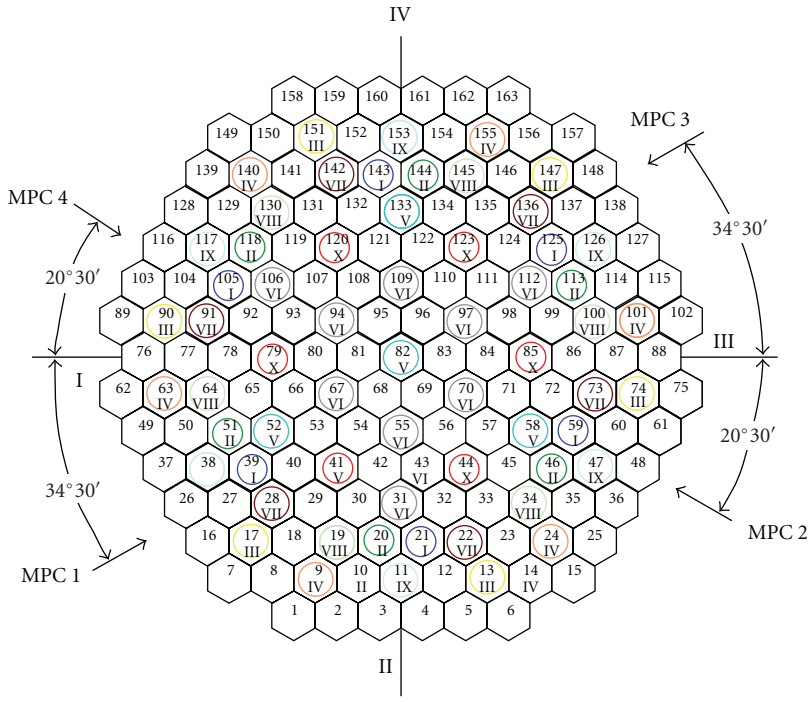

Figure 2: The asymmetrical arrangement of the loops (I, II, III, and IV) related to the core.

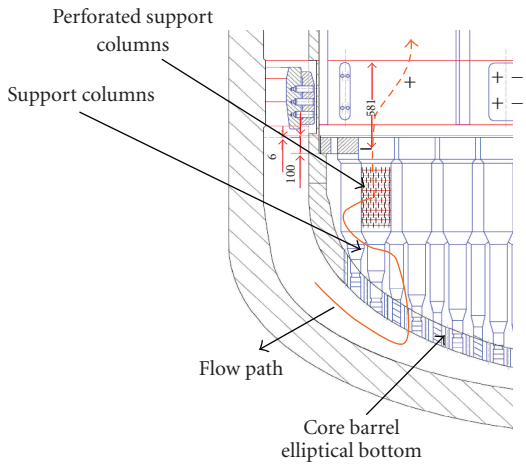

Figure 3: Constructive details of the lower plenum and complex flow path.

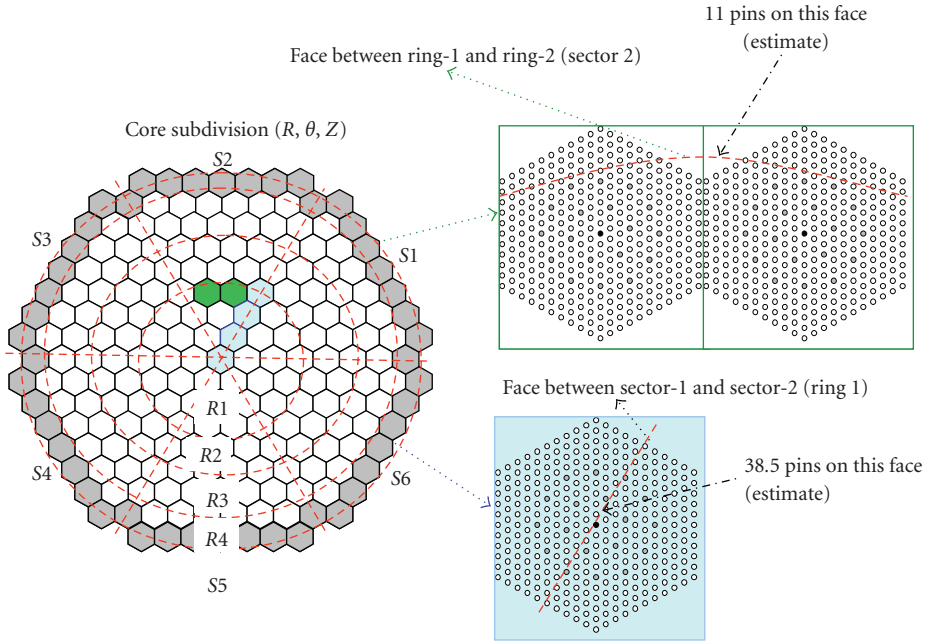

Figure 4: Pin arrangement regarding the nodalisation lines in radial and azimuthal direction.

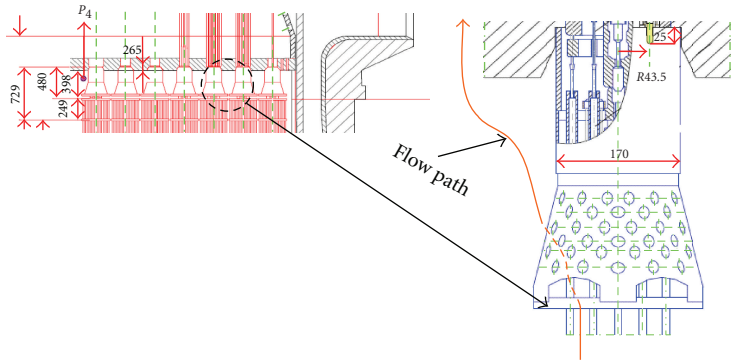

Figure 5: Flow conditions at the fuel assembly head and upper grid plate.

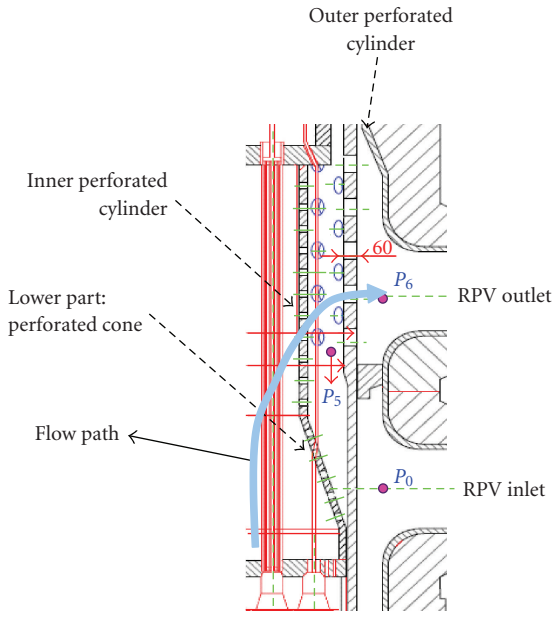

Figure 6: Vertical arrangement of the VVER-1000 primary components.

flow system code, developed to simulate any kind of operational events, transients, and design basis accidents of both boiling water reactor (BWR) and PWR. The component VESSEL allows the 3D simulation of the flow in the reactor pressure vessel. In addition, different working fluids such as gas and liquid metals are included in TRACE so that it can be also used to assess the safety features of innovative reactors such as GEN IV reactors. The in-build point kinetics model, based on the Kaganove-approach, is extended by the coupling or direct incorporation of the three dimensional core reactor simulation tool PARCS [8]. Thanks to the coupling of RELAP5 and TRACE to PARCS, a powerful system is created that is appropriate for the simulation of transients and accident scenarios where a strong power perturbation within the core exists and where the thermal hydraulic core behavior is strongly related to the core neutronic processes (e.g., MSLB scenarios, ATWS, boron dilution). CFX [7] is a commercial CFD tool widely used to simulate 3D flow in complex geometries. Its application in the nuclear reactor safety is rapidly increasing, especially for single phase flow situations.

4. Thermal Hydraulic Models of the Reactor Pressure Vessel

4.1. The 3D TRACE Model of the Reactor Pressure Vessel. A detailed 3D model of the RPV of the VVER-1000 reactor representing the most relevant internals was developed for TRACE [9]. Before that, a complete model for the VVER-1000 reactor with RELAP5/PARCS was developed [10]. It includes, for example, the downcomer, lower plenum, core, core outlet, upper plenum, and RPV inlet and outlet pipes. A detailed description of this model can be read in [9]. The 3D VESSEL component of TRACE was used for the representation of the RPV. According to this, the whole RPV is subdivided in 30 axial levels, six radial rings and six azimuthal sectors (Figures 7 and 8). The sizes of the respective nodes depend on the existing flow conditions along the main flow paths within the RPV determined by the constructive peculiarities of the RPV internals. From the 30 axial levels of the RPV, 10 axial nodes belong to the core region while two belong to the lower and upper axial reflector. The azimuthal sectors (S1 to S6) were defined in a way that the cold legs are connected to sector 4 (cold leg 1), sector 6 (cold leg 2) sector 1 (cold leg 3), and sector 3 (cold leg 3).

Figure 9 shows radial nodalization of the RPV into 6 rings, 3 of which are for the core. For each of the 3D volume elements, the main thermal hydraulic parameters for each direction such as hydraulic diameter, flow area, heated diameter, and form loss coefficients are derived from the detailed plant data. To catch the asymmetrical coolant mixing expected to occur mainly in the downcomer and lower/upper plenum a rather fine nodalization of the RPV in azimuthal and radial direction is needed. One has to keep in mind that the finer nodalization leads to a higher CPU time. A reasonable compromise between accuracy and CPU cost is here mandatory. In Figure 8, the radial and azimuthal nodalization of the core is shown. In developing the 3D model using the VESSEL component the following aspects had to be kept in mind.

(i) Make use of geometrical symmetry (R, θ, Z).

(ii) Select the size of cells (radial, axial, angular) as small as necessary (based on underlying physics).

(iii) Consider the details of flow paths as much as necessary.

(iv) Otherwise the 3D model may become unnecessary complex.

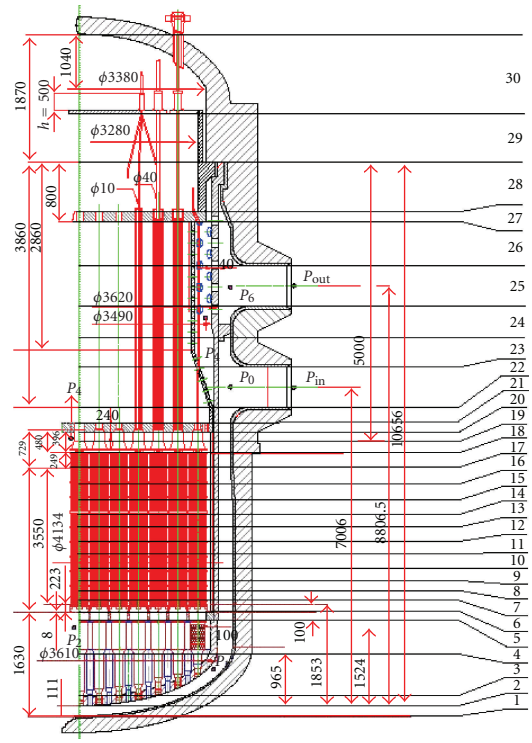

Figure 7: TRACE axial nodalization of the RPV.

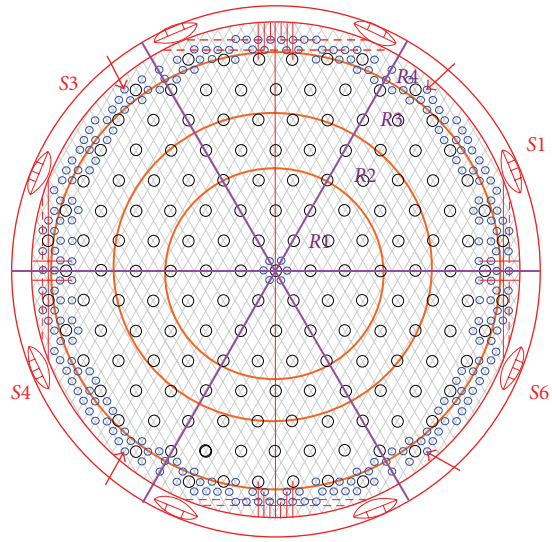

Figure 8: TRACE radial and azimuthal subdivision of the core.

The complete TRACE model as represented by SNAP (pre- and postprocessor) is shown in Figure 10. Part of the hot and cold legs, as well as the mass source and sinks, is represented with PIPE, FILL, and BREAK components. They are necessary to define the initial and boundary conditions of the problem being investigated. These boundary conditions are coolant temperature and mass flow rate (FILL) and system pressure (BREAK).

4.2. Combined 1D RELAP5 and CFX Model. Detailed models of the RPV, including the core, were developed for RELAP5 [11] and CFX [12]. Since the coolant mixing experiment is almost a thermal hydraulic problem with very weak reactivity feedbacks, it represents a unique opportunity for the simulation of the RPV and core behavior using a combination of CFD and system codes.

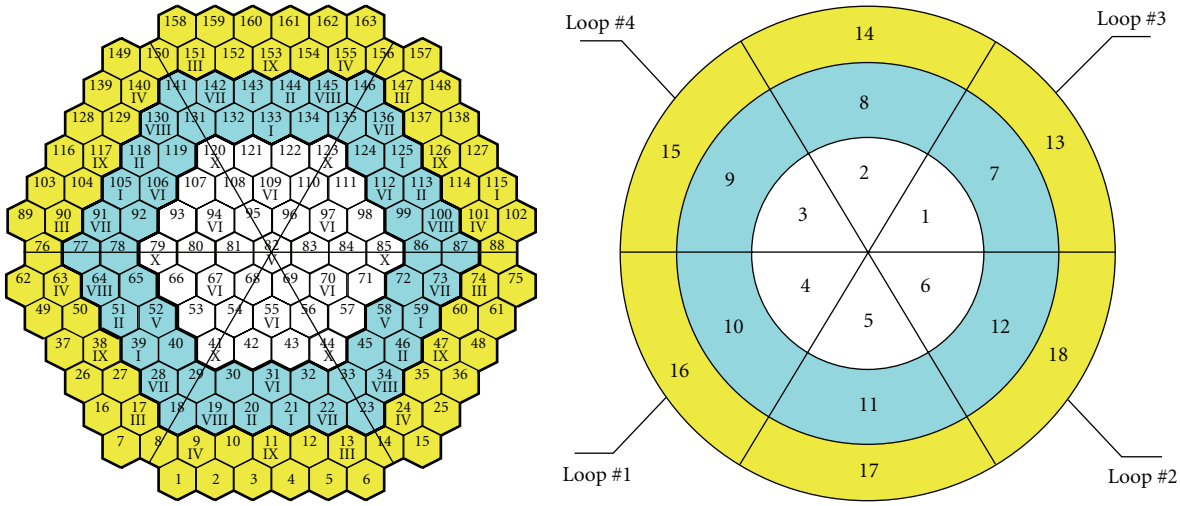

Figure 9: TRACE Nodalization of the core and relative position of the cold/hot legs.

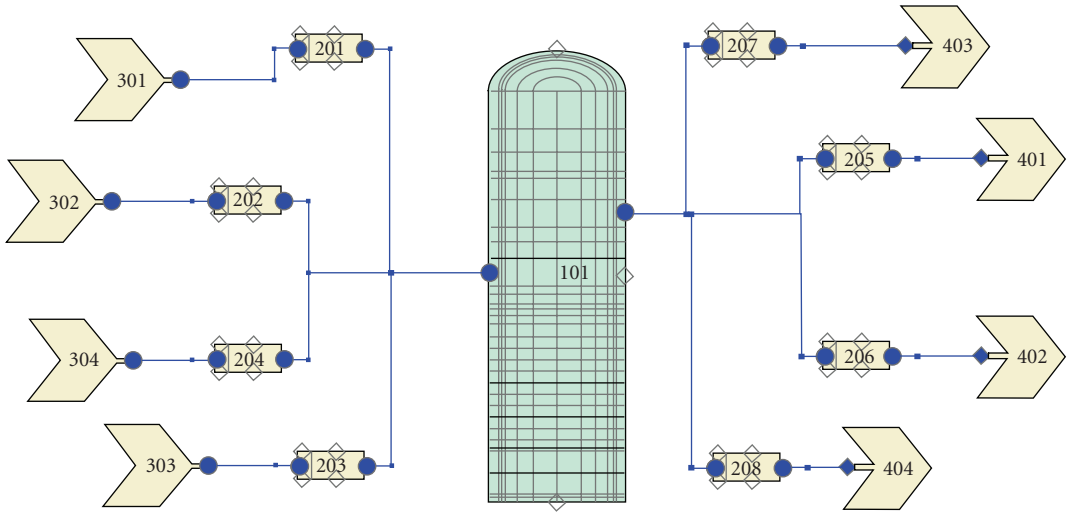

Figure 10: TRACE 3D Nodalization of the RPV with cold/hot legs.

All important RPV volumes, where coolant mixing is expected to occur such as downcomer and lower plenum till the core entrance, are simulated with CFX-5 (Figure 12). The core and the upper plenum, including the RPV outlets, are described by RELAP5 volumes (Figure 11). In this off-line coupling of CFX with RELAP, the data exchange between both models is realized at the core entrance, that is, at the inlet of each fuel assembly by time dependent boundary conditions (coolant temperature, mass flow rate and pressure). In the RELAP5 model, the core is represented by 164 parallel channels (163 represent FAs, 1 represents the bypass) together with their corresponding heat structures. Axially, the core region is divided in 10 axial levels and two additional more for the lower and upper axial reflector region. The core outlet and the upper plenum are represented by six equal sized sectors, modeled as parallel channels. Sector 1 (vol 860), sector 2 (vol 861), and sector 3 (vol 862) belong to the "affected" core half and the other three sectors (vol 863, vol 864, and vol 865) to the "unaffected" core half. The RPV head is represented by single volumes (vol 870 and vol 880).

The CFD domain is represented by a detailed CFX-5 model [12] of the downcomer and lower plenum including all the constructive details of the complicated flow paths. A detailed description of this model is given in [12] (see Figure 12).

This CFX model is part of a complete CFX model of the RPV, including the core and upper plenum, that was developed for the V1000-CT-2 benchmark [12].

The coupling of RELAP5 and CFX presented here is an offline coupling realized for this specific problem. It can be improved by the development of a versatile interface module

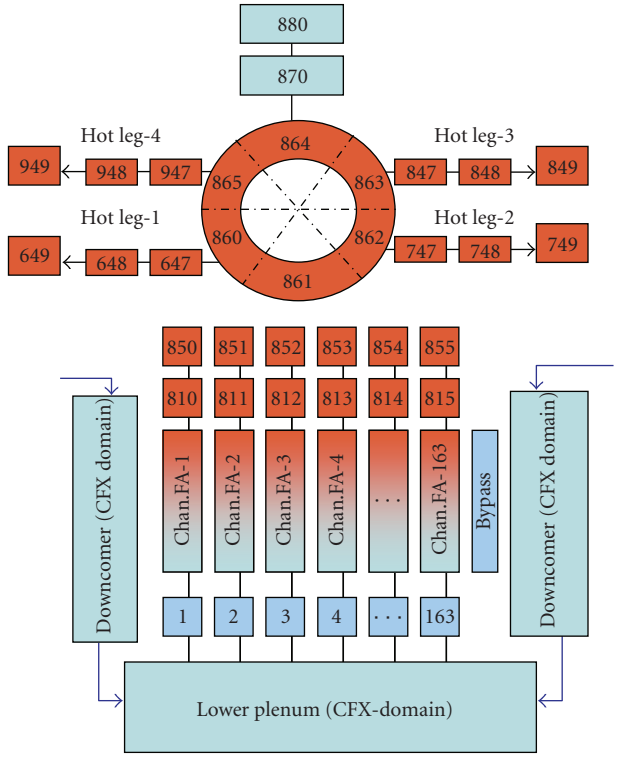

Figure 11: Sketch of the RPV Model with the CFX and RELAP5 domain.

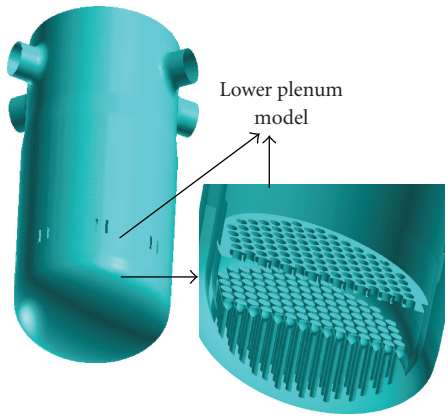

Figure 12: Detailed CFX-5 model of the downcomer and upper plenum of the RPV.

that allows more universal use of these codes to investigate combined 3D and 1D thermal-hydraulic process within the RPV of light water reactors. In the CFX, the constructive details of the lower plenum are treated as porous media mainly. This can be enhanced by a direct resolution of the constructive peculiarities of the lower plenum structures resulting in an increase of the number of cells, too.

5. Simulation of the Heat-Up Experiment

5.1. Short Description of the Experiment

5.1.1. Pretest Phase. Before the test, the nuclear power plant Kozloduy was operated at around 9.36% of the nominal power, that is, 281 MWth, with all main coolant pumps running. The main operational parameters are summarized in Table 2, together with the measurement accuracy. On the secondary side all steam generators were available. The core was loaded with fresh fuel, that is, at the beginning of cycle conditions (BOC) with a core-averaged exposure of 0.4 effective full power days (EFPDs) and a boron concentration of 7.2 g/kg. The positions of the control rod groups were as follows: groups #9 and #10 are fully inserted; groups #1–#7 are fully withdrawn; the regulating rod group #8 was about 84% withdrawn from the bottom of the core. The coolant temperature at core inlet was 20 K lower that the one at nominal conditions. Finally the steam generator levels were as high as the ones at nominal conditions. The main steam

Table 2: Main parameters of the four loops before the test.

Parameter	Initial state	Accuracy
Thermal power, MW	281	±60
Pressure above core, MPa	15.593	±0.300
Pressure drop over RPV, MPa	0.418	±0.043
Coolant temperature at core inlet #1, K	541.75	±1.50
Coolant temperature at core inlet #2, K	541.85	±1.50
Coolant temperature at core inlet #3, K	541.75	±1.50
Coolant temperature at core inlet #4, K	541.75	±1.50
Coolant temperature at core outlet #1, K	545.00	±2.00
Coolant temperature at core outlet #2, K	545.00	±2.00
Coolant temperature at core outlet #3, K	544.90	±2.00
Coolant temperature at core outlet #4, K	545.00	±2.00
Mass flow rate of loop #1, kg/s	4737	±110
Mass flow rate of loop #2, kg/s	4718	±110
Mass flow rate of loop #3, kg/s	4682	±110
Mass flow rate of loop #4, kg/s	4834	±110

header pressure amounts to 5.07 MPa, meaning 1.0 MPa lower than the nominal value.

5.1.2. Test Phase. The test was performed in 1991 at the Kozloduy NPP [6]. It was initiated by the isolation of the steam generator of loop 1 due to the closure of the main steam isolation valve. As a consequence, the primary coolant temperature of loop 1 started to increase up to about 14 K higher than the coolant temperature of the other loops. Under such conditions, coolant mixing occurred, first of all in the downcomer region. The resulting mixing pattern propagates through the lower plenum, core, and upper plenum. Since the power was relatively low, the feedbacks between thermal hydraulics and core neutronics are negligible according to the recorded data. Due to the mixing, the temperature of the unaffected loops especially of the loop close to the loop 1 (loop 2) increased. The test lasted for 1800 seconds. At that time the power increased up to 286 MW. Different data were recorded at the Kozloduy plant during the test. The coolant temperature at the cold/hot legs was measured with one thermal resistor at the level of pipe axis and two thermocouples in the lower part of the flow section. At some fuel assembly positions the coolant temperature at the core outlet was also measured. Fuel outlet temperatures and experimentally determined mixing coefficients from cold legs to fuel assembly outlets were also measured for the qualification of CFD codes. From this data, the fuel assembly inlet temperatures were derived, assuming that the relative temperature rise distribution does not change during the transient.

In Figure 13, the recorded data of the four hot legs are given for the whole test, that is, 1800 seconds. There it can be seen that the coolant temperature of the affected loop 1 starts to increase very rapidly at around 130 seconds due to the deteriorated heat transfer over the SG 1. From 500 seconds onward the increasing rate becomes smaller, stabilizing at a value below 556 K. Due to the coolant mixing in the downcomer the temperature of the loop 2 experienced

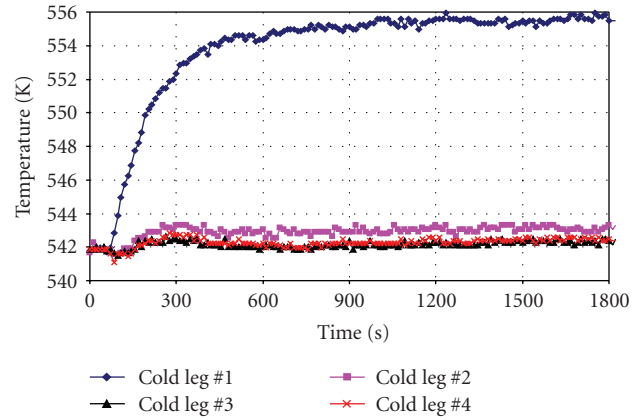

Figure 13: Measured evolution of the hot legs during the test at the KNPP.

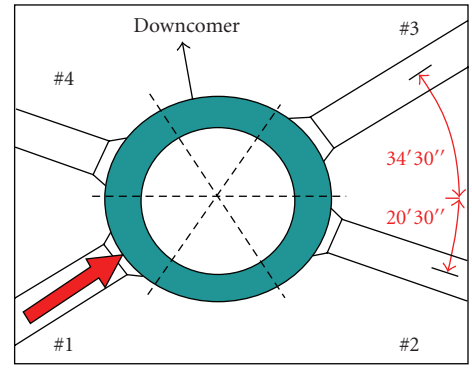

Figure 14: Location of the loops with respect to the downcomer.

a higher temperature than the one of loop 4, indicating that the mixing pattern is not in clockwise direction. Note that the position of the loops is not symmetrical (Figure 14). The core parameters at the end of the test (at 1800 seconds) are given in Table 5.

5.2. Selected TRACE Results. The TRACE posttest calculations of the coolant mixing experiment were performed in two steps. First of all, a steady-state calculation was carried out to predict the plant conditions just before the test. Secondly, a transient run was made for 1800 seconds to determine the final state of the plant. The time dependent boundary conditions, for example, loops flow rate, coolant temperature of the cold legs, and the system pressure were defined in the benchmark specifications [6].

5.2.1. Prediction of the Initial Plant State. In Table 3, a comparison of the TRACE predictions and the plant data is given for the initial plant state to be exhibit. It can be seen that the agreement between data and prediction is quite good. At the initial state the coolant temperature at the core inlet/outlet is uniformly since all pumps and steam generators are in operation. This will change drastically during the heat-up test progression. Note that the largest deviation between the prediction and the data is below 4%.

Table 3: Comparison of TRACE predictions with plant data for the initial state.

Parameter	Initial state	Accuracy	TRACE	Deviation
Thermal power, MW	281	±60	281	0
Pressure above core, MPa	15.593	±0.300	15.592	0.001
Pressure drop over RPV, MPa	0.418	±0.043	0.404	0.014
Coolant temperature at core inlet #1, K	541.75	±1.50	541.78	−0.03
Coolant temperature at core inlet #2, K	541.85	±1.50	541.88	−0.03
Coolant temperature at core inlet #3, K	541.75	±1.50	541.78	−0.03
Coolant temperature at core inlet #4, K	541.75	±1.50	541.78	−0.03
Coolant temperature at core outlet #1, K	545.00	±2.00	544.63	0.37
Coolant temperature at core outlet #2, K	545.00	±2.00	544.70	0.30
Coolant temperature at core outlet #3, K	544.90	±2.00	544.61	0.29
Coolant temperature at core outlet #4, K	545.00	±2.00	544.62	0.38
Mass flow rate of loop #1, kg/s	4737	±110	4749	−12
Mass flow rate of loop #2, kg/s	4718	±110	4735	−17
Mass flow rate of loop #3, kg/s	4682	±110	4750	−68
Mass flow rate of loop #4, kg/s	4834	±110	4737	97

5.2.2. Predicted Final Plant State. The transient phase started with the isolation of the main steam isolation valve and lasted for 1800 seconds. The final plant state predicted by TRACE is compared to the plant data and shown in Table 4. There, it can be observed that the code predictions are close to the plant data. In addition to the hot/cold leg temperatures, the pressure drop is also in good agreement with the data. Since during the test the hot leg temperature of the loop 1 (Figure 13) was continuously increasing while the one of the other loops were not, a considerable coolant mixing took place in the downcomer. The predicted temperatures in the six sectors of the downcomer are shown in Figure 15. The increase of the temperature in sector two and three was due to the mixing process. It is worth to mention that the mixing took place in counter clockwise direction.

The predicted coolant temperature of each fuel assembly at the core outlet for the beginning and end state of the test is given in Figures 15, 16, and 17. In Figure 17 the mixing pattern within the core can be observed. The hotter fluid of the loop 1 get mixed with the one of the sector between the loop 1 and loop 2, that is, in counter-clockwise direction as observed in the tests.

A comparison of the measured coolant temperature at the fuel assembly outlet with the predicted values by TRACE is given in Figure 18. It can be seen that the TRACE predictions follow qualitatively the trend of the measured data. In some positions, TRACE tends to over predict and in others to under predict the data. But the differences between data and predictions are within the measurement error. These trends are comparable to the trends predicted by CFX-5 [12].

5.3. Performed RELAP5/CFX Simulations. In this offline coupling approach, the CFX calculations [12] were performed first taking into account the initial and boundary conditions at the vessel inlet (cold legs1 to 4). From these investigations, the detailed flow conditions at the core inlet for each fuel assembly (RELAP5 PIPE component) like coolant temperature, mass flow rate, were derived as time dependent tables for the RELAP5 simulation [11]. Afterwards, these tables were used in the detailed whole core model of RELAP5 as time dependent boundary conditions. By this way, the RPV behavior could be analyzed in a more detailed sense as it can be done if only a whole 1D model of the RPV for RELAP5 is used. The focus here was to explore the possible way of combination of CFX and system codes for dedicated

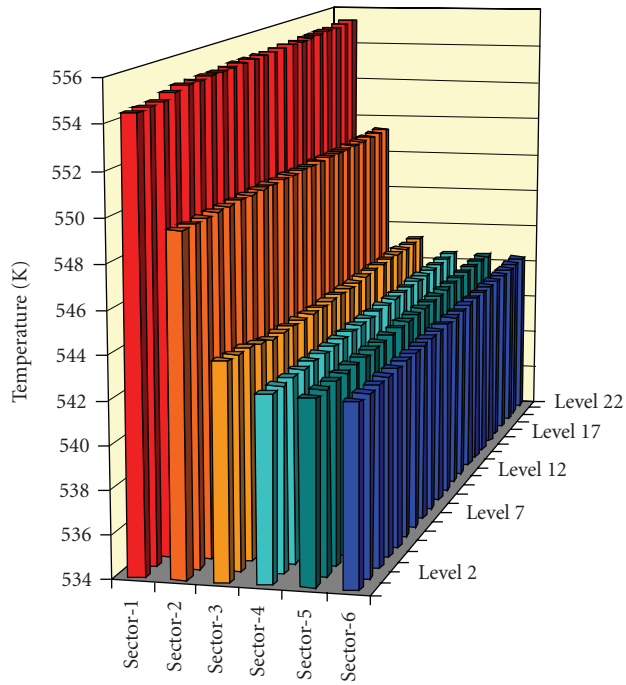

Figure 15: Predicted coolant temperature in the sectors of the downcomer (levels: 2 to 22).

Table 4: Comparison of TRACE predictions with plant data for the final state.

Parameter	Final state	Accuracy	TRACE	Deviation
Thermal power, MW	286	±60	286	0.000
Pressure above core, MPa	15.593	±0.300	15.591	0.002
Pressure drop over RPV, MPa	0.417	±0.043	0.404	0.013
Coolant temperature at core inlet #1, K	555.35	±1.50	555.39	−0.04
Coolant temperature at core inlet #2, K	543.05	±1.50	543.08	−0.03
Coolant temperature at core inlet #3, K	542.15	±1.50	542.18	−0.03
Coolant temperature at core inlet #4, K	542.35	±1.50	542.38	−0.03
Coolant temperature at core outlet #1, K	554.85	±2.00	555.14	−0.29
Coolant temperature at core outlet #2, K	548.55	±2.00	548.66	−0.11
Coolant temperature at core outlet #3, K	545.75	±2.00	545.44	0.31
Coolant temperature at core outlet #4, K	546.45	±2.00	545.69	0.76
Mass flow rate of loop #1, kg/s	4566	±110	4657	−91
Mass flow rate of loop #2, kg/s	4676	±110	4693	−17
Mass flow rate of loop #3, kg/s	4669	±110	4724	−55
Mass flow rate of loop #4, kg/s	4816	±110	4724	92

Table 5: Main parameters of the NPP at the end of the test (1800 seconds).

Parameter	Final state	Accuracy
Thermal power, MW	286	±60
Pressure above core, MPa	15.593	±0.300
Pressure drop over RPV, MPa	0.417	±0.043
Coolant temperature at core inlet #1, K	555.35	±1.50
Coolant temperature at core inlet #2, K	543.05	±1.50
Coolant temperature at core inlet #3, K	542.15	±1.50
Coolant temperature at core inlet #4, K	542.35	±1.50
Coolant temperature at core outlet #1, K	554.85	±2.00
Coolant temperature at core outlet #2, K	548.55	±2.00
Coolant temperature at core outlet #3, K	545.75	±2.00
Coolant temperature at core outlet #4, K	546.45	±2.00
Mass flow rate of loop #1, kg/s	4566	±110
Mass flow rate of loop #2, kg/s	4676	±110
Mass flow rate of loop #3, kg/s	4669	±110
Mass flow rate of loop #4, kg/s	4816	±110

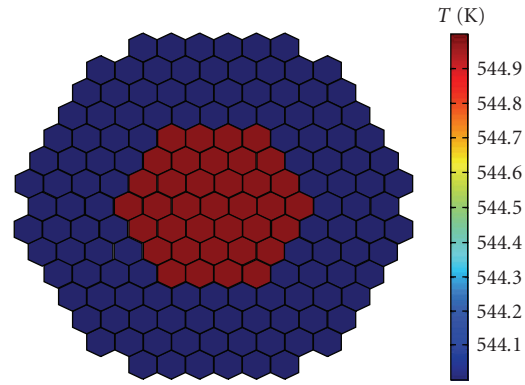

Figure 16: Predicted coolant temperature at the core outlet at initial state (0 second).

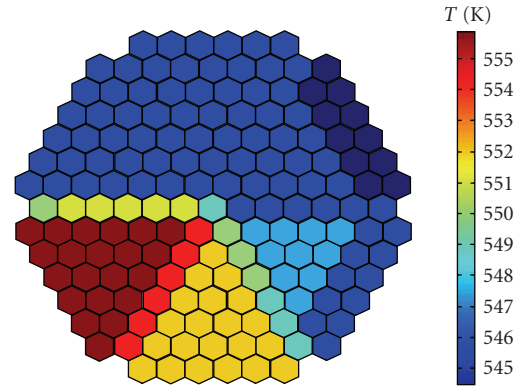

Figure 17: Predicted coolant temperature at core outlet at final state (1800 seconds).

applications. Hereafter, the transient evolution of the hot loop temperatures predicted by TRACE and RELA5/CFX, in comparison with measured data, will be presented and discussed.

5.4. Comparison of TRACE and RELAP5/CFX Transient Results. Different parameters of the Kozloduy plant were measured during the test like the hot leg temperatures at the RPV outlet. Time dependent data were derived from these measurements. These data are compared in Figures 19, 20, 21, and 22.

In these figures, it can be seen that the predictions of TRACE and RELAP5/CFX are in very good agreement with the experimental data. The temperature evolution of all loops shows a mixing effect that starts in the downcomer and propagates through the core to the upper plenum since all pumps are running and high coolant velocities prevail during the transient. Apparently, this is not the case for loop 2. But reevaluation [13] of this experiment performed

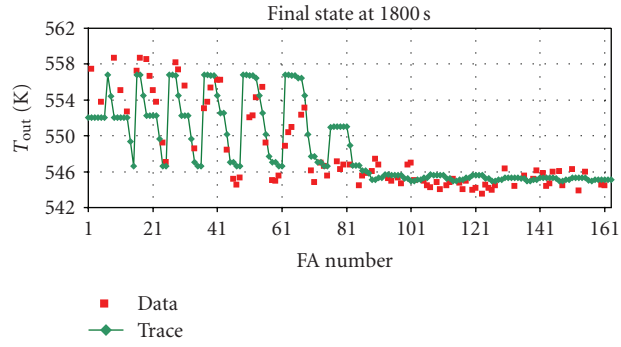

Figure 18: Comparison of the predicted coolant temperature at each FA outlet with data.

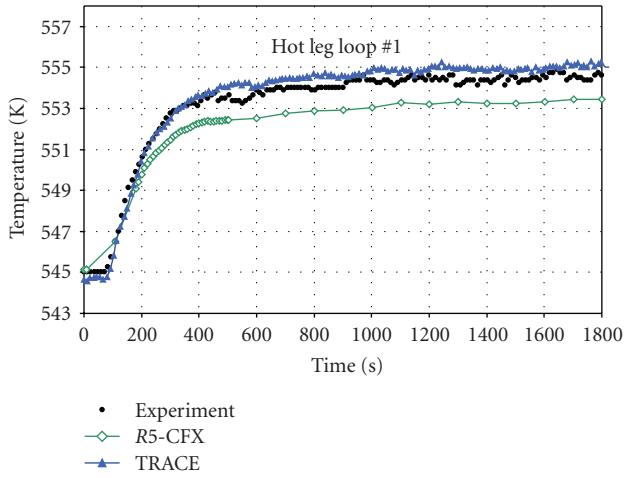

Figure 19: Comparison of the data with the predictions for loop 1.

by the benchmark team leads to the conclusion that the measured value for loop 2 should be around 548 K instead of 545 K. Only for loop 1 the TRACE results are closer to the data compared to the RELAP5/CFX ones. But for the other loops the RELAP5/CFX results are in better agreement with the data, which is expected since the coolant mixing is better described by CFD tools than by coarse mesh 3D thermal hydraulic codes such as TRACE.

6. Conclusions and Further Work

In this paper, investigations performed to validate the 3D thermal hydraulic model of TRACE based on plant data (Kozloduy nuclear power plant) were presented and discussed. Detailed models for a 3D coarse mesh system code (TRACE) and for RELAP5/CFX were developed for the analysis of the heap-up test, where the coolant mixing within the RPV was the dominating process. The constructive peculiarities of the RPV, important for the elaboration of the 3D models, are also outlined. Although the azimuthal subdivision of the 3D reactor pressure level consists of only six sectors, this model is useful for global comparison of coolant temperatures at the hot legs against data and RELAP5/CFX simulations.

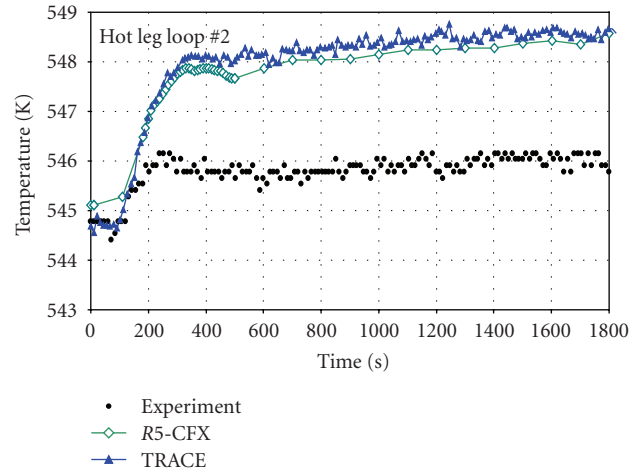

Figure 20: Comparison of the data with the predictions for loop 2.

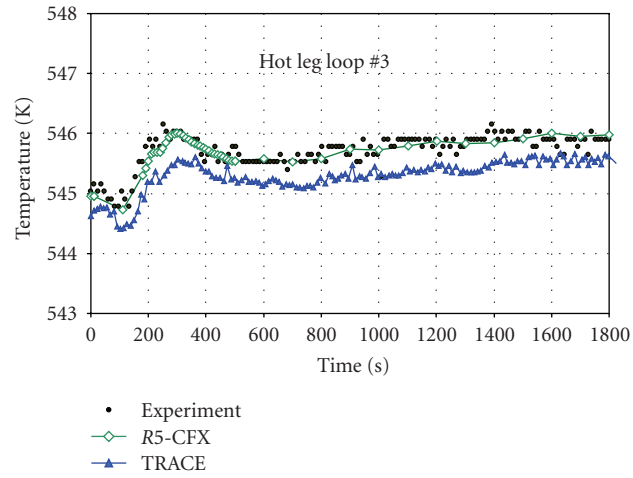

Figure 21: Comparison of the data with the predictions for loop 3.

From the comparison of the calculated parameters by TRACE with the available measurement data the following conclusions can be drawn.

(i) The initial plant conditions just predicted by TRACE are in a very good agreement with the plant data.

(ii) The final plant state predicted by TRACE is close to the plant data and the deviations are within the measurement error band.

(iii) The evolution of important plant parameter, predicted by TRACE, follows nicely the measured trends, indicating that the mixing within the RPV is well described by the simulations (hot leg temperature of all loops).

(iv) A detailed comparison of the calculated coolant temperature at the core outlet for each fuel assembly position with available data showed good trends.

(v) TRACE was also able to predict the counter-clockwise rotation, that is, the mixing preferably in direction of loops 2 and 3 instead of loop 4.

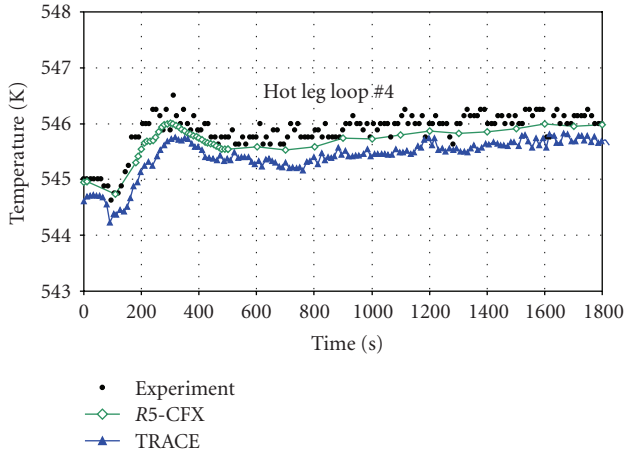

Figure 22: Comparison of the data with the predictions for loop 4.

In general, it can be stated that the chosen 3D thermal hydraulic nodalization scheme using the VESSEL component of TRACE seems to be appropriate to catch the underling physics of the coolant mixing process of VVER-1000 reactors.

These results are very encouraging and they underline the capability of the 3D VESSEL component of TRACE, which is very flexible, allowing simulations ranging from 1D over 2D to 3D. Consequently, the validated 3D model of the RPV of the VVER-1000 reactor can be used to investigate transients where the coolant mixing is a key issue such as deboration, main steam line break, and so forth.

The performed investigations, to assess the capability of the offline coupling RELAP5/CFX, have shown the potential of such coupling and the need for the development of more sophisticated multiscale coupling schemes for system codes and CFD codes. The combination of RELAP5 with CFX improved the quality of the obtained results for the coolant mixing phenomena of VVER-1000 reactors. The developed models regard the constructive and design peculiarities of this reactor type, and hence, it cannot be applied for another reactor design.

Additional refinement of the 3D vessel TRACE model will be done to perform detailed comparison of the TRACE predictions with the available data at a local, more detailed, spatial level in the downcomer, core entrance, and core outlet. The obtained results with the six azimuthal sectors are encouraging the extension of this model to at least 12 azimuthal sectors to really catch the physical phenomena measured in the heat-up test.

List of Acronyms

ATHLET: Analysis of thermal-hydraulics of leaks and transients
ATWS: Anticipated transients without scram
BWR: Boiling water reactor
BOC: Begin of cycle
CATHARE: Code for analysis of thermal-hydraulics during an accident of reactor and safety evaluation
CFD: Computational fluid dynamics
EFPD: Effective full power days
INR: Institute of Neutron Physics and Reactor Technology
KNPP: Kozlody nuclear power plant
LANL: Los Alamos National Laboratory
MSLB: Main steam line break
PARCS: Purdue advanced reactor core simulator
PWR: Pressurized water reactor
RELAP: Reactor excursion and leak analysis program
RPV: Reactor pressure vessel
SG: Steam generator
SNAP: Symbolic nuclear analysis package
TRACE: TRAC/RELAP advanced computational engine
TRAC: Transient reactor analysis code
VVER: Water-water energy reactor.

References

[1] R. Riemke, "RELAP5 multi-dimensional constitutive models," in *RELAP5/TRAC-B International Users Seminar*, Baton Rouge, La, USA, November 1991.

[2] "TRAC-BF/MOD1: An advanced best-estimate computer program for BWR accident analysis," US Nuclear Regulatory Commission Report NUREG/CR-4356-Vol.1, Idaho National Engineering Laboratory, August 1992.

[3] P. Bazin and M. Pelissier, "CATHARE 2 V25_1: description of the base revision 6.1 physical laws used in the 1D, 0D and 3D modules," CEA/DER/SSTH/LDAS/EM/2005-038, 2006.

[4] U. Graf, "Implicit coupling of fluid-dynamic systems: application to multidimensional counter-current two-phase flow of water and steam," *Nuclear Science and Engineering*, vol. 129, no. 3, pp. 305–310, 1998.

[5] F. Odar, et al., "TRACE V4.0 User's Manual," US NRC, 2005.

[6] N. Kolev, S. Aniel, E. Royer, U. Bieder, D. Popov, and Ts. Topalov, "The OECD VVER-1000 Coolant Transient Benchmark Phase 2 (V1000CT-2) Volume I: Specifications of the Coolant mixing problem," NEA/NC DOC, 2004.

[7] ANSYS Inc., "ANSYS CFX Release 11.0," *Reference Guide*, 2007.

[8] H. G. Joo, D. Barber, G. Jiang, and T. Downar, "PARCS: a multidimensional two-group reactor kinetics code based on the nonlinear analytical nodal method," School of Nuclear Engineering, Purdue University, July 2002.

[9] W. Jaeger, W. Lischke, and V. H. Sánchez Espinoza, "Safety related investigations of the VVER-1000 reactor type by the coupled code system TRACE/PARCS," in *Proceedings 15th International Conference on Nuclear Engineering (ICONE '07)*, Nagoya, Japan, April 2007.

[10] V. Sánchez, et al., "Analysis of the VVER-1000 coolant transient benchmark phase 1 with RELAP5/PARCS," *Progress of Nuclear Energy*, vol. 48, pp. 865–879, 2006.

[11] B. Truong, "Application of RELAP5/PARCS coupled-code system in studying coolant mixing and main steam line break transients behavior of VVER-1000 reactor," Tech. Rep., FZK, August 2006.

[12] M. Boettcher, "Investigations of the coolant mixing phenomena within reactor pressure vessel of the VVER-1000 reactor," *Nuclear Engineering and Design*, vol. 238, pp. 445–545, 2008.

[13] N. Kolev, et al., "Comparative analysis of exercise 2 results of the OECD VVER-1000 MSLB benchmark," in *Proceedings of the 16th Symposium of AER on VVER Reactor Physics and Safety*, Bratislava, Slovak Republic, September 2006.

Hindawi Publishing Corporation
Science and Technology of Nuclear Installations
Volume 2010, Article ID 783204, 8 pages
doi:10.1155/2010/783204

Research Article

CATHARE Assessment of PACTEL LOCA Experiments with Accident Management

Luben Sabotinov,[1] Heikki Purhonen,[2] and Vesa Riikonen[2]

[1] *IRSN, B. P.17 - 92262 Fontenay-aux-Roses, France*
[2] *LTKK, P.O. Box 20, 53851 Lappeenranta, Finland*

Correspondence should be addressed to Luben Sabotinov, luben.sabotinov@irsn.fr

Received 19 May 2009; Revised 27 January 2010; Accepted 1 February 2010

Academic Editor: Dubravko Pevec

This paper summarizes the analysis results of three PACTEL experiments, carried out with the advanced thermal-hydraulic system computer CATHARE 2 code as a part of the second work package WP2 (analytical work) of the EC project "Improved Accident Management of VVER nuclear power plants" (IMPAM-VVER). The three LOCA experiments, conducted on the Finnish test facility PACTEL (VVER-440 model), represent 7.4% cold leg breaks with combination of secondary bleed and primary bleed and feed and different actuation modes of the passive safety injection. The code was used for both defining and analyzing the experiments, and to assess its capabilities in predicting the associated complex VVER-related phenomena. The code results are in reasonable agreement with the measurements, and the important physical phenomena are well predicted, although still further improvement and validation might be necessary.

1. Introduction

This study was carried out in the framework of the EC project "Improved Accident Management of VVER nuclear power plants" (IMPAM-VVER) with participation of Finland, France, Germany, Hungary, Czech Republic, Slovakia, and Bulgaria. The objective of the project was to gain experimental and analytical results in order to improve the safety management practices and provide information for both utilities and safety authorities. In some VVER small break LOCA scenarios, it has been found out that there may be problems to depressurize the primary system in order to allow the emergency core coolant injection from the low-pressure system. The main objective of this project was to investigate which means and criteria for starting depressurization measures, like feed and bleed, would be the most efficient. Also it had to assesse the capability of computer codes like APROS, ATHLET, CATHARE and RELAP to predict the associated complex VVER-related phenomena. The experiments have been performed on the Finnish test facility PACTEL and Hungarian rig PMK-2. This paper presents the modeling and the results of CATHARE calculations, compared to the three PACTEL experiments. More details and results are provided in [1].

2. Description of the PACTEL Experimental Facility

The PACTEL experimental facility (Figure 1) was designed to model the thermal-hydraulic behavior of VVER-440-type pressurized water reactors (PWR). These reactors have several unique features that differ from other PWR designs. PACTEL simulates all the major components and systems of the reference VVER-440, making it a realistic tool to examine a broad range of postulated accidents and operational transients [2].

PACTEL is a volumetrically scaled (1 : 305) facility including core, cold and hot legs, steam generators, main coolant pumps, pressurizer, high- and low-pressure emergency core cooling systems, and hydro-accumulators. The maximum operating pressures on the primary and secondary sides are 8 MPa and 4.6 MPa, respectively. The corresponding values in VVER-440 are 12.3 MPa and 4.6 MPa. The reactor

vessel is simulated with separate downcomer and core sections. The core itself consists of 144 full-length, electrically heated fuel rod simulators with a heated length of 2.42 m. The axial power distribution is a chopped cosine with a peaking factor of 1.4. The maximum total core power output is 1 MW, 20% of scaled full power. The fuel rod pitch (12.2 mm) and diameter (9.1 mm) are identical to those of the reference reactor. The rods are divided into three roughly triangular-shaped parallel channels representing the intersection of the corners of three hexagonal VVER rod bundles.

Component heights and relative elevations correspond to those of the full-scale reactor to match the natural circulation gravitational heads in the reference system. The hot and cold leg elevations of the reference plant have been maintained, including the loop seals. To preserve flow regime transitions in the horizontal sections of the loop seals under two-phase flow conditions, the Froude number has been applied to select the diameter and length of the hot and cold legs. Three coolant loops with double capacity steam generators are used to model six loops of the reference power plant. The steam generators (SG) have vertical primary collectors and horizontal heat exchanging tubes. The external and internal SG tube diameters are 16 mm and 13 mm as in real NPP. The scaled heat transfer area of the tubes is preserved. Secondary side steam production is vented through control valves directly to the atmosphere.

3. PACTEL Modeling by CATHARE

The calculations have been performed with the system thermal-hydraulic code CATHARE 2, version V1.3L_1.

The input data deck has been prepared on the basis of the CATHARE nodalization [3] of the PACTEL facility, which was used for ISP-33 analysis [4]. The input model has been modified in order to correspond to the PACTEL state [2] of the experiments.

The main modifications are as follows:

(i) the full-length steam generators have been replaced by the model of Large Diameter SGs with shorter heat exchange tubes but with real SG collectors,

(ii) main coolant pumps have been added,

(iii) ECCS has been modeled (Hydro-Accumulators and LPSI pump).

The three real loops of PACTEL are modeled *separately* because of some differences in the lengths, elevations, and so forth.

The *core vessel* (Figure 2) is modeled by an *average core channel* with 11 axial meshes and weight 144 and a *bypass* with 11 axial meshes. The model of the upper plenum consists of a volume with 2 core and bypass inlet junctions and 3 outlet junctions (hot legs).

The *pressurizer* presents a volume with an external wall and 3 internal walls, modeling the heaters. For the modeling of the *steam generator* a *multitube* approach is applied. The heat exchange tubes of every SG, primary side, are presented as *9 axial elements*, located at different horizontal elevations.

PACTEL experimental facility

Figure 1: PACTEL experimental facility

Every axial element is divided in *10 meshes*. The *pressurizer* is connected in the hot leg of *Loop 1*. The *break* is located in the *cold leg* of *Loop 3* close to the reactor vessel.

As a whole, the primary side contains 92 junctions, 1 tee element, 10 volumes, and 40 axial elements with 539 segments. Figure 3 illustrates the modeling of the primary circuit of PACTEL.

The *secondary side* of the SG is presented by *recirculation* model. Every one of the secondary circuits comprises 4 junctions, 1 volume for the steam dome and 2 axial elements, modeling the SG liquid pool and the steam line with 22 segments.

The *heat losses* to the environment are modeled based on the information of the previous PACTEL configuration with some corrections taking into account the PACTEL heat losses test [5] (e.g., 9.5 kW per RCP etc.).

In the junction between the core, and upper plenum the CATHARE *Kutateladze model for CCFL* has been applied. The CATHARE CCFL operator allows the user to specify the parameters M, C, E, and X in the flooding equation:

$$\left[J_G^* Bo^{E/2}\right]^X + M\left[J_L^* Bo^{E/2}\right]^X = C, \quad (1)$$

where Bo is the Bound number and J_G^* and J_L^* are the dimensionless superficial velocity of gas and liquid, respectively.

The peak cladding temperature is very sensitive to CCFL model and plays an important role in the considered scenario of the transient.

4. Results of the CATHARE Calculations and Comparison with the Experiments

4.1. Test T2.1 Analysis. The test T2.1 represents a *7.4% (7.8 mm) cold leg break with secondary bleed and primary*

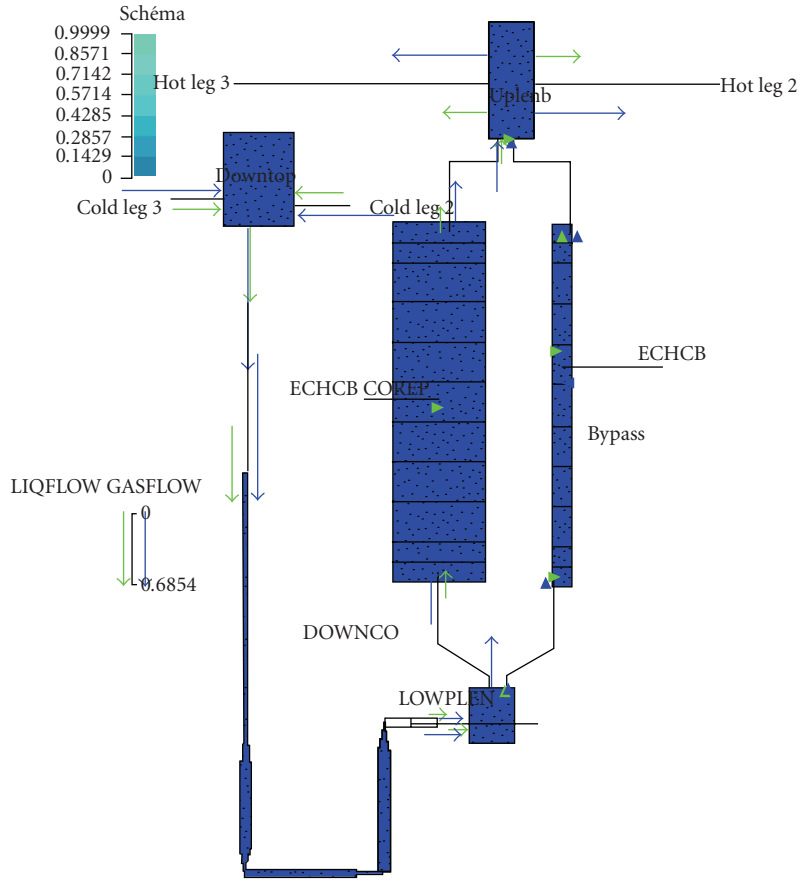

Figure 2: CATHARE core model of PACTEL.

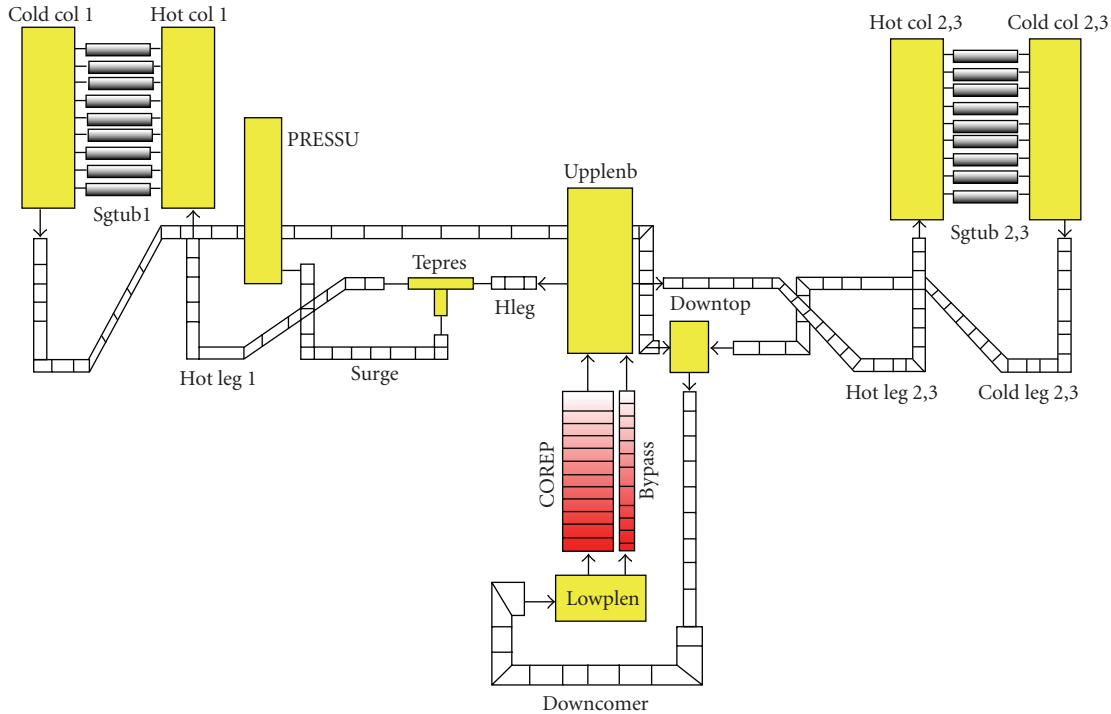

Figure 3: CATHARE nodalization of the PACTEL primary circuit.

bleed and feed. The bleed and feed occur if predefined core heat-up takes place. Regarding the ECCS configuration, the hydro-accumulators and the LPSI pump are available [6].

> *The objective of Test T2.1 was to investigate whether the primary pressure can be reduced to the LPSI delivery pressure without high-pressure injection in LOCA scenario.*

The initial primary pressure in the experiment was close to the maximum operating pressure of the facility and the lower-maximum power was compensated by decreasing the primary mass flow so that temperature distribution in the initial phase in the facility is as close as possible to the nominal temperature distribution in the plant.

The main conditions of the test are the following:

(i) the test is started from nominal conditions of the loop by opening the break in cold leg and initiating simultaneously:

  (a) scram,
  (b) steam line and feedwater isolation,
  (c) pump coast down;

(ii) injection of 1 accumulator to upper plenum starts, and 2 accumulators to downcomer;

(iii) secondary bleed starts at $T_{\text{wall}} > 350^{\circ}\text{C}$;

(iv) primary bleed starts if $T_{\text{wall}} > 400^{\circ}\text{C}$;

(v) LPSI starts at $P < 0.7$ MPa;

(vi) test is terminated if $T_{\text{wall}} > 450^{\circ}\text{C}$.

The sequence of the main events of the pretest and posttest calculations and comparison with the measured parameters are provided in the Table 1.

Regarding the boundary conditions, the posttest calculations are based on the specification and measurements of test T2.1. In the posttest analysis also some modification of the singularity in the hydroaccumulator line modeling has been introduced in order to get better timing in the prediction of the maximal fuel cladding temperature, although even in the pretest calculations the timing and the amplitude of the core heat up were predicted quite well.

Due to the coolant leakage, a rapid primary pressure drop takes place (Figure 4). The pressure calculations are in good agreement with the experiment. Some overprediction can be observed during the HA injection phase.

The primary pressure decrease below 5.5 MPa (after 50 seconds) leads to Hydro-Accumulators injection (Figure 5), which lasts until 450 seconds. In the calculations, the HA injection is relatively well predicted, but is slightly longer compared to the experiment.

Intensive core boiling takes place (Figure 6). The core liquid mass is going down and steam mass is increasing. The liquid flow in the core, downcomer and loops is stagnating around zero.

After the emptying of the HA, the further decrease of the primary mass inventory leads to core uncover, and core heat

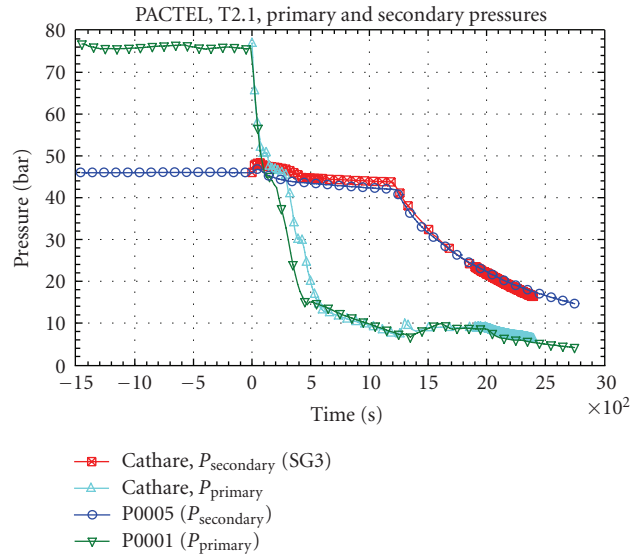

Figure 4: Primary and secondary pressures.

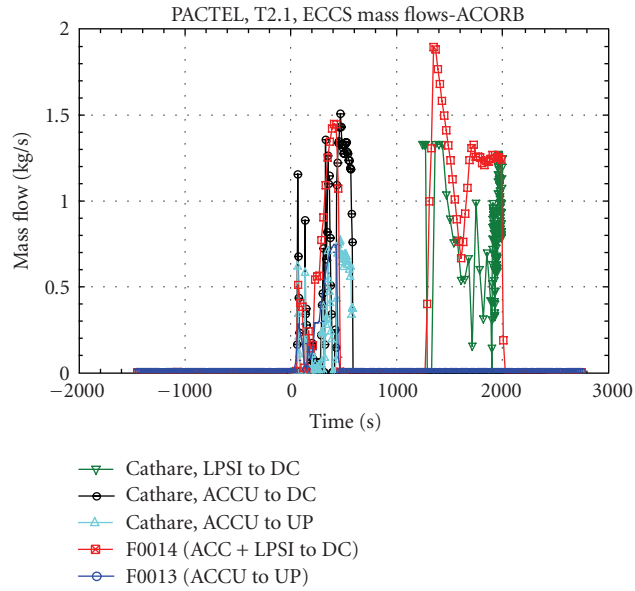

Figure 5: ECCS mass flows.

up starts at $t = 940$ seconds in the test, at $t = 920$ seconds in the posttest calculations (Figure 7), and at 900 seconds in the pretest. The timing and the temperature peaks are very well predicted by the calculations.

According to the scenario when the maximal cladding temperature exceeds 350°C, the operator starts the secondary bleed by opening the steam dump device to the atmosphere BRU-A ($t = 1230$ seconds experiment, $t = 1202$ posttest, $t = 1166$ seconds pretest). The calculated secondary pressure is decreasing in good agreement with the experiment (Figure 4).

The further decrease of the primary pressure leads very soon after the operator intervention to LPSI pump injection, (Figure 5, $t = 1250$ seconds test, $t = 1244$ seconds posttest

Table 1: Test T2.1: Timing of the main events, CATHARE versus experiment

Event	Time [S] Exp.	Time [S] Pretest	Time [S] Posttest	Comment
Start of calculation	−1500	−5000	−5000	Stabilization
Opening break valve	0	0	0	7.4% cold leg break (∅ 7.8 mm)
Reactor scram	0	0	0	
Pumps coast-down	0	0	0	Coast-down linear (0–150 s)
Isolation of feedwater and steam lines	0	0	0	Closing time is 3 s and 10 s, respectively
Pressurizer heaters off		18.9	18.9	Level in PRZ < 2.7 m
ACCU injection initiated to Downcomer to Upper plenum	50	60 61	60 61	Primary pressure < 5.5 MPa
END of HA injection to UP to DC	450	582 586.4	582 586	HA empty
Increase of fuel cladding temperature start	940	900	920	Core uncovery and heat-up start
Secondary bleed	1230	1166	1202	Cladding temperature > 350°C,
Primary bleed	—	—	—	Cladding temperature > 400°C,
LPSI start	1250	1205	1244	Primary pressure < 0.7 MPa
Maximal fuel cladding temperature	1261	1215	1267	Tclad, exp = 379°C Tclad, calc = 394°C posttest Tclad, calc = 391°C pretest
LPSI pump switched off	2000		2000	
End of test	2750	3600	2400	

and $t = 1205$ seconds pretest). With the LPSI, the core heat up is stopped, core quenching occurs, and the T_{max} is going down (Figure 7). So T_{max} does not reach the criterion for primary bleed (400°C), neither in the test nor in the posttest and pretest calculations. A stable cool down of the reactor vessel and primary circuit is achieved without primary bleed. It should be noted that the threshold for LPSI (0.7 MPa) could be reached even without operator intervention.

4.2. Test T2.3 Analysis. The test T2.3 is similar to test T2.1, but the pressure set-point for hydroaccumulators injection is lower: *3.5 MPa instead of 5.5 MPa* and the *water volume is increased*.

> *The objective of Test T2.3 was to investigate whether the primary pressure can be reduced to the LPSI pressure without high-pressure injection in LOCA scenario and if delayed hydroaccumulators injection with lower pressure set-point is more favorable for core cooling (to reach LPSI before core overheating occurs).*

Until 500 seconds, the primary pressure is very well predicted (Figure 8). Between 500 seconds and 900 seconds, the pressure drop is faster in the experiment than in the calculations. Probably this is related to the start of HA injection and stronger condensation in the experiment than in the calculations in the upper plenum. The cold water penetration into the core is quite sensitive to the CCFL modeling in CATHARE (strong dependence on the geometry and corresponding relationships).

The primary pressure decrease below 35 bars (after 422 seconds in the test and 441 seconds in the calculations) leads to Hydro-Accumulators injection.

Intensive core boiling takes place. In the calculations a small core uncovery occurs between 287 seconds and 441 seconds, which is not observed in the experiment. The core liquid mass is going down and steam mass is increasing. The liquid flow in the core and in the down comer is stagnating around zero. The maximal fuel cladding temperature (Figure 9) remains below the threshold values to begin operator actions of secondary and then primary bleed (350°C and 400°C, resp.).

The further decrease of the primary pressure leads to LPSI pump actuation. It should be noted that the threshold for LPSI (0.7 MPa) has been reached without operator intervention. A stable cool down of the reactor vessel and primary circuit is achieved (Figures 9 and 10) without

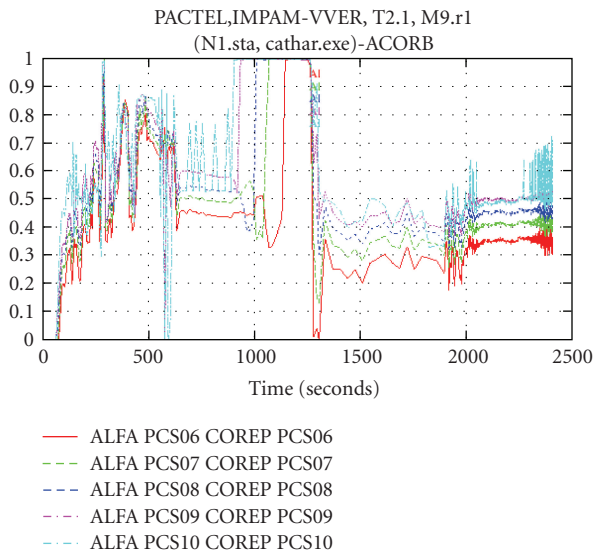

Figure 6: Void fractions (core upper half part).

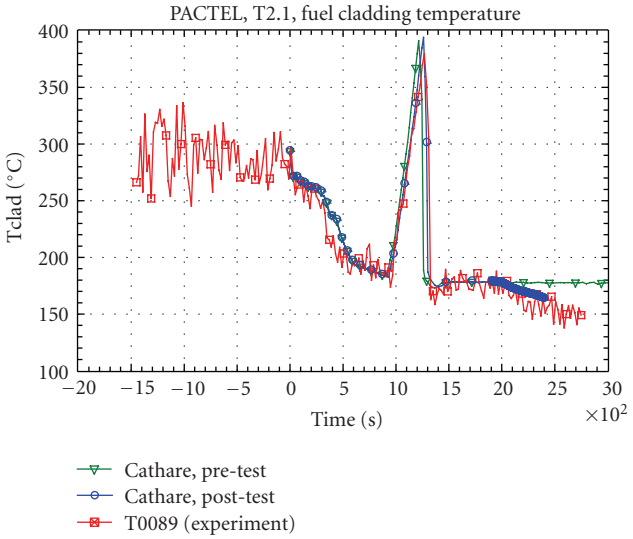

Figure 7: Fuel cladding temperature.

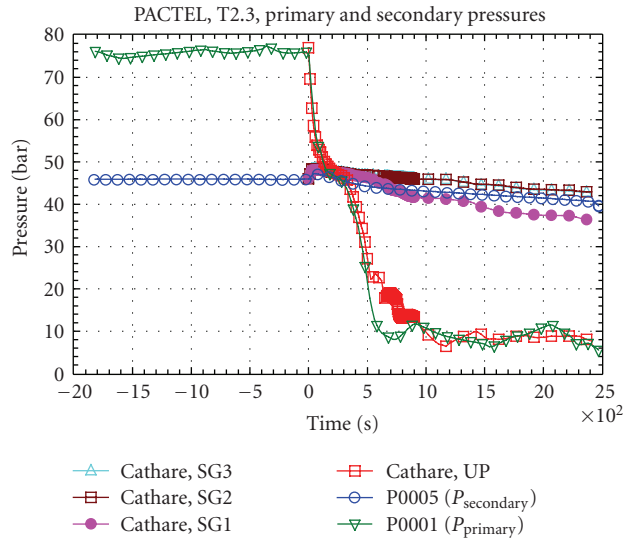

Figure 8: Primary and secondary pressures.

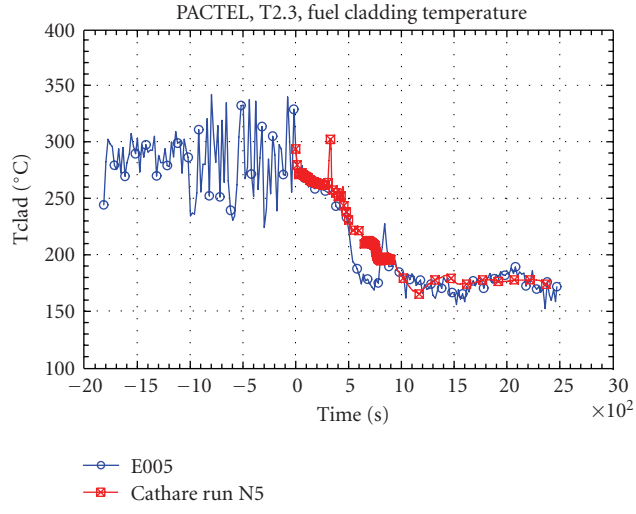

Figure 9: Fuel cladding temperature.

secondary and primary bleed. The delayed HA injection (reduced HA pressure set-point) had a favorable effect on the core cooling: no overheating occurred.

4.3. Test T3.2 Analysis. The test T3.2 is similar to test T2.1, but *secondary bleed is not actuated even if there are conditions to start it*. The primary bleed and feed occur if predefined core heat-up takes place. Based on the experience from the earlier tests the temperature criterion to start the primary bleed was *increased*.

> *The objective of Test T3.2 was to investigate the effect of low-pressure injection in the conditions in which the secondary side pressure remains high.*

The main conditions of the test are similar to T2.1 with exception of the following:

(i) no secondary bleed starts even if $T_{\text{wall}} > 350^{\circ}\text{C}$;

(ii) primary bleed starts if $T_{\text{wall}} > 500^{\circ}\text{C}$;

(iii) test is terminated if $T_{\text{wall}} > 550^{\circ}\text{C}$.

The calculated primary and secondary pressures are in good agreement with the measurements (Figure 11). Small overprediction of the primary pressure can be observed during the HA injection period. It is due probably to the modeling of HA and some underestimation by CATHARE of the condensation effects.

The primary pressure decrease below 55 bars leads to Hydro-Accumulators injection (Figure 12), which is well predicted by the pretest and posttest calculations.

With the LPSI, start the break flow is increasing again (Figure 13). The comparison of the calculated and measured break flows shows a good agreement.

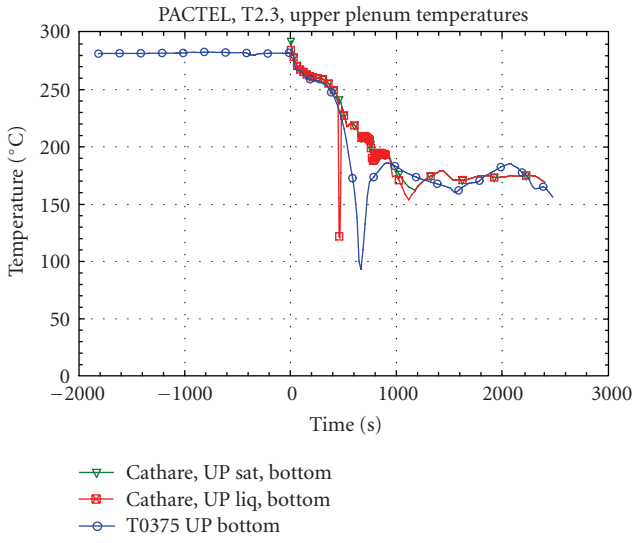

Figure 10: Upper plenum temperatures.

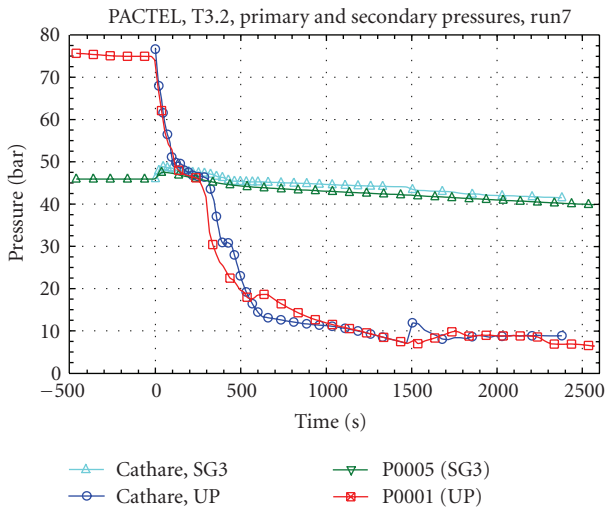

Figure 11: Primary and secondary pressures.

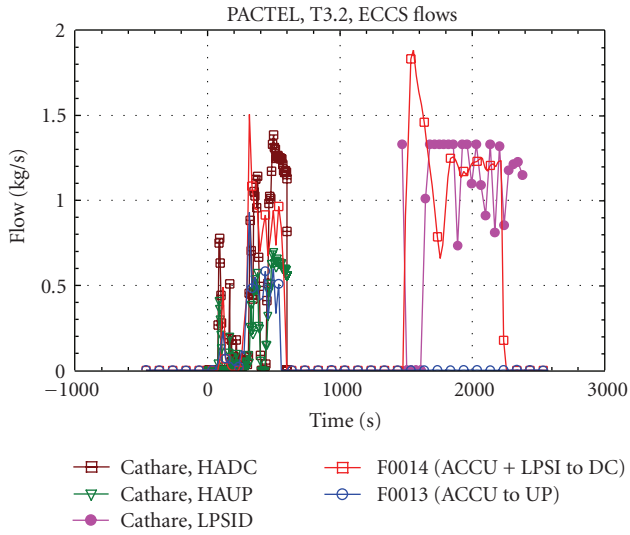

Figure 12: ECCS mass flows.

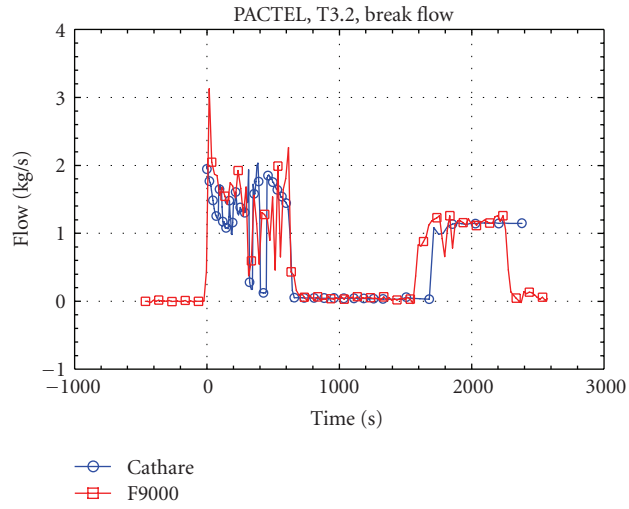

Figure 13: Break flow.

After the emptying of the HA, the further decrease of the primary mass inventory leads to core uncover, and core heat up starts at $t = 1082$ seconds in the test, at $t = 900$ seconds in the pretest calculations, and 1055 seconds in the posttest (Figure 14). The maximal fuel cladding temperature is achieved at 1476 seconds in the experiment and 1470 seconds in the posttest. So the posttest results have been largely improved in the timing and amplitude and a very good agreement can be observed. It should be pointed out that T_{max} is an extremely sensitive parameter.

The further decrease of the primary pressure ($P1 < 0.7$ MPa) leads to LPSI pump injection, which is well predicted in the posttest calculations (Figure 12). With the LPSI, the core heat up is stopped, core quenching occurs, and the cladding temperature is going down (Figure 14). So T_{max} does not reach the criterion for primary bleed (500°C), neither in the test nor in the posttest and pretest calculations. A stable cool down of the reactor vessel and primary circuit is achieved without primary bleed. The threshold for LPSI was reached without operator intervention.

5. Conclusions

The main objective of the IMPAM-VVER project was to investigate experimentally and analytically the means and criteria in case of SB LOCA to depressurize the primary circuit to the value of the LPSI pump head without high-pressure injection before core heat up takes place. The available measures for cooldown and pressure reduction are the hydroaccumulator injection and operator actions of secondary bleed and primary feed and bleed.

Correct definition of the initial and boundary condition of the tests is important for the proper code predictions. Global parameters as pressures, mass inventory, and so forth. are less sensitive compared to fuel cladding temperature,

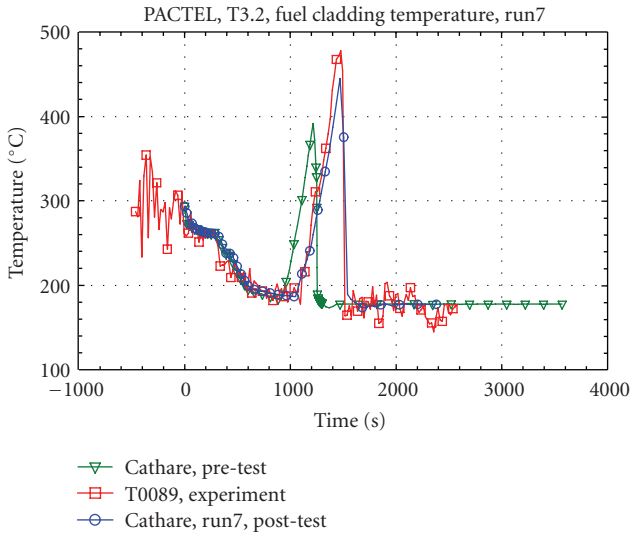

Figure 14: Fuel cladding temperature.

which is a key criterion in the safety studies and in the test scenarios.

The investigated break size of 7.4% is close to the spectrum of intermediate break LOCAs. Because of the relatively big break size, it was observed relatively fast that primary pressure decrease and the value of LPSI pump head (0.7 MPa) were reached even without operator actions in the code calculations as in the tests.

In the code calculations of test T2.1 and T3.2 (higher HA pressure set-point actuation), boiling crisis and core heat up took place, but the maximal heater rod wall temperatures did not exceed the predefined criteria for primary bleed. Timing and value of T_{max} are well computed by CATHARE code.

With the start of LPSI, the core heat up is stopped, core quenching occurs and the maximal cladding temperature starts to decrease. So T_{max} does not reach the criterion for primary bleed, neither in the tests nor in the calculations.

Test T2.3 was carried out with delayed HA injection (reduced HA pressure set-point). This measure had a favorable effect on the core cooling: no overheating occurred. T_{max} remained below 350°C. This effect was reproduced well by CATHARE code calculations. No secondary and no primary bleed took place.

Acknowledgments

This study was carried out in the framework of the European Commission project "Improved Accident Management of VVER nuclear power plants (IMPAM-VVER)." The authors express their gratitude to EC for the administrative and financial support of the work.

References

[1] L. Sabotinov, I. Karppinen, F. Lahovsky, and P. Matejovic, "Analyses of PACTEL experiments," IMPAM-VVER Project N° FIS5-2001-00117, 2004.

[2] J. Tuunanen, J. Kouhia, H. Purhonen, et al., "General description of the PACTEL test facility," VTT, Technical Research Center of Finland, 1998.

[3] L. Sabotinov and E. Laugier, "Pre-test and post-test sensitivity study of PACTEL ISP-33. CATHARE calculations," in *Proceedings of the 17th Chandra User's Committee Meeting (CUC '93)*, Grenoble, France, February 1993.

[4] OECD/NEA/CSNI International Standard Problem No.33, "PACTEL Natural Circulation Stepwise Coolant Inventory Reduction Experiment," Comparison Report, Volume 1 and 2 NEA/CSNI/R(94)24, December 1994.

[5] H. Purhonen, "Heat losses at the PACTEL facility," Version 2, 2003.

[6] H. Purhonen, "Test specification for PACTEL Test 2.1," April 2003.

Hindawi Publishing Corporation
Science and Technology of Nuclear Installations
Volume 2010, Article ID 864709, 12 pages
doi:10.1155/2010/864709

Research Article

Experimental Characterization of a Passive Emergency Heat Removal System for a GenIII+ Reactor

Lorenzo Santini, Davide Papini, and Marco E. Ricotti

Department of Energy, CeSNEF-Nuclear Engineering Division, Politecnico di Milano, Via La Masa, 34, 20156 Milano, Italy

Correspondence should be addressed to Davide Papini, davide.papini@mail.polimi.it

Received 28 April 2009; Accepted 3 October 2009

Academic Editor: Dubravko Pevec

Among the several types of passive safety systems adopted in new generation reactor designs, the experimental investigation of a closed loop, two-phase flow, natural circulation system is depicted. Emergency Heat Removal Systems (EHRSs) based on this solution are envisaged as safety-engineered features for advanced nuclear reactors, as in the IRIS reactor. An experimental facility simulating one EHRS-like loop has been built and operated at SIET labs in Piacenza (Italy). The facility is a natural circulation, sliding pressure, and electrically heated loop, with a helical coil steam generator as a heat source and a horizontal tube pool condenser as a heat sink. A steady-state analysis is provided to characterize the system behaviour and its key parameters. Because of the loop limited volume, oscillations of the main parameters (temperatures, flowrate, pressure) may be expected. The oscillating phenomena detected during the experimental campaign are discussed; a reasonable explanation is at last proposed.

1. Introduction

The innovative passive safety systems of advanced LWRs are based on natural laws, such as gravity and natural circulation [1]. They can be considered more reliable than active systems, since the lack of mechanical moving parts or other active components should reduce the probability of hardware failure.

Natural Circulation (NC) principle has been widely adopted in the past in several power conversion systems. Subcritical fossil fuelled power stations use NC as boiler flow driving mechanism, with the great advantage of a higher simplicity and of the reduction in operation costs related to the absence of pumps. In the nuclear field, pressurized water reactors use the same principle in U-tube steam generators. In recent years, NC has become very attractive even for emergency core cooling applications [2], relying on elements which always exist in a nuclear reactor: the heat source, the heat sink, the piping, and the gravity law.

The apparent simplicity of this physical principle in reality covers the complexity of the phenomena mutually interacting in a natural circulation loop [3, 4]: operating pressure, flowrate, flow quality, and heat transfer coefficients are all linked together. The behaviour of the NC passive systems usually entails oscillations in the thermal-hydraulic parameters, for example, the flowrate, hence leading to possible fluid dynamic instabilities. In particular, the problem of thermal-hydraulic instabilities [5] is one of the most crucial drawbacks on natural circulation systems. Instabilities could cause oscillations of the main loop parameters, inducing mechanical and thermal fatigue problems as well as making the system unable to perform its duty due to excessive deviations from the expected behaviour. For passive systems, it is thus necessary to introduce the concept of "functional failure" [6], considering the possibility that the loads will exceed the capacity in a reliability physics framework. To give an example, too high frictional pressure drops could cause a cancellation of loop driving force, preventing the system to accomplish its goal.

IRIS reactor [7] belongs to the innovative NPPs making an extensive use of natural circulation principle for safety purposes. IRIS is a low/medium power (335 MW_e) pressurized water reactor for electricity production developed by an international consortium led by Westinghouse. IRIS

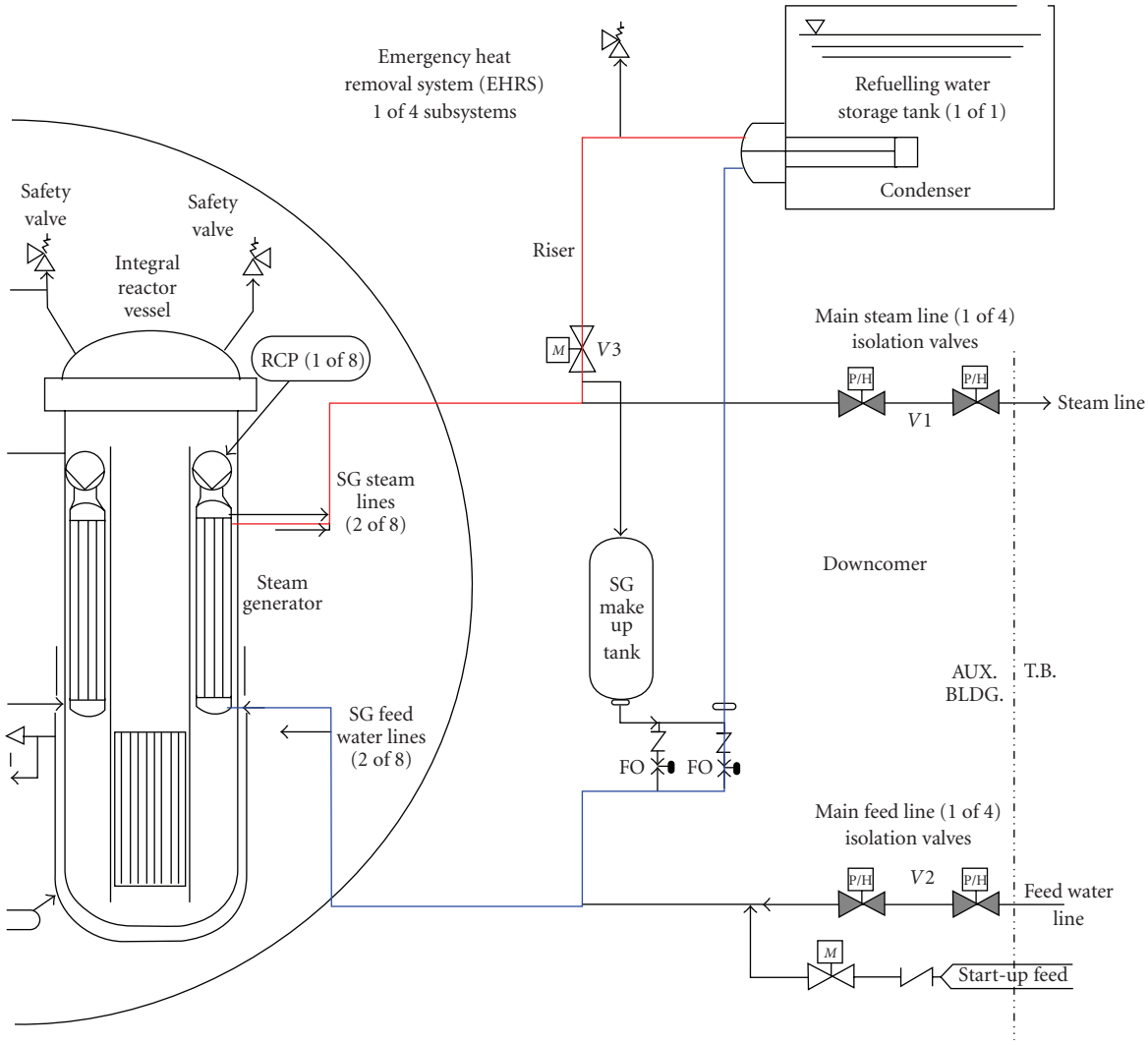

Figure 1: Sketch of IRIS emergency heat removal system (EHRS).

development started in late 1999 as part of the NERI program and has rapidly progressed to a nuclear reactor design with market entry targeted for deployment in the 2012–2015 time frame. The plant conceptual design was completed in 2001 and the preliminary design is currently underway. The preapplication licensing process with NRC started in October, 2002 and IRIS is one of the designs considered by US utilities as part of the ESP (Early Site Permit) process.

The main safety system of IRIS reactor is the Emergency Heat Removal System (EHRS), aimed to transfer core decay heat and sensible heat from the reactor coolant to the environment during transients, accidents, or whenever the normal heat removal paths are lost. It consists of four trains, each provided with a pair of steam generators (heat source), a hot leg (loop riser), a heat sink composed by a heat exchanger bundle submerged in the Refuelling Water Storage Tank (RWST), and a cold leg (downcomer), which closes the loop by bringing cold condensed water to the steam generators (Figure 1). Each of the four IRIS EHRS loops [8] is connected to one of the four steam and feedwater lines in the penetration area outside the containment (two of them are required to provide sufficient heat removal to match core decay heat). During normal plant operations V1 and V2 valves are open and V3 valve is closed (Figure 1); preheated water coming from the regeneration line is pushed into the steam generator where it is evaporated, slightly superheated, and sent to the turbine. If a reactor trip occurs, the core decay heat will be normally removed by the SGs thanks to the start-up feedwater system and the steam will be directed to the condenser via the steam dump valves. In case of malfunctioning of the start-up feedwater system, the EHRS is available to remove decay heat by means of the closure of V1 and V2 valves and the opening of V3 valve.

The challenge in analyzing the complex physics involved in the behaviour of a natural circulation loop requires relying not only on sophisticated modelling tools, for example, best estimate codes, but also on suitable experimental facilities, fundamental tools to provide data for validation of computer

codes and safety system design. In this paper the results of an experimental campaign on a facility simulating a two-phase, natural circulation, closed loop, sliding pressure safety system, similar to the type adopted for IRIS EHRS, are presented. As a preliminary step, a steady-state analysis has been performed to characterize the system behaviour. No accidents/transients have been investigated, the main goal being the dynamics of the loop at given primary thermal power to be rejected to the heat sink, at different system configurations (e.g., water mass inventories into the loop). A specific feature of the system and the facility is the closed loop, sliding pressure behaviour. Usually, in innovative BWR [9] and PWR [10, 11] designs the two-phase NC loops for passive safety systems are connected to large primary volumes, that is, the primary circuit, acting as a large expansion volume similar to a pressurizer. In the IRIS EHRS the loop is limited in volume since the in-pool condenser is directly connected to the helical coil steam generator tube bundle, hence a small volume when compared with the above mentioned configurations. It is expected that a dynamics with large pressure variations might occur, with possible feedbacks on the general behaviour. Moreover, the water mass inventory entrapped into the loop when the isolation valves activate should affect the system behaviour in a more sensible way with respect to the mentioned BWRs and PWRs safety systems, where larger mass inventories are expected.

The main simplification adopted in the facility is the imposed electrical power to obtain the heat source simulation, instead of the imposed temperature given by primary fluid, as in the real safety system. Although not strictly representative of the real loop conditions, it allows investigating a preliminary stability level for the system, apart from the thermal coupling with the primary loop which could introduce further complexity. Anyway, a useful experimental database for model validation is one of the main results.

2. The Experimental Facility

The IES facility (IRIS EHRS Simulator) was built and operated at SIET labs in Piacenza, as an extension of an electrically heated test section used for the investigation on the full-scale helical-coil steam generator tube [12]. The experimental loop is composed by a heat source, a riser, a heat sink, and a downcomer (Figure 2). It is scaled 1 : 1300 on power with respect to the real one, whereas it is full scale on height (~20 m) and on thermal-hydraulic conditions (pressure and temperature). The full height allows reproducing the driving force.

The heat source is the electrically heated steam generator, previously built for the study of two-phase pressure drops and critical flux in the helical-coil. The tube, as well as the piping, is thermally insulated by means of rock wool. The thermal losses were measured via runs with single phase hot pressurized water flowing inside the steam generator and estimated as a function of the temperature difference between external tube wall and the environment. The riser is a 21.3 m long AISI 316 stainless steel tube with an inner

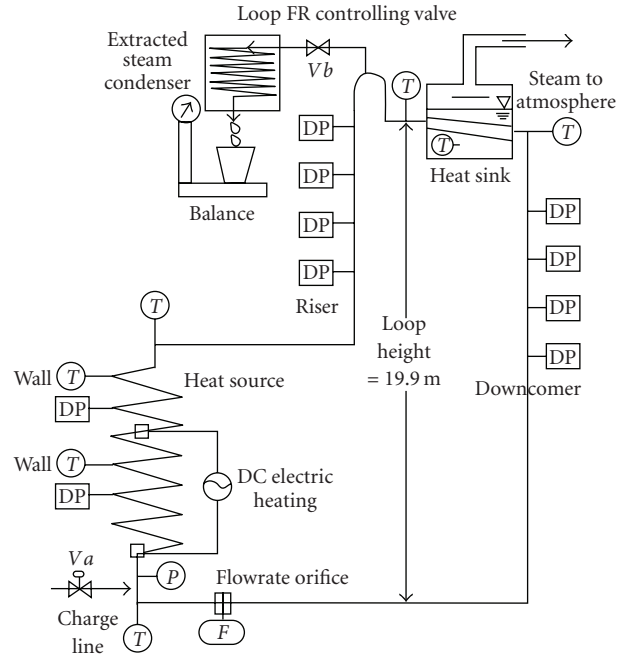

Figure 2: Sketch of IRIS EHRS Simulator facility (IES) at SIET labs.

diameter of 20.93 mm and an outer diameter of 26.67 mm. Downcomer tube is a 31.8 m long AISI 316 stainless steel tube with the same dimensions as the riser. Riser and downcomer diameters have not been scaled with respect to IRIS EHRS riser and downcomer expected pressure drops. The facility operates with one pool condenser tube, 1 m long with 59 and 73 mm of inner and outer diameters. The tube simulates a condenser with nearly horizontal tubes, inclined of 3° (corresponding to an early IRIS EHRS condenser design). A different solution with vertical tube arrangement will be investigated in the near future. The condenser tube is submerged into a 250-liter pool. A metallic slab is placed few centimetres before the vapour release duct in order to reduce the presence of liquid droplets in the exiting steam. The evaporated water is continuously replaced, according to a pool water level control.

The quantities measured in the loop (more than 200 measuring points) are flowrates, pressures (absolute and differential), temperatures, and powers. The loop flowrate has been measured by a calibrated orifice (5 mm diameter) placed at steam generator inlet and instrumented with a differential pressure transducer calibrated at SIET-labs (all the measurement devices are calibrated at SIET certified lab, SIT certified) with an estimated maximum uncertainty of 2%. The loop absolute pressure is measured at steam generator inlet via an absolute pressure transducer with a maximum uncertainty of 0.1%. Differential pressure transmitters are placed along the steam generator tube, the riser as well along the downcomer, with the aim of evaluating the possible presence of two-phase mixture at condenser tube outlet. Fluid temperature measurements are obtained with K-class thermocouples, with a maximum error of 0.4°C at 100°C. They are located at steam generator inlet and outlet headers,

Table 1: IES facility main geometrical data.

	Inner diameter (m)	Outer diameter (m)	L (m)	$\alpha(^\circ)$	R (m)
Orifice	0.01253	0.01715 (3/8″ S40)	0.56	90	0
Heated test section	0.01253	0.01715 (3/8″ S40)	24	14.3	0
Unheated test section	0.01253	0.01715 (3/8″ S40)	8	14.3	0
Upper header	0.0381	0.04826 (1.1/2″ S80)	1.1	0	0
Elbow	0.02093	0.02667 (3/4″ S40)	0.6	90	0.15
Horizontal riser	0.02093	0.02667 (3/4″ S40)	9.45	0	0
Elbow	0.02093	0.02667 (3/4″ S40)	0.2		0.15
Vertical riser	0.02093	0.02667 (3/4″ S40)	10.7	87	0
Siphon	0.02093	0.02667 (3/4″ S40)	1		0
Condenser	0.059	0.073025 (2.1/2″ S80)	1	−3	0
Elbows	0.02093	0.02667 (3/4″ S40)	3		0
Vertical downcomer A	0.02093	0.02667 (3/4″ S40)	9.45	−90	0
Elbow	0.02093	0.02667 (3/4″ S40)	0.2		0.15
Horizontal downcomer	0.02093	0.02667 (3/4″ S40)	8	0	0
Vertical downcomer B	0.02093	0.02667 (3/4″ S40)	9.23	−85	0
Elbows	0.02093	0.02667 (3/4″ S40)	2.1		0
Test section inlet header	0.02664	0.0334 (1″ S40)	1.1	0	0

at condenser tube inlet and outlet, and inside the pool. The electrical power is measured via a digital instrument with a relative uncertainty of 2.5%. The main geometrical data of the facility are summarized in Table 1.

2.1. The Filling Procedure. The constant volume of the loop makes its performance dependent on the water mass actually stored in it. The loop Filling Ratio (FR) is defined as the ratio between the total mass in the closed loop and the total mass of cold water that could be stored into the loop. The investigation of the effects of different FRs [13] is one of the main goals of the experimental campaign [14], since it is anticipated that this parameter deeply affects loop behaviour, in terms of heat rejection capability (in fluid heated systems) and working pressure.

In the real EHRS loop, the designed filling ratio would be obtained by properly timing the closure of the two valves which isolate the passive system from secondary circuit. In IES test section, a specific FR was obtained according to the following procedure, starting from an empty loop (with reference to Figure 2):

(i) Va and Vb valves open: the loop is completely filled with cold water via an external feed pump (the total measured mass of cold water storable in the system was nearly 25 kg);

(ii) Va valve closed;

(iii) warm up of the steam generator;

(iv) extraction, condensation, and weighting of the extracted water-steam;

(v) Vb valve closed when the desired FR is obtained;

(vi) operation of the loop at the desired power level conditions.

2.2. The Heat Losses Compensation. The larger surface over volume ratio of the facility with respect to the real system makes the thermal losses of riser and downcomer rather significant, notwithstanding the thermal insulation. These heat losses have been compensated by heating the riser and downcomer piping with an electrical wire and tuneable power. Since the heat losses are proportional to tube wall temperature, hence two-phase mixture temperature, hence system pressure, the suitable power needed to compensate the heat losses is a function of the system operating pressure. Therefore, a dynamic compensation was required, until the steady state was reached.

The inherent dynamic nature of the procedure and the time periods needed to run out the transient make the procedure quite time consuming. On the other hand, a precise evaluation of the heat losses is achievable by measuring the offset electrical power, according to the results of the first experiences with this compensating practice.

2.3. Test Matrix. The test matrix is composed of 45 runs, which allowed studying the variations of the following parameters: filling ratio (0.18, 0.31, 0.49, 0.61, 0.79), electric power supplied to the fluid, noncondensable gas content, and riser/downcomer heat losses compensation. The summary of the investigated parameters is provided in Table 2.

The lowest tested filling ratio (FR equal to 0.18) did not permit to reach the maximum power value (43 kW) due to large amplitude instabilities and dryout inception occurred in the test section. As far as the highest filling ratio/power points (FR of 0.79 and power of 43 kW) are concerned, it was instead not possible to compensate the thermal losses because of their too high values.

Table 2: Test matrix on IES loop.

Filling Ratio (FR)	Test section electrical power (kW)	Heat losses compensation	Noncondensable gas presence
0.18	13	yes	no
	23	yes	
	33	yes	
0.31	23	yes	no
	33	yes	
	43	yes	
0.49	23	yes	yes
	33	yes	
	43	yes	
0.61	23	yes	no
	33	yes	
	43	yes	
0.79	23	yes	no
	33	yes	
	43	no	

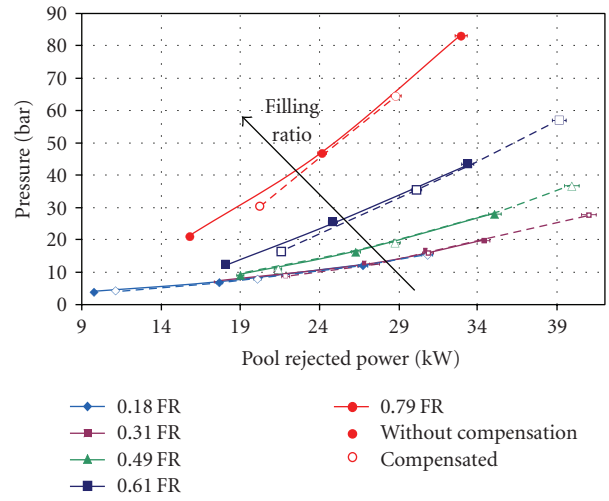

Figure 3: Effects of filling ratio and pool condenser rejected power on system pressure (both with and without heat losses compensation) [14].

3. Steady-State Results

3.1. Effects of Test Section Power and Filling Ratio on System Pressure. The most important effect of test section electrical power on system behaviour, at constant FR, is the setup of loop working pressure. A physical explanation is related to the working principle of pool condenser, assuming a steady-state condition with an equal balance between power supplied to the fluid and power rejected to the pool. The general formula describing the heat sink performance is

$$Q = U \cdot S \cdot \Delta T_{lm}. \quad (1)$$

The only way for transferring a higher thermal power to the pool is to increase U or ΔT_{lm} (or both). The possibility of increasing U is very small due to the strong thermal resistance of tube wall (thickness of 7 mm) and to the weak dependence of two-phase condensation and boiling heat transfer coefficients on flowrate. Thus, to increase the mean temperature difference implies an increase in loop pressure, being the pool water boiling temperature fixed by atmospheric pressure (neglected pool condenser outlet subcooling influence on the phenomenon).

FR effect is physically more difficult to explain, and it seems to be strictly linked to condenser outlet subcooling. Pool condenser outlet subcooling plays a key role in terms of the loop capacity in storing the water mass. High FRs turn into long subcooled zones both in the steam generator and in the condenser: usually these zones, together with the downcomer piping, host the largest amount of charged water, being small the mass stored in the two-phase zones due to the rapid grow of void fraction with quality. An increase of FR implies wider single-phase zones and higher subcooling at condenser outlet, which would result in principle in a reduction of the exchanging power capability. The rejected power is anyway fixed by the electrical heating; thus ΔT_{lm} and hence loop pressure must increase.

Figure 3 resumes all the runs carried out on the loop for different values of power and FR, with and without riser and downcomer heat losses compensation: it is apparent that the system pressure increases as a function of FR and test section power (through pool rejected power).

The role of pool condenser rejected power as the controlling parameter on system operating behaviour is fundamental, whichever are electrical power and thermal dispersions (mainly dependent on loop pressure). System pressure variations are, as a matter of fact, always driven by (1), which needs to be respected in response to perturbations on the other loop parameters, as deeply explained even in the following section.

Besides, in order to summarize the experienced loop behaviour (Figure 3 data), a simple correlation between system pressure and pool condenser rejected power has been proposed, which is valid in the explored range of filling ratios (between 0.18 and 0.79):

$$\frac{p^{0.7}}{T_{\text{sat}}} \frac{\Delta h_{lg}}{Q^{0.86}} = 136 \cdot \text{FR}^2 - 78 \cdot \text{FR} + 49, \quad (2)$$

where the pressure p is expressed in kPa, the heat of vaporization Δh_{lg} is expressed in kJ/kg, saturation temperature T_{sat} is expressed in K, and pool condenser rejected power Q is expressed in kW. System pressure is predicted with a mean error of −1% and an RMS error of 7.3%. These predictive capabilities, of course, have to be considered strictly limited to the specific characteristics of the loop investigated in this work.

3.2. Effects of Filling Ratio and Power on Pool Condenser Outlet Subcooling. The effects of FR and electrical power on pool condenser outlet subcooling are shown in Figure 4. Both

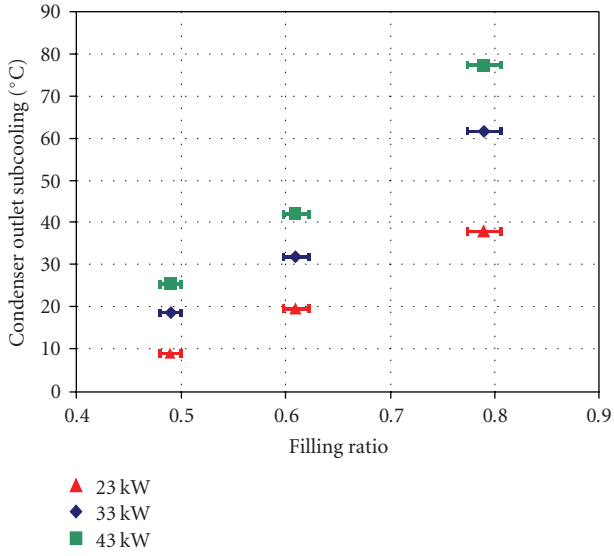

Figure 4: Effects of filling ratio and electrical power on pool condenser outlet subcooling (without heat losses compensation) [14].

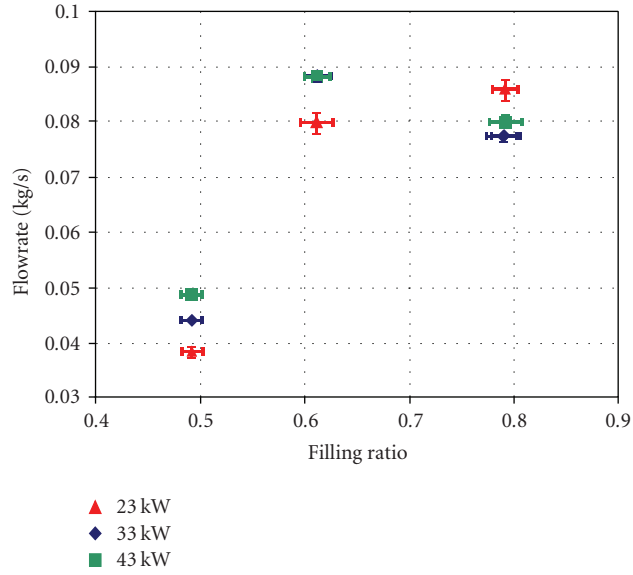

Figure 5: Effects of filling ratio and electrical power on system flowrate (without heat losses compensation) [14].

the FR and the power increase the pool condenser outlet subcooling. The data at FR equal to 0.18 and 0.31 have been omitted, due to the presence of a two-phase mixture in the downcomer piping.

The central role of pool condenser power is still confirmed. Loop pressure variations are driven by the condenser outlet subcooling perturbations following a change in FR. As discussed in the previous section, an increase in FR, that is, loop mass content, induces the circuit to increase pool condenser and steam generator tube subcooling lengths, in order to allocate the increased mass. This augmented mass inventory cannot be otherwise hosted in the two-phase leg, since the void fraction shows typically high values (and moreover the downcomer is already filled with water). The increased subcooled zone lengths have a direct impact on pool condenser overall heat transfer coefficient; according to (1), U must be smaller due to the increased importance of the liquid zone (which gives lower HTCs); thus an increase of mean logarithmic delta temperature between loop and pool water, the latest being always fixed at 100°C, is needed. This demonstrates the necessary increase in system pressure from lower to higher FRs, which is consistent with the outcomes of Figure 3. Taking into account what discussed in Section 3.1, it is evident that both, effects of FR and of test section power on condenser outlet subcooling, require a corresponding increase in system pressure in order to achieve heat balance in steady state. Loop pressure acts therefore as the hidden thermal-hydraulic variable always involved when perturbing system input parameters.

In the previous reasoning the flowrate impact on pool condenser exchanging capabilities has been neglected. As it will be discussed in the next section, flowrate changes due to a change in power, but not monotonically, due to the complex interactions between downcomer gravitational driving force, riser gravitational counter-driving force, and loop friction. By neglecting any change in loop flowrate with respect to thermal power, which is indeed small, the loop allocates a larger water mass content by increasing the pool condenser outlet subcooling.

3.3. Effects of Filling Ratio and Power on Loop Flowrate. Figure 5 shows that the effect of FR and electrical power on system flowrate is not monotonic. At low-medium FRs, an increase in power (considering pressure, FR and subcooling unchanged) increases the flow quality in the riser piping, reducing the gravitational counter-driving force. Thus, the flowrate would increase until a higher steam generator outlet quality reestablishes the balance between the friction pressure drops and the overall gravitational driving force (i.e., the density difference between riser and downcomer piping). This explanation is valid when the increase in power slightly changes steam generator inlet subcooling, that is, the case of the smallest value of FR (0.49) reported in Figure 5.

At higher FRs, the increased SG single phase zone length, as a consequence of the effect discussed in Section 3.2, makes the counter-driving force higher despite the increased power, causing a reduction in flowrate.

3.4. Noncondensable Gas Effect on System Pressure. In order to investigate the effect of the presence of noncondensable gases (e.g., air) on system behaviour, some tests were performed after the introduction of a certain amount of air into the system. The presence of noncondensable gas may come from several potential sources:

(i) the air naturally dissolved in the secondary circuit, due to a not perfect behaviour of the de-aerator of the secondary cycle;

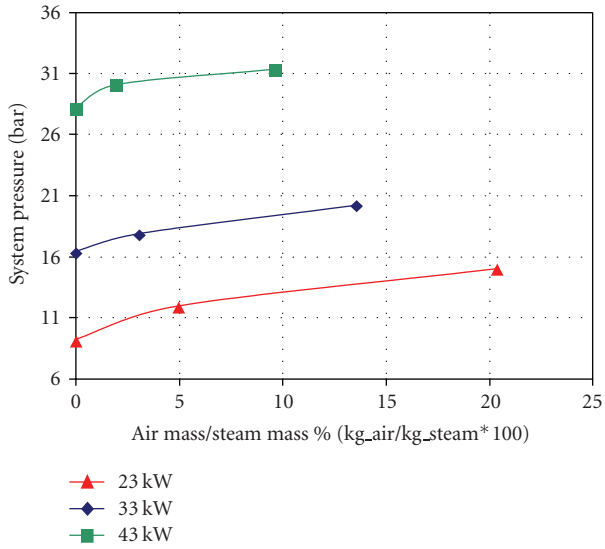

Figure 6: Noncondensable gas concentration effect on system pressure [14].

(ii) the introduction of helium or hydrogen into the secondary circuit, coming from primary circuit, due to a steam generator tube rupture or leakage;

(iii) the possibility of maintenance errors.

Condensation heat transfer coefficients are reduced if a noncondensable gas is added in the condensing fluid [15]. In fact, the gas collects at the interface between liquid film and condensing steam, reducing vapour partial pressure and thus its temperature (which drives the thermal exchange). This degradation in convective coefficients is more pronounced if system pressure is reduced and in stagnant mixtures rather than in forced convective condensation. A typical parameter introduced in order to quantify the amount of noncondensable gas is the ratio between the mass of air and the mass of steam (M_a/M_g). The total quantity of steam, dependent on FR and system pressure, is obtained with the simplifying hypothesis that air content does not influence steam presence. Therefore, the loop is schematized as a volume with a defined portion occupied by liquid and the remaining portion by steam in saturated conditions, resulting

$$M_g = \frac{V_{\text{loop}} - v_l \cdot \text{FR} \cdot M_0}{v_g - v_l}, \tag{3}$$

being M_0 the maximum mass of liquid storable in the loop in cold conditions ($\approx$25 kg).

The effect of noncondensable gas presence on system pressure is summarized in Figure 6. Air mass over steam mass ratio covered a range from 0% to 20%, though the highest values must be considered not realistic in real system operation and were achieved only with the aim of emphasizing noncondensable content effect on system performance. The degradation of heat transfer coefficients at pool condenser tube results in a system pressure increase. The effect is marked just with the first percentages of air introduced into the loop, as confirmed by the jump in pressure corresponding to noncondensable gas collecting at interface between saturated liquid and saturated steam; then such effect has to be considered small, being the rate observed equal to 0.2 bar of pressure increase every 1% of air content increase, and almost independent on the power level investigated.

4. Limiting Boundaries for Loop Filling Ratio

Simple considerations allowed identifying the effects of the main thermal-hydraulic parameters, especially water mass content, on loop steady-state conditions. As far as the dynamic oscillating behaviour of the loop is concerned, typical for a natural circulation system, a performance map has been obtained, where the limiting working conditions of the closed loop system are referred to the FRs and are function of system pressure, hence of thermal power to be rejected. Once an estimation of the loop pressure is obtained, the map allows defining the maximum and the minimum FRs ensuring a suitable dynamics for the system. It is important to point out that the map does not refer to a strict and thorough stability analysis, while the range of FRs leading to a suitable dynamics for the loop is related to engineering evaluations: working conditions, where flowrate inversion in the loop or two-phase mixture at steam generator inlet or loop completely filled with liquid occur, are evaluated as unfitted for a two-phase flow, closed loop safety system.

Oscillations of the circuit thermal-hydraulic parameters have been observed at the very low FRs experimentally investigated. Taking into account the SG tube, it can be assumed that a necessary but not sufficient condition for the stability is to have a negative thermodynamic quality at inlet: an increase in inlet quality, at fixed power, causes a wider two-phase zone length, leading to higher frictional pressure drops which are destabilizing. As previously stated, a boundary case to be avoided as prone to unstable behaviour is the operating condition with two-phase mixture entering the heated channel. This limit is in practice related to the volume of the downcomer with respect to the total volume of the loop. If the water initially stored into the loop is not enough to completely fill in the downcomer (i.e., small FR), the configuration previously described will occur. Obviously this minimum value must depend on system pressure because of the dependence of liquid density on pressure in saturated conditions. In order to quantify this limiting boundary by computing the minimum water inventory to be stored in the loop, the following simple conservative assumptions are made:

(i) homogeneous mixture flowing in the loop;

(ii) downcomer completely filled with liquid water at saturation temperature;

(iii) steam generator with complete evaporation of the mixture and linear increase of quality (from $x = 0$ to $x = 1$);

(iv) riser filled with saturated steam;

(v) condenser tube with complete condensation and linear decrease of quality (from $x = 1$ to $x = 0$).

According to the previous assumptions, the masses stored in the four components of the loop (steam generator, riser, condenser and downcomer) are, respectively,

$$M_{SG} = V_{SG} \frac{\ln\left(v_g/v_l\right)}{v_g - v_l}, \tag{4}$$

$$M_{riser} = \frac{V_{riser}}{v_g}, \tag{5}$$

$$M_{cond} = V_{cond} \frac{\ln\left(v_g/v_l\right)}{v_g - v_l}, \tag{6}$$

$$M_{down} = \frac{V_{down}}{v_l}. \tag{7}$$

The minimum value of the mass stored in the system in order to ensure a downcomer full of liquid water is thus

$$M_{min}(p) = M_{SG} + M_{riser} + M_{cond} + M_{down}, \tag{8}$$

and the corresponding minimum filling ratio (FR_{min}) for the loop is:

$$FR_{min}(p) = \frac{M_{min}(p)}{M_0}. \tag{9}$$

At very high FRs, that is, very high liquid contents, there must be a temperature hence a pressure in correspondence of which liquid specific volume is high enough to fill the entire loop volume. In this case, the degree of subcooling of the liquid leaving pool condenser allows the loop to store a higher quantity of mass, thus rising the maximum allowable FR. For a simple evaluation of the maximum FR, the entire loop is assumed filled with saturated liquid, except for the downcomer which is filled with subcooled water. With these assumptions the total mass stored is

$$M_{max}(p, \text{subcooling}) = \frac{V_{loop} - V_{down}}{v_l(p)} + \frac{V_{down}}{v_{l\_sc}(\text{subcooling})} \tag{10}$$

resulting in a maximum allowable FR equal to

$$FR_{max}(p, \text{subcooling}) = \frac{M_{max}(p, \text{subcooling})}{M_0}. \tag{11}$$

The map with loop maximum and minimum FR as a function of system pressure is drawn both for IES experimental facility and for IRIS EHRS loop design, as shown in Figures 7 and 8. It has to be intended as a quick tool to define the range for the mass to be charged into the system, in order to ensure a suitable functioning. The different shapes of lower curves in the two diagrams between IES facility and IRIS EHRS are due to their different volume distributions. In particular, in IES loop the steam generator volume is just

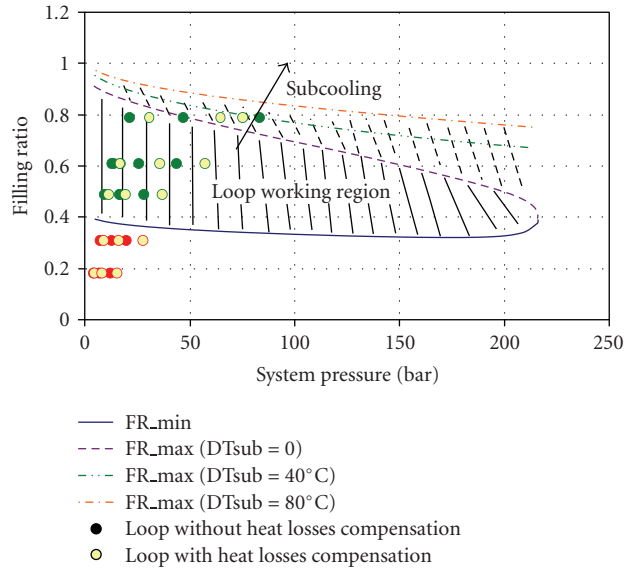

Figure 7: Filling ratio boundaries as a function of pressure and downcomer subcooling for IES loop.

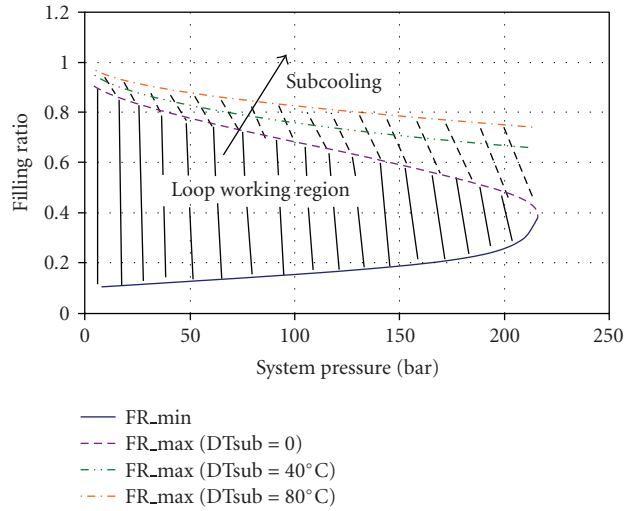

Figure 8: Filling ratio boundaries as a function of pressure and downcomer subcooling for IRIS EHRS loop.

16% of total loop volume, whereas it is about 40% in IRIS EHRS loop. The increased importance of SG volume in the EHRS makes possible to store more mass in the component; thus the system minimum mass could increase passing from low to high pressures, due to the decrease of steam specific volume with pressure in (4). On the contrary, IES loop has a smaller SG volume, and hence an increase in system pressure has the main effect of reducing liquid inventory into the downcomer.

The map in Figure 7, related to IES facility, reports even the experimental data (FR versus system pressure) provided by the test matrix execution, already used to set up the graph in Figure 3. Both the cases with and without heat losses compensation are taken into account; it is evident how the

compensation contributes to enhance system pressure. The dynamics and behaviour of the runs with FR equal to 0.49, 0.61, and 0.79 always fall inside the loop working region, whereas the smallest FRs explored (0.18 and 0.31) are below the minimum acceptable FR. The measurements for these runs show as a matter of fact the presence of a two-phase mixture in the downcomer piping, hence leading to large uncertainties in the system flowrate monitoring.

5. Stability Analysis

Many Authors in the past studied the stability features of a natural circulation loop, both with analytical tools and with experimental works. Instability phenomena can be produced by appropriate combinations of geometrical and operating parameters, namely, loop height and length as well as heating power and friction. A pioneering work in this field is due to Welander [16], who showed these instabilities turn into the amplification of perturbed temperature slugs generated in the heated and cooled sections. These analyses have been recently resumed by Ambrosini et al., facing both analytically [17] and with numerical codes [18, 19] the linear and nonlinear stability of a single-phase natural circulation loop. As far as the analytical approach is concerned, the main technique consists in linearizing the momentum and the energy equations as well as the boundary conditions, and adopting a first-order perturbation method. Suitable physical and geometrical parameters, evaluated in accordance with specific heat transfer laws and friction factor correlations, are used to completely identify the dynamic behaviour of the system. On this basis, stability maps [20] can be drawn, discriminating between stable and unstable regions according to the sign of the real part of the dynamic matrix eigenvalues (negative for stability and positive for instability conditions).

Other Authors referred the stability analysis to the interpretation of the dynamic flow oscillations [21, 22] which can appear in the loop. In particular, Jiang et al. experimentally studied a peculiar configuration which is named flow excursion [23], a new kind of static flow instability occurring at very low steam quality conditions and determined by the loop flow resistance and the internal driving head inside the natural circulation loop. Characteristic curves, operational curves, and bifurcation curves are the available methods to analyze these instabilities, as proposed by Yang et al. [24]. The same works show moreover how this flow excursion is prior to the low steam quality density wave oscillation [25], characterized by a dynamic interrelation between void fraction, pressure drops, and flowrate and by a strong coupling between the heated section and the heat sink condenser outlet.

In this paper, a particular kind of low-frequency oscillations, detected during the IES experimental campaign at the highest explored FRs, is discussed and interpreted in accordance with literature results. At the very low qualities which derive from a high FR, small flowrate variations can in fact cause large variations in riser void fraction, changing its gravitational pressure drops. The perturbation of loop

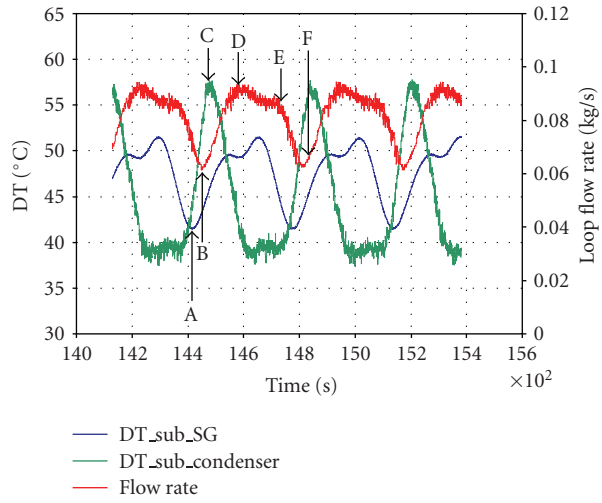

Figure 9: Low-frequency oscillations: steam generator inlet subcooling, pool condenser outlet subcooling, and loop flowrate as a function of time (Data obtained with power = 23 kW − FR = 0.79- with heat losses compensation).

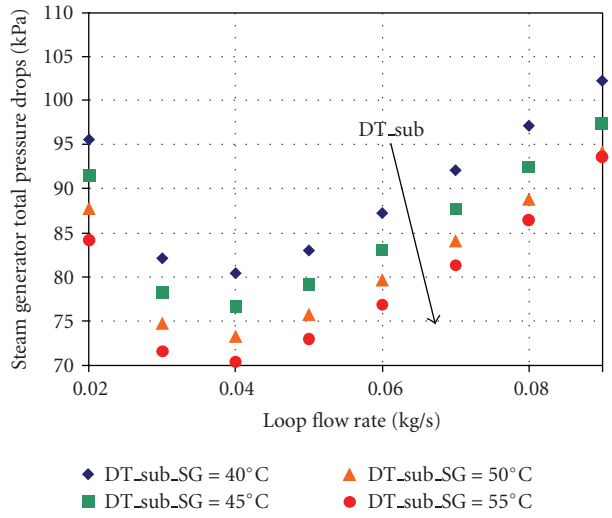

Figure 10: Steam generator pressure drops as a function of inlet subcooling (Data obtained with p = 30.5 bar − power = 23 kW).

pressure drops has a direct impact on the flowrate, influencing also pool condenser outlet subcooling. The coupling and the time delays between flowrate, pressure drops, and downcomer subcooling become the main responsible for the observed low-frequency oscillations. These oscillations occur at equilibrium conditions and do not affect the steady-state behaviour of the system, since the average values of the oscillating parameters are constant over a long-time period. They are mainly induced by the specific boundary conditions, that is, the imposed power at the heat source, the imposed temperature at the heat sink, and the unavoidable phase displacement due to the fluid running in the loop.

PHYSICAL EXPLANATION:

A. Perturbing cause represented by an enthalpy wave with a temperature decreasing ramp entering the SG.

B. Increasing inlet subcooling induces a reduction in SG pressure drops (Figure 10) which increases loop flowrate.

C. Increased flowrate causes a temperature ascending ramp exiting pool condenser due to the non-stationary heat exchange process.

D. The growing riser counter-driving force due to SG outlet quality decrease is responsible for a first reduction in flowrate.

E. Further decrease of flowrate when the temperature ascending ramp reaches SG inlet giving a rise in its pressure drops.

F. Reduced flowrate causes a temperature descending ramp exiting pool condenser due to the non-stationary heat exchange process, thus creating the conditions for a new oscillating cycle of the system.

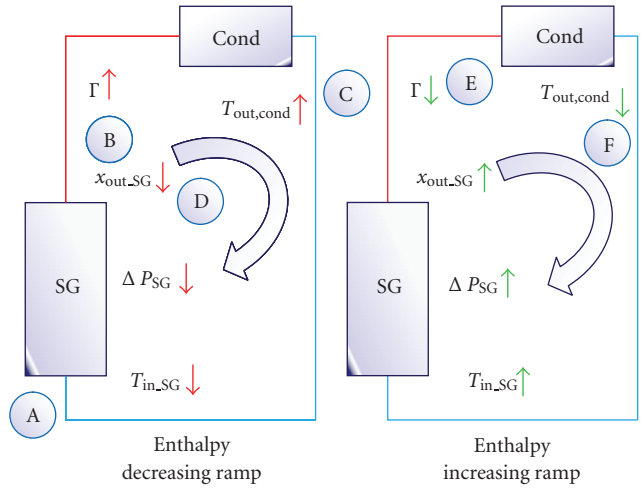

Figure 11: Schematic description of the physics involved in the low-frequency oscillations.

More in detail, the mentioned low-frequency oscillations, with periods of about 300 seconds, were detected only in the runs with the highest FR (0.79) and with the lowest power, that is, 23 kW and 33 kW. In Figure 9 mass flowrate, pool condenser outlet temperature, and steam generator inlet temperature are plotted for a run in which such high-amplitude long-period phenomena were observed. The period of the oscillations is 347 seconds. The transit time for a particle flowing in the loop, that is, the time period needed to travel the entire closed loop, is

$$\tau_{\text{loop}} = \frac{M}{\Gamma}, \tag{12}$$

being M the stored mass and Γ the flowrate. The run reported in Figure 9 refers to an FR of 0.79, that is, a stored mass of 19.75 kg, while the measured mean flowrate was 0.086 kg/s, resulting in a particle transit time equal to 230 seconds. The oscillation period reveals itself nearly 1.5 times the fluid transit time during that run. The similarity between the oscillation period and the particle residence time in the loop suggests that this oscillatory mode is somehow related to very slow enthalpy waves which travel in the loop with the same mean velocity of the mixture. These waves create a strong coupling between heated test section flowrate, riser pressure drops, and condenser outlet subcooling. This type of oscillations, widely investigated in mentioned works, for example, in [23], is probably related to the specific shape of the hot leg (steam generator and riser) characteristic (pressure drops dependence on loop flowrate, at different subcooling). Steam generator calculated pressure drops are shown in Figure 10. All the terms of pressure drops are included, except for the negligible acceleration term. The main result is that, everything else being the same, an increase in steam generator inlet subcooling reduces its total pressure drops.

Observing the curves reported in Figure 9, the similarity between SG inlet subcooling and loop flowrate supports the existence of a link between the two. In particular, SG inlet subcooling increase (point A) is always anticipating loop flowrate increase (point B), suggesting that the former is causing the latter. In order to understand the low-frequency oscillations propagation phenomenon, it is useful to consider a perturbation in the operating conditions, for instance, an enthalpy wave characterized by a decreasing temperature ramp exiting pool condenser. The enthalpy decreasing ramp entering the SG is equivalent to an increasing subcooling. According to the results of Figure 10, this subcooling wave will cause a reduction of SG total pressure drops which will increase loop flowrate (point B in Figure 9). The increased flowrate has the main effect of causing an ascending temperature ramp at pool condenser outlet (point C). This fact can be explained by a transient behaviour of the heat exchanger where, due to the increased flowrate, tube wall and liquid bulk are not able to reach a steady-state condition and have not enough time to exchange the power, resulting in a reduced extracted power and thus an increased outlet temperature. The increase in flowrate brings a decreasing SG outlet quality, which is then responsible for a first reduction in loop flowrate (from point D to point E), due to the growing of riser counter-driving force caused by the increased gravitational pressure drops. Loop flowrate will be further reduced when the temperature ascending ramp, travelling along the downcomer, will reach steam generator inlet. A reduction in SG inlet subcooling has in fact the effect of increasing its total pressure drops, thus reducing the flowrate. This reduction in loop flowrate will finally cause an enthalpy wave in the form of a temperature descending ramp starting from the pool condenser, which will create the conditions for a new oscillating cycle of the system. The whole line of reasoning can be clearly followed relying on the schematic of Figure 11.

6. Conclusions

The experimental campaign carried out in SIET labs on the IES facility simulating an IRIS EHRS-like loop has been described in the paper, the main goal being to investigate the influence of the mass inventory charged in the fixed volume system. The controlling parameter on system behaviour resulted to be pool condenser rejected power. Its balance equation is sufficient to explain how loop pressure responses to a change in loop FR and in test section electrical power. The most important effect of FR on loop performance is strictly linked to condenser outlet subcooling. High FRs turn into long subcooled zones both in the steam generator and in the condenser. The increased subcooled zone lengths have a direct impact on pool condenser overall heat transfer coefficient: the HTC is smaller due to the increased importance of single-phase heat transfer, resulting in an increase of mean logarithmic temperature drop, hence of pressure. The effects of FR and electrical power on system flowrate have been evaluated as well as the influence of the noncondensibles. The latter cause a reduction in condensation heat transfer, bringing to a slight loop pressure increase.

A simplified characterization of the facility has been proposed, to identify the FRs suitable for an effective behaviour of the system. The evaluation of the bounding values for FR has been summarized into a map, where the possible working conditions of the natural circulation loop are represented as a function of the achievable system pressure, both for IES experimental facility and for IRIS EHRS. The map is useful to quickly identify how much water has to be stored, according to the pressure level hence to the power to be rejected. The experimental runs on the IES facility and corresponding measurements and behaviour have confirmed the validity of the map.

A particular type of low-frequency oscillations, detected during the runs with the highest explored FR, has been investigated. These high-amplitude long-period oscillations are related to the particular boundary conditions of the system, that is, the imposed power at the heat source, the imposed temperature at the heat sink, and the unavoidable phase displacement due to the fluid running in the loop. At low qualities, a small SG inlet subcooling variation leads to sensible variations in SG and riser void fractions. The pressure drops influence loop flowrate which impacts also on pool condenser outlet subcooling. The coupling and the time delays between flowrate, pressure drops, and downcomer subcooling cause the observed phenomenon of low-frequency oscillations. The period of these oscillations (about 300 seconds) has been interpreted according to the concept of transit time for a particle flowing in the loop.

The explanation of the low-frequency oscillations proposed in the paper appears physically reasonable, being in accordance with all the observed phenomena and without any contradictions with the experimental results. Nevertheless, a confirmation of the mentioned cause-effect relations could come from a quantitative model of the system. The experimental campaign has indeed to be intended also as an important database useful to validate the accuracy of analytical models devoted to the dynamics of natural circulation thermosyphon loops. Both a simplified analytical model and a best-estimate (e.g., RELAP5) numerical model of IES facility are under development and will be validated on the experimental data.

Acronyms

BWR: Boiling water reactor
EHRS: Emergency heat removal system
ESP: Early site permit
FR: Filling ratio
HTC: Heat transfer coefficient
HX: Heat eXchanger
IC: Isolation condenser
IES: IRIS EHRS simulator
IRIS: International reactor innovative and secure
LWR: Light water reactor
NC: Natural circulation
NERI: Nuclear energy research initiative
NPP: Nuclear power plant
NRC: Nuclear regulatory commission
PWR: Pressurized water reactor
RMS: Root mean square
RWST: Refuelling water storage tank
SBWR: Simplified boiling water reactor
SG: Steam generator
SIET: Società informazioni esperienze termoidrauliche (company for information on thermal-hydraulic experimentation).

Nomenclature and Symbols

M: Mass stored in the loop (kg)
p: System pressure (kPa)
Q: Heat sink thermal power (kW)
S: Heat transfer surface (m^2)
T: Temperature (K)
U: Overall heat transfer coefficient ($kW/(m^2K)$)
V: Loop volume (m^3)
v: Specific volume (m^3/kg)
Δh_{lg}: Latent heat of vaporization (kJ/kg)
ΔT_{lm}: Logarithmic mean temperature difference (K)
Γ: System mass flowrate (kg/s)
τ: Particle transit time (s).

Subscripts

a: Air
cond: Pool condenser
down: Downcomer
g: Saturated steam
loop: Entire loop
l: Saturated liquid
l_sc: Subcooled liquid
riser: Riser
sat: Saturation
SG: Steam generator.

Acknowledgments

A special thanks to Professor Carlo Lombardi for his expertise, criticism, and invaluable help in following every part of the work. The Authors are grateful to Gustavo Cattadori, Andrea Achilli, and Stefano Gandolfi from SIET labs for their valuable collaboration and deep expertise. A dear thought also to Barbara Zito, worthy companion during the whole experimental campaign. Last but not least, the Authors are grateful to Mario Carelli and the colleagues of the IRIS project for the opportunity to work in such a stimulating and challenging adventure.

References

[1] IAEA-TECDOC-1281, "Natural circulation data and methods for advanced water cooled nuclear power plant designs," in *Proceedings of a Technical Committee Meeting*, Vienna, Austria, July 2000.

[2] Y.-J. Chung, S.-H. Yang, H.-C. Kim, and S.-Q. Zee, "Thermal hydraulic calculation in a passive residual heat removal system of the SMART-P plant for forced and natural convection conditions," *Nuclear Engineering and Design*, vol. 232, no. 3, pp. 277–288, 2004.

[3] P. K. Vijayan and A. K. Nayak, "Natural circulation systems: advantages and challenges," in *Natural Circulation in Water Cooled Power Plants*, IAEA-TECDOC-1474, 2005.

[4] N. Aksan, "Application of natural circulation systems: advantages and challenges II," in *Natural Circulation in Water Cooled Power Plants*, IAEA-TECDOC-1474, 2005.

[5] P. K. Vijayan and A. K. Nayak, "Introduction to instabilities in natural circulation systems," in *Natural Circulation in Water Cooled Power Plants*, IAEA-TECDOC-1474, 2005.

[6] L. P. Pagani, G. E. Apostolakis, and P. Hejzlar, "The impact of uncertainties on the performance of passive systems," *Nuclear Technology*, vol. 149, no. 2, pp. 129–140, 2005.

[7] M. D. Carelli, L. E. Conway, L. Oriani, et al., "The design and safety features of the IRIS reactor," *Nuclear Engineering and Design*, vol. 230, no. 1–3, pp. 151–167, 2004.

[8] A. Cammi and A. Cioncolini, "IRIS Passive Emergency Heat Removal System—PEHRS: state of the art design and RELAP model," IRIS Internal Report, Westinghouse Proprietary Class 2, 2003.

[9] J. Meseth, "Natural circulation and stratification in the various passive safety systems of the SWR1000," in *Natural Circulation Data and Methods for Advanced Water Cooled Nuclear Power Plant Designs*, IAEA-TECDOC-1281, 2002.

[10] F. D'Auria and M. Frogheri, "Natural circulation limits achievable in a PWR," in *Natural Circulation Data and Methods for Advanced Water Cooled Nuclear Power Plant Designs*, IAEA-TECDOC-1281, 2002.

[11] S. Zhang, "Experimental research and calculation method of natural circulation flow for AC600/1000," in *Natural Circulation Data and Methods for Advanced Water Cooled Nuclear Power Plant Designs*, IAEA-TECDOC-1281, 2002.

[12] L. Santini, A. Cioncolini, C. Lombardi, and M. Ricotti, "Two-phase pressure drops in a helically coiled steam generator," *International Journal of Heat and Mass Transfer*, vol. 51, no. 19-20, pp. 4926–4939, 2008.

[13] Y. J. Park, H. K. Kang, and C. J. Kim, "Heat transfer characteristics of a two-phase closed thermosyphon to the fill charge ratio," *International Journal of Heat and Mass Transfer*, vol. 45, no. 23, pp. 4655–4661, 2002.

[14] C. Lombardi, M. Ricotti, L. Santini, and B. Zito, "Experimental results on a two-phase closed loop system," in *Proceedings of Congresso Nazionale UIT sulla Trasmissione del Calore*, Trieste, Italy, June 2007.

[15] J. C. Collier, *Convective Boiling and Condensation*, McGraw-Hill, New York, NY, USA, 1981.

[16] P. Welander, "On the oscillatory instability of a differentially heated fluid loop," *Journal of Fluid Mechanics*, vol. 29, pp. 17–30, 1967.

[17] M. Maiani, W. J. M. de Kruijf, and W. Ambrosini, "An analytical model for the determination of stability boundaries in a natural circulation single-phase thermosyphon loop," *International Journal of Heat and Fluid Flow*, vol. 24, no. 6, pp. 853–863, 2003.

[18] W. Ambrosini and J. C. Ferreri, "Prediction of stability of one-dimensional natural circulation with a low diffusion numerical scheme," *Annals of Nuclear Energy*, vol. 30, no. 15, pp. 1505–1537, 2003.

[19] D. S. Pilkhwal, W. Ambrosini, N. Forgione, P. K. Vijayan, D. Saha, and J. C. Ferreri, "Analysis of the unstable behaviour of a single-phase natural circulation loop with one-dimensional and computational fluid-dynamic models," *Annals of Nuclear Energy*, vol. 34, no. 5, pp. 339–355, 2007.

[20] F. D'Auria, A. Del Nevo, and N. Muellner, "Insights into natural circulation stability," in *Natural Circulation in Water Cooled Power Plants*, IAEA-TECDOC-1474, 2005.

[21] C. Y. Wu, S. B. Wang, and C. Pan, "Chaotic oscillations in a low pressure two-phase natural circulation loop under low power and high inlet subcooling conditions," *Nuclear Engineering and Design*, vol. 162, no. 2-3, pp. 223–232, 1996.

[22] J.-T. Hsu, M. Ishii, and T. Hibiki, "Experimental study on two-phase natural circulation and flow termination in a loop," *Nuclear Engineering and Design*, vol. 186, no. 3, pp. 395–409, 1998.

[23] S. Y. Jiang, Y. J. Zhang, X. X. Wu, J. H. Bo, and H. J. Jia, "Flow excursion phenomenon and its mechanism in natural circulation," *Nuclear Engineering and Design*, vol. 202, no. 1, pp. 17–26, 2000.

[24] X. T. Yang, S. Y. Jiang, and Y. J. Zhang, "Mechanism analysis on flow excursion of a natural circulation with low steam quality," *Nuclear Engineering and Design*, vol. 235, no. 22, pp. 2391–2406, 2005.

[25] S. Guanghui, J. Dounan, K. Fukuda, and G. Yujun, "Theoretical and experimental study on density wave oscillation of two-phase natural circulation of low equilibrium quality," *Nuclear Engineering and Design*, vol. 215, no. 3, pp. 187–198, 2002.

Hindawi Publishing Corporation
Science and Technology of Nuclear Installations
Volume 2010, Article ID 815754, 16 pages
doi:10.1155/2010/815754

Review Article

Modelling of Heat Transfer Phenomena for Vertical and Horizontal Configurations of In-Pool Condensers and Comparison with Experimental Findings

Davide Papini and Antonio Cammi

Department of Energy, CeSNEF-Nuclear Engineering Division, Politecnico di Milano, Via La Masa, 34, 20156 Milano, Italy

Correspondence should be addressed to Davide Papini, davide.papini@mail.polimi.it

Received 30 April 2009; Revised 30 September 2009; Accepted 28 December 2009

Academic Editor: Dubravko Pevec

Decay Heat Removal (DHR) is a fundamental safety function which is often accomplished in the advanced LWRs relying on natural phenomena. A typical passive DHR system is the two-phase flow, natural circulation, closed loop system, where heat is removed by means of a steam generator or heat exchanger, a condenser, and a pool. Different condenser tube arrangements have been developed for applications to the next generation NPPs. The two most used configurations, namely, horizontal and vertical tube condensers, are thoroughly investigated in this paper. Several thermal-hydraulic features were explored, being the analysis mainly devoted to the description of the best-estimate correlations and models for heat transfer coefficient prediction. In spite of a more critical behaviour concerning thermal expansion issues, vertical tube condensers offer remarkably better thermal-hydraulic performances. An experimental validation of the vertical tube correlations is provided by PERSEO facility (SIET labs, Piacenza), showing a fairly good agreement.

1. Introduction

Nuclear advanced water reactor design is primarily focused on the achieving of innovative safety characteristics. The main goal of a safety design is to establish and maintain core cooling and ensure containment integrity for any transient situation, thus to minimize core damage and fission product release probabilities. The adoption of an integral layout, where the vessel hosts all the principal components of the primary circuit (reactor core, cooling pumps, steam generators, pressurizer, etc.), addresses a safety-by-design approach which increases the reactor safety.

Another important strategy in an advanced safety concept is the large utilization of passive systems, characterized by their full reliance upon natural laws (e.g., gravity and natural circulation) to accomplish their designated safety functions. Components and systems are called passive when they do not need any external input to operate. AC power sources as well as manual initiations are excluded, being the presence of moving mechanical parts and energized actuation valves limited according to the passivity level category [1].

A typical passive safety system is the natural circulation loop able to transfer core decay heat and sensible heat from the reactor coolant to the environment during transients, accidents or whenever the normal heat removal paths are lost. Such a system consists usually of a steam generator (providing the hot well), a hot leg (circuit riser), a heat sink given by a heat exchanger bundle submerged in a pool, and a cold leg (circuit downcomer). Its operation is based on the high heat transfer capability of the steam generator, able to remove decay heat producing steam which is driven into riser piping. Steam condensation in a suitable heat exchanger permits to reject this heat to the environment via the pool. The circuit is closed by downcomer piping, which drains cold condensed water back to the steam generator.

Primary objective of this paper is to provide a deep analysis on the heat transfer phenomena involved in a component of the mentioned circuit, namely the condenser submerged in the pool. The two simplest and most used tube

configurations, which are horizontal tube and vertical tube arrangements, have been considered. Condensation under the typical working conditions of a passive safety system for decay heat removal represents hence the topic of the paper. A key point is to carry out an open literature review on the most updated and reliable models and correlations to deal with flow pattern identification and heat transfer coefficient prediction, both for horizontal tube and vertical tube applications. Most of the proposed correlations were validated in the recent past thanks to suitable experimental campaigns in properly scaled facilities. Therefore, a short review on the experimental facilities in the frame of the explored condensation models has been provided to fully accomplish the review purpose of the paper.

A simple Matlab code has been then developed in order to test and compare the various condensation models described in the paper, with the main purpose to quantify the better thermal-hydraulic performances offered by vertical tube arrangement for the in-pool condensers (fixed the proper reference conditions for the comparison with horizontal tube arrangement). As a second goal, the accuracy and the wide applicability range of the classical modelling approach based on film condensation theory for vertical tube applications have been corroborated thanks to experimental findings from PERSEO facility [2].

The present work is structured as follows: in Section 2 an overview on the various passive safety systems for decay heat removal implemented in GenIII+ nuclear reactors is presented; in Section 3 the review of condensation models (both for horizontal tube and vertical tube applications) is provided. The Section 4 is dedicated to the short review of the experimental facilities of main interest for condensation modelling issues. In the Section 5 the results obtained with the simple in-house code are discussed; finally in the Section 6 the validation of the proposed vertical tube condensation model based on film condensation theory is provided by means of PERSEO experimental data.

2. Review of Passive Safety Systems for Decay Heat Removal

A first concept of in-pool immersed heat exchangers deals with a parallel arrangement of horizontal U-tubes between two common headers. This configuration has been provided in the emergency condenser of a SWR1000 [3], as shown in Figure 1. The top header is connected via piping to the reactor pressure vessel steam plenum, while the lower header is connected to the reactor vessel below the water level. The heat exchangers are located in a lateral pool filled with cold water, forming a system of communicating pipes with the vessel. At normal reactor water level the emergency condensers are flooded with cold water; if a reactor trip occurs the level can drop so that the heat exchanging surfaces inside the tubes are gradually uncovered. The incoming steam condenses on the cold surfaces, and the condensate is simply returned to the reactor vessel, avoiding any core uncovering.

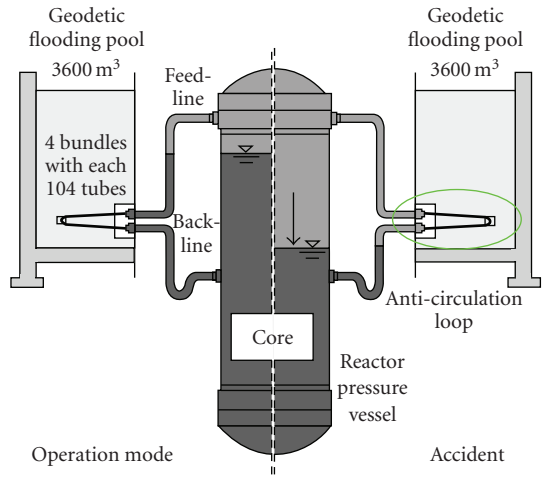

Figure 1: Emergency condenser of the SWR1000.

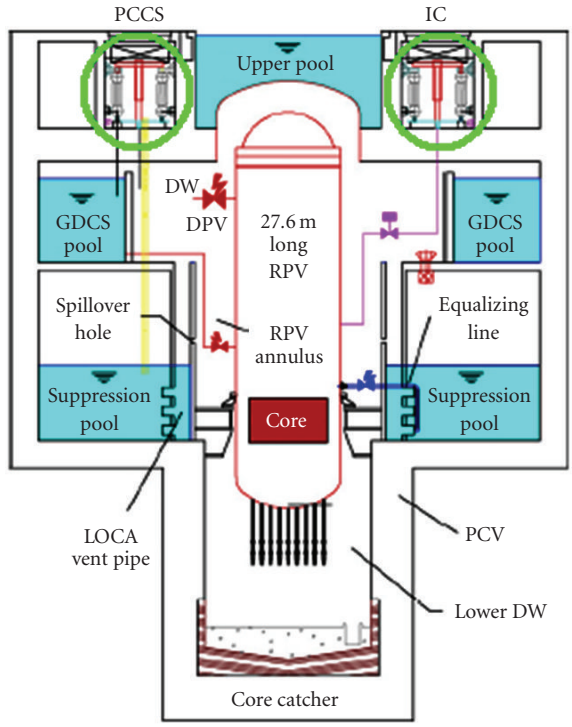

Figure 2: Isolation Condenser (IC) of the SBWR.

Other advanced water reactors implemented a vertical tube arrangement. This configuration has been carried out, for example, in the Isolation Condenser (IC) of an SBWR and in the Passive Containment Cooling System (PCCS) of a KNGR. In both cases decay heat is removed passively from the containment by the condenser submerged in a suitable pool [4].

In an SBWR [5] the system ICs are designed to passively limit the reactor pressure under accident conditions, whereas the containment ICs have to remove the decay heat after a LOCA. The physical location of the ICs is above the RPV, Suppression Pools and Gravity Driven Cooling System

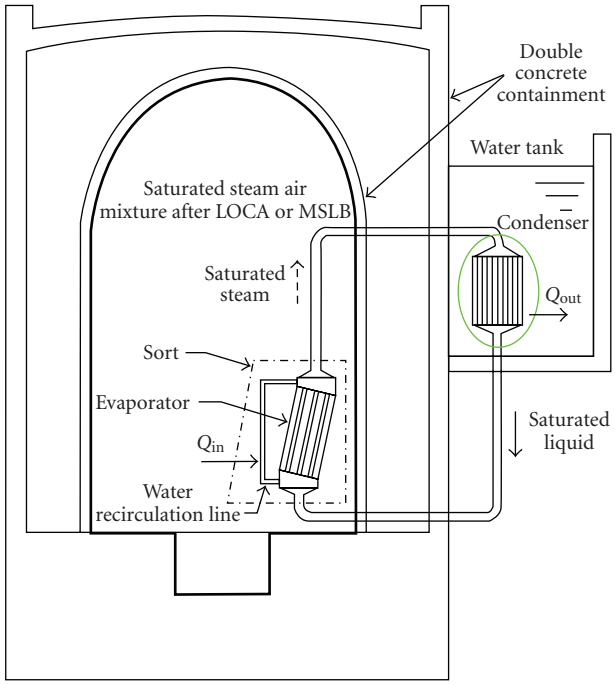

Figure 3: PCCS condenser of the KNGR.

(GDCS) in order to utilize the gravity induced return flow of the condensate from the ICs to the respective ports. Reactor layout is reported in Figure 2. Steam flows into the system ICs directly from the RPV, while the ICs of the PCCS receive a pressurized steam-nitrogen mixture from the drywell of the containment. Condensate is returned to the vessel by drain lines or through GDCS.

The PCCS of a KNGR [6] (Figure 3) is rather similar to the passive containment cooling system described for the SBWR ICs. It is provided with two heat exchangers, relevant lines and water tanks, and guarantees a way of external containment cooling through a natural circulation circuit. Heat transferred from the containment atmosphere to the coolant through the primary heat exchanger tubes is simply removed by condenser tubes to the water tank, located outside the containment.

A suitable passive safety system for decay heat removal, namely the Emergency Heat Removal System (EHRS) depicted in Figure 4, is foreseen also for IRIS reactor [7]. A previous in-pool condenser concept with horizontal U-tubes moved to a vertical tube arrangement; the utilization of the Isolation Condenser adopted from SBWR is now envisaged within the current design status. The Korean SMART reactor is conceived according to a similar idea of modular and integral-layout reactor; decay heat removal function is accomplished by the natural circulation in the PRHRS [8] (Figure 5), based again on steam generators for heat extraction and on in-pool heat exchangers (submerged in the Emergency Cooldown Tank -ECT-) for heat removal to the environment. A vertical tube arrangement is proposed.

The various decay heat removal systems developed for GenIII+ reactors point out a predominance of vertical tube condensers, which offer on the whole better thermal-hydraulic performances, as it is shown in the followings. It is just mentioned that the heat transfer performance is not the only figure of merit to be accounted when choosing the most proper configuration for an in-pool condenser. Thermo-mechanical issues are indeed of critical importance: horizontal tube condensers, allowing inherently thermal expansions, are of course preferable rather than a straight single-pass vertical solution which could induce dangerous thermal stresses due to prevented dilatations. These issues lie anyway outside the interests of the paper, hence will not be covered in the analysis.

3. Literature Review of Condensation Models

The better heat transfer performances assured by a vertical pipe condenser, mainly in terms of higher heat transfer coefficient and more predictable in-tube flow distribution, are first briefly summarized. The typical conditions for the utilization of an in-tube condenser within one of the passive safety systems mentioned above have been taken as reference. The capability to remove about 20–30 MW of thermal power, inducing low mass fluxes –G < 100 kg/sm^2– in the loop, is required.

Condensation in horizontal tubes is strongly influenced by the flow pattern, which can range from annular to stratified without avoiding the intermittent regimes (slug-plug). In a defined interval of mass fluxes and qualities, in fact, the possibility of fluid pulsation is concrete, driven by large amplitude waves that wash the top of the tube; flow reversal can be induced, as well as mechanical and thermal fatigue problems on the tube wall. A fully stratified–stratified wavy regime occurs according to the low flowrates and the medium-high pressures which characterize a natural circulation loop for DHR (typically 60–100 bar). A thin condensate film drains down from the upper part of the tube under the influence of gravity force, while a water sump accumulates and flows on the bottom. The HTC is negatively affected by this sump, in particular when it approaches subcooling conditions at the end of the pipe. Interfacial wave effects, increasing with the flowrate, do not balance this drawback. The result is an average heat transfer coefficient of approximately 4000–6000 W/m^{2}K (considered a G equal to 60 kg/sm^2). Therefore, condensation in a horizontal tube deals with a whole of complex phenomena, which require a careful analysis.

Two-phase flow path is instead well defined in a vertical tube, in case of a downflow streaming. An annular film of condensate forms on the wall and falls down driven by gravity, filling up the cross-section only at the end and assuring a better condensation process along major portion of the pipe. Condensate flows with a higher velocity, reducing fouling and corrosion effects as well as assuring higher HTCs. At fixed quality, the higher velocities (pulled by gravity) lead to a thinner film, with a lower thermal resistance, a thinner laminar boundary layer and thus higher turbulence. Average heat transfer coefficients are strongly enhanced with respect to the horizontal solution, providing

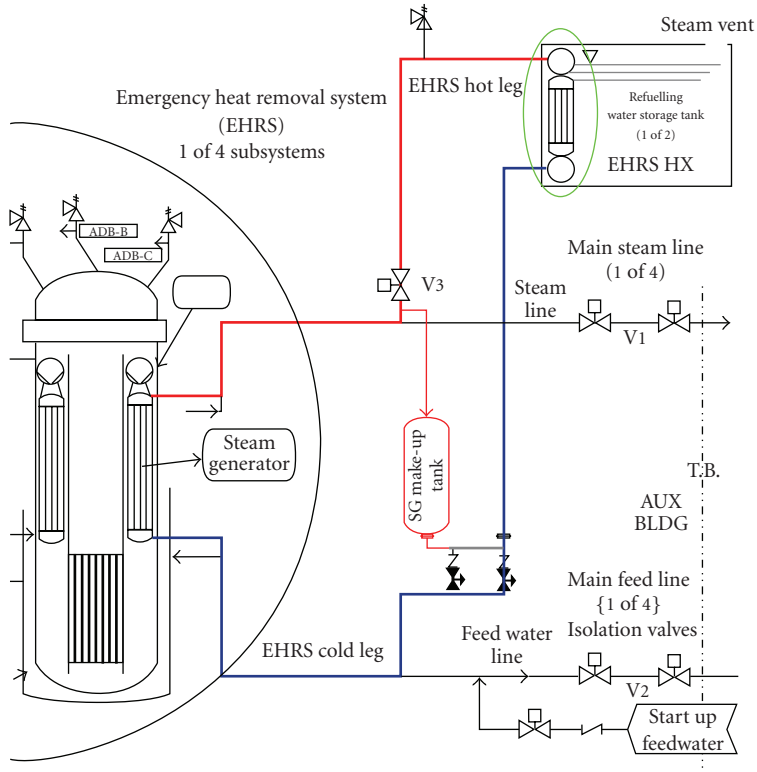

Figure 4: EHRS condenser of the IRIS.

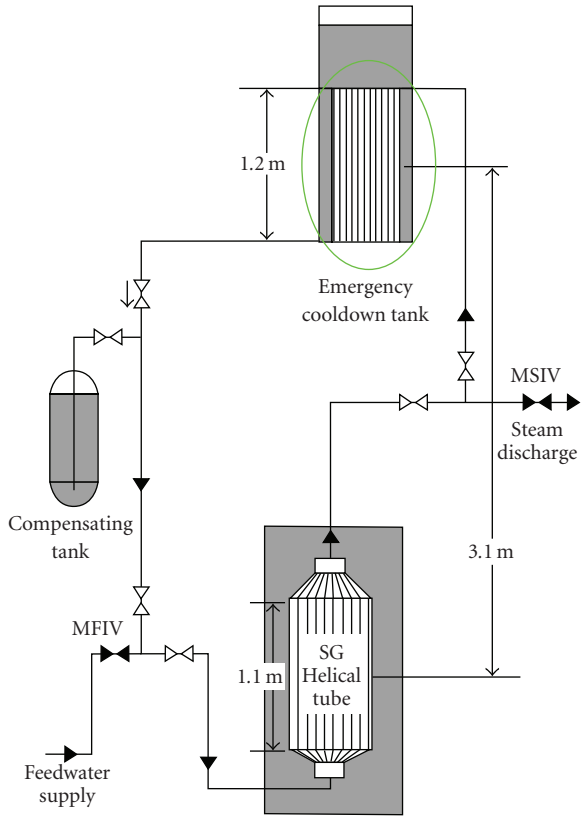

Figure 5: PRHRS condenser of the SMART.

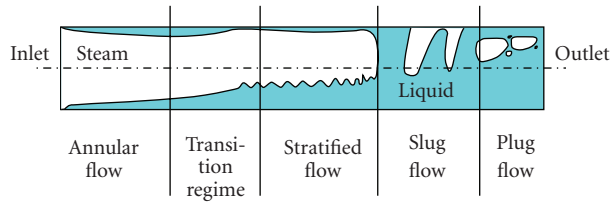

Figure 6: Different flow patterns during condensation in a horizontal tube.

values of approximately 8000–11000 W/m^{2}K. A lack of high pressure steam condensation data for large diameter vertical tubes, which is indeed the case of the IC adopted from SBWR to IRIS, has been noticed in open literature works. A comprehensive investigation on how condensation is provided in a downflow vertical tube appears hence of great interest. The different physical phenomena involved within horizontal and vertical tubes are clearly shown by the drafts reported in Figures 6 and 7.

3.1. Modelling of Condensation in a Horizontal Tube. In early models [9–12], the flow patterns were classified just under two categories, that is, stratified or annular. The first, dominated by gravity forces, is characterized by a thick condensate layer flowing along the bottom of the tube, while a thin liquid film forms on the wall in the upper portion of

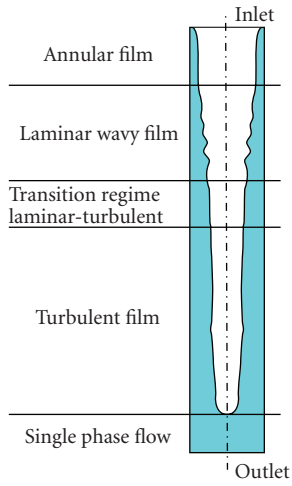

Figure 7: Different flow patterns during condensation in a vertical tube.

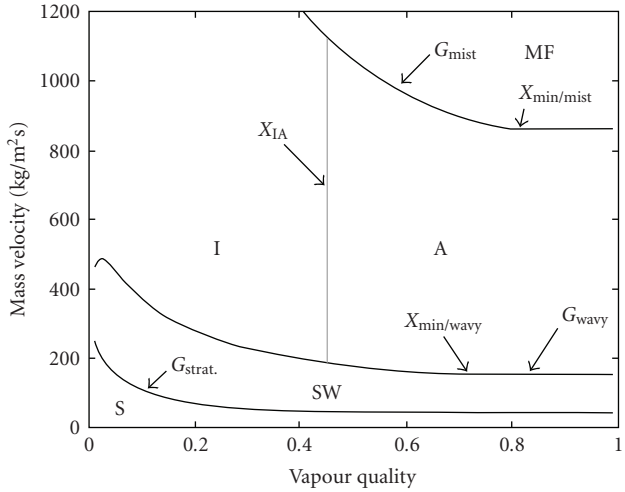

Figure 8: Thome's flow pattern map for condensation in a horizontal tube. S → stratified SW → stratified wavy A → annular I → intermittent MF → mist flow.

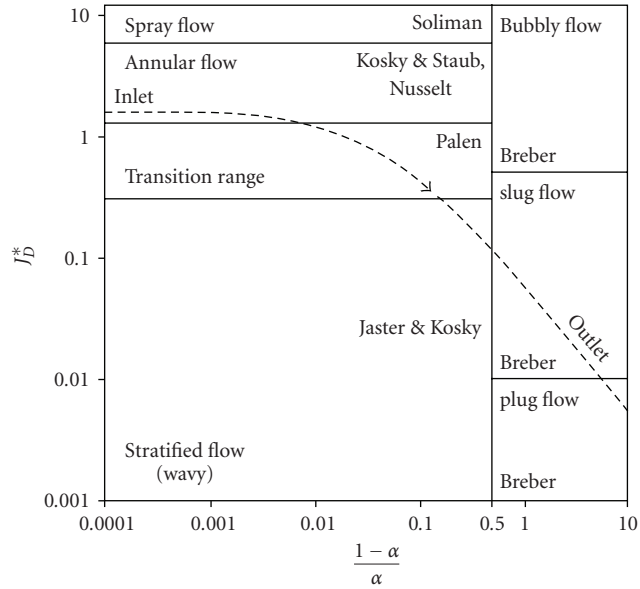

Figure 9: Tandon's flow pattern map for condensation in a horizontal tube.

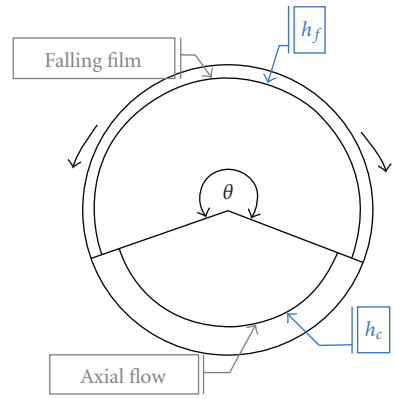

Figure 10: Heat transfer model showing convective and falling film.

the tube. The latter, dominated by shear effects, leads to an annular ring of condensate flowing uniformly along the tube. Different flow regimes can be instead induced. When the stratified condensate layer in the tube sump reaches medium-high velocities, ripples or waves are often generated at the phase surface (stratified wavy). If these waves become so large to wash the top of the tube, an intermittent flow pattern (slug-plug) can be established, presenting a very complex flow structure. At very high velocities, finally, a mist (spray) regime can occur, characterized by impinging droplets on the thin unsteady liquid film.

Two models are proposed in this paper as the most updated and reliable concerning the condensation in a horizontal tube, each one based on a proper flow pattern map for the identification of the actual flow regime (reported, resp. in Figures 8 and 9).

In Thome's model [13–15] the intermittent (both slug and plug) and mist flows are considered and evaluated as annular flow. For annular flow a uniform film thickness is assumed and the actual larger thickness of the film at the bottom rather than the top due to gravity is ignored. Stratified and stratified wavy are instead characterized by the so named stratification angle, which subtends the cross-sectional area occupied by the liquid, assumed as truncated annular ring of uniform thickness. Figure 10 is useful to understand the provided simplifications. Two different heat transfer mechanisms are considered within the tube: convective condensation and film condensation. The first refers to the axial flow of condensate along the channel due to the imposed pressure gradient; the second refers to the flow of condensate from the top of the tube towards the bottom due to gravity. The convective condensation heat transfer coefficient h_c is applied to the perimeter wetted by the axial flow of liquid film, which is the entire perimeter in annular flow, but only part of the perimeter in stratified wavy and stratified one. The film condensation

heat transfer coefficient h_f, affecting only stratified–stratified wavy regime, is obtained by applying the Nusselt's falling film theory [16] to the inside of the horizontal tube, assumed a laminar falling film. Hence, the condensation HTC is given combining these two coefficients according to

$$h = \frac{h_f \theta D_i/2 + h_c(2\pi - \theta)D_i/2}{\pi D_i}. \quad (1)$$

The convective condensation heat transfer coefficient h_c can be obtained from the following film equation, assumed the axial flow as turbulent

$$h_c = 0.003\,\mathrm{Re}_l^{0.74}\mathrm{Pr}_l^{0.5}\frac{k_l}{\delta}f_i \quad (2)$$

where δ is the film thickness, considered uniform in all the cross-section. This is an only liquid correlation type, that is, just the liquid part of the two-phase flowrate has to be considered, resulting

$$\mathrm{Re}_l = \frac{4G(1-x)\delta}{(1-\alpha)\mu_l}. \quad (3)$$

The interfacial roughness correction factor f_i takes into account the shear effects which dominate an annular flow regime. First of all, the shear of the high speed vapour is transmitted to the liquid film across the interface. Magnitude and number of the interfacial waves are increased and hence available surface area for condensation, inducing an enhancement in heat transfer. Secondly, these interfacial waves tend to reduce the mean thickness of the film (and thus its thermal resistance), again increasing heat transfer. Interfacial roughness and wave formation are also directly relatable to entrainment of liquid droplets into vapour phase, which reduces the thickness of the liquid film and increases heat transfer. Finally, interfacial shear creates vortices within the liquid film, which also increase heat transfer.

The film condensation heat transfer coefficient h_f, instead, is given from a modification of the Nusselt's theory for laminar flow of a falling film outside a horizontal tube (around the perimeter, from top to bottom) applied indeed to the condensation on the inside. Any effect of axial shear on the falling film is ignored. According to theory, heat transfer coefficients are known to be a function of tube wall temperature difference (not noticeable nevertheless for annular flow). Typical heat exchanger design codes are being implemented taking as variable the heat flux in each incremental zone along the exchanger (rather than wall temperature difference); therefore the heat flux version of Nusselt's equation is better to be considered:

$$h_f = 0.655\left[\frac{\rho_l\left(\rho_l - \rho_g\right)g\Delta h_{\mathrm{lg}}k_l^3}{\mu_l D_i \Phi_i}\right]^{1/3}, \quad (4)$$

where Φ_i is the heat flux related to the internal diameter.

The heat transfer coefficient given by (4) has to be intended as average HTC when referred to tube average heat flux, whereas represents a local value when the tube length is divided into different nodes and local heat flux for each node is accounted. In the same way, (2) gives a local HTC when the mean quality at half cell is considered in (3). All the computational details to calculate h_c and h_f can be anyway found in [13–15].

Schaffrath's model [17] was developed for the investigation of the operation mode of the SWR1000 emergency condenser (NOKO test facility). It is based on Tandon's flow regime map [18] for the determination of the actual flow regime and switches to flow regime semi-empirical correlations for the HTC calculation: Soliman for spray flow [19], Nusselt for laminar annular flow, Kosky and Staub for turbulent annular flow [20], Rufer and Kezios for stratified flow [21], Breber et al. for slug-plug flow [22]. The parameters chosen to identify the flow pattern are the dimensionless vapour velocity j_D^* and the volume ratio of liquid and gas in a cross-sectional area $(1-\alpha)/\alpha$.

3.2. Modelling of Condensation in a Vertical Tube. In a downflow vertical pipe condensation takes place with a condensate film growing up in contact with the wall, while vapour phase flows along the bulk of the channel. Many methods have been proposed for predicting the film condensation heat transfer coefficient; these range from empirical or semi-empirical correlations to highly sophisticated analytical treatments of the transport phenomena [23–25].

In this work the classical modelling approach, based on Nusselt's analysis [26] for film condensation on a vertical plate, is adapted to the inside of a vertical tube. Mass, momentum and energy equations for the condensate film are dealt according to the following assumptions [16]:

(i) Pure vapour and at saturation temperature is considered. With no temperature gradient in the steam, heat transfer can occur only by condensation at the interface.

(ii) Shear stress at the liquid-vapour interface is neglected.

(iii) Advection terms in the equations are assumed to be negligible. Heat transfer across the film occurs only by conduction. Liquid temperature distribution is thus linear, and this concern can be expressed as

$$Nu_l = \frac{h\delta}{k_l} = 1. \quad (5)$$

The distinction of film condensation into three different regimes has been provided, according to the different physical phenomena which can occur: laminar, laminar wavy and turbulent. Figure 11 is useful to understand the flow patterns induced inside the tube.

The analytical solution of the governing equations, passing through the calculation of condensate film thickness δ, allows treating laminar regime. Semi-empirical correlations are recommended for laminar wavy and turbulent regimes. The main parameter governing the process is the condensate velocity, expressed by its Reynolds number Re_l as follows:

$$\mathrm{Re}_l = \frac{4\Gamma_l}{\pi D_i \mu_l}, \quad (6)$$

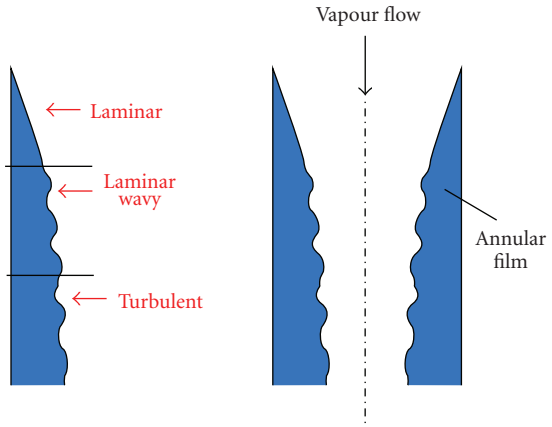

Figure 11: Sketch of film condensation inside a vertical tube.

where Γ_l is the liquid flowrate, to be expressed according to an only liquid approach:

$$\Gamma_l = \Gamma(1 - x). \tag{7}$$

(i) Laminar $\mathrm{Re}_l < 30$. Condensation HTCs decrease in the laminar region with increasing film thickness due to the increased thermal resistance. Nevertheless, laminar condensation occupies a very short portion of the tube and hence can be neglected in the calculations:

$$h = k_l \left(\frac{\nu_l^2}{g}\right)^{-1/3} 1.1\,\mathrm{Re}_l^{-1/3} \quad \text{Nusselt correlation.} \tag{8}$$

(ii) Laminar wavy $30 < \mathrm{Re}_l < \mathrm{Re}_{\mathrm{tr}} = 4658\,\mathrm{Pr}_l^{-1.05}$. Condensation HTCs (still a decreasing function of film thickness) are enhanced when the film becomes wavy, because waves promote turbulence in the film and increase heat exchange surface [27]. $\mathrm{Re}_{\mathrm{tr}}$ represents the transition value between laminar (wavy) and turbulent film condensation:

$$h = k_l \left(\frac{\nu_l^2}{g}\right)^{-1/3} 0.756\,\mathrm{Re}_l^{-0.22} \quad \text{Kutateladze correlation.} \tag{9}$$

(iii) Turbulent $\mathrm{Re}_l > \mathrm{Re}_{\mathrm{tr}} = 4658\mathrm{Pr}_l^{-1.05}$. The highest HTCs are provided once the film has become turbulent; the trend is now different from previous case (being the HTC an increasing function of film thickness), due to mixing effects which exceed the higher thermal resistance. Two different semi-empirical correlations can be applied [28, 29]:

$$h = k_l \left(\frac{\nu_l^2}{g}\right)^{-1/3} 0.023\,\mathrm{Re}_l^{0.25}\mathrm{Pr}_l^{0.5} \quad \text{Labuntsov correlation,} \tag{10}$$

$$h = k_l \left(\frac{\nu_l^2}{g}\right)^{-1/3} 0.00402\,\mathrm{Re}_l^{0.4}\mathrm{Pr}_l^{0.65} \quad \text{Chen correlation.} \tag{11}$$

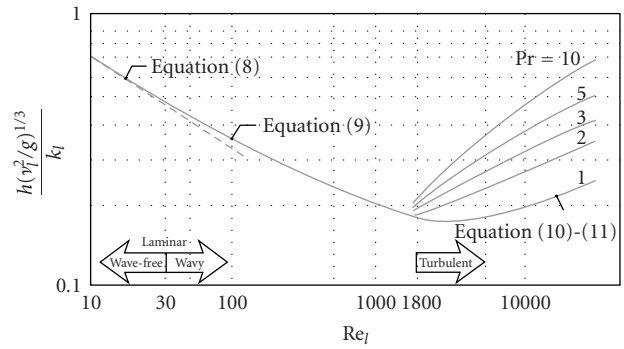

Figure 12: Nondimensional HTC dependence on condensate Reynolds number, for condensation on a vertical plate [16].

Figure 12 shows nondimensional heat transfer coefficient dependence on condensate Reynolds number Re_l, which increases in the downward direction inside the tube [16]. Above discussed HTC trends find their confirmation.

All the proposed correlations give a local HTC value. A general expression providing an average heat transfer coefficient is more useful especially in design applications. The easiest way to calculate average heat transfer coefficients is to integrate the equations for local coefficients along the tube length, resulting:

$$\bar{h}_L = \frac{1}{L}\int_0^L h(s)ds. \tag{12}$$

The following correlations can be considered in order to compute the mean HTC for the various flow regimes:

(i) *Nusselt* correlation for laminar zone, obtained analytically integrating (8) from $s = 0$ to $s = L$ [16]:

$$\bar{h}_{\mathrm{lam}} = k_l \left(\frac{\nu_l^2}{g}\right)^{-1/3} 1.47\,\mathrm{Re}_L^{-1/3}. \tag{13}$$

(ii) *Kutateladze* correlation for laminar wavy zone [27]:

$$\bar{h}_{\mathrm{lam\_wavy}} = k_l \left(\frac{\nu_l^2}{g}\right)^{-1/3} \frac{\mathrm{Re}_L}{1.08\,\mathrm{Re}_L^{1.22} - 5.2}. \tag{14}$$

(iii) *Labuntsov* correlation for turbulent zone [28]:

$$\bar{h}_{\mathrm{turb}} = k_l \left(\frac{\nu_l^2}{g}\right)^{-1/3} \frac{\mathrm{Re}_L}{8750 + 58\,\mathrm{Pr}_l^{-0.5}\left(\mathrm{Re}_L^{0.75} - 253\right)}. \tag{15}$$

(iv) *Blangetti* correlation for turbulent zone [30]:

$$\bar{h}_{\mathrm{turb}} = k_l \left(\frac{\nu_l^2}{g}\right)^{-1/3} \frac{\mathrm{Re}_L}{414.6\,\mathrm{Re}_L^{0.6}\,\mathrm{Pr}_l^{-0.65} - 5.182 - 33514\,\mathrm{Pr}_l^{-1.27}}. \tag{16}$$

(v) *Chen* correlation for the total film condensation (neglecting laminar and considering both laminar wavy and turbulent zones) [29]:

$$\bar{h} = k_l \left(\frac{\nu_l^2}{g}\right)^{-1/3} \left(\mathrm{Re}_L^{-0.44} + 5.82 \cdot 10^{-6}\mathrm{Re}_L^{0.8}\mathrm{Pr}_l^{1/3}\right)^{1/2}. \tag{17}$$

Usually the Shah correlation [31], which is an empirical correlation based on a wide range of experimental data, is mostly considered as the best correlation for the turbulent film condensation heat transfer both in horizontal, vertical and inclined pipes. It is based on a liquid only approach, referring the two-phase HTC to the single-phase coefficient computed with Dittus-Boelter correlation, assumed all the flowrate being liquid:

$$h = h_l\left[(1-x)^{0.8} + \frac{3.8x^{0.76}(1-x)^{0.04}}{p_r^{0.38}}\right] \quad \text{local HTC,} \quad (18)$$

$$\overline{h} = h_l(0.55 + 2.09p_r^{-0.38}) \quad \text{mean HTC.} \quad (19)$$

Nevertheless the validity of Shah correlation is questionable for high pressure and large diameter tube applications with water, as recently experimentally confirmed by Kim and No [32]. Moreover, this correlation predicts a decreasing HTC with a decreasing quality, exactly the opposite trend of film condensation theory. It is also questionable how the same correlation could be suitable for all the flow orientations, since the physical phenomena involved are rather different.

4. Short Review on Experimental Facilities

In the frame of advanced water reactors development, the construction of experimental facilities is required to study the behaviour of integral systems during postulated accidents as well as separate effect phenomena on specific innovative components. This section is dedicated to the brief discussion of the experimental works carried out to fully qualify in-pool condenser systems and validate the proper modelling tools for condensation analyses.

Suitable facilities, built and operated in the recent years, provided a large amount of data, based on which the heat transfer correlations (both for horizontal and vertical tube configurations) were validated. Best-estimate thermal-hydraulic code assessment on such data is then the final task in order to guarantee the availability of reliable computational tools to duly perform special components design and reactor safety analyses.

The NOKO test facility was constructed at the Forschungszentrum Jülich for the experimental investigation of the SWR1000 emergency condenser effectiveness [3]. The design of the facility, provided with an operating pressure of 10 MPa and an electrical heater with a maximum power of 4 MW, permits to adjust the same thermal-hydraulic conditions as in the real plant; moreover, prototypical elevations, water levels, dimensions and HX tubes material have been reproduced. A phenomenological evaluation was performed to determine the operation conditions of the emergency condenser. The HX capacity was determined as a function of primary pressure, pool pressure and water level, as well as of concentration of the non-condensables in the vessel. The experimental results showed that extracted thermal power increases with a primary side pressure increase and decreases with a pool side pressure increase. The emergency condenser characterization was accomplished calculating the tube surface available for condensation by means of the evaluation of geodetic pressure drops variation in consequence of vessel water level decrease. A single tube test, besides, was provided to clarify the condensation flow regimes inside a horizontal tube and to validate Tandon's flow map condensation model (reported in Figure 9). This experimental campaign led finally to the improvement of ATHLET thermal-hydraulic code [17], implementing the correlations discussed at the end of Section 3.1.

The long-term decay heat removal from the containment of advanced light water reactors, and in particular the long-term LOCA response of the Passive Containment Cooling System of the ESBWR, were tested in the large scale PANDA facility [33]. Constructed at the Paul Scherrer Institute (PSI) for the investigation of both overall dynamic response and key phenomena of passive containment systems, it consists briefly of six vertical cylindrical vessels, four water pools and a variety of connecting lines available to compose different facility configurations. The major aspect of the tests dealt with the evaluation of the ESBWR PCCS performance in case of main steam line break. Released steam flows into the drywell where it is mixed to the air contained inside; then the mixture is vented into the wetwell where the steam content is condensed and the air content is separated, inducing an increase in system pressure. When the heat exchangers in the pool start their operation, condensation of the steam-air mixture allows stopping pressure increase. Pressure time behaviour defines thus the response of the whole system to the specific transient. As far as condensation issues are concerned, PANDA facility was very useful for investigating the degradation of HTC (and then the influence on the effective condensing length) in presence of non-condensable gases [34], both heavier than steam, initially filling the containment compartments (nitrogen or air), and lighter than steam, released later in the course of the transient from the reactor core (hydrogen, simulated by helium). The provided tests permitted moreover to extend the database available for containment analysis code qualification.

The VISTA facility is the experimental facility developed by the KAERI to simulate the primary and secondary systems as well as the PRHRS of the SMART reactor [8]. The main objective of the study was to investigate the characteristics of natural circulation flows, passive system pressure drops and heat transfer performances of the PRHRS heat exchangers. The secondary objective was to confirm the capability of MARS best-estimate code to predict the overall thermal-hydraulic behaviour of the PRHRS. One of the most important results was that the code underestimated heat transfer at the heat exchanger, predicting fluid temperatures at HX bottom higher than the experimental results. The condensation model used in the code, exactly the same of that adopted by RELAP5 code [35], considers the maximum value between Nusselt correlation (8) for laminar flow and Shah correlation (18) for turbulent flow. The implementation in MARS and RELAP5 codes of suitable heat transfer correlations, as the ones proposed in this paper on the bases of film condensation theory, would guarantee a more accurate heat transfer package to duly carry out transient and safety analyses.

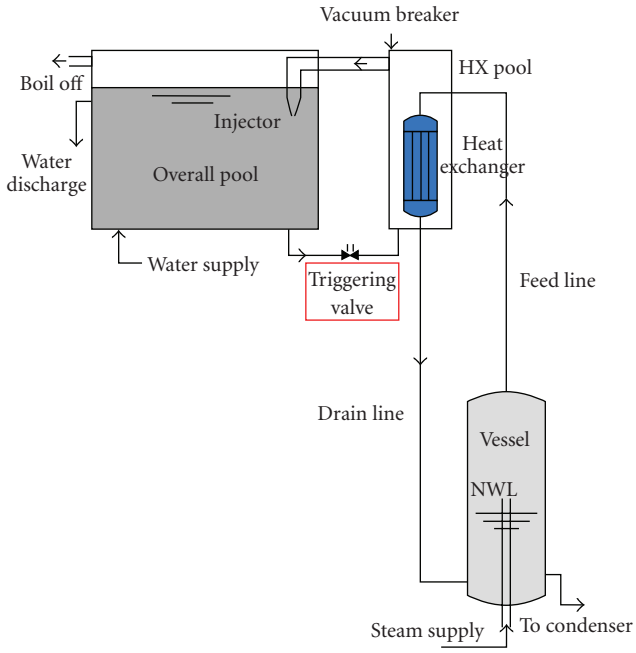

Figure 13: PERSEO facility scheme.

In spite of the common belief that passive systems should not require any operator actions, the actuation of such systems needs to be started by active valves, whose reliability is of fundamental importance. A new concept of a valve liquid side, instead of steam side in the primary system, located on a line connecting two pools at the bottom, has been proposed in the PERSEO facility [2] (Figure 13), developed in SIET labs (Piacenza) for testing a full scaled module for the GE-SBWR in-pool heat exchanger. The full scale module of the SBWR IC consists in two horizontal cylindrical headers and 120 vertical pipes; prototypical thermal-hydraulic conditions were respected, reproducing the removal to the pool of heat exchanger nominal power (20 MW_{th}) by means of the supply of saturated steam at 7 MPa from the nearby EDIPOWER power station. The new kind of actuation valve (named triggering valve) is closed during normal operations and the pool containing the heat exchanger (HX pool) is empty; the other pool (Overall pool) is full of cold water. Under emergency conditions the valve is opened and the heat exchanger is flooded, with consequent heat transfer from the primary side to the pool. The effectiveness of the actuation valve movement, from the high pressure primary side of the reactor to the low pressure pool side, was tested during the experimental campaign, both in steady and in unsteady conditions. Two kinds of tests were performed: integral tests and stability tests. The integral tests were aimed at demonstrating the behaviour and performance of the system following a request of operation and during all phases of a long accident transient. The stability tests, instead, were aimed at studying particular critical problems happening in case of sudden condensation at the steam water interface in the injector or in case of triggering valve re-opening, with cold water inlet in presence of steam in the HX pool. The experimental testing of the IC in-pool condenser concept provided moreover a useful database for condensation models validation. Within the postprocessing analysis on PERSEO project results [36], the finding of experimental data for condensation inside a vertical tube has been envisaged in order to validate the heat transfer correlations proposed in this paper.

Table 1: IC data, taken as reference for the calculations.

Parameter	*Choice*
Tube outer diameter	50.8 mm
Tube inner diameter	46.2 mm
Tube thickness	2.3 mm
Thermal conductivity	17.4 W/mK
Pressure	72.4 bar
Fouling	$5 \cdot 10^{-5} m^2K/W$
Plugging	5% of tubes
Thermal power	35 MW
Number of tubes	240 (2 units of IC)
Flowrate per tube	0.103 kg/s
Mass flux G	61.47 kg/sm^2

5. Calculation Results

Proposed condensation heat transfer models, both for application within horizontal and vertical tubes, have been firstly verified through the development of a simple Matlab code. The reference case was taken from set of PERSEO test data, being the primary aim to show with simple calculations (without the utilization of a best-estimate code) how a vertical tube configuration can guarantee the highest HTCs in condensation, as well as the best trend (i.e., increasing along tube abscissa). The step-by-step computational procedure followed in the calculations, in order to obtain condensation HTC trend along tube abscissa and the actual length required to accomplish design prescriptions, is described in the appendix.

Table 1 summarizes the data of SBWR IC mean tube design representing the basis for the analysis. The reference tube is thus a vertical tube, with an inner diameter of 46.2 mm and an outer diameter of 50.8 mm, submerged in a pool of boiling water at 100°C. Tube material is INCONEL 600 (17.4 W/mK of thermal conductivity), and fluid inlet conditions are represented by saturated steam at 72.4 bar. The utilization of this HX within the EHRS of IRIS reactor has been taken into account. Hence, following design prescriptions, two units of the condenser (with 120 tubes each one) have to exchange altogether a thermal power of 35 MW. Fouling effects, both for internal and external side, are quantified with an additional thermal resistance of $5 \cdot 10^{-5}$ m^{2}K/W, while a possible plugging of the 5% of the tubes is also considered. The resulting reference value of flowrate per tube is equal to 0.103 kg/s, which gives a mass flux G equal to 61.47 kg/sm^2.

Reference data for the calculations are related to a condenser with vertical tube arrangement. Nevertheless, they

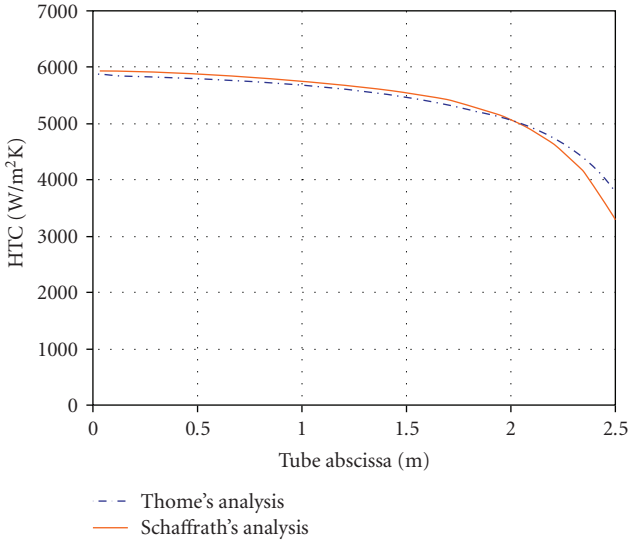

Figure 14: Comparison between Thome's analysis and Schaffrath's analysis in stratified flow (G = 61.5 kg/sm^2).

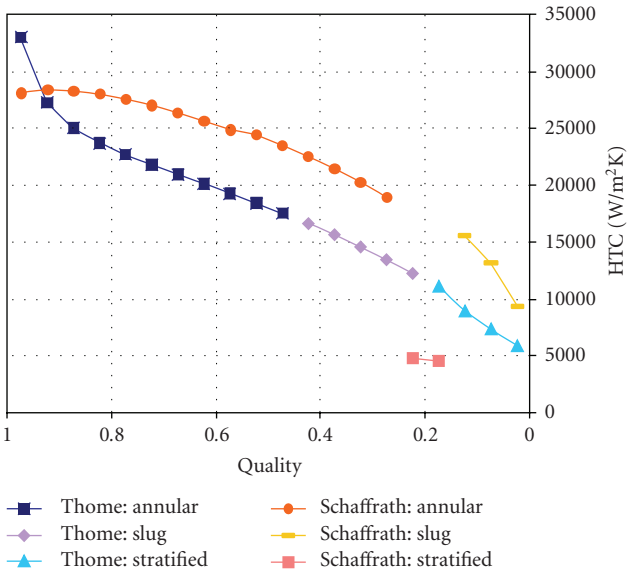

Figure 15: Comparison between Thome's analysis and Schaffrath's analysis with dominant annular flow (G = 417.6 kg/sm^2).

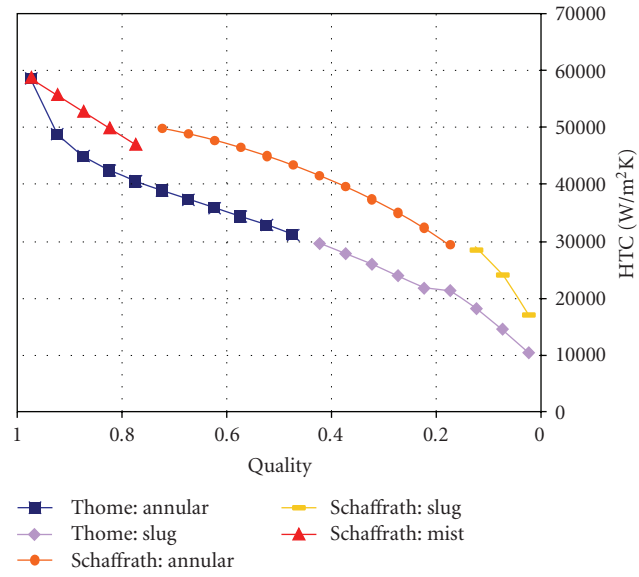

Figure 16: Comparison between Thome's analysis and Schaffrath's analysis at very high flowrates (G = 984.8 kg/sm^2).

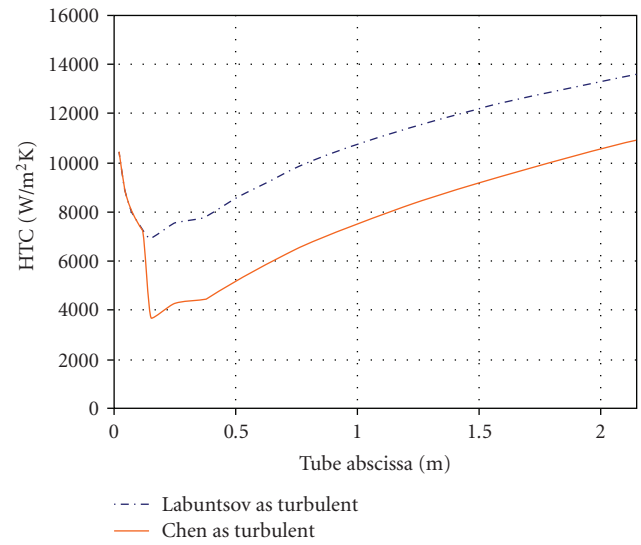

Figure 17: Condensation HTC along tube abscissa, according to film condensation theory (G = 61.5 kg/sm^2).

have been applied also to test the models for horizontal in-tube condensation and provide thus a proper comparison with the vertical tube arrangement results. In case of condensation within a horizontal tube, reference value of mass flux leads to a stratified pattern. Heat transfer coefficient trend along the pipe has been predicted, applying first Thome's analysis and then Schaffrath's model, selected the proper correlation (Rufer and Kezios formula). The tube length required to completely condense the inlet steam (with saturated liquid at condenser outlet) is evaluated as 2.50 m. A pretty fair agreement can be observed between the two distinct models, as shown in Figure 14: an average heat transfer coefficient of approximately 5500 W/m^{2}K involves almost the entire length, decreasing just at the end. When condensate starts to occupy the major portion of cross-sectional area, in fact, the condensate sump dominates any type of film condensation at the top of the tube. The higher thermal resistance causes the lower heat transfer coefficient. Moreover, the possibility of a slug-plug flow (at low qualities, with $x < 0.1$) is envisaged by Schaffrath's analysis. Condensation in a horizontal tube proves thus to be a complex phenomenon, considered the risk of instabilities which could derive from the intermittent flow regimes.

Thome's and Schaffrath's models have been tested even under high flowrate conditions, establishing flow regimes different from stratified pattern. Two distinct values of

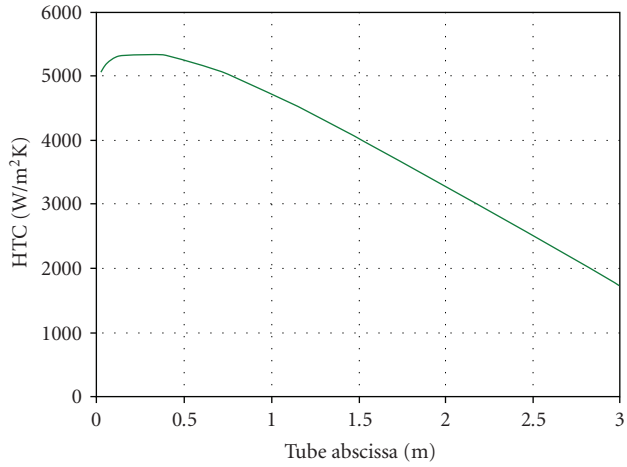

Figure 18: Condensation HTC along tube abscissa, according to Shah correlation (G = 61.5 kg/sm^2).

inlet flowrate have been considered: 0.7 kg/s, which gives a dominant annular flow, and 1.5 kg/s, which induces a mist flow at tube entrance. Respective results are reported in Figures 15 and 16. It is evident that heat transfer coefficient increases with flowrate (for turbulence development). Such trend is confirmed in similar ways by the two models. Tandon's map provides for annular flow ($\Gamma = 0.7$ kg/s) a HTC value slightly higher and less variable along the tube. Thome's analysis, finally, is not capable of treating separately the spray flow; nevertheless, the results obtained when dealing with annular flow at $\Gamma = 1.5$ kg/s are rather similar to HTC values given by Soliman correlation, the one selected in Tandon's map for the mist regime.

The same calculational model has been then applied implementing the vertical tube correlations. Predicted tube length is equal to 2.17 m according to film condensation correlations, and to 3.04 m for Shah correlation. The first model is certainly more accurate, being based on physical principles; hence, it is evident that for the IC conditions of pressure, flowrate and tube diameter (globally representative of the typical working conditions for an in-pool immersed HX within DHR applications), Shah's model broadly underpredicts the condensation HTC. Moreover, an opposite trend of turbulent heat transfer coefficient with a quality decrease is confirmed between the two models (increasing for film condensation, but decreasing for Shah's model). The comparison is provided by the graphs reported in Figures 17 and 18. As far as film condensation is concerned, laminar zone is absolutely negligible, and laminar wavy zone (with its decreasing trend of HTC with tube abscissa) is noticed up to a quality value of 0.95. As regards turbulent zone, both Labuntsov and Chen correlations have been implemented. The latter gives lower HTCs, proving to be more conservative (and hence it has been used in sizing calculations). Chen correlation for mean HTC along the tube predicts a value of approximately 8000 W/m^{2}K. When comparing these outcomes (except for the ones obtained with Shah correlation, whose validity is however highly questionable) with the predictions of horizontal tube models, it is evident that the vertical tube is in position to assure better performances, first just resulting in higher heat transfer coefficients. A direct consequence of this concern is the increased length required by horizontal tubes to completely condense the inlet steam (i.e., 2.50 m compared to 2.17 m of the vertical configuration). At the end, it is noted that Shah correlation prescriptions limit its validity to 40 mm of inner diameter, below the inner diameter of the IC tube under examination. The extrapolation of Shah correlation outside the range of the covered parameters appears a sufficient explanation for the wrong HTCs predicted.

6. Experimental Findings from Perseo Facility

Experimental findings useful for validating the vertical tube condensation model proposed in this paper represent one important result of PERSEO facility campaign. Thanks to the collaboration between POLIMI and SIET, such experimental findings have been analyzed, focusing the interest on condenser inner side performance. Main results are discussed in this section.

Some IC tubes were monitored with wall thermocouples (K-type, nominal accuracy of $\pm 1.5^\circ$C), applied on the outer surface at three different axial positions: at the top, at the middle and at the bottom of tubes. Circuit pressure (equal to 7 MPa) was measured with a pressure transmitter installed inside HX upper header, whereas primary flowrate (on average 0.1 kg/s per tube) was measured by an orifice differential pressure transmitter (with an uncertainty of $\pm 0.25\%$ of the instrument full scale). Due to the lack of accuracy of fluid thermocouples, saturated steam has been considered at condenser inlet and saturated liquid at condenser outlet. This assumption permitted to calculate the exchanged thermal power, and then to obtain the local heat flux required for heat transfer coefficients computation. Saturation temperature at the circuit pressure has been adopted as fluid bulk temperature, while inner wall temperature has been calculated from tube external value (measured) adding the thermal jump in the metal, resulting

$$T_{w,i} = T_{w,e} + \frac{D_i \ln(D_e/D_i)}{2k_{\text{tube}}} \Phi_i. \tag{20}$$

For each thermocouple position the local heat flux value Φ and the local HTC h_{cond} have been obtained by solving the following system of two equations, where $T_{w,i}$ must be calculated according to (20):

$$U_i = \frac{\Phi}{T_{\text{sat},i} - T_{\text{sat},e}} = \left(\frac{1}{h_{\text{cond}}} + \frac{D_i \ln(D_e/D_i)}{2k_{\text{tube}}} + \frac{1}{h_{\text{pool}}(D_e/D_i)} \right)^{-1}, \tag{21}$$

$$h_{\text{cond}} = \frac{\Phi}{T_{\text{sat},i} - T_{w,i}}.$$

The sketch of the accounted situation is depicted in Figure 19. The obtained results are presented in Figure 20,

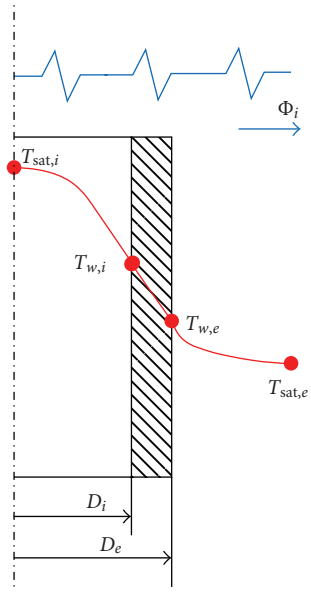

Figure 19: Sketch of heat transfer and temperature distribution in a single tube.

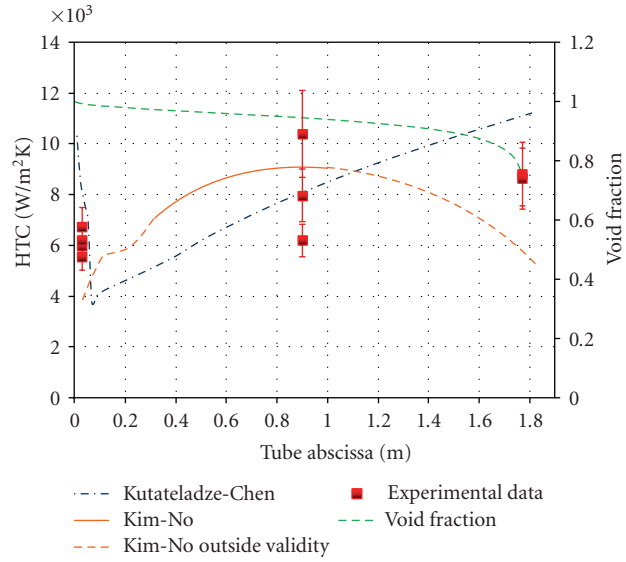

Figure 20: PERSEO facility experimental data compared with film condensation theory and Kim's model [32] predictions.

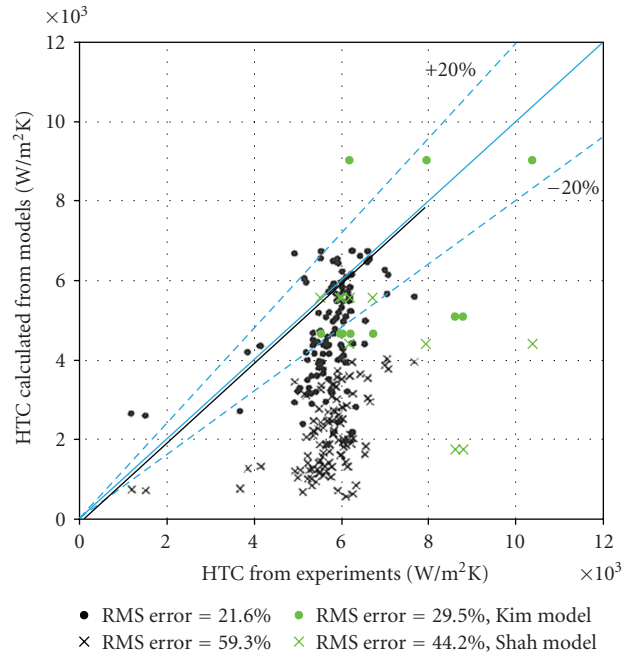

Figure 21: Comparison between PERSEO facility data (green) and Kim's data (black).

where they are compared to the predictions of film condensation theory (in particular, Kutateladze correlation for laminar wavy zone and Chen correlation for turbulent zone) and of a semi-empirical model proposed by Kim and No [32]. The increasing HTC trend and the good accordance with the experimental values confirm the validity of the proposed correlations, confuting therefore the Shah correlation under these particular thermal-hydraulic conditions (i.e. condensation of water steam at high pressure in large diameter vertical tubes). Among the works available in literature questioning about the validity of Shah's model, the experimental work of Kim and No has been selected since the investigated test section consists in a tube with the same geometrical features of the SBWR IC tested in PERSEO facility (i.e., outer diameter of 50.8 mm, thickness of 2.3 mm and length of 1.8 m). The semi-empirical model validated on Kim's data is a turbulent film condensation model based on the similarity between the single-phase turbulent convective heat transfer and the annular film condensation heat transfer. For any computational detail, refer to [32].

Figure 20 shows a remarkable shifting between theory and experimental data only at the end of the tube, where the liquid film at the wall cannot be considered any more as thin. This is proved by the void fraction damping down at the bottom of the pipe, which questions the validity of the presented theory. Figure 21 presents the comparison of PERSEO data with Kim's data; both Kim's model and Shah correlation (18) have been considered in order to predict the experimental values. HTCs calculated from PERSEO data are rather higher than HTCs calculated from Kim's data; the higher condensate Reynolds numbers reached in PERSEO facility are a plausible explanation of this concern. The order of magnitude is however well captured. Moreover, both the databases confirm that Shah's model is not accurate when dealing with condensation phenomena at high pressure, whereas the semi-empirical model validated on Kim's data gives more satisfactory results.

At the end, the film condensation model based on Kutateladze correlation (9) and Chen correlation (11) has been considered to predict PERSEO data. The results, distinguishing between the predictions at the top, at the middle and at the bottom of tubes, are reported in Figure 22. The set of correlations proposed in this paper offers the best agreement with PERSEO data, whereas the turbulent annular

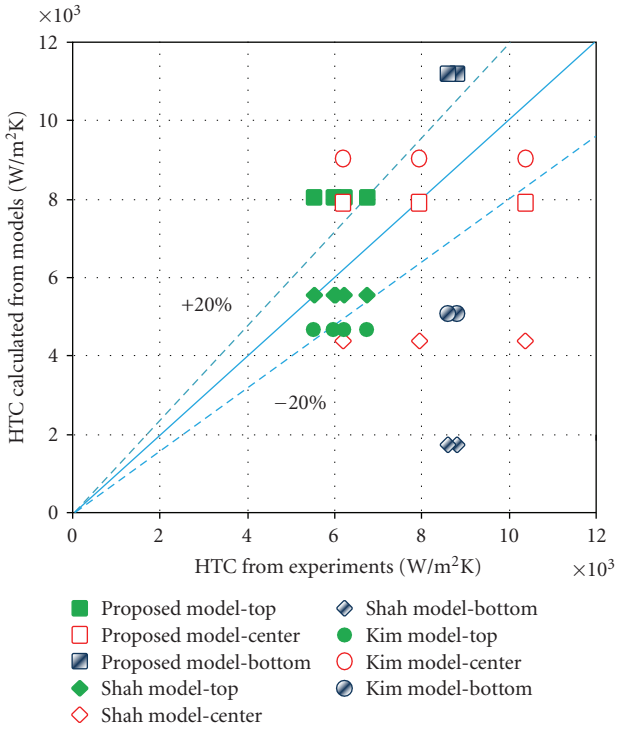

FIGURE 22: Benchmark evaluation of PERSEO data according to the various condensation models.

condensation model proposed by Kim fails at low qualities (when condensate Reynolds number becomes too high at the end of the tube). Except for tube inlet (high qualities), Shah's model broadly underestimates the condensation HTC.

7. Conclusions

In the frame of the study on innovative passive safety systems and components, which require the proper modelling tools for the analysis of the heat transfer phenomena involved, an accurate review on the concept of in-pool condenser for DHR applications has been the main purpose of the work. Primary objective has been to provide a literature review of the most updated and reliable heat transfer models for condensation both in horizontal and in vertical tube condensers, which are the two most used configurations. The conditions at which condensation has been considered in the paper are such that are typical of passive safety systems for decay heat removal.

An overview on the concept of in-pool condenser within a DHR passive safety system has been firstly carried out. A preponderance of vertical tube arrangement solution has been pointed out for applications to GenIII+ nuclear reactors. The main advantages offered by a downflow vertical configuration are

(i) higher heat transfer coefficients (even doubled with respect to horizontal solution),

(ii) more predictable in-tube flow distribution.

Two calculational models have been presented as far as horizontal in-tube condensation is concerned. The first model is based on Thome's work, distinguishes between three different flow regimes (annular, stratified and stratified wavy) and takes into account two heat transfer mechanisms: convective condensation and film condensation. The second model is based on Tandon's map, as proposed by Schaffrath. Condensation within a vertical tube has been addressed according to a physical principle analysis, relied on film condensation theory for a vertical plate. In this paper the classical modelling approach based on the Nusselt's theory for laminar film condensation has been presented. Suitable semi-empirical correlations have been proposed for laminar wavy regime (Kutateladze correlation) and for turbulent regime (Chen correlation).

In order to prove the better thermal-hydraulic performance of a vertical tube condenser, a comparison between all the models has been provided through a simple Matlab code, taking as reference the SBWR IC mean tube data and considering the utilization of this condenser within the IRIS EHRS. A stratified flow is induced in case of horizontal tube, giving a pretty constant value of HTC (about 5500 W/m^{2}K), except for tube end ($x < 0.1$) where condensate sump effects become dominant. The possibility of a slug-plug flow at low qualities is envisaged by Schaffrath's analysis, making the condensation process in a horizontal tube a rather complex phenomenon, considered the risk of instabilities which could derive from intermittent flow regimes. Vertical tube film condensation theory, applied to the same set of data, shows that laminar wavy film condensation occurs only at tube entrance (up to a quality value of 0.95). The main process is governed by turbulent film condensation, which gives the dominant increasing trend of HTC with tube abscissa. Chen correlation predicts a mean HTC value of about 8000 W/m^{2}K, rather higher when compared to the mean value of horizontal in-tube condensation.

Amongst the advanced LWR reactors adopting a vertical tube in-pool condenser for DHR applications, IRIS reactor is still in a conceptual design and pre-application phase. The better thermal-hydraulic behaviour of the vertical tube solution, stressed in the paper, can be intended as a scientific validation of the provided design choices.

Second goal of the work has been to validate the film condensation model for vertical tubes by means of experimental findings from PERSEO facility. Experimental HTC trend along tube abscissa has been reproduced for the SBWR IC tubes provided with wall thermocouples. The obtained results, in good agreement with the experimental work of Kim and No available in open literature, show an increasing HTC trend with tube abscissa, validating the proposed correlations and definitely confuting the Shah correlation under the particular conditions investigated.

As well as the commonly adopted Nusselt correlation for laminar film condensation, the two semi-empirical relationships proposed for laminar wavy regime (Kutateladze correlation) and turbulent regime (Chen correlation) appear preferable than any completely empirical relationship, as Shah correlation. This concern should be properly accounted when dealing with condensation phenomena, for example,

when a transient event on a nuclear reactor is simulated with a best-estimate thermal-hydraulic code. The implementation of the recommended heat transfer model is thus required for system codes like RELAP5, in which turbulent condensation is still dealt according to Shah correlation.

Appendix

This section describes how to apply the correlations presented for HTC evaluation dealing with condensation in a horizontal tube (Section 3.1) and in a vertical tube (Section 3.2), to predict condenser tube length required to accomplish the complete condensation of inlet steam.

Computational procedure, based on a subdivision of the pipe in many cells, is step-by-step shown in the followings.

Step 1. From the known thermal power to be exchanged and the chosen number of discretization intervals, evaluate the thermal power exchanged per cell W_{cell}:

$$W_{\text{cell}} = \frac{W}{N_{\text{cell}}}. \tag{A.1}$$

Step 2. Calculate internal side (condensation) heat transfer coefficient h_{cond}, using one of the models/correlations proposed in the paper.

Step 3. Calculate external side (pool boiling) heat transfer coefficient h_{pool}, using one of the available correlations for a single tube submerged in a boiling pool, as the correlation due to Borishanski-Mostinsky [37], specifically valid for water:

$$h_{\text{pool}} = 0.10111\, p_{\text{cr}}^{0.69}\left(1.8\, p_r^{0.17} + 4\, p_r^{1.2} + 10\, p_r^{10}\right)\Phi^{0.7}. \tag{A.2}$$

Step 4. Heat exchange process requires to be dealt considering every thermal resistance involved, representative respectively of internal side, tube metal side, external side, as well as fouling effects (both internal and external). Once each of these terms is known, calculate overall heat transfer coefficient as follows (internal surface is chosen as reference):

$$U_i = \left[\frac{1}{h_{\text{cond}}} + R_{f,i} + \frac{D_i \ln(D_e/D_i)}{2k_{\text{tube}}} + \frac{R_{f,e}}{D_e/D_i} + \frac{1}{h_{\text{pool}}(D_e/D_i)}\right]^{-1} \tag{A.3}$$

Step 5. Evaluate heat transfer surface for each cell S_i:

$$S_i = \frac{W_{\text{cell}}}{U_i\left(T_{\text{sat},i} - T_{\text{sat},e}\right)}. \tag{A.4}$$

Step 6. Compute the length of each cell, and, by adding the differential lengths L', compute tube total length L:

$$L' = \frac{S_i}{\pi D_i}, \qquad L = \sum L'. \tag{A.5}$$

Step 7. Evaluate local heat flux for each cell Φ':

$$\Phi' = \frac{W_{\text{cell}}}{\pi D_i L'}. \tag{A.6}$$

Step 8. Because of the dependence of pool boiling HTC on heat flux Φ, according to (A.2), an iterative procedure is required. The heat flux value obtained in Step 7 has to be considered for pool boiling HTC calculation in Step 3. Iterate from Step 3 to Step 7 until a check error on the resulting heat flux becomes smaller than a fixed value.

Acronyms

DHR:	Decay Heat Removal
ECT:	Emergency Cooldown Tank
EHRS:	Emergency Heat Removal System
ESBWR:	European Simplified Boiling Water Reactor
GDCS:	Gravity Driven Cooling System
HTC:	Heat Transfer Coefficient
HX:	Heat eXchanger
IC:	Isolation Condenser
IRIS:	International Reactor Innovative and Secure
LOCA:	Loss Of Coolant Accident
KAERI:	Korea Atomic Energy Research Institute
KNGR:	Korea Next Generation Reactor
LWR:	Light Water Reactor
NOKO:	NOtKOndensator (emergency condenser)
NPP:	Nuclear Power Plant
PANDA:	PAssive Nachwärmeabfuhr- und DruckAbbau- testanlange (passive decay heat removal and depressurization test facility)
PCCS:	Passive Containment Cooling System
PERSEO:	in-Pool Energy Removal System for Emergency Operation
POLIMI:	POLItecnico di Milano (Polytechnic of Milan)
PRHRS:	Passive Residual Heat Removal System
PSI:	Paul Scherrer Institute
RPV:	Reactor Pressure Vessel
SBWR:	Simplified Boiling Water Reactor
SIET:	Società Informazioni Esperienze Termoidrauliche (company for information on thermal-hydraulic experimentation)
SMART:	System integrated Modular Advanced ReacTor
SWR1000:	Siede Wasser Reaktor–1000 MW_e (boiling water reactor – 1000 MW_e)
VISTA:	experimental Verification by Integral Simulation of Transient and Accidents

Nomenclature and Symbols

D: Tube diameter (m)
f_i: Interfacial roughness factor
G: Mass flux (kg/(m^{2}s))

g: Acceleration of gravity (m/s^2)
h: Condensation heat transfer coefficient (W/(m^{2}K))
h_c: Convective condensation heat transfer coefficient (W/(m^{2}K))
h_f: Film condensation heat transfer coefficient (W/(m^{2}K))
h_l: Single-phase heat transfer coefficient (from Dittus-Boelter correlation) (W/(m^{2}K))
j_D^*: Dimensionless vapour velocity
k: Thermal conductivity (W/(mK))
L: Tube length (m)
N_{cell}: Number of tube discretization intervals
Nu_l: Condensate Nusselt number
p_{cr}: Critical pressure (bar)
p_r: Reduced pressure (p/p_{cr})
Pr_l: Condensate Prandtl number
R_f: Fouling thermal resistance (m^{2}K/W)
Re_l: Local condensate Reynolds number
Re_L: Condensate Reynolds number evaluated at the end of the considered regime
S: Heat transfer surface (m^2)
T: Temperature (K)
U: Overall heat transfer coefficient (W/(m^{2}K))
W: Exchanged thermal power (W)
x: Thermodynamic equilibrium quality
α: void fraction
Δh_{lg}: Latent heat of vaporization (J/kg)
δ: Film thickness of annular ring (horizontal tube) (m)
Film thickness of condensate at the wall (vertical tube) (m)
Φ: Heat flux (W/m^2)
Γ: Mass flowrate (kg/s)
Γ_l: Condensate mass flowrate (kg/s)
μ_l: Liquid dynamic viscosity (Pa s)
ν_l: Liquid kinematic viscosity (m^2/s)
θ: Falling film stratification angle
ρ: Density (kg/m^3).

Subscripts

cell: Discretization interval
cond: Condensation
e: External
g: Saturated steam
i: Internal
l: Saturated liquid
lam: Laminar regime
lam_wavy: Laminar wavy regime
pool: pool boiling
sat: Saturation
tube: Tube metal
turb: Turbulent regime
w: wall.

Aknowledgments

The authors wish to thank Fosco Bianchi (ENEA) for providing the experimental data from an integral test carried out during PERSEO project, and Roberta Ferri (SIET labs) for the deep and pleasant explanations on the facility behaviour. The authors are also grateful to the anonymous reviewers whose remarks have allowed significantly improving the paper organization and readability.

References

[1] IAEA-TECDOC-626, "Safety related terms for advanced nuclear plants," September 1991.
[2] R. Ferri, A. Achilli, G. Cattadori, F. Bianchi, and P. Meloni, "Design, experiments and Relap5 code calculations for the perseo facility," *Nuclear Engineering and Design*, vol. 235, no. 10-12, pp. 1201–1214, 2005.
[3] A. Schaffrath, E. F. Hicken, H. Jaegers, and H.-M. Prasser, "Operation conditions of the emergency condenser of the SWR1000," *Nuclear Engineering and Design*, vol. 188, no. 3, pp. 303–318, 1999.
[4] T. Sato and Y. Kojima, "Variations of a passive safety containment for a BWR with active and passive safety systems," *Nuclear Engineering and Design*, vol. 237, no. 1, pp. 74–86, 2007.
[5] H. J. Kahn and U. S. Rohatgi, "Performance characterization of isolation condenser of SBWR," Tech. Rep. BNL-NUREG-47960, 1992.
[6] S. J. Cho, B. S. Kim, M. G. Kang, and H. G. Kim, "The development of passive design features for the Korean Next Generation Reactor," *Nuclear Engineering and Design*, vol. 201, no. 2, pp. 259–271, 2000.
[7] M. D. Carelli, L. E. Conway, L. Oriani, et al., "The design and safety features of the IRIS reactor," *Nuclear Engineering and Design*, vol. 230, no. 1-3, pp. 151–167, 2004.
[8] Y.-J. Chung, H.-C. Kim, B.-D. Chung, M.-K. Chung, and S.-Q. Zee, "Two phase natural circulation and the heat transfer in the passive residual heat removal system of an integral type reactor," *Annals of Nuclear Energy*, vol. 33, no. 3, pp. 262–270, 2006.
[9] H. Jaster and P. G. Kosky, "Condensation heat transfer in a mixed flow regime," *International Journal of Heat and Mass Transfer*, vol. 19, no. 1, pp. 95–99, 1976.
[10] W. W. Akers, H. A. Deans, and O. K. Crosser, "Condensing heat transfer within horizontal tubes," *Chemical Engineering Progress Symposium Series*, vol. 55, pp. 171–176, 1959.
[11] A. Cavallini and R. Zecchin, "High velocity condensation of organic refrigerants inside tubes," in *Proceedings of the 13th International Congress of Refrigeration*, vol. 2, pp. 193–200, Washington, DC, USA, August-September 1971.
[12] M. K. Dobson and J. C. Chato, "Condensation in smooth horizontal tubes," *Journal of Heat Transfer*, vol. 120, no. 1, pp. 193–213, 1998.
[13] J. El Hajal, J. R. Thome, and A. Cavallini, "Condensation in horizontal tubes—part 1: two-phase flow pattern map," *International Journal of Heat and Mass Transfer*, vol. 46, no. 18, pp. 3349–3363, 2003.
[14] J. R. Thome, J. El Hajal, and A. Cavallini, "Condensation in horizontal tubes—part 2: new heat transfer model based on flow regimes," *International Journal of Heat and Mass Transfer*, vol. 46, no. 18, pp. 3365–3387, 2003.

[15] J. R. Thome, "Condensation in plain horizontal tubes: recent advances in modelling of heat transfer to pure fluids and mixtures," *Journal of the Brazilian Society of Mechanical Sciences and Engineering*, vol. 27, no. 1, pp. 23–30, 2005.

[16] F. P. Incropera, D. P. Dewitt, T. L. Bergman, and A. S. Lavine, *Fundamentals of Heat and Mass Transfer*, John Wiley & Sons, New York, NY, USA, 2007.

[17] A. Schaffrath, A.-K. Krüssenberg, A. Fjodorow, U. Gocht, and W. Lischke, "Modeling of condensation in horizontal tubes," *Nuclear Engineering and Design*, vol. 204, no. 1-3, pp. 251–265, 2001.

[18] T. N. Tandon, H. K. Varma, and C. P. Gupta, "A new flow regimes map for condensation inside horizontal tubes," *Journal of Heat Transfer*, vol. 104, no. 4, pp. 763–768, 1982.

[19] H. M. Soliman, "The mist-annular transition during condensation and its influence on the heat transfer mechanism," *International Journal of Multiphase Flow*, vol. 12, no. 2, pp. 277–288, 1986.

[20] P. G. Kosky and W. F. Staub, "Local condensing heat transfer coefficients in the annular flow regime," *AIChE Journal*, vol. 17, no. 5, pp. 1037–1043, 1971.

[21] C. E. Rufer and S. P. Kezios, "Analysis of two-phase, one-component stratified flow with condensation," *Journal of Heat Transfer*, vol. 88, pp. 265–275, 1966.

[22] G. Breber, J. W. Palen, and J. Taborek, "Prediction of horizontal tubeside condensation of pure components using flow regime criteria," *Journal of Heat Transfer*, vol. 102, no. 3, pp. 471–476, 1980.

[23] L. E. Herranz, J. L. Muñoz-Cobo, and G. Verdú, "Heat transfer modeling in the vertical tubes of the passive containment cooling system of the simplified boiling water reactor," *Nuclear Engineering and Design*, vol. 178, no. 1, pp. 29–44, 1997.

[24] S. Z. Kuhn, V. E. Schrock, and P. F. Peterson, "An investigation of condensation from steam-gas mixtures flowing downward inside a vertical tube," *Nuclear Engineering and Design*, vol. 177, no. 1–3, pp. 53–69, 1997.

[25] H. C. No and H. S. Park, "Non-iterative condensation modeling for steam condensation with non-condensable gas in a vertical tube," *International Journal of Heat and Mass Transfer*, vol. 45, no. 4, pp. 845–854, 2001.

[26] W. Nusselt, "The surface condensation of water vapour," *Zeitschrift des Vereins Deutscher Ingenieure*, vol. 60, pp. 541–546, 569–575, 1916.

[27] S. S. Kutateladze, *Fundamentals of Heat Transfer*, Academic Press, New York, NY, USA, 1963.

[28] D. A. Labuntsov, "Heat transfer in film condensation of pure steam on vertical surfaces and horizontal tubes," *Teploenergetika*, vol. 4, no. 7, pp. 72–79, 1957.

[29] S. L. Chen, F. M. Gerner, and C. L. Tien, "General film condensation correlations," *Experimental Heat Transfer*, vol. 1, no. 2, pp. 93–107, 1987.

[30] J. M. McNaught and D. Butterworth, "Film condensation of pure vapours," in *Heat Exchanger Design Handbook 2002*, vol. 2, Begell House, London, UK, 2002.

[31] M. M. Shah, "A general correlation for heat transfer during film condensation inside pipes," *International Journal of Heat and Mass Transfer*, vol. 22, no. 4, pp. 547–556, 1979.

[32] S. J. Kim and H. C. No, "Turbulent film condensation of high pressure steam in a vertical tube," *International Journal of Heat and Mass Transfer*, vol. 43, no. 21, pp. 4031–4042, 2000.

[33] N. Aksan, "Overview on PANDA test facility and ISP-42 PANDA tests data base," in *Natural Circulation in Water Cooled Power Plants, IAEA-TECDOC-1474,* November 2005.

[34] T. Bandurski, M. Huggenberger, J. Dreier, et al., "Influence of the distribution of noncondensibles on passive containment condenser performance in PANDA," *Nuclear Engineering and Design*, vol. 204, no. 1–3, pp. 285–298, 2001.

[35] RELAP5/MOD3.3 Code, "Manual Volume IV: Models and Correlations," *NUREG/CR-5525 Rev 1*, 2001.

[36] R. Ferri, A. Achilli, and S. Gandolfi, "PERSEO PROJECT: experimental data report," Tech. Rep. SIET 01 014 RP 02 Rev 1, 2003.

[37] J. W. Palen, "Shell and tube reboilers," in *Heat Exchanger Design Handbook 2002*, vol. 3, Begell House, London, UK, 2002.

Hindawi Publishing Corporation
Science and Technology of Nuclear Installations
Volume 2010, Article ID 797193, 12 pages
doi:10.1155/2010/797193

Research Article

RELAP5/MOD3.3 Best Estimate Analyses for Human Reliability Analysis

Andrej Prošek and Borut Mavko

Reactor Engineering Division, Jožef Stefan Institute, Jamova cesta 39, 1000 Ljubljana, Slovenia

Correspondence should be addressed to Andrej Prošek, andrej.prosek@ijs.si

Received 29 April 2009; Accepted 11 September 2009

Academic Editor: Nikola Čavlina

To estimate the success criteria time windows of operator actions the conservative approach was used in the conventional probabilistic safety assessment (PSA). The current PSA standard recommends the use of best-estimate codes. The purpose of the study was to estimate the operator action success criteria time windows in scenarios in which the human actions are supplement to safety systems actuations, needed for updated human reliability analysis (HRA). For calculations the RELAP5/MOD3.3 best estimate thermal-hydraulic computer code and the qualified RELAP5 input model representing a two-loop pressurized water reactor, Westinghouse type, were used. The results of deterministic safety analysis were examined what is the latest time to perform the operator action and still satisfy the safety criteria. The results showed that uncertainty analysis of realistic calculation in general is not needed for human reliability analysis when additional time is available and/or the event is not significant contributor to the risk.

1. Introduction

The experience accumulated in the last few decades has shown that human factors play a significant role in the risk of system failures and accidents, throughout the life cycle of a system. This explains significant focus on human reliability analysis (HRA) and on its full integration within systematic risk analysis and reliability assessment procedures [1]. A major problem in meeting this growing importance of HRA is the lack of empirical plant specific data needed for assessment of human reliability. In general, there are several information requirements for HRA, including the available time for diagnosis and correct execution of a tasks, steps, and actions (i.e., time window for action) [2]. This information comes from the deterministic analysis.

The time window for human action actually represents the success criteria for the action. It represents the time interval in which operators have to perform the action in order that the plant is put in a safer state, that is, the plant is put into a scenario that leads to a safe state and not to an accident state.

To estimate the time windows for operator actions the results of fast running severe accident code such as the MAAP code have been used in the conventional probabilistic safety assessment (PSA). However, information from these is often too conservative to perform a realistic PSA for a risk-informed application [3]. In the last years a few comparative studies were performed to justify the use of MAAP4 for the PSA Level 1 analysis of advanced reactors [4, 5]. In the comparison between MAAP4.07 and S-RELAP5 for U.S. EPR reactor [4] MAAP4 has demonstrated that it is a rather good simulator of nuclear plant transient trends. However, MAAP4's prediction of clad temperature magnitude is not sufficiently accurate to accept without compensation. For example, shortly after steam generator dryout the MAAP4 predicted much larger core heatup than S-RELAP5. Also, there are certain nuclear plant scenarios for which MAAP4 is clearly not applicable, such as early transient of large-break LOCA (at break sizes beyond the area of the largest attached pipe). In the study for APR1400 (Advanced Power Reactor) [5] comparison between MAAP4.03 and RELAP5/MOD3.2.2 was done for large break loss-of-coolant accident (LOCA). It was concluded that for a more mechanistic simulation of the initial stage of the LOCA using MAAP4.03, more detailed calculations of the primary system are required. Namely, for the break flow and the emergency core cooling flow rates,

MAAP4.03 predicted considerably higher values in the initial stage than RELAP5/MOD3.2.2. As a consequence, the two codes predicted different sequences for essentially the same initiating condition.

To reduce the undue conservatism, the use of best-estimate thermal hydraulic code has become an essential issue in the latest PSA. An example is the use of MARS code for small break LOCA calculations of Korea standard nuclear power plant [3] and the use of RELAP5/MOD3.2 code for LOCA calculations of RBMK-1500 [6]. Also the PSA standard [7] recommends the use of best-estimate code to improve the quality of a PSA. Severe accident codes are needed for simulation of phases with core damage [8].

Therefore for updated human reliability analysis the RELAP5/MOD3.3 best-estimate computer code [9] was used. The specified time windows are important for HRA to determine the likelihood of operator actions. The human error probability of certain action is lower if operators have more time available. In the control room of a nuclear power plant there is a team of operators, which is supervised by a shift supervisor. If operators, for example, have 10 or more minutes of additional time for action, it can be expected that colleagues or shift supervisor can observe and correct a possible error of their colleague [10]. Consideration of recovery causes lower human error probability and may cause a different impact of human error to the overall probabilistic safety assessment results. The actual times needed for performing the action were assessed based on real simulator scenarios [11], while the time windows determination is the aim of this study. Calculations were performed for the scenarios in which human actions are supplement to safety systems actuations by establishing auxiliary feedwater in case of small or medium loss of coolant accident (LOCA), establishing auxiliary feedwater in case of transients, and manual actuation of safety injection (SI) signal at LOCA. For calculations the qualified RELAP5 input model representing a two-loop pressurized water reactor, Westinghouse type, was used [12].

2. Deterministic Analysis Methodology Description

The realistic code calculations were performed by RELAP5/MOD3.3 Patch 03 thermal hydraulic computer code [9]. The parameters selected were best-estimate values. No conservative assumptions were taken into account such as single failure criterion. The systems performance was in accordance with the assumptions specified for scenarios. The core damage criteria used for determination of time windows are described first. Then the input model for the RELAP5 is described. Finally, each scenario is briefly described.

2.1. Description of General Core Damage Criterion. The typical core cooling success criteria for Westinghouse-type PWR as defined in [13] were used. These criteria are defined in terms of the average fuel/clad temperature instead of hot rod fuel/clad temperature, considering also the period of high temperature. It is assumed if the hottest core fuel/clad node temperature in the reactor core exceeds 923 K for more than 30 minutes or if temperature exceeds 1348 K, the core damage may occur, which may lead to accident state. Based on the core damage criteria the time windows were determined. Sensitivity studies were performed which include variations of timing of human action to determine the latest time, when operators have to perform the needed action in order that the main plant parameters are not exceeded their limits.

2.2. RELAP5 Input Model Description. To perform this analysis, Krško nuclear power plant (NPP) has provided the base RELAP5 input model, so-called "Master input deck," which has been used for several analyses, including reference calculations for Krško full scope simulator verification [12, 14]. A full two-loop plant input model has been used for the analysis. It includes the new Siemens-Framatome (now Areva) replacement steam generators type SG 72 W/D4-2. The model consists of 469 control volumes, 497 junctions, and 378 heat structures with 2107 radial mesh points. Besides, 574 control variables and 405 logical conditions (trips) represent the instrumentation, regulation isolation, safety injection (SI) and auxiliary feedwater (AFW) triggering logic, steamline isolation, and so on. Secondary side is modelled up to the turbine.

Figure 1 shows animation mask of RELAP5 input model. Animation mask has been created by Symbolic Nuclear Analysis Package (SNAP) [15]. Modelled are important components as the reactor vessel (RV), pressurizer surge line (SL), pressurizer (PRZ) vessel, pressurizer spray lines and spray valves, pressurizer power operated relief valves (PORVs), and safety valves. Primary piping includes hot leg (HL), primary side of steam generator by inlet and outlet plenum, among which a single pipe is representing the U-tube bundle, intermediate leg (IL), and cold leg (CL) with reactor coolant pump (RCP). Loops are symmetrical except for the pressurizer surge line and chemical and volume control system connections layout (charging and letdown). Modelled is emergency cooling system (ECCS) with high pressure injection system (HPIS), accumulators, and low pressure injection system (LPIS).

The parts of the steam generator secondary side are represented by riser, separator and separator pool, downcomer, and steam dome. Each loop of main steamline has main steam isolation valve (MSIV), five SG safety valves, and one SG PORV. Turbine valve and steam dump (SD) flow are regulated by corresponding logic. Main feedwater (MFW) piping is modelled till the MFW pump, which is modelled as time dependent junction. Auxiliary feedwater (AFW) piping is modelled from pumps, which are modelled as time dependent junction. The AFW system is injecting above the SG riser.

Besides the model layout, in Figure 1 are shown initial conditions of the main plant parameters at full power, status of the pumps and valves, and how the systems are filled. Green colour means operating pump and open valve, while red colour means stopped pump and closed valve. Besides, void fraction is shown across the primary and secondary

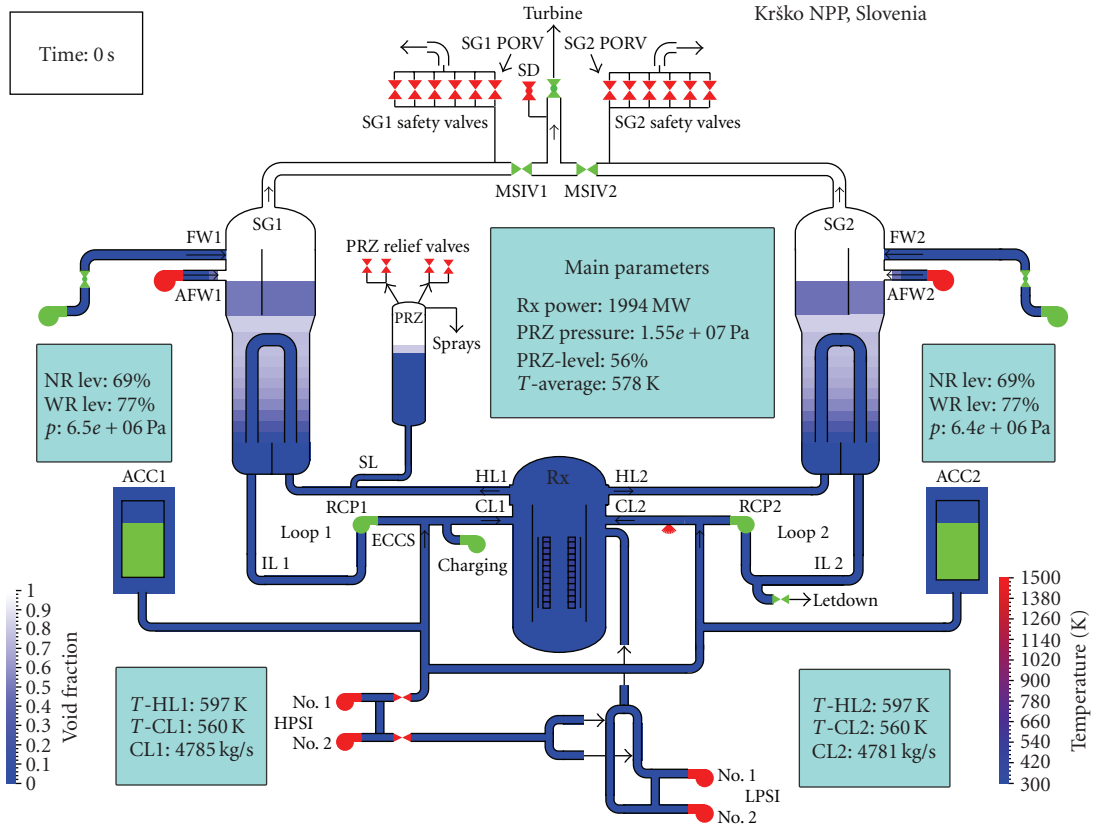

Figure 1: Krško NPP animation mask at 0 second.

systems. Blue colour represents a fluid, white colour represents a steam, while the colours between represent a two-phase mixture.

2.3. Scenarios Description. Three scenarios are described, which were needed for updated human reliability analysis. In these scenarios the human actions are supplement to safety systems actuations. In the first scenario the human action was establishing AFW in case of small or medium LOCA assuming that high pressure safety injection (HPSI) system fails. In the second scenario the human action was establishing AFW in case of loss of feedwater (LOFW) transient. In the third scenario the human action was actuation of SI signal for the most limiting accident (excluding large break LOCA), that is, small and medium LOCA. For each scenario the success criteria as defined in original HRA analysis are described, while acceptance criteria are core damage criteria described in Section 2.1. Success criteria establish the minimum number or combinations of systems required to operate, during a specified period of time, to ensure that the critical safety functions are met within the limits of the acceptance criteria.

In the case of small or medium LOCA in a nuclear power plant with the assumption that HPSI system fails, one of the means to cool the reactor is through the secondary side depressurization providing that AFW system is operating. Normally, AFW system is automatically put into operation when main feedwater is lost. If the AFW pumps would not start automatically, operators should intervene. The success criterion requires operation of one of three AFW pumps to maintain the flow in order to depressurize the primary system below the accumulator injection setpoint at 4.9 MPa and secondary steam relief via one SG PORV. Besides passive accumulators it was assumed that low pressure safety injection (LPSI) is available too. The parameter to indicate depressurization was primary pressure and the parameter to indicate core cooling was average rod cladding temperature of hottest node. As larger breaks can depressurize through the break in any case below accumulator injection setpoint pressure after some time, AFW is not needed for depressurization. Therefore the analysis was performed for a spectrum of break sizes from 1.27 cm (0.5 inch) to 15.24 cm (6 inch) to determine, for which break sizes is needed the operation of one AFW pump and for them the time available to start AFW was determined based on the parametric study varying delay of AFW start. The break was located in the cold leg between the reactor coolant pump and the reactor vessel (see Figure 1).

The most limiting transient requiring operation of AFW is LOFW. The success criterion is that capacity of one train of AFW is adequate to remove the decay heat, to prevent overpressurization of primary system, and to prevent uncovering of the core resulting in core heatup. Success for AFW start also assumes adequate steam relieving capability. The time when the operator succeeds to start AFW pump was varied. When the AFW pump started to inject into the

Table 1: Sequence of main events for LOCA calculations.

	Time (s)					
Analyzed cases (break sizes)	1.27 cm	1.91 cm	2.54 cm	5.08 cm	7.62 cm	15.24 cm
Break occurrence	0.0	0.0	0.0	0.0	0.0	0.0
Rx trip signal generation	880.7	274.2	112.5	21.5	3.3	2.6
Turbine trip	880.7	274.2	112.5	21.7	3.3	2.7
SI signal generation	891.4	282.4	122.9	29.9	13.4	6.3
MFW isolation	891.4	282.5	122.9	29.9	13.5	6.3
LPSI 1 and 2 pump running	901.4	292.4	132.9	39.9	23.5	16.3
RCP 1 and 2 trip	1105.0	432.0	260.9	120.4	91.2	68.7
SG PORVs first discharge	1230	538	372	223	232	N.A.
PRZ PORV 2 first discharge	8340	N.A.	N.A.	N.A.	N.A.	N.A.
Accumulator no. 1 injection	N.A.	N.A.	N.A.	1802.2	712.5	188.3
Accumulator no. 2 injection	N.A.	N.A.	N.A.	1802.0	712.5	188.3
Accumulator no. 1 isolation	N.A.	N.A.	N.A.	8612.3	4111.3	634.1
Accumulator no. 2 isolation	N.A.	N.A.	N.A.	8612.3	4111.8	634.0
LPSI 1 and 2 first injection	N.A.	N.A.	N.A.	N.A.	4910	864

secondary side, cooling of the secondary side caused the pressurizer pressure to drop below the pressurizer PORV closure setpoint and then below the maximum pressure capacity of HPSI pump. The HPSI injection efficiently prevents further core uncovery.

The third considered scenario was LOCA without automatic SI signal actuation. This means that none of the safety systems including HPSI system, LPSI system, and AFW system was assumed available. The whole spectrum of LOCAs from 1.91 cm (0.75") to 15.24 cm (case 6") equivalent diameter break size was evaluated. For the most critical break regarding the time available to the operator the manual SI signal was simulated at the time the core started to heatup and at the time the core average temperature approaches the core average temperature criterion.

3. Results

In the next three subsections the results for the selected scenarios are shown, based on which the time windows for operator actions were determined. In Figures 1 through 7 are shown the most important variables to understand the scenario progression. The time available to perform operator action was determined from average core cladding temperature. Finally, the obtained time windows were compared to the actual times needed for performing the actions, which was assessed based on real simulator scenarios [11].

3.1. LOCA Calculations with Manual Actuation of AFW. The spectrum of break sizes was analyzed. For the most limiting break regarding time available it was shown that operation of AFW is not enough if not supported by manual opening of steam generator (SG) power operated relief valve (PORV). These two actions were assumed to be performed with the same time delay. The results for a spectrum of break sizes are shown in Table 1 and Figure 2.

Table 1 shows the sequence of main events. After break occurrence the reactor trips on low pressurizer pressure and it is followed by turbine trip. The SI signal is actuated on low-low pressurizer signal what cause main feedwater isolation and LPSI pumps running with 10 seconds delay. Next reactor coolant pumps are tripped by operator on subcooling criterion. After turbine trip and steam dump closure the SG pressure started to increase, resulting in discharging the SG mass.

From Table 1 and Figure 2(a) it can be seen that 5.08 cm (2 inch) and larger breaks depressurize (through the break) in any case below accumulator injection setpoint pressure at 4.9 MPa after some time and therefore AFW is not needed for depressurization. When accumulators are emptied after some time the primary pressure drops below the LPSI pumps shutoff head. On the other hand, 2.54 cm (1 inch) equivalent diameter break size and smaller need depressurization. As reactor coolant system (RCS) mass depletion (see Figure 2(c)) and core heatup (see Figure 2(b)) are earlier for 2.54 cm (1 inch) break than for 1.91 cm (0.75 inch) and 1.27 cm (0.5 inch) break, the 2.54 cm break was identified as the most critical regarding the time available to start AFW. Figure 2(d) shows that for break 2.54 cm (and smaller), the steam generators start to dry out as their inventory is lost through SG PORVs, what caused core heatup. This can be seen from Figures 2(e) and 2(f) for SG pressure and SG PORV flow for steamline no. 1, respectively. Similar is situation in the steamline no. 2. In the case of 15.24 cm break LPSI pump injection removes decay heat through the break. This cooling is sufficient to cool the secondary side what can be seen from SG no. 1 pressure shown in Figure 2(e) .

To establish the depressurization by cooling through the secondary side, one AFW is needed. However, as shown in Figure 3(a), just by operating AFW and automatic SG PORV operation the RCS pressure could not be depressurized and the core heated up (see Figure 3(b)). The reason is that the SG PORV is cycling. Once SG is filled to normal level, the

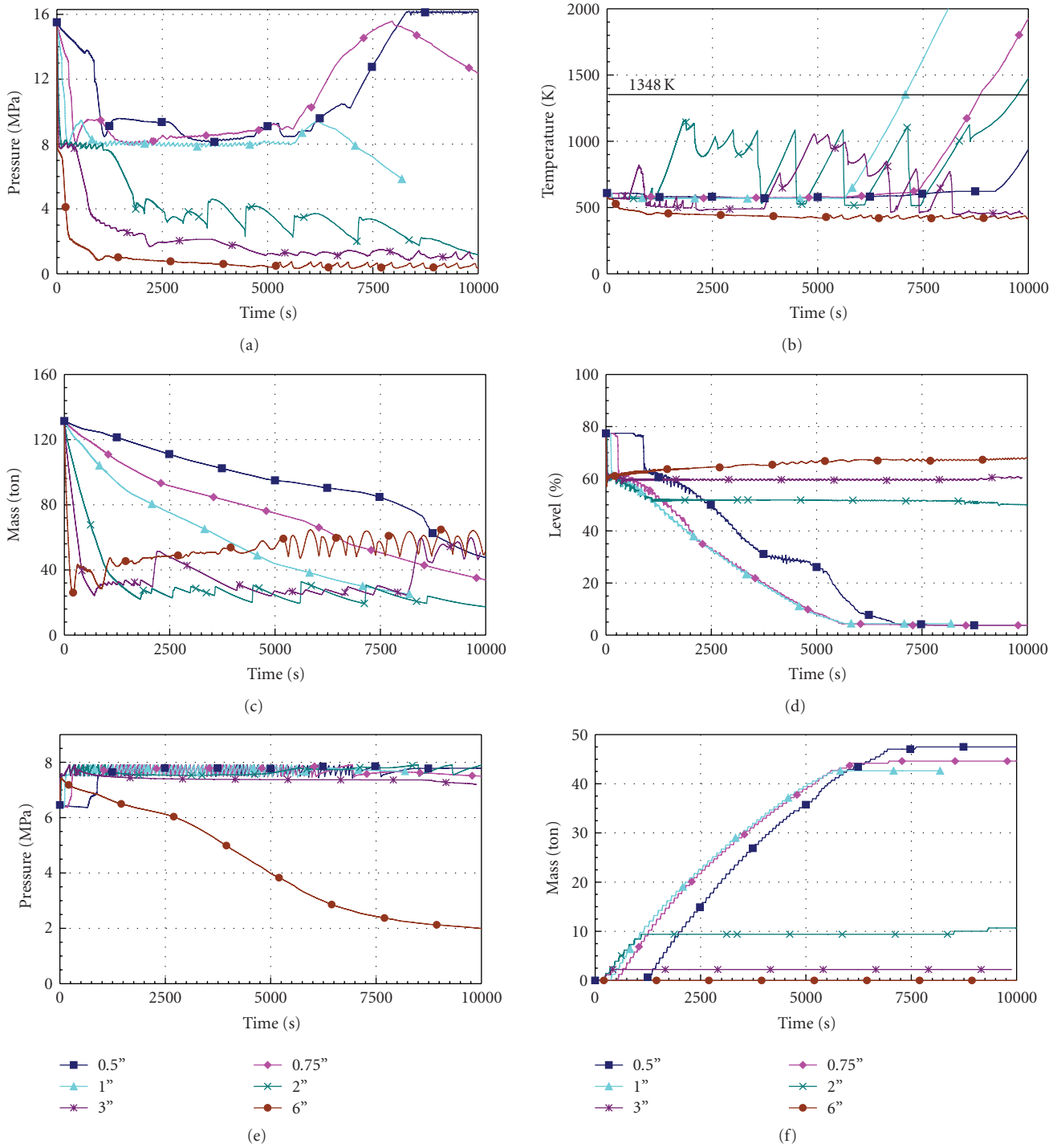

Figure 2: Calculated results for spectrum of break sizes: (a) RCS pressure, (b) core cladding temperature, (c) RCS mass inventory, (d) SG no. 1 wide range level, (e) SG no. 1 pressure, (f) mass discharged through SG no. 1 PORV.

AFW injected intermittently following cycling of the PORVs. Depressurization could be efficiently achieved by manual full opening of SG PORV providing that SG level is maintained above the minimum level by AFW.

As can be seen from Table 2 six cases were analyzed for the selected 2.54 cm break size. Case A was analyzed in order to determine how long cooling can be done with available SG inventory. In the cases B to F different delays of manual AFW start and full PORV opening were analysed.

Table 3 shows the time sequence of main events. Scenario A is different from scenarios B to F, as it was performed with the intention to see how long it takes the SG to dry out with assumed SG PORV opened. Due to opened SG no. 1 PORV both steam generators were emptying until steamline

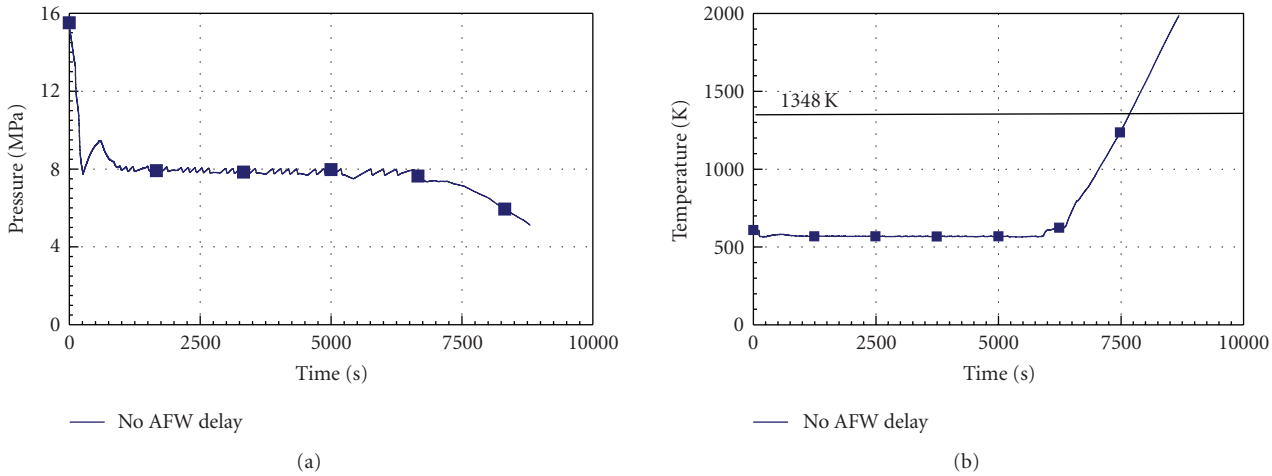

Figure 3: Scenario with AFW available: (a) RCS pressure, (b) core cladding temperature.

Table 2: Operator actions delay for 2.54 cm LOCA calculations.

Case	Operator action	
	AFW start delay (minute)	SG PORV full opening delay (minute)
A	Not available	0
B	30	30
C	50	50
D	80	80
E	100	100
F	120	120

isolation. Later each steam generator was discharging its inventory through its PORV. In the case of SG no. 2 the PORV was cycling. Due to secondary cooling the primary pressure droped below the accumulator injection setpoint. The accumulator emptied in approximately 1100 seconds. Later no cooling is available leading to core heatup. The results for scenario A showed that SG no. 1 drys out in approximately 40 minutes. In scenarios B to F the time available to the operators was determined. Until AFW no. 1 is started both SG PORVs cycled. After full opening of SG no. 1 PORV, the SG no. 2 PORV remains closed. It is important to note that it takes approximately 5 to 10 minutes that the secondary cooling reduces the pressure below the accumulator injection setpoint.

Figure 4(a) shows that RCS depressurization with SG no. 1 PORV fully open is efficient in preventing the core heatup (see Figure 4(b)), when delay of AFW pump start is not too large. Following the AFW pump no. 1 injection the RCS pressure depressurized below the accumulator injection setpoint and the RCS system started to fill as shown in Figure 4(c). Case A was analyzed in order to see how long inventory in SG is available for cooling through fully open SG PORV. The SG is emptied in 40 minutes and core started to heat up 25 minutes after SG is emptied. In another 20 minutes the core temperature exceeds the criterion. From Figure 4(d) it can be seen that for cases B to D the SG no. 1 level is dropping approximately linearly and that cooling is sufficient, because the SG is not completely emptied. In cases A, E, and F both SGs emptied below the minimum needed level for cooling and the core heatup was therefore unavoidable. The SG pressure is shown in Figure 4(e) and SG PORV discharge in Figure 4(f). From Figure 4(f) it can be seen that after full SG no. 1 PORV opening the mass discharge rate initially increased and later stabilized when the pressure drops to stable value. It should be also noted that both steam generators emptied through SG no. 1 PORV until main steamline isolation. Main steamline isolation resulted from low steamline pressure after full SG no. 1 PORV opening.

From case E it can be seen that if operator actions are performed immediately after SGs emptying the further heat up could still be prevented. Based on the set criteria 100 minutes are available to the operators.

3.2. LOFW Calculations with Manual Actuation of AFW. The delays of AFW pump start from 30 minutes to 70 minutes were simulated to determine the time window for manual AFW start. Table 4 shows the sequence of main events. The reactor trips on low SG level, followed by turbine trip. SI signal is generated on low steamline pressure, which also actuates main steamline isolation. The RCPs were tripped manually by operator on subcooling criterion. At the time when one AFW pump started to inject into the secondary side, cooling of the secondary side caused the

Table 3: Sequence of main events for 2.54 cm LOCA calculations.

	Time (s)					
Analyzed cases	A	B	C	D	E	F
Break occurrence	0.0	0.0	0.0	0.0	0.0	0.0
Rx trip signal generation	108.6	112.5	112.5	112.5	112.5	112.5
Turbine trip	108.7	112.5	112.5	112.5	112.5	112.5
SI signal generation	118.9	122.9	122.9	122.9	122.9	122.9
MFW isolation	118.9	122.9	122.9	122.9	122.9	122.9
steamline isolation	1568.8	2338.2	3437.5	5124.0	6124.9	7320.8
Accumulator no. 1 injection	2202.1	2541.1	3617.0	5274.2	6497.7	7631.4
Accumulator no. 2 injection	2202.0	2541.1	3617.0	5274.0	6497.5	7631.3
Accumulator no. 1 isolation	3299.0	5511.5	5706.1	6157.1	7325.4	8575.3
Accumulator no. 2 isolation	3298.0	5510.4	5705.1	6157.2	7325.3	8575.0

pressurizer pressure to drop below the pressurizer PORV closure setpoint and then below the maximum pressure capacity of HPSI pump (see Figure 5(a)). The closure of the pressurizer PORV and coolant injection into primary system resulted in recovering the RCS inventory as shown in Figure 5(c) and quenching the core as shown in Figure 5(b). From Figure 5(c) it can be seen that the RCS mass depletion depends mainly on the delay of AFW pump start. The parametric analysis showed that the core significantly heats up when the start of AFW pump is delayed for 60 minutes or more. The case with start of AFW pump delayed for 50 minutes cause small core heatup and with delay of 60 minutes the core temperature is still below the criterion 1348 K for core damage, while in the case with delay of 70 minutes this value is exceeded. In Figure 5(d) is shown the steam generator no. 1 wide range level. As already mentioned the start of AFW caused filling of steam generator no. 1 and RCS system depressurization. Initial filling of steam generator is slower due to SG PORV discharge. As HPSI pump is also injecting, the SG PORV cooling is not needed until SI is terminated. SI termination can be done as the primary system is refilled and there is no break on the primary side. After SI termination the secondary pressure started to increase again (see Figure 5(e)) until SG PORV setpoint is reached causing further steam release as shown in Figure 5(f).

3.3. LOCA Calculations with Manual Actuation of SI. The sequence of events for LOCA spectrum calculations is shown in Table 5. The only safety system operating was passive accumulators. For 5.08 cm and larger breaks they emptied in the calculated time interval of 10 000 seconds. The results for RCS pressure and core cladding temperature are shown in Figure 6. At breaks smaller than 5.08 cm the RCS was not sufficiently depressurized as shown in Figure 6(a) to enable accumulator injection, while larger breaks depressurize the RCS. Figure 6(b) shows that the temperature criterion 1348 K is first exceeded for 15.24 cm (case 6"), then for 10.16 cm break (case 4"), 7.62 cm (case 3"), 1.91 cm (case 0.75"), and the last for 5.08 cm (case 2"). The reason is that for 5.08 cm break the accumulators were sufficient to cool the core until they emptied. At breaks larger than 5.08 cm the core starts to significantly heatup after the accumulators emptied. In general it can be concluded that the larger is the break the faster is the core uncovery. From the point of operator action the 15.24 cm break size calculation is therefore limiting.

Table 6 shows for 5.08 cm and 15.24 cm break size the times of emergency core coolant injections. Passive accumulators injected in all cases, while HPSI and LPSI pumps injected after manual SI signal was actuated and the primary pressure was below the shutoff pressure of the injection pumps. For 15.24 cm break size the pressure is sufficiently low to allow injection of both HPSI and LPSI pumps once SI signal is manually actuated. In the case of 5.08 cm break size only HPSI pumps started to inject at the time of SI signal actuation. For both break sizes the injection is sufficient to terminate the core heatup as shown in Figure 7. It can also be seen that when delay of SI signal actuation is 20 minutes, there is negligible core heatup, while in the case of 30 minutes delay of SI signal actuation the criterion is not exceeded, but consideration of uncertainties could cause the criterion to be exceeded. Therefore 20 minutes time window was conservatively selected as time available to the operators.

3.4. Results Discussion. The times needed for performing operator actions were determined based on the simulator experience [11]. For starting the AFW the operator needs from 1 to 10 minutes, while for SI signal actuation 2 minutes are needed. When the time window is large, much of the additional time is available and there is no need to very accurately determine the time window even if the human factor event is an important contributor to the risk. For example, the time needed to start SI signal is 2 minutes and there is additional 18 minutes to perform this action. Considering typical uncertainties in the peak cladding temperatures of 200 K based on the previous uncertainty evaluations [16] and adiabatic heatup rate for 15.24 cm break, the criterion would be reached 3 minutes earlier. Equally important is also time uncertainty of reaching maximum temperature which is approximately 2 minutes according to [17]. The additional time considering uncertainties is still sufficient.

In the case of small and medium break LOCAs with the assumption that HPSI is not available, the depressurization is

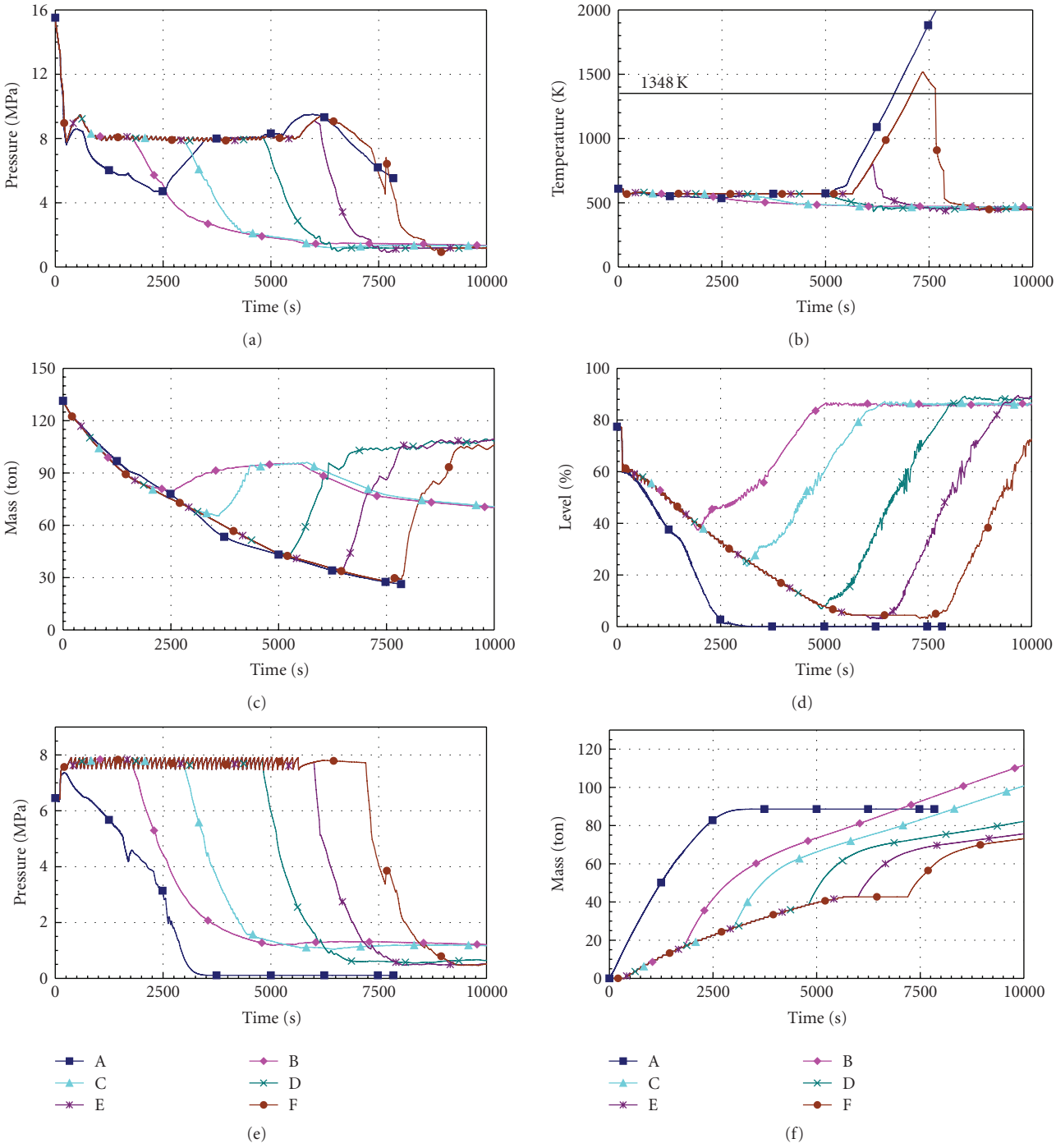

FIGURE 4: 2.54 cm break scenarios with two operator actions: (a) RCS pressure, (b) core cladding temperature, (c) RCS mass inventory, (d) SG no. 1 wide range level, (e) SG no. 1 pressure, (f) mass discharged through SG no. 1 PORV.

needed for breaks smaller than 5.08 cm. The break 5.08 cm is limiting as for this and larger breaks the RCS depressurizes by itself. However, when the pressure drops below the accumulator injection setpoint, the core is already heated up for 5.08 cm break. Considering the typical cladding temperature uncertainty of the best estimate calculation to be 200 K [16] the criterion 1348 K could be exceeded. The recovery action would be questionable because of short time window. The uncertainty analysis was not needed, as the risk contribution of this event to the plant risk is insignificant.

On the other hand, establishing AFW at LOFW event is significant contributor to the risk, but the calculated time window gives sufficient additional time, even if conservative time window is considered in the human reliability analysis.

For the case of LOCA with delayed SI signal actuation it was shown that the additional time available is sufficient,

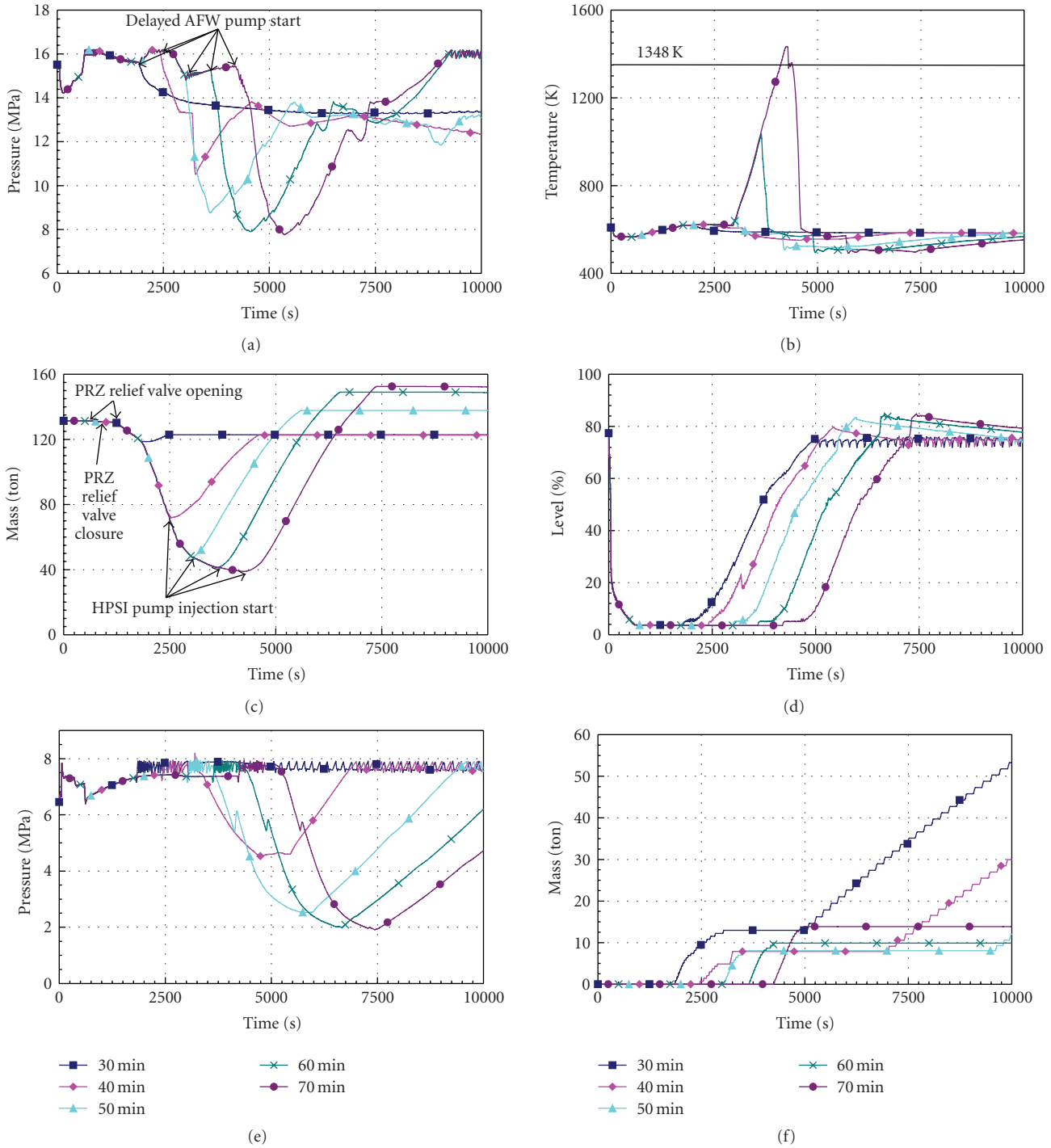

Figure 5: LOFW transient: (a) RCS pressure, (b) core cladding temperature, (c) RCS mass inventory, (d) SG no. 1 wide range level, (e) SG no. 1 pressure, (f) mass discharged through SG no. 1 PORV.

therefore uncertainty analysis is not needed in spite of the fact that event is significant contributor to the risk.

All these examples showed that uncertainty analysis was not needed, as additional time was available and/or the event was not significant contributor to the risk. If the event is significant contributor to the risk or not, it is answered by PSA. Based on this it can be concluded that uncertainty analysis may be valuable only for significant risk contributors, when additional available time is small. For the cases needed for updated human reliability analysis it was demonstrated that PSA reduces the number of uncertainty analysis. So there was no case requiring uncertainty analysis. If uncertainty analysis would be needed same approach could be followed as for licensing LOCA calculations, for example,

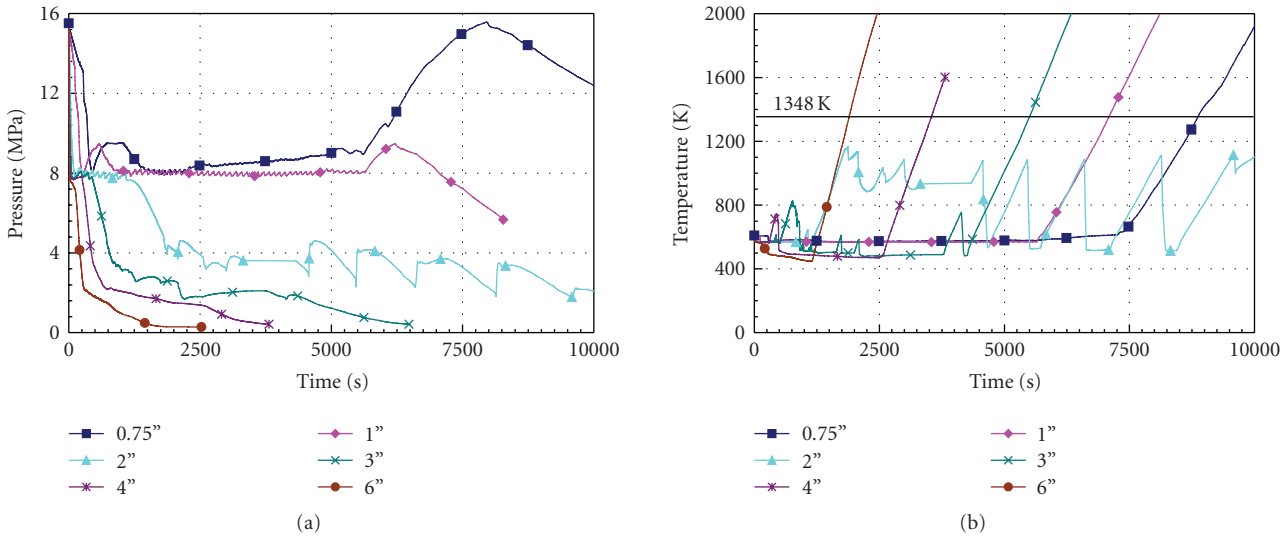

Figure 6: LOCA spectrum without SI actuation: (a) RCS pressure, (b) core cladding temperature.

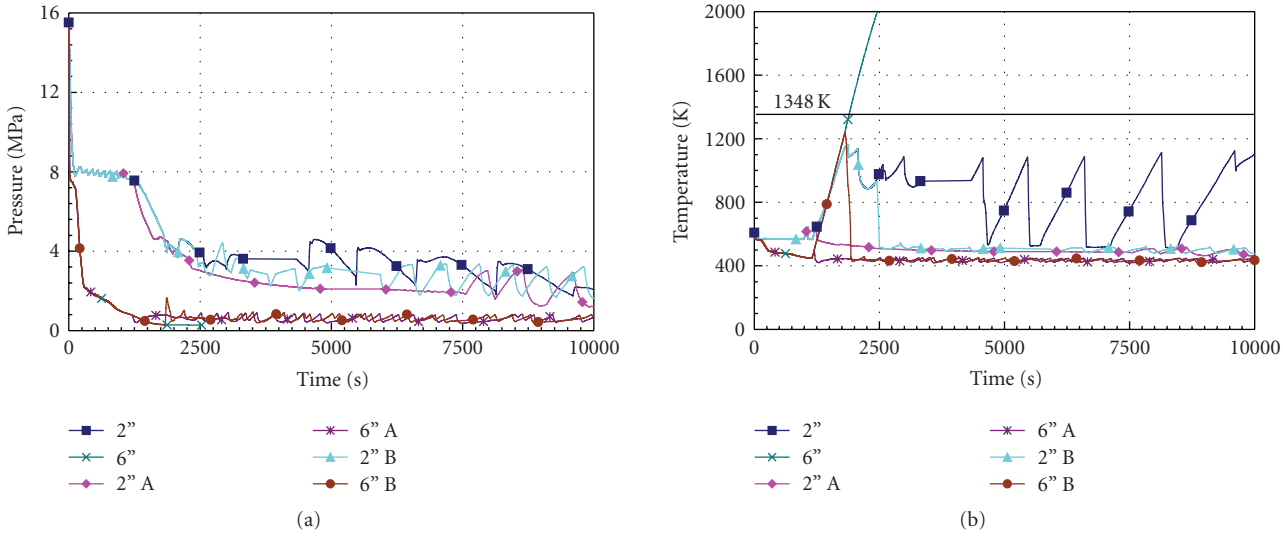

Figure 7: LOCA with manual actuation of SI: (a) RCS pressure, (b) core cladding temperature.

Table 4: Sequence of main events for LOFW calculations.

Scenario	Time (s)				
Analyzed cases (AFW delay)	30 minutes	40 minutes	50 minutes	60 minutes	70 minutes
Main feedwater closure	0.1	0.1	0.1	0.1	0.1
Rx trip signal generation	52.9	52.9	52.9	52.9	52.9
Turbine trip	52.9	52.9	52.9	52.9	52.9
Steam dump discharge	30–617	30–617	30–617	30–617	30–617
SI signal generation	616.9	616.9	616.9	616.9	616.9
Steam line 1 and 2 isolation	617.0	617.0	617.0	617.0	617.0
RCP 1 and 2 trip	1587.2	1587.2	1587.2	1587.2	1587.2
AFW 1 start (by assumption)	1805	2405	3005	3605	4205
SG PORV first discharge	1855	2460	3060	3660	4260
HPSI pump injection start	2020	2560	3010	3630	4300
HPSI termination	2450	4585	5594	6512	7372

Table 5: Sequence of main events for LOCA calculations without SI signal.

	Time (second)					
Analyzed break sizes	1.91 cm	2.54 cm	5.08 cm	7.62 cm	10.16 cm	15.24 cm
Break occurrence	0.0	0.0	0.0	0.0	0.0	0.0
Rx trip signal generation	274.2	112.5	21.5	3.3	2.9	2.6
Turbine trip	274.2	112.5	21.5	3.3	2.9	2.7
conditions for automatic SI signal generation	282.4	122.9	29.6	13.4	8.9	6.3
Accumulator no. 1 injection	N.A.	N.A.	1802.2	712.2	391.8	189.0
Accumulator no.2 injection	N.A.	N.A.	1802.0	712.0	391.7	188.9
Accumulator no. 1 isolation	N.A.	N.A.	8612.3	4146.3	1720.2	625.9
Accumulator no.2 isolation	N.A.	N.A.	8612.3	4146.9	1752.9	625.7

Table 6: Coolant injection times for LOCA calculations with/without SI signal.

	Time (second)					
Break size		5.08 cm			15.24 cm	
Analyzed case	2”	2” A	2” B	6”	6” A	6” B
(delay of manual SI signal)	(N.A.)	(20 minutes)	(40 minutes)	(N.A.)	(20 minutes)	(30 minutes)
Accumulator no. 1 injection	1802.2	1557.6	1802.2	189.0	189.0	189.0
Accumulator no. 2 injection	1802.0	1560.6	1802.0	188.9	188.9	188.9
Accumulator no. 1 isolation	8612.3	7115.1	8278.6	625.9	625.9	625.9
Accumulator no. 2 isolation	8612.3	7115.0	8279.2	625.7	625.7	625.7
HPSI 1 and 2 first injection	N.A.	1222	2422	N.A.	1203	1803
LPSI 1 and 2 first injection	N.A.	9920	N.A.	N.A.	1203	1803

[18]. On the other hand, the authors in [19] are of the opinion that the uncertainty is a less important issue for the treatment of an operator's action in a thermal hydraulic simulation and that better approach is to estimate the time window conservatively. Nevertheless, such a statement could be used only when additional available time is sufficient to take into account conservatism.

4. Conclusions

The operator action success criteria time windows were estimated using the RELAP5/MOD3.3 Patch 03 thermal-hydraulic computer code for updated human reliability analysis. For the three selected cases the results of deterministic safety analysis were examined in sense how late after the required human intervention the operator performs its action that the safety criteria are not exceeded. This gives available time for operator to act. The results of deterministic analyses showed that in some cases the treatment of uncertainty for variables compared with safety criterion could significantly change the time window. However, based on the information from PSA regarding the contribution to the risk, uncertainty analysis was not needed, what greatly support the use of best estimate codes for probabilistic safety assessment. It can be concluded that uncertainty evaluation of realistic safety analysis may be needed only when there is little time for recovery action and the affected human factor event is an important contributor to risk.

Acknowledgments

The authors acknowledge the financial support from the state budget by the Slovenian Research Agency Program no. P2-0026 and the financial support from Slovenian Nuclear Safety Administration and Krško NPP by Project no. POG-3473. The RELAP5/MOD3.3 Krško NPP base input model is courtesy of Krško NPP.

References

[1] E. Zio, “Reliability engineering: old problems and new challenges,” *Reliability Engineering and System Safety*, vol. 94, no. 2, pp. 125–141, 2009.

[2] J. Park, W. Jung, J. Ha, and Y. Shin, “Analysis of operator's performance under emergencies using a training simulator of the nuclear power plant,” *Reliability Engineering and System Safety*, vol. 83, no. 2, pp. 179–186, 2004.

[3] S. J. Han, H. G. Lim, and J. E. Yang, “An estimation of an operator's action time by using the MARS code in a small break LOCA without a HPSI for a PWR,” *Nuclear Engineering and Design*, vol. 237, no. 7, pp. 749–760, 2007.

[4] J. S. Butler, D. Kapitz, R. K. Sundaram, and R. P. Martin, “MAAP4.0.7 analysis and justification for PRA level 1 mission success criteria,” in *Proceedings of the International Congress on Advances in Nuclear Power Plants (ICAPP '08)*, Anaheim, Calif, USA, June 2008, paper 8200.

[5] C. H. Park, D. J. Lee, I. J. U. C. Lee, K. Y. Suh, and G. C. Park, “Comparative study of loss-of-coolant accident using

MAAP4.03 and RELAP5/MOD3.2.2," in *Proceedings of the International Conference on Nuclear Engineering (ICONE '02)*, vol. 3, pp. 729–733, Arlington, Va, USA, April 2002.

[6] A. Kaliatka, E. Uspuras, and S. Rimkevicius, "Thermal hydraulic analysis of LOCA for justification of RBMK-1500 success criteria," in *Proceedings of the International Congress on Advances in Nuclear Power Plants (ICAPP '07)*, vol. 2, pp. 1056–1064, May 2007, paper 7184.

[7] ASME, *Standard for Probabilistic Risk Assessment for Nuclear Power Plant Applications RA-S-2002*, The American Society of Mechanical Engineers, New York, NY, USA, 2002.

[8] M. Leskovar and B. Mavko, "Simulation of the Phebus FPT1 severe accident experiment with the MELCOR computer code," *Journal of Mechanical Engineering*, vol. 52, no. 3, pp. 142–160, 2006.

[9] USNRC, *RELAP5/MOD3.3 Code Manual*, vol. 1–8, Information Systems Laboratories, Rockville, Md, USA, 2006, prepared for USNRC.

[10] M. Čepin, "Human reliability analysis within probabilistic safety assessment for other modes than power operation," in *Proceedings of the International Topical Meeting on Probabilistic Safety Assessment & Analysis—Challenges to PSA during the Nuclear Renaissance*, Knoxville, Tenn, USA, September 2008.

[11] A. Prošek and M. Čepin, "Impact of deterministic safety analysis on human reliability analysis," in *Proceedings of the Risk, Quality and Reliability Conference (RQR '07)*, pp. 233–237, Ostrava, Czech Republic, September 2007.

[12] A. Prošek, I. Parzer, and B. Krajnc, "Simulation of hypothetical small-break loss-of-coolant accident in modernized nuclear power plant," *Electrotechnical Review*, vol. 71, no. 4, pp. 199–204, 2004.

[13] R. P. Prior, J. P. Chaboteaux, F. P. Wolvaardt, M. T. Longton, and R. Schene, "Best estimate success criteria in the Krsko IPE," in *Proceedings of the PSA/PRA and Severe Accidents*, pp. 2–12, Nuclear Society of Slovenia, Ljubljana, Slovenia, April 1994.

[14] I. Parzar, B. Mavko, and B. Krajnc, "Simulation of a hypothetical loss-of-feedwater accident in a modernized nuclear power plant," *Journal of Mechanical Engineering*, vol. 49, no. 9, pp. 430–444, 2003.

[15] Applied Programming Technology, "Symbolic nuclear analysis package (SNAP)," User's Manual, April 2007.

[16] A. Prošek and B. Mavko, "Evaluating code uncertainty—I: using the csau method for uncertainty analysis of a two-loop PWR SBLOCA," *Nuclear Technology*, vol. 126, no. 2, pp. 170–185, 1999.

[17] A. Prošek and B. Mavko, "Evaluating code uncertainty—II: an optimal statistical estimator method to evaluate the uncertainties of calculated time trends," *Nuclear Technology*, vol. 126, no. 2, pp. 186–195, 1999.

[18] R. P. Martin and L. D. O'Dell, "Development considerations of AREVA NP Inc.'s realistic LBLOCA analysis methodology," *Science and Technology of Nuclear Installations*, vol. 2008, Article ID 239718, 13 pages, 2008.

[19] S. J. Han, H. G. Lim, and J. E. Yang, "An estimation of an operator's action time by using the MARS code in a small break LOCA without a HPSI for a PWR," *Nuclear Engineering and Design*, vol. 237, no. 7, pp. 749–760, 2007.